SPATIALLY EXPLICIT MODELING OF HYDROLOGICALLY CONTROLLED CARBON CYCLES IN A BOREAL ECOSYSTEM

By

Ajit Govind

A thesis submitted in conformity with the requirements
for the degree of Doctor of Philosophy
Graduate Department of Geography
University of Toronto

© Copyright by Ajit Govind (2008)

Spatially Explicit Modeling of Hydrologically Controlled Carbon Cycles in a Boreal Ecosystem.

Doctor of Philosophy, 2008

Ajit Govind

Graduate Department of Geography, University of Toronto

Current estimates of terrestrial carbon (C) fluxes overlook explicit hydrological controls. In this research project, a spatially explicit hydro-ecological model, BEPS-TerrainLab V2.0 was further developed to improve our understanding of the non-linearities associated with various hydro-ecological processes. A modeling study was conducted in a humid boreal ecosystem in north central Quebec, Canada. The sizes and nature of various ecosystem-C-pools were comprehensively reconstructed under a climate change and disturbance scenario prior to simulation in order to ensure realistic biogeochemical modeling. Further, several ecosystem processes were simulated and validated using field measurements for two years. A sensitivity analysis was also performed. After gaining confidence in the model's ability to simulate various hydrologically controlled ecophysiological and biogeochemical processes and having understood that topographically driven sub-surface baseflow is the main process determining the soil moisture regime in humid boreal ecosystem, its influence on ecophysiological and biogeochemical processes were investigated. Three modeling scenarios were designed that represent strategies that are currently used in ecological models to represent hydrological controls. These scenarios were: 1) *Explicit,* where realistic lateral water routing was considered 2) *Implicit,* where calculations were based on a bucket-modeling approach 3) *NoFlow*, where the lateral sub-surface flow was turned off in the model. In general, the *Implicit* scenario overestimated GPP, ET and NEP, as opposed to the *Explicit* scenario. The *NoFlow* scenario underestimated GPP and ET but overestimated NEP. The key processes controlling the differences were due to the combined effects of variations in plant physiology, photosynthesis, heterotrophic respiration, autotrophic respiration and nitrogen mineralization; all of which occurred simultaneously in different directions, at different rates, affecting the spatio-temporal distribution of terrestrial C-sources or sinks (NEP). From these results it was clear that lateral water flow does play a significant role in the net terrestrial C distribution and it was discovered that non-explicit forms of hydrological representations underestimate the sizes of terrestrial C-sources rather than C-sinks.

The scientific implication of this work demonstrates that regional or global scale terrestrial C estimates could have significant errors if proper hydrological constraints are not considered for modeling ecological processes due to large topographic variations of the Earth's surface.

Acknowledgements

This thesis is the result of four and half years of work whereby I have been accompanied and supported by many people. It is a good occasion to express my earnest gratitude to all of them.

First of all I thank my supervisor, Prof. Jing Ming Chen for accepting me and introducing me to this exciting research project. His easy grasp of environmental physics and intuitive skills helped nurture my rational thinking. He carefully guided the progress of this research and provided immense support for both my scientific and scholastic development. He was always reachable and responded to all of my questions even during his busiest times. Thank you for giving me an opportunity to work with you. Next, I am grateful to all the members of my advisory committee. I take this opportunity to express my gratitude to Late Prof. Ferenč Csillag who served as a committee member between 2003 and 2005. He motivated me during my initial stages at U *of* T, a critical period for an international student. I thank Prof. Sharon Cowling, Prof. John Caspersen and Prof. Anthony G. Price who have had a critical role in the success of this thesis. I learnt a lot from them by attending their graduate courses which had a great impact on this research work.

I was also fortunate to be involved with the Fluxnet Canada Research Netwrok (FCRN), now the Canadian Carbon Program. FCRN has given me ample opportunity to attend various conferences (financial support) and interact with many well known scientists, which immensely contributed to my scientific development. In this regard, I sincerely thank Prof. Hank Margolis, PI of FCRN, Prof. Carolle Coursolle, FCRN manager and other FCRN staff Ms. Debbie Christiansen Stowe and Ms. Stefanie Guimond (Faculty of Forestry, Universite Laval). I would also like to thank Prof. Larry B. Flanagan (University of Lethbridge) who organized the *Carbon Cycle Course* and Dr. Alan Barr (Environment Canada) for the *Eddy Covariance Tower Climbing Course*, sponsored by the FCRN. From these courses I learnt a lot on global C cycle and state of the art terrestrial carbon monitoring techniques by interacting with many scientists and students.

I have been closely interacting with many individuals doing field measurements at the Chibougamau site of FCRN (EOBS) since 2003. I thank Dr. Onil Bergeron (McGill University), Mr. Marc André Giasson (manager, EOBS site) for promptly responding to all my site-specific questions in a welcoming manner. I also thank scientists and technical personnel at the Laurentian Forestry Centre of the Canadian Forest Service, Sainte Fye. These individuals include Dr. Pierre Bernier, Dr. Andre Beaodoin, Mr. Luc Guindon and Mr. Sebastian Degnault.

I would like to express my gratitude to all the folks in the remote sensing and carbon modeling lab since 2003. They include Dr. Mustapha El Maayar, Dr. Lisa Zhang, Ms. Anita Simic, Mr. Jan Pisek, Mr. Feng Deng, Prof. Baozhang Chen, Mr. Gang Mo, and Dr. Mingzhen Chen. I thank Mrs. Jane Liu (Department of Physics, U*of*T) who created the initial version of the model. I thank Mr. Andrei Bulynkov, computer programmer who created the first version of the model interface. This was a great platform for me to further develop the model and the interface. I would like to give my sincere appreciation to the Centre for Global Change Science (CGCS) which generously supported my visit to the Hill slope and Watershed Hydrology lab at the Department of Forest Engineering, Oregon State University (OSU). It was in OSU that I interacted with Prof. Jeff McDonnell, who has been a constant source of inspiration for this PhD research. At this juncture, I thank several OSU professors namely Prof. Barbara Bond, Prof. Kate Lajtha, Prof. Richard Waring, Prof. Michael Unsworth, Prof. Richard Cuenca, Prof. Mark Harmon and Dr. Bob McKane (EPA), for encouraging me and giving me many research ideas.

I greatly appreciate the generous financial assistance provided by University of Toronto while I pursued this research work. I value the support from many individuals at the Department of Geography, U*of*T. I would like to specially thank Ms. Marianne Ishibashi, Ms.Donna Jeynes, Ms. Marika Maslej, Ms. Susan Calanza, Mr. Bruce Huang and Mr. Mirchea Pilaf.

I worked with Mr. Oliver Sonnentag and Prof. Weimin Ju (Nanjing University, China) very closely for the past several years. Weimin nurtured my programming skills and Oliver tirelessly helped me during the field campaigns and laboratory analyses. We also had useful discussions on several modeling topics. I learnt a lot from these individuals and I cherish collaborating with them. I also take this opportunity to give my gratitude to my previous teachers, professors and colleagues who have indirectly contributed to the success of this research work. I thank my brother Arun, who always praised my research work and kept me going. Words are few to express my thanks to my parents who always created an air of academia in my life and encouraged me to pursue higher studies.

Finally, I thank my wife Jyothi for her patience and support during the course of this research work.

Ajit Govind

Table of Contents

Topic	Page No.
Thesis Abstract	ii
Acknowledgements	iii
Table of Contents	v
List of Figures	x
List of Tables	xvi
1. Introduction	1
1.1. Carbon emissions, global warming and climate change	1
1.2. Terrestrial carbon cycling	3
1.3. The boreal ecosystem	7
1.4. Monitoring carbon cycling in terrestrial ecosystems	8
1.5. Need for modeling of carbon cycling in terrestrial ecosystems	11
1.5.1 Modeling hydrological controls on terrestrial C and N dynamics	12
1.5.1.1. Controls on photosynthesis and respiration	14
1.6. Towards a better understanding of terrestrial C cycling processes: Ecohydrological and hydroecological approaches	17
1.7. Hypothesis and objectives	22
1.8. A road map to the thesis	23
2. Development of a Spatially Explicit Hydro-ecological Modeling Framework *BEPS-TerrainLab V2.0:* Model Description and Test in a Boreal Ecosystem.	
2.1. Abstract	42
2.2. Introduction	43
2.3. Model description	44
2.4. Site description	48

2.5. Spatial data set preparations 49
2.6. Flux and meteorological measurements 55
2.7. Initialization of water table and ecosystem carbon pools 56
2.8. Results and discussion 57
2.8.1. Spatio-temporal patterns of ET 57
2.8.2. Soil volumetric water content and water table depth 61
2.8.3. Sub-surface baseflow, surface overland flow and water balance 64
2.8.4. Spatio-temporal patterns of GPP 70
2.9. Summary and conclusions 72
2.10. Appendix 74
2.10. 1. Hydro-ecological processes considered in BEPS-TerrainLab V 2.0 74
2.10. 1.1. Canopy hydrological processes 74
2.10.1.1.1. Spatial upscaling of evapotranspiration 79
2.10.1.1.2. Leaf fractions in a canopy corresponding to varying water and light regimes 80
2.10.1.1.3. Forest floor evapotranspiration 81
2.10. 1.2. Unsaturated zone hydrological processes 81
2.10. 1.3. Saturated zone hydrological processes 83
2.10. 1.4. Stomatal conductance, moss conductance and soil conductance 85
2.10.1.5. Photosynthesis 92

3. Effects of Sub-surface Baseflow on Photosynthesis and Evapotranspiration
3.1. Abstract 101
3.2. Introduction 102
3.3. Model description 103
3.4. Site description 104
3.5. Datasets used 105
3.6. Water balance of a Beps-TerrainLab v2.0 modeling unit (pixel) 106
3.7. Numerical experiment 107

3.8. Results 111
3.8.1. ET and GPP sub-components under hydrological scenarios 111
3.8.2. Temporal dynamics of GPP and ET under hydrological scenarios 113
3.8.3. Spatial variability of GPP under hydrological scenarios 116
3.8.4. Spatial variability of ET under hydrological scenarios 119
3.8.5. Variation of soil water balance under hydrological scenarios 122
3.9. Discussion 124
3.9.1 Stomatal dynamics 125
3.9.2. Nitrogen mineralization 126
3.9.3. Dynamics of root fractions within a soil saturation regime 128
3.10. Model sensitivity to different parameters for GPP and ET 131
3.11. Summary and conclusions 135

4. Reconstruction of Carbon pools of a Boreal Ecosystem under the Influence of Climate Change, CO_2 Fertilization, N Deposition and Disturbance
4.1. Abstract 139
4.2. Introduction 140
4.3. Model and theory 143
4.4. Site description 149
4.5. Spatial data set preparation 151
4.5.1. Land-cover map 152
4.5.2. Reference year leaf area index map 152
4.5.3. Disturbance history and current stand age map 153
4.5.4. Reference year NPP and ET maps 154
4.5.5. Soil texture map 155
4.5.6. Data on N-deposition 155
4.5.7. Meteorological data 156
4.6. Measurement of ecosystem C-stocks 158
4.6.1. Measurement of biomass C-stocks 158

4.6.2. Measurement of soil C-stocks *159*
4.7. Indirect PAI measurements 160
4.8. Results and discussion 160
4.8.1. Dynamics of ecosystem C-processes *160*
4.8.2. Dynamics of ecosystem C-pools *164*
4.8.2.1. Temporal dynamics of ecosystem C-pools *164*
4.8.2.2. Spatial distribution of ecosystem C-pools *170*
4.8.3. Validation of current biomass C-pools *174*
4.8.4. Validation of current soil C-pool sizes *179*
4.9. Summary and conclusions 180
4.10. Appendix 1 182

5. Spatially Explicit Simulation of Hydrologically Controlled Carbon and Nitrogen Cycles and Associated Feedback Mechanisms in a Boreal Ecosystem.
5.1. Abstract 194
5.2. Introduction 195
5.3. Model description 197
5.3.1 Carbon cycling processes within BEPS-TerrainLab V2.0 ..... *199*
5.3.1.1. Autotrophic respiration *199*
5.3.1.2. Heterotrophic respiration *200*
5.3.2. Soil nitrogen cycle within BEPS-TerrainLab V2.0 ..... *204*
5.3.3. Feedback relationships within Beps-TerrainLab V2.0 ..... *206*
5.4. Site description 206
5.5. Flux measurements 208
5.6. Spatial and meteorological datasets and initialization of c-pools 209
5.7. Modeling experiments 210
5.8. Results and discussion 211
5.8.1. Snow depth and soil temperature *211*
5.8.2. Spatio-temporal patterns of NEP and respiration *212*

5.8.3. Differences in the simulated NEP under hydrological scenarios 217
5.8.4. Mechanisms of hydrological control on NEP 222
5.8.5. Dynamics of ecosystem C-pools under hydrological scenarios 224
5.8.6. Nutrient (N) availability and associated feedback mechanisms 227
5.9. Summary and conclusions 228
5.10. Appendix 1 230
5.10.1. Daily change in ecosystem carbon pool 231
5.11. Appendix 2 233
5.11.1. Soil nitrogen dynamics 233

6. Summary and Conclusions.
6.1. Lessons learned from this research 240
6.1.1. Understanding the hydroecology of humid boreal forests using Beps-Terrainlab V2.0 240
6.1.2. Effect of sub-surface baseflow on ecophysiological processes 241
6.1.3. Long-term dynamics of C-cycling processes 242
6.1.4. Effect of sub-surface baseflow on biogeochemical processes 243
6.2. Uncertainties in the simulated results 245
6.2.1. Parameters and coefficients used in the models 245
6.2.2. Quality of input datasets used in the models 245
6.2.3. Quality of long-term meteorological records used in InTEC 246
6.2.4. Quasi-empiricism in the process model, BEPS-TerrainLab V2.0 247
6.3. Current modeling gaps or topics for future research 247
6.3.1. Simulation of other forms of hydrologically controlled C-fluxes 247
6.3.2. Multilayer soil water replacing the two-layered approach 248
6.3.3. Root water uptake schemes 248
6.3.4. Temporal upscaling of the Penman-Monteith equation 249
6.3.5. C-allocation mechanism in InTEC and BEPS-TerrainLab V2.0 249
6.4. Contribution to science 249

List of Figures

Figure **Page No.**

Figure 1-1. (a) Canada wide distribution of eddy covariance tower sites administered by Fluxnet Canada Research Network (Canadian Carbon Program), and (b) Global distribution of eddy covariance based measurement of the fluxes of carbon, water and energy between the biosphere and the atmosphere. (GIS Data source: http://daac.ornl.gov/FLUXNET/) 10

Figure 2-1. A schematic representation of a BEPS-TerrainLab V2.0 modelling unit. Most hydro-ecological processes are represented in this modeling unit. The soil profile is divided into saturated and unsaturated zones by the position of the water table. The lateral water fluxes that link neighboring pixels include sub-surface baseflow and surface overland flow that are topographically driven 47

Figure 2-2. Various spatial datasets required to run BEPS-TerrainLabV2.0 at a daily time step. These datasets include (A) A validated land cover map (B) Digital elevation model (DEM) that was further processed to make it hydrologically consistent. Aspect and slope were derived from the DEM. (C) Leaf area index (LAI) map derived using remote sensing and ground based LAI measurements and (D) Soil textural class. All the data sets have a spatial resolution of 25 x 25 m. Projection is UTM Zone 18N; (E) The ~1km^2 foot print region of the tower; and (F) Wetness Index used for a topography-based initialization of WTD. 51

Figure 2-3. NDVI-LAI algorithm developed using ground based LAI measurements (taken along an east –west transect during the 2003 growing season) and remote sensing derived NDVI values. This algorithm was inverted and applied to the entire watershed to derive a watershed scale LAI map 52

Figure 2-4. Comparison of simulated and measured ET time-series (5-day moving average for visual clarity) for the years 2004 and 2005, at the EOBS tower footprint region. (b)One to one comparison of the simulated and measured ET for the years 2004 and 2005 (combined) 58

Figure 2-5. Spatial distributions of annual total ET simulated by BEPS-TerrainLab V2.0 for (a) 2004 and (b) 2005 for the watershed surrounding the EOBS flux tower. 59

Figure 2-6. Simulated vs. modeled VSWC at the EOBS flux tower footprint for the years (a) 2004 and (b) 2005 62

Figure 2-7. Comparison of simulated and measured WTD fluctuations at the EOBS flux tower site for the years (a) 2004 and (b) 2005 63

Figure 2-8. Simulated footprint average sub-surface baseflow fluctuations for the years 2004 and 2005 65

Figure 2-9. Spatial distribution of water table depths (WTD) during (a) spring (DOY=130) and (b) growing season (DOY=260) 67

Figure 2-10. Comparison of hydrographs of three representative locations showing the dominant flow-path 68

Figure 2-11. Simulated magnitudes of soil water balance components in the EOBS foot print region in 2004 and 2005, between days 1 to 365 69

Figure 2-12. (a) Comparison of simulated and measured GPP time-series (5-day moving average) for the years 2004 and 2005, at the EOBS tower footprint region. (b) One-to-one comparison of simulated and measured GPP for the years 2004 and 2005 71

Figure 2-13. Spatial distribution of GPP simulated for the years 2004 and 2005. 72

Figure 2-A1. Schematic representation of the vertical wind profile and aerodynamic resistances to the vertical scaler transfer within and above the canopy 78

Figure 2-A2. Calculation of hydraulic head gradient using water-table slope. This approach seems to work well in boreal landscapes where the topographic differences are subtle 84

Figure 2-A3. Variation of saturated hydraulic conductivity (Ks_{peat}) with soil-depth for a moss-peat system. This decay scheme is used to parameterize baseflow once the WTD reaches a land-cover specific "*peat layer criteria*". This procedure implicitly captures the preferential flow of water on boreal landscapes. Values displayed here (each points) represent the average for five treatments for each depth. A constant head permeameter approach was used to measure Ks_{peat} in the laboratory 86

Figure 2-A4. (a) The soil temperature scalar $f(T_s)$ used to constrain g_{max} for a wide range of soil temperature values. (b) Footprint average (all leaf types) simulated g_s in comparison to measurements taken using an ADC LC-Pro-photosynthesis system in the growing season of 2005 91

Figure 3-1. Variations among ET and GPP sub-component partitioning under various hydrological scenarios (a) Differences in ET sub-component partitioning; and (b) Differences in GPP sub-component partitioning 112

Figure 3-2. Annual variations of GPP and Total ET in the footpint area of the EOBS tower, under various hydrological scenarios 114

Figure 3-3. A pixel to pixel comparison of the annual GPP for the entire watershed under (a) The *Explicit* and the *NoFlow* scenarios and (b) the *Explicit* and the *Implicit* scenarios. (c)

The spatial variation of the GPP difference between the *Explicit* and the *NoFlow* scenarios (*Explicit- NoFlow*). Note that the maximum positive difference (underestimation by the *NoFlow* scenario) is seen on the hill-slopes where the baseflow is intense. (d) The spatial variation of the GPP difference between the *Implicit and* the *Explicit* scenarios (*Implicit-Explicit*). Note that the maximum positive difference is seen in most parts of the watershed where the surface is near flat 117

Figure 3-4. A pixel to pixel comparison of annual ET for the entire watershed under (a) *Explicit* and *NoFlow* scenarios and (b) *Explicit* and *Implicit* scenarios.(c) The spatial variation of the ET difference between the *Explicit* and *NoFlow* scenarios. Note that the maximum positive difference (underestimation by the *NoFlow* scenario) is seen on the depressions that are otherwise saturated with water. This is due to rapid reduction in soil and moss evaporation. (d) The spatial variation of the ET difference between *Implicit and Explicit* scenarios. Note that the maximum positive difference is seen in most flat parts of the watershed because of "more than normal" unrealistically created baseflow under the *Implicit* scenario that lowers soil water content to the field capacity 120

Figure 3-5. Nature of water balance under various hydrological scenarios in the footprint region of the EOBS tower in 2004 123

Figure 3-6. Seasonal dynamics of the average g_s in the footprint region, under different scenarios. Note the pronounced underestimation by the *NoFlow* scenario and overestimation by the *Implicit* scenario in comparison to the *Explicit* scenario 125

Figure 3-7. Relationship between stomatal conductance and GPP simulated using the temporally integrated Farquhar model (Chen et al., 1999), at various levels of plant N, for a given set of conditions. Both stomatal conductance and N availability are hydrologically controlled 127

Figure 3-8. A schematic representation of the separation of roots into unsaturated and saturated fractions as a function of root geometry factor, β, and water table, z. These fractions are used to constrain the physiological status of leafs in a proportionate manner, in order to calculate the stomatal conductance g_s 128

Figure 3-9. (a). Nature of the soil water scalar for a wide range of soil moisture conditions , for different soil texture types. This scalar is used to constrain the maximum stomatal conductance $g_{s,\max}$. (b). Nature of partitioning of the unsaturated (μ) and saturated (1-μ) root fractions as a function of water table position (z cm from the surface) and the root decay constant (β), a land cover specific parameter describing the root geometry 129

Figure 4-1. Strategy adopted for spatially explicit short-term modeling of biogeochemical cycles using BEPS-TerrainLab V2.0 with C-pools initialized through long-term modeling using InTEC 142

Figure 4-2. A schematic representation of the InTEC modeling framework (Chen et al., 2000) 144

Figure 4-3. A conceptual diagram showing the long-term C-balance modeling strategy adopted by InTEC. Note how the current estimates of NPP (NPP_{ref}) is used to retrospectively estimate NPP at the *equilibrium age* (NPP= Rh), which is further used for prospective modeling. The sketch shown here is applicable for an undisturbed stand. For disturbed stands, *equilibrium age* is assumed to be the year of disturbance 146

Figure 4-4. Location of the study site, Chibougamau watershed, which includes the Eastern Old Black Spruce (EOBS) tower site of FCRN where near-continuous high-frequency measurements of carbon, water and energy fluxes are being made using the eddy covariance technique. The scale shown in the figure applies to the watershed 150

Figure 4-5. Various spatial datasets required to drive InTEC at annual time steps. These datasets include (A) Validated reference year land cover map, obtained from the Canadian Forest Service (EOSD project); (B) Reference year leaf area index (LAI) map derived from remote sensing imagery using an algorithm derived from ground based LAI measurements;(C) Current forest stand age map derived using photogrammetry, satellite remote sensing and GIS; (D) Soil texture derived from soil deposit dataset (Quebec Ministry of Natural Resources), land cover type (CFS-LFC) and intensive point analysis; (E) Reference year evapotranspiration from Govind et al. (2008 a); and (F) Reference year NPP from the hydro-ecological simulation conducted by Govind et al. (2008a). All the data sets have a spatial resolution of 25 x 25 m. Projection is UTM Zone 18N. The scale of the ~40km^2 watershed is shown in Figure 4 151

Figure 4-6. Temporal patterns of the non disturbance factors used for reconstructing the C balance using the InTEC model. (a) Temporal pattern of CO2 concentration according to SRES-A2 emission scenario. (b) Rate of green house gas emission. (c) Mean annual spring temperature as the average of daily mean temperatures between DOY 85 to 125. (d) Mean annual temperature as the average of daily mean temperatures between DOY 1 to 365. (e) Mean annual growing season temperature as the average of daily mean temperatures between DOY 85 to 240.(f) Mean annual precipitation as the sum of daily sum of precipitation between DOY 1 to 365 157

Figure 4-7. Locations of the CFS inventory plots in the footprint region of the FCRN's EOBS tower site 158

Figure 4-8. Reconstructed ecosystem C fluxes and biomass simulated by InTEC model. (A) Historical dynamics of the EOBS tower footprint-averaged NPP . (B) Historical NPP dynamics of a disturbed (1963) site located at 74°19′ 54.5″ W and 49° 42′ 38.2″N. (C) Historical dynamics of the footprint-averaged NBP (E) Historical dynamics of the footprint-averaged C in the aboveground biomass (D) Historical dynamics of the NBP of a disturbed (1963) site. (F) Historical dynamics of the aboveground biomass C of a disturbed (1963) site 162

Figure 4-9. Temporal variation of the footprint averaged (A) Woody biomass pool, C_w (B) Coarse-root biomass pool, C_{cr} (C) Fine-root biomass pool, C_{fr} (D) Foliage biomass pool, C_l (E) Coarse and dead wood detritus pool, C_{cd} (F) Surface structural pool, C_{ssd} (G) Surface metabolic pool, C_{smd} (H) Fine-root structural litter pool , C_{fsd} (I) Fine-root metabolic pool, C_{fmd} (J) Surface microbial pool, C_{sm} (K) Soil microbial pool, C_m and (L) Slow C pool, C_s 166

Figure 4-10. (A) Aboveground biomass as the sum of woody biomass pool (C_w) and foliage biomass pool(C_l); (B) Belowground biomass as the sum of coarse-root biomass pool (C_{cr}) and fine root biomass pool (C_{fr}); (C) soil surface C-pools as the sum of coarse and dead wood detritus pool (C_{cd}), surface structural pool (C_{ssd}), surface metabolic pool(C_{smd}), and surface microbial pool (C_{sm}); and (D) Soil C-pools as the sum of fine-root structural litter pool (C_{fsd}), fine-root metabolic pool (C_{fmd}), soil microbial pool (C_m), slow C pool (C_s), and passive C pool (C_p).The scale of the ~40km² watershed is shown in Figure 4 173

Figure 4-11. Correlation between the simulated aboveground biomass C and the average plant area index measured by digital hemispherical photography and plant canopy analyzer (LAI 2000) in 2003 along a westbound transact from the EOBS tower and at the 12 NFI plots 177

Figure 4-12. Digital hemispherical photographs taken at the 12 NFI plots for calculating plant area index in conjunction with plant canopy analyzer (LAI-2000). Note the relatively high biomass in 16T and 17T as opposed to relatively open canopy in 11T 178

Figure 5-1. Schematic representation of a BEPS-TerrainLab V2.0 modeling unit adopted from Govind et al. (2008a). Biogeochemical processes and their feedback relationships as influenced by hydrology is the focus of this paper 198

Figure 5-2. Nature of (a) Soil temperature scalar for heterotrophic respiration. (b) Soil moisture scalar for heterotrophic respiration 203

Figure 5-3. Location of the study site, Chibougamau watershed, which includes the Eastern Old Black Spruce (EOBS) tower site of FCRN where continuous high precision measurements of fluxes of mass and energy are being made using eddy covariance technique 207

Figure 5-4. Temporal dynamics of the snow depth and near-surface (20 cm) soil temperature measured and modeled 211

Figure 5-5. Spatial distribution of the annual NEP simulated for the years, 2004 and 2005 in the Chibougamau watershed 213

Figure 5-6. Comparison of measured and simulated (A) GPP (B) NEP (B) and (C) Ecosystem respiration (all 5 day moving averages shown for visual clarity) at the footprint region of the EOBS tower site, for two years 2004 and 2005 215

Figure 5-7. Plots between the NEP simulated under different baseflow scenarios. Left panel is the plot between the *Implicit* and the *Explicit* scenarios and right panel is between the *NoFlow* and the *Explicit* scenarios. In both, the line on slope=1 is the *Explicit* scenario, and departure from this line is considered as the bias 218

Figure 5-8. The spatial distribution of NEP bias under various hydrological scenarios. (A) by the *Implicit* scenario and (D) by the *NoFlow* scenario. Panels B and D show the spatial distribution of NEP difference-types for the *Implicit* and the *No Flow* scenarios, respectively 220

Figure 5-9. Relative occurrence of various NEP bias types under hydrological scenarios. Note that in both the *Non Explicit* scenarios, Type 5 is the dominant type 222

Figure 5-10. Temporal dynamics of various ecosystem C-pools under hydrological scenarios. The C-pools shown here are Woody biomass pool (C_w), Foliage biomass pool (C_l), Coarse root biomass pool (C_{cr}), Fine root biomass pool (C_{fr}), Coarse detritus pool (C_{cd}), Surface structural pool (C_{ssd}), Surface metabolic pool (C_{smd}), Surface microbial pool (C_{sm}), Soil structural litter pool (C_{fsd}),Soil metabolic pool (C_{fmd}), Soil microbial pool (C_m), Slow C pool(C_s), and Passive C pool(C_p) 225

Figure 5-11. Temporal dynamics the total soil C-pools (sum of all the pools) under various hydrological scenarios 226

Figure 5-12. Temporal dynamics of leaf-N content under various hydrological scenarios. Note the pronounced N limitation under the *NoFlow* scenario which is primarily due to reduced soil C decomposition and N mineralization. 227

List of Tables

Table **Page No.**

Table 2-1. Hydraulic properties of various soil types in the watershed 53

Table 2-2. Landcover Specific Biophysical Parameters used in BEPS-TerrainLab V2.0 54

Table 3-1. Characteristic features of the three hydrological scenarios considered in this numerical experiment 110

Table 3-2. Statistical measures of model performance under the three hydrological scenarios. 115

Table 3-3. Sensitivity of various parameters considered in BEPS-TerrainLab V2.0 for ET and GPP simulation 134

Table 4-1. Description of various conceptual carbon pools considered in the InTEC model 148

Table 4-2. Species specific allometric equations used to convert DBH to tree biomass 159

Table 4-3. Comparison of InTEC simulated above ground biomass (2003) with inventory plot measurements 175

Table 4-4. Comparison of modeled and measured soil C-pools in the foot print region of EOBS tower site 180

Table 4-A1. Ecosystem C-pools and their decomposition products and rates of decomposition 186

Table 5-1. Various land-cover specific parameters used for biogeochemical modeling with BEPS-TerrainLab V2.0 202

Table 5-2. Differences in the magnitudes of various C-fluxes within various NEP-difference as a result of *Non-Explicit* hydrological representation 223

CHAPTER 1

Introduction

1.1. Carbon Emissions, Global Warming and Climate Change

The greenhouse effect of the Earth's atmosphere due to the radiative forcing of polyatomic gases contained in it was first explained by the French scientist, Fourier as early as 18th century. However, it was only in the seminal work of Arrhenius (1896) that the first quantification of the influence of increasing atmospheric carbon dioxide (CO_2) on increasing the Earth's surface temperature was made. Since the industrial revolution, the mean global CO_2 concentration has risen from about 280 ppm to over 379 ppm (Keeling et al., 1995 ; IPCC, 2007). This rapid rise in atmospheric carbon dioxide concentrations occurred due to the imbalances between the rates at which anthropogenic and natural sources emit CO_2 and the rate at which the global C sinks remove CO_2 from the atmosphere (Baldocchi et al., 2001).

The first order effect of increased atmospheric CO_2 is the increase in surface temperature of the Earth which subsequently leads to climate change (Hansen et al., 1997; Frolking et al., 2004). However, climate change will further enhance CO_2 emissions due the presence of several feedback mechanisms operating among various biogeochemical cycles, thus leading to further intensification of climate change (Joos et al., 2001b). Potential consequences of elevated CO_2 concentrations include increasing air and ocean temperatures, melting of polar ice-caps and rising of sea levels (Jackson et al., 2001), plant composition and ecosystem scale physiological changes (Norby et al., 1997). Some other effects include decreasing portions of the surface of the Earth that are covered with snow, and decreasing spatial extent of permafrost (IPCC, 2007).

The first major international initiative to address climate change was the *First World Climate Conference* in 1979. This led to the establishment of the Intergovernmental Panel on Climate Change (IPCC) in 1988. Since then, the effects of climate change has been increasingly recognized by many countries that lead to various international agreements to reduce greenhouse gas emissions such as the United Nations Framework Convention for Climate Change(UNFCC) in 1992, and the Kyoto Protocol in December 1997. As of June, 2006, 189 nations, including the United States, adopted the UNFCCC, which has as its objective of "stabilization of greenhouse gas concentrations in the atmosphere at a level that would prevent dangerous anthropogenic interference with the climate system" (Houghton, 2007). The conclusion drawn by IPCC scientists is that the concentration of greenhouse gases in the atmosphere has been rising mainly due to human activities and that this would lead to rising temperatures and a human-induced climate change (Grubb, 1999). The global average surface temperature has increased over the 20th century by about 0.6°C, and most of the warming that was observed over the last 50 years was caused by anthropogenic activities (IPCC., 2001). It is quite probable that global average temperature can further increase by about 0.4°C over the next two decades and by 1.8 to 4.0°C by the end of this century (IPCC, 2007).

This thesis is a small segment of Canada's attempt to better understand the global C cycle and the associated climate change through the Canadian Carbon Program. This work is directed towards improving our understanding of the meso-scale terrestrial C cycling processes that govern the exchange of C between the terrestrial biosphere and the atmosphere through modeling techniques. Terrestrial C cycle is sensitive to climate change because of its direct and indirect connections to anthropogenic activities (due to factors such as deforestation, desertification, N-deposition,) and also difficult to estimate because of its heterogeneous nature.

1.2. Terrestrial Carbon Cycling

Terrestrial ecosystems modify atmospheric C balance through many mechanisms. In pristine terrestrial ecosystems C cycling is mainly controlled by photosynthesis and respiration. Other mechanisms that govern the C balance in these ecosystems include methane fluxes, lateral transport of dissolved organic carbon, and spontaneous release of terrestrial C in the event of forest fires. On the other hand, in other regions of the Earth, processes that determine terrestrial C balance are dominated by human-induced processes such as fossil fuel burning, industrial emissions such as calcination of limestone, fermentation processes, deforestation, etc. Since pristine ecosystems have a dominance of vegetation and are spatially extensive, they are considered to be important in global C-cycling because of their potential to sequester atmospheric C.

In recent years, scientists have learnt that terrestrial ecosystems' vegetation , soil (Melillo et al., 1989; Knapp et al., 1993) and animals (Naeem et al., 1995; Hattenschwiler and Bretscher, 2001) play key roles in mediating terrestrial C cycle. Vegetation being the primary producers, it is from the plants that mass and energy gets transformed to other living beings (Engel and Odum, 1999), within an ecosystem. The process of photosynthesis fixes atmospheric C into the biosphere. Atmospheric C enters the plant through stomatal opening that are controlled by a variety of environmental factors (Jarvis, 1976; Griffis et al., 2003). These factors include ambient temperature, atmospheric CO_2 concentration, nutrient availability, soil water availability and forest age (Schimel, 1995; Prentice et al., 2001). Changes in the atmospheric C concentration and the corresponding changes in the climate have altered the magnitudes of terrestrial C cycling. For example, a climate change induced vegetation growth due to earlier spring and lengthened growing season was detected by the phase shift of seasonal atmospheric CO_2 cycle by Keeling et al.(1996) and satellite-based vegetation index analysis by Myneni et al.

(1997). Studies indicate that increase in atmospheric CO_2 enhances photosynthesis (e.g. Woodward and Friend, 1988) and hence increase assimilation of atmospheric C by the terrestrial vegetation.

Nitrogen (N) availability to plants is another factor that can affect photosynthesis. This is because N is a primary nutrient for plant growth. In the recent years, variations in plant N-availability have also altered the trends in the terrestrial C cycles. Variations in plant N availability occur mainly due to natural and anthropogenic N-deposition. Based on modeling studies, Townsend et al. (1996); Asner et al. (1997) and Holland et al. (1997) have demonstrated that N deposition is responsible for about 0.1-2.3 GtC yr^{-1} fixed by terrestrial vegetation which is almost half of the magnitude of C flux due to fossil fuel emission. Another factor that determines the nature of terrestrial C balance of an ecosystem is the age-effects of the vegetation. Schimel et al. (1995) have demonstrated that forest re-growth can account for part of terrestrial C uptake as much as 0.5±0.5 GtC yr^{-1}, especially in northern mid and high latitude. This is because younger vegetation actively grows and hence sequesters more atmospheric C as opposed to mature forest stands.

There are many other processes that directly and indirectly affect photosynthesis and thus, the C cycle. They include land use and land cover change (Caspersen et al., 2000; Houghton and Hackler, 2006; Easter et al., 2007), reforestation (House et al., 2002; Paul et al., 2002), agricultural and grazing activities (Cerri et al., 2005), insect attack (Chapman et al., 2003; Throop et al., 2004) and invasive species (Szlavecz et al., 2006).

Respiration is a process by which C is added to the atmosphere from the biosphere. There are studies that indicate that total ecosystem respiration is a major determinant of terrestrial C balances (Valentini et al., 2000). Total ecosystem respiration includes respiration by aboveground plant parts (boles, branches, twigs, and leaves) and soil respiration, which is the

sum of the heterotrophic respiration, and root respiration including respiration of symbiotic microorganisms. The temporal variability of respiratory metabolism is influenced mostly by temperature and humidity conditions (Davidson and Janssens, 2006). Although ecosystem respiration has received considerable attention in recent decades, much less is known about the relative contributions of its sub- components (Jassal et al., 2007), and our understanding of how they will respond to global warming is poor. Soil respiration (root + heterotrophic respiration) is a dominant component of C exchange in terrestrial ecosystems which accounts for more than half of the total ecosystem respiration (Black et al. 2005). This is because soils of terrestrial ecosystems contain more C than atmosphere and live biomass together (Eswaran et al., 1993). Components of respiration can have different responses to temperature and soil water content (Boone et al., 1998; Lavigne et al., 2004), thus the effects of these environmental controls needs to be understood in order to fully comprehend the soil C cycling mechanism.

There are many other mechanisms that can release terrestrial C to atmosphere. This includes both natural and anthropogenic reasons. Emission of large amounts of C to the atmosphere from vegetation can occur during forest fires (Amiro et al., 2002; Soja et al., 2004; Amiro et al., 2004) or biomass burning (Fernandez et al., 1999; Tanaka et al., 2001) . These C emissions are of very high magnitudes although their duration is very short. Forest fires and biomass burning also affect the nutrient status of the soil which could have positive effects on the succeeding vegetation (Prietofernandez et al., 1993; Deluca and Sala, 2006). Another form of C-flux in almost all terrestrial ecosystems is the import and export of dissolved organic carbon (DOC) (Neff and Asner 2001; Hornberger et al. 1994). DOC fluxes include C in the form of simple amino acids to large molecules that are transported through water flows. Fluxes of DOC into the ocean via runoff from terrestrial ecosystems are estimated to be 0.2 (Harrison et al., 2005) to 0.4 x 1015 g (IPCC,2001). Since these fluxes are very small compared to the C fluxes due

to photosynthesis and respiration in terrestrial ecosystems DOC fluxes are not generally considered for the global C cycle (Schimmel 1995). Moreover, since DOC fluxes are small compared to the total C stocks in the ecosystem and more over, DOC fluxes do not affect the fluxing of C between the biosphere and the atmosphere, it is often not considered in the annual net ecosystem productivity (NEP) calculations. However, on a long-term basis, DOC can be considered as an essential component of the net biome productivity, NBP (Janssens et al. 2003). Methane emission is yet another form of C-flux between the biosphere the atmosphere (Blodau et al., 2007; Zhuang et al., 2007; Curry, 2007; Einola et al., 2007). This mode of C-flux occurs mostly in anoxic conditions such as water-logged areas and peat lands.

In spite of the various mechanisms of exchange of C between biosphere and the atmosphere, many studies demonstrate that the terrestrial ecosystem is a net C sink due to the presence of soil C-pools having much longer residence times (Thompson et al., 1996; Chen et al., 2003; Canadell et al., 2007; Schulze, 2006). The strength of the terrestrial C sink was estimated to be 0.5-2.0 GtC yr^{-1} (Schimel et al., 1995). By sequestering atmospheric C, the terrestrial ecosystems help decrease the rate of accumulation of anthropogenic CO_2 in the atmosphere, and its associated climate change (Cihlar, 2007). Terrestrial C sinks may be responsible for taking up about one-third of all the carbon dioxide that is released into the atmosphere (Canadell et al., 2007). The terrestrial C sink, inferred based on our current understanding, may not be permanent (Luo et al., 2003; Cox et al., 2000 ; Friedlingstein et al., 2003). Over the last few years there have been several studies suggesting that the size of this terrestrial C sink is vulnerable to global warming (Martin et al., 1998; Nemani et al., 2002; Canadell et al., 2007).

1.3. The Boreal Ecosystem

The boreal forests represent one of the world's largest terrestrial biomes (Bonan and Shugart, 1989). Boreal forests are spread in North American (Bonan and Vancleve, 1992), Scandinavian (Rinne et al., 2007) and Eurasian landmasses (Kolchugina and Vinson, 1993). Globally, these forests have an aerial extent of 15 million km^2 (Schlesinger and Andrews, 2000; Schlesinger, 2000). Of this aerial extent, nearly 3 million km^2 are present in Canada alone (Coursolle et al., 2006). Globally it is the second largest forest biome that contains 49% of all forest C (Dixon et al., 1994), and has the potential to play a major role in the global C balance (D'Arrigo et al., 1987; Hall et al., 2004). Studies have shown that boreal ecosystems are net terrestrial C sinks because accumulation of C by photosynthesis is greater than the losses of C due to respiration (autotrophic and heterotrophic) because of lower temperatures. Boreal forests are also significant because majority of the terrestrial fresh water resources (including ice and snow) and soil C stocks are distributed in high latitudes where boreal forests exist. Since these high latitude regions are subjected to increased warming due to climate change, processes such as melting of ice, snow and permafrost could exacerbate hydrological processes in such a way that their consequences on biogeochemical processes and the C-exchange between the biosphere and the atmosphere remains quite speculative (Van Hees et al., 2005; Zhuang et al., 2003; White et al., 2000; Kravchenko, 2002). The C cycling in the boreal forest is driven by both natural and human disturbances (Kurz and Apps, 1995), the most important being fire, insects, diseases, wind throw, and harvesting. Although on a long-term basis, C cycling in boreal forests is driven by climate and natural and anthropogenic disturbances, on a short-term basis, inter-annual variability are primarily determined by a large number of environmental controls (Fenton et al., 2005; Lal, 2005; Panikova et al., 2006; Kane et al., 2006; Prokushkin et al., 2006). Thus, it is of utmost importance to understand and predict the short-term and long-term

dynamics of its ecosystem functioning, in order to improve our understanding of how these ecosystems would respond under climate change. Moreover, the northern extent of the boreal biome is the tree-line which has been showing rapid migration towards the north in the recent years, under climate change (Epstein et al., 2004; Beringer et al., 2005). The northern parts of boreal ecosystem also have permafrost that shows significant fluctuations in the recent past, which is closely linked to global warming (Nelson, 2003; Zimov et al., 2006).

1.4. Monitoring Carbon Cycling in Terrestrial Ecosystems

Currently, several techniques exist for measuring the exchange of CO_2 and trace gases from an ecosystem to the atmosphere at various spatial scales. The technique that is most commonly used is the eddy covariance technique (EC), which directly measures the fluxes of CO_2, water-vapor and energy from a land surface. It is based on the principle that the vertical flux of an entity in the turbulent surface layer is proportional to the covariance of the vertical velocity and its concentration (Baldocchi et al., 1988). Over the last few years, EC measurements have provided vital information about terrestrial C balances on a variety of ecosystems such as boreal forests (Amiro et al., 2006 Coursolle et al., 2005), boreal and arctic peat-lands (Moore et al., 2002; Lafleur et al., 2005; Syed et al., 2006), tropical rainforest (Turnipseed et al., 2003; Kumagai et al., 2004; Iwata et al., 2005), tropical savannah (Beringer et al., 2007; Baldocchi et al., 2000; Hutley et al., 2001), tropical seasonal forest (Dou et al., 2006; Zhang et al., 2006), tundra (Corradi et al., 2005; Oechel et al., 2000;), tropical wetlands, mangrove and tropical swamps (Jones and Humphries, 2002); and temperate grasslands (Novick et al., 2004; Gilmanov et al., 2007).

Since the early 1990's, there has been a large increase in the use of EC technique to monitor CO_2 exchange at the ecosystem level (Baldocchi, 2003). Ecosystems that have been

subjected to natural and human induced disturbances such as fire (e.g. Amiro et al., 2003), and managed and regenerated stands (Kowalski et al., 2004) are also being studied using the EC technique. When a EC system is mounted on a tall structure such as a scaffold tower, it is possible to estimate a spatially-averaged flux for a "footprint" that extends 200-800 m in radius depending the height of the tower. The EC measurements are done without disturbing the vegetation. The measurements made are continuous, long-term flux records. The EC technique measures the ecosystem response to short-term (hourly) and long-term (seasonal and annual) variations. These important datasets provide a great deal of information on the processes controlling CO_2 and water vapor exchange, as well as ecosystem sensitivity to climate variability.

EC measurements also provide a direct means of testing ecological models (Grant et al., 2007; Ju et al., 2006c; Arain et al., 2006;). During the Boreal Ecosystem-Atmosphere Study (BOREAS) between 1994 and 1996, EC measurements of CO_2 and water vapor fluxes were made on towers in nine different boreal ecosystems (Sellers et al., 1997), which provided invaluable data concerning the mechanism of C energy and water exchanges on boreal ecosystems. Consequently, scientists advocate that long-term EC flux measurements above terrestrial ecosystems can be undertaken on different ecosystems to better understand regional and global C and water budgets (Baldocchi and Vogel, 1996). As a result, several EC flux networks *Euro flux* in Europe, Scandinavia and Russia, *Ameriflux* in United States, *Fluxnet-Canada* in Canada, *China flux* in China, *Koflux* in Korea, and *Ozflux* in Australia, were initiated (Figure 1b). With the launch of the Fluxnet-Canada Research Network (FCRN) in 2003 as a continuation of the BOREAS project, several EC towers (see Figure 1-1a) were established across several ecosystems on the Canadian landmass (Margolis et al., 2006).

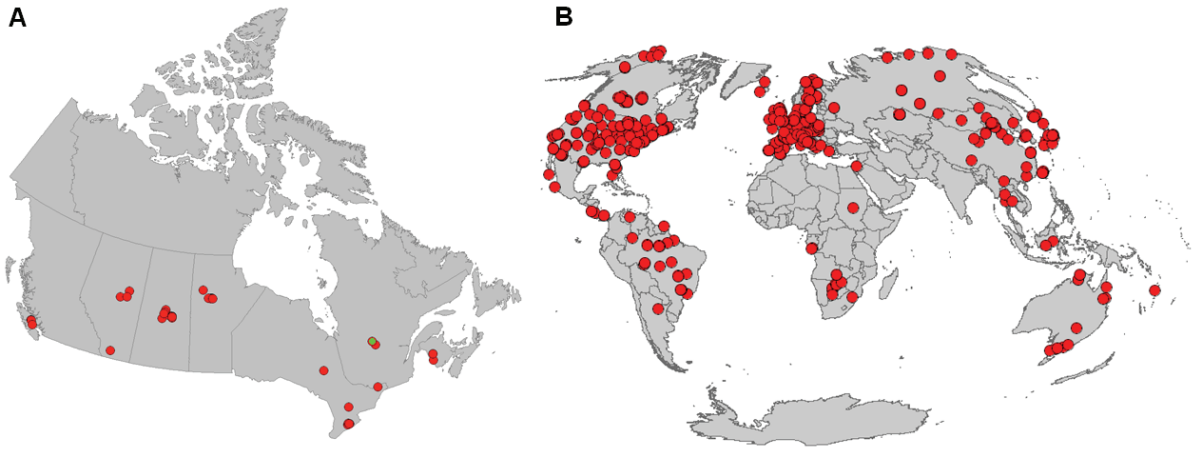

Figure 1-1. (a) Canada wide distribution of eddy covariance tower sites administered by Fluxnet Canada Research Network (Canadian Carbon Program), and (b) Global distribution of eddy covariance based measurement of the fluxes of carbon, water and energy between the biosphere and the atmosphere. (GIS Data source: http://daac.ornl.gov/FLUXNET/)

The establishment of EC towers facilitates high-frequency, multi-year measurement of C, water and energy exchanges between the biosphere and the atmosphere across several ecosystems in Canada. In March 2007, Fluxnet-Canada was transformed into the Canadian Carbon Program with three year tenure (2007-2010) with similar objectives as FCRN with increased emphasized on national and continental scale integrated modeling. Within FCRN, scientists focus either on measurement and empirical studies on one hand, or simulation modeling and development of upscaling strategies using remote sensing and numerical methods, on the other. This thesis originates as a part of the *integrated modeling* component of and the *historical carbon modeling* sub groups within FCRN.

The network of EC flux towers around the world greatly assists in the better understanding of biosphere-atmosphere exchanges of carbon, water and energy. However, it does not provide reliable evidence of the magnitude and location of C sinks because an EC tower does not operate over a large and sufficiently unbiased sample area to represent a land

cover (Steinfeld et al., 2007). Furthermore, the method is limited to generally flat terrain with uniform vegetation (Su et al., 2004). In order to generalize ecosystem scale C-exchanges between the biosphere and atmosphere, inclusion of techniques that operate at higher spatial scales are warranted in addition to EC technique. These include the measurement of build-up of CO_2 concentrations above an ecosystem during temperature inversions (Yi et al., 2004). At a larger scale (upward of 50 km^2), concentration measurements are made from tall tower (Denning et al., 2003; Bakwin et al., 2004; Wang et al., 2006) or balloons that reach the top of the boundary layer of the Earth. An example of a technique that infers flux at this intermediate scale is the Convective Boundary Layer (CBL) budgeting approach (Vinuesa and De Arellano, 2003; Kim et al., 2006; Linne et al., 2007). Aircraft based flux estimations can measure at still larger scales (Prueger et al., 2005; Buzorius et al., 2006; Shashkov et al., 2007; Miglietta et al., 2007). These measurements are very useful for validating large scale modeling efforts.

1.5. Need for Modeling of C cycling Terrestrial Ecosystems

Thermodynamically, a terrestrial ecosystem is an open system. Therefore, biogeochemical cycles strongly interact with one another along with positive or negative feedback relationships (e.g., Joos et al., 2001b; Sitch et al., 2005; Manzoni and Porporato, 2007). Due to the complex nature of the system, simplified empirically-based studies cannot provide a complete description of the non-linearity that exists in various aspects of terrestrial ecosystem responses. Interactions between components at different spatio-temporal scales are quite variable and therefore, create uncertainties in our understanding of their behavior as climate changes (Bottcher, 2004; Rannik et al., 2006). The only way to improve our understanding of the non-linearities and associated feedback mechanisms that exist in biogeochemical processes is to

use a systems approach that adequately considers the scales at which these processes operate (Shibu et al., 2006).

Recently, various studies using Earth system models that integrate climate models (GCM) and the C-cycle (Land Surface Schemes) show that the feedback mechanisms between various processes could accelerate climate change (Cox et al., 2000 ; Friedlingstein et al., 2003; Gedney et al., 2006). Although such projections have much uncertainty, through model inter-comparison studies (e.g., the PILPS project, Pitman et al., 1999; Mcguffie and Henderson-Sellers, 2001; or Friedlingstein et al., 2006), much of the uncertainty associated with models may be clarified and this may further aid in policy making. Moreover, with a large wealth of data on fluxes of mass and energy between the biosphere and the atmosphere, meteorological data, remote sensing technology and rapidly increasing computational capabilities, simulation models can be used both to better understand how ecosystems function and to reduce uncertainty. The picture that is evolving from long-term measurement records is that different combinations of environmental factors affect the inter-annual variability of exchange of C between the biosphere and the atmosphere and generalizations are hard to make in ecosystem processes. Therefore, we need modeling tools to explain variability in a cogent manner.

1.5.1. Modeling Hydrological Controls on Terrestrial C and N Dynamics

Hydrological and biogeochemical processes are closely linked because of the unique physicochemical properties of water as a chemical compound. The association between hydrological and biogeochemical cycles is multifaceted and is often difficult to comprehend when based only on empirical studies. It is therefore necessary to employ simulation models that take a systems approach to better understand the intricacies involved (Waelbroeck, 1993; Andersson and Sobek, 2006). There are several ecological processes that are highly sensitive to

hydrological controls, both directly and indirectly. These include photosynthesis, heterotrophic respiration and soil organic carbon decomposition, redox condition mediated methane production, transport of dissolved organic C (DOC), snow mediated insulation on soil respiration, controls on evapotranspiration (ET), and nutrient mineralization. These processes occur at various spatial and temporal scales.

Hydrological controls on biogeochemical cycles and their implications for global climate change have recently gained recognition, especially among regional and global scale modelers (e.g., Gedney et al., 2006, Ju et al., 2007b, Betts et al., 2007; Sellers et al., 1997). This body of work demonstrates that climate change may be explained by alteration in hydrological controls that govern the exchange of C between the atmosphere and the biosphere, with vegetative controls as intermediate processes. Some studies also highlight that for high latitude ecosystems, it is possible that the melting of permafrost could intensify biogeochemical processes such as the decomposition of soil C (Deming, 1995; Overpeck et al., 1997; Nelson, 2003; Zimov et al., 2006). This warrants serious attention to hydrological controls that affect biogeochemical processes, which could appreciably alter plant growth, nutrient and C dynamics, as well as physical growth conditions.

There are many studies that suggest that snow has the capacity to insulate the soil surface in high latitude ecosystems, and this may significantly affect the C-cycling of these ecosystems by controlling winter soil respiration (Davidson and Janssens, 2006; Monson et al., 2006; Kielland et al., 2006). In arid and semi-arid ecosystems, hydrological controls may be evident through conditions of water insufficiency. Dry conditions may directly or indirectly control biogeochemical cycles. Therefore, adequate representations of hydrological controls must be incorporated in models that predict biogeochemical processes.

1.5.1.1. Controls on Photosynthesis and Respiration.

Hydrological controls on photosynthesis are manifested through deficits or excesses of soil water (Wong et al., 1985; Kozlowski, 2000; Zgallai et al., 2006; Galmes et al., 2007). Although there are many hypotheses regarding the physiological mechanism of the control of soil water on primary production, the most accepted school of thought is that of Schulze et al. (1994) who hypothesized that abscisic acid (ABA), a phyto-hormone produced by stressed root tips when transported through xylem, triggers leaves to close stomata and reduce transpiration losses. During this process, the entry of CO_2 declines and photosynthesis decreases. Tardieu et al. (1992) found that stomatal conductance (g_s) depends both on ABA and leaf water content and hence, both factors are required to properly model this physiological control of stomatal conductance. Some models (e.g., Nikolov et al., 1995) attempted to simultaneously represent ABA and hydraulic signals from the roots to the stomata as proposed by Tardieu and Davies (1992) but a quantitative description of the ABA is not yet developed for any of the models. To link soil water and stomatal conductance, various conceptualizations have been adopted by the modeling community.

There are two distinct approaches for modeling stomatal conductance. They are the Ball–Berry (Ball et al., 1987; Leuning et al., 1998) and the Jarvis (Jarvis, 1976) approaches. The Ball–Berry types of models take the form:

$$gs = m\left[\frac{A_n.h_s}{c_s}\right] + b \qquad (1)$$

where m and b are empirical constants, A_n is net photosynthetic rate, h_s is relative humidity at the leaf surface, and c_s is the CO_2 mole fraction at the leaf surface. Ball–Berry models adequately estimate C assimilation by simultaneously accounting for C assimilation and

conductance response using a biochemical model of photosynthesis such as the Farquhar model (Farquhar et al., 1980). These types of stomatal conductance models require iterative calculations to update current stomatal conductance by equilibrating photosynthesis at a previous time step against the ambient stomatal conductance for CO_2. Ecological models that employ this formulation are SiB2 (Sellers et al., 1996b); CTEM(Arora, 2003); CN-CLASS(Arain et al., 2006); *Ecosys* (Zhang et al., 2005; Grant and Flanagan, 2007), to name a few.

An alternative way to model stomatal conductance is to use the Jarvis (Jarvis, 1976) multiplicative algorithm. Jarvis-type models have the general form:

$$g_s = g_{s,\max} \cdot \prod f_i \qquad (2)$$

where $g_{s,\max}$ is a species specific maximum stomatal conductance that may occur under optimal environmental and plant physiological conditions. A series of environmental factors in the form of scalars (f_i) constrain the potential stomatal conductance. The $g_{s,\max}$ parameter can vary widely among and within species (Kelliher et al., 1995; Dang et al., 1997; Dang et al., 1998) and g_s increases with $g_{s,\max}$ (Arain et al., 2002; Landsberg and Waring, 1997). Most of the ecological models currently use a process-based instantaneous biogeochemical leaf-level photosynthesis model postulated by Farquhar et al. (1980) with various modifications for upscaling the photosynthetic processes in space (leaf to canopy) and time (instantaneous to daily). Some of the spatial upscaling strategies are *big-leaf* (e.g., Friend and Cox, 1995, Sellers et al., 1996a), *sunlit-shaded* or *two leaves* (e.g., Wang and Leuning, 1998), *multi-layered* (e.g., Grant et al., 2001), and *multi-layered with sunlit-shaded* among others. An example for temporal upscaling is the analytical solution developed by Chen et al. (1999). All these approaches rely heavily on accurate estimates of g_s.

In addition to the hydrologically controlled g_s, another biophysical parameter, the maximum carboxylation rate of the Rubisco enzyme ($Vc\max$) is used in photosynthesis modeling. $Vc\max$ has a strong association with leaf N content (Mooney, 1986; Dang et al., 1997; Field and Reich et al., 1997). Leaf N is directly related to the available soil N. Several environmental factors such as temperature, precipitation and soil moisture, directly or indirectly affect the availability of soil N. Some studies have reported that in northern ecosystems, particularly in forests, N availability limits plant growth (e.g., Schlesinger and Lichter, 2001). In these ecosystems, decomposition of soil C-pools and the consequent N mineralization, atmospheric deposition and biological N fixation are the sources of available soil N. Under conditions of global warming, as the decomposition of soil C-pools intensify due to increased soil temperature and moisture inducing increased heterotrophic respiration, N mineralization can increase (Schroter et al., 2003; Arain et al., 2006; Traore et al., 2007; Tan and Chang, 2007). Since water, N and soil C-cycles are strongly linked, it is often difficult to separate the extent to which net primary production or net ecosystem productivity is controlled by the combined action of water or nutrient availability. N is mineralized in the soil when soil organic matter decomposes under optimal hydrothermal conditions (Schroter et al., 2003). Recently Ju et al. (2006) demonstrated that mineralized N in soil may also be a factor that is responsible for the decomposition of some of the soil organic matter pools, which in turn mineralize N. In an ideal modeling domain, one needs to tightly couple N availability through organic matter decomposition as a function of soil temperature and soil water fluctuations on plant growth and C assimilation (Arain et al., 2006).

Ecosystem respiration is an important form of C flux. There are many environmental controls that affect respiration, especially soil respiration. They include soil temperature and moisture, substrate availability and quality, soil C decomposition and microbial growth

dynamics, soil hydraulic properties, as well as root maintenance and growth requirements on rates of respired CO_2 from soils (Borken et al., 2002; Davidson et al., 2002). Soil respiration is highly controlled by soil water status. Studies demonstrate that at low soil water content, respiration is reduced (Irvine et al., 2002; Joffre et al., 2003; Harper et al., 2005). This has been mainly attributed to a reduction in decomposition of the soil organic matter due to microbial activity.

From this discussion it is clear that a proper representation of soil water dynamics, stomatal dynamics, photosynthesis, soil C dynamics, and soil N dynamics is required in a coupled manner to properly model the exchange of C between the soil-plant–atmospheric continuums. A set of other related processes should also be accurately represented e.g., radiation regimes, soil temperature, and the dynamics of snow depth. In the current ecosystem models, all of these processes are not explicitly described. Imbalances exist in the current models in terms of the processes they describe. For example, when one process is described in a sophisticated manner, another process is highly abstracted. This is mainly because of technical variations associated with models with regard to their ability to handle both various spatial and temporal scales and resolutions, and the scientific background of the modeler. Although significant progress has been made by the ecological modeling community in the area of representing the soil-plant-atmospheric continuum of mass and energy, the dynamics of soil water remain highly abstracted, despite being a crucial parameter of ecological processes.

1.6. Towards a Better Understanding of Terrestrial C-cycling Processes: Ecohydrological or Hydro-ecological approaches?

Even though ambient soil water content is the net result of precipitation, soil characteristics (infiltration capacity, porosity, etc), extraction of water by plants, and the

topography of the landscape, an integrated approach representing the complete hydrological cycle is not often adopted in most ecological models (Kuchment et al., 2006). Soil water can be accurately simulated only if the complete hydrological cycle is "represented" within a modeling domain. Hydrologists and ecologists differ in their view of soil water dynamics. While hydrologists consider the physical laws that determine water flow between locations in the soil body or landscape, ecologists and agriculturists are more concerned with the volume of water *available* for plant use during ecophysiological processes such as transpiration. They often ignore the amount of water that drains laterally across the landscape, which could significantly alter local scale hydrological regimes. Likewise, hydrologists also abstract vegetation controls on the hydrological cycle. For both hydrologists and ecologists, vegetation is the common bridge that links the water-potential gradient between soil and air.

Until now, ecological modeling studies focus either on point scale details (e.g., Grant et al., 2006; Ju et al., 2006a) or large-scale generalizations (Running, 1994; Liu et al., 1997a; Potter et al., 2001; Coops et al., 2007). Most existing ecological models are lumped or point scale formulations that assume that a modeling unit is isolated from its neighboring areas (e.g., Bonan, 1989; Verseghy, 1991; Zhang et al., 2002; Arora and Boer, 2006; Grant et al., 2006). As such, only vertical hydrological processes can be realistically modeled using "soil layers" employing some implicit procedures to account for the lateral water flow although the vertical movement of water in between layers is modeled at various levels of sophistication.

On one hand, the conceptualizations used to describe the vertical movement of water in lumped models include single layered soil, double layered soils that demarcate saturated and unsaturated zones, multi layered soil, or multilayered soil with root water uptake schemes. Almost all of conventional models employ Richard's equation to calculate the unsaturated flow of soil water. On the other hand, spatially distributed models that are driven on a remote

sensing framework, where modeling units (pixels) remain isolated, soil moisture is calculated simply as "available soil moisture" (e.g., Liu et al., 1997) or some form of scalars may be used to represent the soil moisture (Heinsch et al., 2006; Coops et al., 2007), in order to circumvent computational difficulties. Although most of the ecological models are sophisticated in terms of modeling the biophysical controls on plant growth, they still abstract the hydrological processes (especially the lateral water fluxes). Absence of, or simplified representations of lateral hydrological processes make the current ecological models hydrologically incomplete. Hence, models that abstract hydrological controls have great vulnerability to simulate the terrestrial C-cycling processes in a biased manner.

Topographic variations on the Earth's surface determine the hydrological, geo-morphological, and ecological processes (Dietrich and Perron, 2006). At small spatial scales (e.g., a soil profile), although electrostatic and osmotic forces govern flow of water, at large spatial scales, topography (through the force of gravity) makes water flow (Wigmosta and Lettenmaier, 1999; Dirnbock et al., 2002). Conventional hydrological models use the digital elevation model, DEM, to simulate lateral flow of water across a terrain (Beven et al., 1984; Ambroise et al., 1996; Armstrong and Martz, 2003; Zhou et al., 2006; Chen et al., 2007; Vazquez and Feyen, 2007). Most of the traditional hydrological models formulate baseflow as an exponential function of the soil water storage deficit (Beven and Kirkby, 1979) or water table depth (Sivapalan et al., 1987) and are generally referred to as TOPMODEL-based runoff schemes. Some models also consider parameterizations of baseflow as an exponential function of the catchments water storage deficit (Koster et al., 2006) or the water table depth (Gordon and Famiglietti, 2004). In earlier land surface models, the baseflow component was formulated as drainage under gravity (Dickinson et al., 1986) or a down-slope lateral drainage (Sellers et al., 1986).

A topographically-driven lateral water flow component that occurs at landscape or watershed scales could have significant influences on ecological processes such as C-cycling. In a soil profile, two regions can be demarcated based on soil saturation, i.e., saturated and unsaturated zones with the water table as the dividing point. Saturated zone dynamics relative to the topographic position control sub-surface lateral water flow across the landscape as baseflow. Although baseflow occurs through the saturated zone, it can significantly influence unsaturated zone soil moisture in regions where the water table is shallow (Lacey and Grayson, 1998; Schilling and Zhang, 2004; Fenicia et al., 2006). To accurately represent hydrological controls on biogeochemical processes within ecological models, the currently existing simplified representation of lateral hydrological processes needs to be changed. Lateral hydrological processes need to be explicitly described considering topography and soil properties that govern the nature of lateral water flow topographically, i.e., surface overland flow or sub-surface baseflow. Ideally, hydrological processes should be simulated according to a hydrologist's perception of the water cycle and should then be linked to an ecological model created according to an ecologist's perception of ecological processes in order to accurately describe what happens in natural systems.

Other forms of hydrological complexities that are specific to various ecosystems also need to be considered when we couple hydrology and ecology. For example, in humid boreal ecosystems, forest floors are dominated by a thick organic layer consisting of a moss-peat complex (Price et al., 1997). This moss-peat complex creates a unique hydrological regime owing to its very high surface infiltration capacity resulting from its ability to facilitate preferential flow either laterally or vertically. Hence, Hortonian types of run-off generation mechanisms seldom exist and sub-surface preferential baseflow may be the dominant form of hydrological process that laterally connect water between neighboring hydrological response

units. Unique flow patterns such as "flow-reversals" may be observed in dry boreal landscapes; this makes water flow against the gravitational gradient due to root water uptake for transpiration and drying of peat matrix (Devito et al.,1997; Devito et al., 2005).

Until now, ecological modelers (mostly biologists) and hydrological modelers (mostly civil engineers) worked in isolation. Even though this resulted in parallel advancements in both the fields, these scientific communities have overlooked the capabilities that the combination of hydrology and ecology can bring to a better understanding of earth surface processes. Only a few studies have attempted to bridge ecology and hydrology from a modeling perspective (e.g., Band et al., 1993; Creed and Band, 1998; Band et al., 2001; Rodriguez-Iturbe et al., 2001; Porporato and Rodriguez-Iturbe, 2002; Porporato et al., 2003; Tague and Band, 2004, Daly et al., 2004; D'odorico et al., 2004; Ju and Chen, 2005; Chen et al., 2005) and further research in this area is required to properly couple water, nutrient and C-cycling processes by adopting various modeling strategies. Lumped formulations need to be replaced by distributed modeling approaches that have inter-pixel connectivity using topographically-driven water fluxes in accordance with the conventional hydrological philosophy. The motivation for this thesis originates here.

The question of linking ecology and hydrology can be conceptualized either as an *Eco-hydrological* or as *Hydro-ecological* issue. It is only in the recent years that scientists have begun taking this approach. Hannah et al. (2004) gives a vivid commentary on the dichotomy of this subject matter. In eco-hydrology, ecology has prominence and this subject matter focuses mainly on plant–water relations that exist in terrestrial ecosystems (e.g., Schulze et al., 1987; Tardieu et al., 1992; Schulze et al., 1995; Grant and Flanagan, 2007). In hydro-ecology, hydrological processes dominate and determine the conditions for ecological processes (Kundzewicz, 2002; Zalewski, 2002; Hannah et al., 2004; Kleynhans et al., 2007). The hydro-

ecological philosophy uses knowledge from hydrological, hydraulic, geomorphological and biological/ecological sciences to predict the response of ecosystems to variation in abiotic factors over a range of spatial and temporal scales (Dunbar and Acreman, 2001). This thesis has a hydro-ecological inclination to study watershed scale ecophysiological and biogeochemical processes.

1.7. Hypothesis and Objectives

With the above-mentioned complexities of terrestrial C-cycling processes, this research project was directed to better understand the key issues concerning the link between meso-scale hydrological and biogeochemical processes. The fundamental hypothesis of this work is that landscape scale hydrological processes significantly affect local scale water balance, which in turn affects various ecophysiological and biogeochemical processes due to their direct and indirect relationships and associated feedback mechanisms. To this end, an intensive hydro-ecological modeling strategy was adopted in a spatially explicit manner, at the watershed scale, with a daily temporal resolution. This modeling study was conducted in a boreal landscape encompassing the Eastern Old Black spruce site of FCRN, Chibougamau, Quebec, Canada, where continuous high precision of measurements of the fluxes of mass and energy across the biosphere and atmosphere have been recorded since mid-2003. The following are the objectives of this research to test the above-mentioned hypothesis.

1. To further develop and test the performance of a hydro-ecological model, BEPS-TerrainLab V2.0 that features a tighter coupling of hydrological, ecological and biogeochemical processes in a spatially explicit manner.
2. To identify the links between topographically driven water fluxes and ecophysiological processes such as ET and photosynthesis and to test the hypothesis that sub-surface

baseflow and its influence on local soil water balance has significant influences on local scale ecophysiological and biogeochemical processes.

3. To reconstruct the historical C-balance (1920-2005) of the study site using a long term ecosystem model and to compare the simulated C-pools in recent years using field measurements.
4. To simulate and validate the spatio-temporal distribution of various boreal hydrothermal and biogeochemical processes using BEPS-TerrainLab V2.0.
5. To test the influence of topographically driven baseflow and the nature of soil water balance on the spatial distribution of C sources and sinks, to identify various sources of bias and to analyze the fate of ecosystem C under various hydrological representations.

1.8. A Road Map to the Thesis

Having identified the objectives, the thesis is organized into different chapters that are tailored towards peer-reviewed publications in scientific journals. In order to ensure that each paper stands on its own, topics such as data preparation, model description and some figures are repeated occasionally.

In Chapter 2, hydro-ecological aspects of the model, BEPS-TerrainLab V2.0 is introduced . Further, the model is tested for various hydro-ecological simulations using field measurements that were taken in a boreal landscape in eastern Canada (the study site). After understanding the intricacies and magnitude of hydro-ecological processes, an investigation is conducted in Chapter 3 to identify the errors associated with currently used hydrological abstractions in ecosystem models that ignore the effects of non-explicit soil water partitioning on ecophysiological processes such as ET or photosynthesis. This investigation was conducted using a numerical experiment employing three scenarios that differed in conceptualizing the

soil water balance and the mechanism of lateral water exchange. A sensitivity analysis was also carried out to ascertain the importance of hydrology vis-à-vis the accuracy of parameters used for ecophysiological computations.

Terrestrial C-balance cannot be fully understood by studying the dynamics of GPP or ET alone. A combination of biogeochemical, hydrological and ecophysiological processes along with feedback relationships controls the net ecosystem C balance. Chapter 4 describes how various ecosystem C-pools are reconstructed using a long-term ecosystem C-balance model in a spatially explicit manner, considering the combined effects of disturbance and non-disturbance factors (climate change, CO_2 fertilization and N deposition) that affects the inter-annual variability of forest growth and C-balance. The reconstructed C-pools are validated using field measurements. These C-pools may be used as "substrates" for biogeochemical processes that simulate net ecosystem productivity (NEP), and the measure of the terrestrial C source or sinks in the present time.

In Chapter 5, the newly introduced biogeochemical module of BEPS-TerrainLab V2.0 is described. Firstly, the model simulations are tested using measurements of snow depth, soil temperature, NEP and total ecosystem respiration. Further, using the same numerical experiment as in Chapter 3, it is demonstrated that unrealistic hydrological representations create large differences in the spatial distribution of C sources and sinks (NEP). Considering the variations in the biogeochemical processes and the fate of C in the ecosystem, the spatial differences in NEP as a result of hydrological influence is understood.

In Chapter 6, the thesis is summarized and the hydrological influence on boreal C cycling processes is established. The uncertainties that exist in current research is discussed and future research directions are proposed.

References

Ambroise, B., Beven, K., and Freer, J.(1996). Toward a Generalization of the Topmodel Concepts: Topographic Indices of Hydrological Similarity, *Water Resources Research* **32**, 2135-2145.

Amiro, B.D., Flannigan, M.D., Stocks, B.J., and Wotton, B.M.(2002). Perspectives on Carbon Emissions From Canadian Forest Fires, *Forestry Chronicle* **78**, 388-390.

Amiro, B.D., Logan, K.A., Wotton, B.M., Flannigan, M.D., Todd, J.B., Stocks, B.J., and Martell, D.L.(2004). Fire Weather Index System Components for Large Fires in the Canadian Boreal Forest, *International Journal of Wildland Fire* **13**, 391-400.

Amiro, B.D., Orchansky, A.L., Barr, A.G., Black, T.A., Chambers, S.D., Chapin, F.S., Gouldenf, M.L., Litvakg, M., Liu, H.P., Mccaughey, J.H., Mcmillan, A., and Randerson, J.T.(2006). The Effect of Post-Fire Stand Age on the Boreal Forest Energy Balance, *Agricultural and Forest Meteorology* **140**, 41-50.

Andersson, E. and Sobek, S.(2006). Comparison of a Mass Balance and an Ecosystem Model Approach When Evaluating the Carbon Cycling in a Lake Ecosystem, *Ambio* **35**, 476-483.

Arain, M.A., Black, T.A., Barr, A.G., Jarvis, P.G., Massheder, J.M., Verseghy, D.L., and Nesic, Z.(2002). Effects of Seasonal and Interannual Climate Variability on Net Ecosystem Productivity of Boreal Deciduous and Conifer Forests, *Canadian Journal of Forest Research-Revue Canadienne De Recherche Forestiere* **32**, 878-891.

Arain, M.A., Yuan, F.M., and Black, T.A.(2006). Soil-Plant Nitrogen Cycling Modulated Carbon Exchanges in a Western Temperate Conifer Forest in Canada, *Agricultural and Forest Meteorology* **140**, 171-192.

Armstrong, R.N. and Martz, L.W.(2003). Topographic Parameterization in Continental Hydrology: a Study in Scale, *Hydrological Processes* **17**, 3763-3781.

Arora, V.K.(2003). Simulating Energy and Carbon Fluxes Over Winter Wheat Using Coupled Land Surface and Terrestrial Ecosystem Models, *Agricultural and Forest Meteorology* **118**, 21-47.

Arora, V.K. and Boer, G.J.(2006). The Temporal Variability of Soil Moisture and Surface Hydrological Quantities in a Climate Model, *Journal of Climate* **19**, 5875-5888.

Arrhenius, S.(1896). On the Influence of Carbonic Acid in the Air Upon the Temperature of the Ground., *Philosophical Magazine and Journal of Science* **5**, 237–275.

Asner, G.P., Seastedt, T.R., and Townsend, A.R.(1997). The Decoupling of Terrestrial Carbon and Nitrogen Cycles, *Bioscience* **47**, 226-234.

Baldocchi, D., Falge, E., Gu, L.H., Olson, R., Hollinger, D., Running, S., Anthoni, P., Bernhofer, C., Davis, K., Evans, R., Fuentes, J., Goldstein, A., Katul, G., Law, B., Lee, X.H., Malhi, Y., Meyers, T., Munger, W., Oechel, W., U, K.T.P., Pilegaard, K., Schmid, H.P., Valentini, R., Verma, S.,

Vesala, T., Wilson, K., and Wofsy, S.(2001). Fluxnet: a New Tool to Study the Temporal and Spatial Variability of Ecosystem-Scale Carbon Dioxide, Water Vapor, and Energy Flux Densities, *Bulletin of the American Meteorological Society* **82**, 2415-2434.

Baldocchi, D.D.(2003). Assessing the Eddy Covariance Technique for Evaluating Carbon Dioxide Exchange Rates of Ecosystems: Past, Present and Future, *Global Change Biology* **9**, 479-492.

Baldocchi, D.D., Hicks, B.B., and Meyers, T.P.(1988). Measuring Biosphere-Atmosphere Exchanges of Biologically Related Gases With Micrometeorological Methods, *Ecology* **69**, 1331-1340.

Baldocchi, D.D., Law, B.E., and Anthoni, P.M.(2000). On Measuring and Modeling Energy Fluxes Above the Floor of a Homogeneous and Heterogeneous Conifer Forest, *Agricultural and Forest Meteorology* **102**, 187-206.

Baldocchi, D.D. and Vogel, C.A.(1996). Energy and Co2 Flux Densities Above and Below a Temperate Broad-Leaved Forest and a Boreal Pine Forest, *Tree Physiology* **16**, 5-16.

Ball, J.T., Woodrow, I.E., and Berry, J.A.: 1987, 'A model predicting stomatal conductnance amd its contribution to the control of photosynthesis under different environmental conditions', *In*Progress in Photosynthesis Research, Martinus Nijhoff Publishers, Dordrecht, pp 221-224.

Band, L.E., Patterson, P., Nemani, R., and Running, S.W.(1993). Forest Ecosystem Processes at the Watershed Scale - Incorporating Hillslope Hydrology, *Agricultural and Forest Meteorology* **63**, 93-126.

Band, L.E., Tague, C.L., Groffman, P., and Belt, K.(2001). Forest Ecosystem Processes at the Watershed Scale: Hydrological and Ecological Controls of Nitrogen Export, *Hydrological Processes* **15**, 2013-2028.

Beringer, J., Chapin, F.S., Thompson, C.C., and Mcguire, A.D.(2005). Surface Energy Exchanges Along a Tundra-Forest Transition and Feedbacks to Climate, *Agricultural and Forest Meteorology* **131**, 143-161.

Beringer, J., Hutley, L.B., Tapper, N.J., and Cernusak, L.A.(2007). Savanna Fires and Their Impact on Net Ecosystem Productivity in North Australia, *Global Change Biology* **13**, 990-1004.

Betts, R.A., Boucher, O., Collins, M., Cox, P.M., Falloon, P.D., Gedney, N., Hemming, D.L., Huntingford, C., Jones, C.D., Sexton, D.M.H., and Webb, M.J.(2007). Projected Increase in Continental Runoff Due to Plant Responses to Increasing Carbon Dioxide, *Nature* **448**, 1037-U5.

Beven, K.J. and Kirkby, M.J.(1979). A Physically Based Variable Contributing Model of Basin Hydrology, *Hydrological Science Bulletin* **24**, 43-69.

Beven, K.J., Kirkby, M.J., Schofield, N., and Tagg, A.F.(1984). Testing a Physically-Based Flood Forecasting-Model (Topmodel) for 3 Uk Catchments, *Journal of Hydrology* **69**, 119-143.

Bonan, G.B.(1989). A Computer-Model of the Solar-Radiation, Soil-Moisture, and Soil Thermal

Regimes in Boreal Forests , *Ecological Modelling* **45**, 275-306.

Bonan, G.B. and Shugart, H.H.(1989). Environmental-Factors and Ecological Processes in Boreal Forests, *Annual Review of Ecology and Systematics* **20**, 1-28.

Bonan, G.B. and Vancleve, K.(1992). Soil-Temperature, Nitrogen Mineralization, and Carbon Source Sink Relationships in Boreal Forests, *Canadian Journal of Forest Research-Revue Canadienne De Recherche Forestiere* **22**, 629-639.

Boone, R.D., Nadelhoffer, K.J., Canary, J.D., and Kaye, J.P.(1998). Roots Exert a Strong Influence on the Temperature Sensitivity of Soil Respiration, *Nature* **396**, 570-572.

Borken, W., Xu, Y.J., Davidson, E.A., and Beese, A.(2002). Site and Temporal Variation of Soil Respiration in European Beech, Norway Spruce, and Scots Pine Forests, *Global Change Biology* **8**, 1205-1216.

Bottcher, J.(2004). Uncertainties of Nonlinearly Estimated Parameters From Incubations of Soil Organic Matter, *Journal of Plant Nutrition and Soil Science-Zeitschrift Fur Pflanzenernahrung Und Bodenkunde* **167**, 293-302.

Buzorius, G., Kalogiros, J., and Varutbangkul, V.(2006). Airborne Aerosol Flux Measurements With Eddy Correlation Above the Ocean in a Coastal Environment, *Journal of Aerosol Science* **37**, 1267-1286.

Canadell, J.G., Kirschbaum, M.U.F., Kurz, W.A., Sanz, M.J., Schlamadinger, B., and Yamagata, Y.(2007). Factoring Out Natural and Indirect Human Effects on Terrestrial Carbon Sources and Sinks, *Environmental Science & Policy* **10**, 370-384.

Caspersen, J.P., Pacala, S.W., Jenkins, J.C., Hurtt, G.C., Moorcroft, P.R., and Birdsey, R.A.(2000). Contributions of Land-Use History to Carbon Accumulation in Us Forests, *Science* **290**, 1148-1151.

Cerri, C.C., Melillo, J.M., Feigl, B.J., Piccolo, M.C., Neill, C., Steudler, P.A., Carvalho, M.D.S., Godinho, V.P., Eduardo, C., Cerri, P., and Bernoux, M.(2005). Recent History of the Agriculture of the Brazilian Amazon Basin - Prospects for Sustainable Development and a First Look at the Biogeochemical Consequences of Pasture Reformation, *Outlook on Agriculture* **34**, 215-223.

Chapman, S.K., Hart, S.C., Cobb, N.S., Whitham, T.G., and Koch, G.W.(2003). Insect Herbivory Increases Litter Quality and Decomposition: an Extension of the Acceleration Hypothesis, *Ecology* **84** , 2867-2876.

Chen, J.M., Chen, B.Z., Higuchi, K., Liu, J., Chan, D., Worthy, D., Tans, P., and Black, A.(2006). Boreal Ecosystems Sequestered More Carbon in Warmer Years, *Geophysical Research Letters* **33**.

Chen, J.M., Chen, X.Y., Ju, W.M., and Geng, X.Y.(2005). Distributed Hydrological Model for Mapping Evapotranspiration Using Remote Sensing Inputs, *Journal of Hydrology* **305**, 15-39.

Chen, J.M., Ju, W.M., Cihlar, J., Price, D., Liu, J., Chen, W.J., Pan, J.J., Black, A., and Barr, A.(2003). Spatial Distribution of Carbon Sources and Sinks in Canada's Forests, *Tellus Series B-Chemical and Physical Meteorology* **55**, 622-641.

Chen, J.M., Liu, J., Cihlar, J., and Goulden, M.L.(1999). Daily Canopy Photosynthesis Model Through Temporal and Spatial Scaling for Remote Sensing Applications, *Ecological Modelling* **124**, 99-119.

Chen, X., Chen, Y.D., and Xu, C.Y.(2007). A Distributed Monthly Hydrological Model for Integrating Spatial Variations of Basin Topography and Rainfall, *Hydrological Processes* **21**, 242-252.

Cihlar, J. Quantification of the regional carbon cycle of the biosphere: Policy, science and land-use decisions: Carbon Sequestration In China's Forest Ecosystems. Journal of Environmental Management 85 [3], 785-790. 2007.

Coops, N.C., Black, T.A., Jassal, R.P.S., Trofymow, J.A.T., and Morgenstern, K.(2007). Comparison of Modis, Eddy Covariance Determined and Physiologically Modelled Gross Primary Production (Gpp) in a Douglas-Fir Forest Stand, *Remote Sensing of Environment* **107**, 385-401.

Corradi, C., Kolle, O., Walter, K., Zimov, S.A., and Schulze, E.D.(2005). Carbon Dioxide and Methane Exchange of a North-East Siberian Tussock Tundra, *Global Change Biology* **11**, 1910-1925.

Coursolle, C., Margolis, H.A., Barr, A.G., Black, T.A., Amiro, B.D., Mccaughey, J.H., Flanagan, L.B., Lafleur, P.M., Roulet, N.T., Bourque, C.P.A., Arain, M.A., Wofsy, S.C., Dunn, A., Morgenstern, K., Orchansky, A.L., Bernier, P.Y., Chen, J.M., Kidston, J., Saigusa, N., and Hedstrom, N.(2006). Late-Summer Carbon Fluxes From Canadian Forests and Peatlands Along an East-West Continental Transect, *Canadian Journal of Forest Research-Revue Canadienne De Recherche Forestiere* **36**, 783-800.

Cox, P.M., Betts, R.A., Jones, C.D., Spall, S.A., and Totterdell, I.J.(2000). Acceleration of Global Warming Due to Carbon-Cycle Feedbacks in a Coupled Climate Model (Vol 408, Pg 184, 2000), *Nature* **408**, 750.

Creed, I.F. and Band, L.E.(1998). Exploring Functional Similarity in the Export of Nitrate-N From Forested Catchments: a Mechanistic Modeling Approach, *Water Resources Research* **34**, 3079-3093.

D'odorico, P., Porporato, A., Laio, F., Ridolfi, L., and Rodriguez-Iturbe, I.(2004). Probabilistic Modeling of Nitrogen and Carbon Dynamics in Water-Limited Ecosystems, *Ecological Modelling* **179**, 205-219.

Daly, E., Porporato, A., and Rodriguez-Iturbe, I.(2004). Coupled Dynamics of Photosynthesis, Transpiration, and Soil Water Balance. Part I: Upscaling From Hourly to Daily Level, *Journal of Hydrometeorology* **5**, 546-558.

Dang, Q.L., Margolis, H.A., and Collatz, G.J.(1998). Parameterization and Testing of a Coupled Photosynthesis Stomatal Conductance Model for Boreal Trees, *Tree Physiology* **18**, 141-153.

Dang, Q.L., Margolis, H.A., Coyea, M.R., Sy, M., and Collatz, G.J.(1997). Regulation of Branch-Level

Gas Exchange of Boreal Trees: Roles of Shoot Water Potential and Vapor Pressure Difference, *Tree Physiology* **17**, 521-535.

Davidson, E.A. and Janssens, I.A.(2006). Temperature Sensitivity of Soil Carbon Decomposition and Feedbacks to Climate Change, *Nature* **440**, 165-173.

Deluca, T.H. and Sala, A.(2006). Frequent Fire Alters Nitrogen Transformations in Ponderosa Pine Stands of the Inland Northwest, *Ecology* **87**, 2511-2522.

Deming, D.(1995). Climatic Warming in North-America - Analysis of Borehole Temperatures, *Science* **268**, 1576-1577.

Denning, A.S., Nicholls, M., Prihodko, L., Baker, I., Vidale, P.L., Davis, K., and Bakwin, P.(2003). Simulated Variations in Atmospheric Co2 Over a Wisconsin Forest Using a Coupled Ecosystem-Atmosphere Model, *Global Change Biology* **9**, 1241-1250.

Devito, K.J., Waddington, J.M., and Branfireun, B.A.(1997). Flow Reversals in Peatlands Influenced by Local Groundwater Systems, *Hydrological Processes* **11**, 103-110.

Devito, K., Creed, I., Gan, T., Mendoza, C., Petrone, R., Silins, U., and Smerdon, B.(2005). A Framework for Broad-Scale Classification of Hydrologic Response Units on the Boreal Plain: Is Topography the Last Thing to Consider?, *Hydrological Processes* **19**, 1705-1714.

Dickinson, R.E., Sellers, A.H., Kennedy, P.J., and Wilson, M.F.: 1986, 'Biosphere-atmosphere transfer scheme (BATS) for the NCAR community climate model', *In*NCAR Tech. Note TN-275, National Center for Atmosphere Research, Boulder, Colorado, USA.

Dietrich, W.E. and Perron, J.T.(2006). The Search for a Topographic Signature of Life, *Nature* **439**, 411-418.

Dirnbock, T., Hobbs, R.J., Lambeck, R.J., and Caccetta, P.A.(2002). Vegetation Distribution in Relation to Topographically Driven Processes in Southwestern Australia, *Applied Vegetation Science* **5**, 147-158.

Dou, J.X., Zhang, Y.P., Yu, G.R., Zhao, S.J., Wang, X., and Song, Q.H.(2006). A Preliminary Study on the Heat Storage Fluxes of a Tropical Seasonal Rain Forest in Xishuangbanna, *Science in China Series D-Earth Sciences* **49**, 163-173.

Engel, V.C. and Odum, H.T.(1999). Simulation of Community Metabolism and Atmospheric Carbon Dioxide and Oxygen Concentrations in Biosphere 2., *Ecological Engineering* **13**, 107-134.

Epstein, H.E., Beringer, J., Gould, W.A., Lloyd, A.H., Thompson, C.D., Chapin, F.S., Michaelson, G.J., Ping, C.L., Rupp, T.S., and Walker, D.A.(2004). The Nature of Spatial Transitions in the Arctic, *Journal of Biogeography* **31**, 1917-1933.

Farquhar, G.D., Caemmerer, S.V., and Berry, J.A.(1980). A Biochemical-Model of Photosynthetic Co2 Assimilation in Leaves of C-3 Species, *Planta* **149**, 78-90.

Fenicia, F., Savenije, H.H.G., Matgen, P., and Pfister, L.(2006). Is the Groundwater Reservoir Linear? Learning From Data in Hydrological Modelling, *Hydrology and Earth System Sciences* **10**, 139-150.

Fenton, N., Lecomte, N., Legare, S., and Bergeron, Y.(2005). Paludification in Black Spruce (Picea Mariana) Forests of Eastern Canada: Potential Factors and Management Implications, *Forest Ecology and Management* **213**, 151-159.

Fernandez, I., Cabaneiro, A., and Carballas, T.(1999). Carbon Mineralization Dynamics in Soils After Wildfires in Two Galician Forests, *Soil Biology & Biochemistry* **31**, 1853-1865.

Friedlingstein, P., Cox, P., Betts, R., Bopp, L., Von Bloh, W., Brovkin, V., Cadule, P., Doney, S., Eby, M., Fung, I., Bala, G., John, J., Jones, C., Joos, F., Kato, T., Kawamiya, M., Knorr, W., Lindsay, K., Matthews, H.D., Raddatz, T., Rayner, P., Reick, C., Roeckner, E., Schnitzler, K.G., Schnur, R., Strassmann, K., Weaver, A.J., Yoshikawa, C., and Zeng, N.(2006). Climate-Carbon Cycle Feedback Analysis: Results From the (Cmip)-M-4 Model Intercomparison, *Journal of Climate* **19**, 3337-3353.

Friedlingstein, P., Dufresne, J.L., Cox, P.M., and Rayner, P.(2003). How Positive Is the Feedback Between Climate Change and the Carbon Cycle?, *Tellus Series B-Chemical and Physical Meteorology* **55**, 692-700.

Friend, A.D. and Cox, P.M.(1995). Modeling the Effects of Atmospheric CO_2 on Vegetation Atmosphere Interactions, *Agricultural and Forest Meteorology* **73**, 285-295.

Frolking, S., Li, C.S., Braswell, R., and Fuglestvedt, J.(2004). Short- and Long-Term Greenhouse Gas and Radiative Forcing Impacts of Changing Water Management in Asian Rice Paddies, *Global Change Biology* **10**, 1180-1196.

Galmes, J., Flexas, J., Save, R., and Medrano, H.(2007). Water Relations and Stomatal Characteristics of Mediterranean Plants With Different Growth Forms and Leaf Habits: Responses to Water Stress and Recovery, *Plant and Soil* **290**, 139-155.

Gedney, N., Cox, P.M., Betts, R.A., Boucher, O., Huntingford, C., and Stott, P.A.(2006). Detection of a Direct Carbon Dioxide Effect in Continental River Runoff Records, *Nature* **439**, 835-838.

Gilmanov, T.G., Soussana, J.E., Aires, L., Allard, V., Ammann, C., Balzarolo, M., Barcza, Z., Bernhofer, C., Campbell, C.L., Cernusca, A., Cescatti, A., Clifton-Brown, J., Dirks, B.O.M., Dore, S., Eugster, W., Fuhrer, J., Gimeno, C., Gruenwald, T., Haszpra, L., Hensen, A., Ibrom, A., Jacobs, A.F.G., Jones, M.B., Lanigan, G., Laurila, T., Lohila, A., Manca, G., Marcolla, B., Nagy, Z., Pilegaard, K., Pinter, K., Pio, C., Raschi, A., Rogiers, N., Sanz, M.J., Stefani, P., Sutton, M., Tuba, Z., Valentini, R., Williams, M.L., and Wohlfahrt, G.(2007). Partitioning European Grassland Net Ecosystem CO_2 Exchange Into Gross Primary Productivity and Ecosystem Respiration Using Light Response Function Analysis, *Agriculture Ecosystems & Environment* **121**, 93-120.

Grant, R.F., Barr, A.G., Black, T.A., Gaumont-Guay, D., Iwashita, H., Kidson, J., Mccaughey, H., Morgenstern, K., Murayama, S., Nesic, Z., Saigusa, N., Shashkov, A., and Zha, T.(2007). Net

Ecosystem Productivity of Boreal Jack Pine Stands Regenerating From Clearcutting Under Current and Future Climates, *Global Change Biology* **13**, 1423-1440.

Grant, R.F. and Flanagan, L.B.(2007). Modeling Stomatal and Nonstomatal Effects of Water Deficits on Co2 Fixation in a Semiarid Grassland, *Journal of Geophysical Research-Biogeosciences* **112**.

Grant, R.F., Kimball, B.A., Brooks, T.J., Wall, G.W., Pinter, P.J., Hunsaker, D.J., Adamsen, F.J., Lamorte, R.L., Leavitt, S.W., Thompson, T.L., and Matthias, A.D.(2001). Modeling Interactions Among Carbon Dioxide, Nitrogen, and Climate on Energy Exchange of Wheat in a Free Air Carbon Dioxide Experiment, *Agronomy Journal* **93**, 638-649.

Grant, R.F., Zhang, Y., Yuan, F., Wang, S., Hanson, P.J., Gaumont-Guay, D., Chen, J., Black, T.A., Barr, A., Baldocchi, D.D., and Arain, A.(2006). Intercomparison of Techniques to Model Water Stress Effects on Co2 and Energy Exchange in Temperate and Boreal Deciduous Forests , *Ecological Modelling* **196**, 289-312 .

Griffis, T.J., Black, T.A., Morgenstern, K., Barr, A.G., Nesic, Z., Drewitt, G.B., Gaumont-Guay, D., and Mccaughey, J.H.(2003). Ecophysiological Controls on the Carbon Balances of Three Southern Boreal Forests, *Agricultural and Forest Meteorology* **117**, 53-71.

Hannah, D.M., Wood, P.J., and Sadler, J.P. (2004). Ecohydrology and Hydroecology: a New Paradigm'?, *Hydrological Processes* **18**, 3439-3445.

Hansen, J., Sato, M., and Ruedy, R.(1997). Radiative Forcing and Climate Response, *Journal of Geophysical Research-Atmospheres* **102**, 6831-6864.

Harper, C.W., Blair, J.M., Fay, P.A., Knapp, A.K., and Carlisle, J.D.(2005). Increased Rainfall Variability and Reduced Rainfall Amount Decreases Soil Co2 Flux in a Grassland Ecosystem, *Global Change Biology* **11**, 322-334.

Harrison, J.A., Caraco, N., and Seitzinger, S.P.(2005). Global Patterns and Sources of Dissolved Organic Matter Export to the Coastal Zone: Results From a Spatially Explicit, Global Model, *Global Biogeochemical Cycles* **19**.

Hattenschwiler, S. and Bretscher, D.(2001). Isopod Effects on Decomposition of Litter Produced Under Elevated Co2, N Deposition and Different Soil Types, *Global Change Biology* **7**, 565-579.

Heinsch, F.A., Zhao, M.S., Running, S.W., Kimball, J.S., Nemani, R.R., Davis, K.J., Bolstad, P.V., Cook, B.D., Desai, A.R., Ricciuto, D.M., Law, B.E., Oechel, W.C., Kwon, H., Luo, H.Y., Wofsy, S.C., Dunn, A.L., Munger, J.W., Baldocchi, D.D., Xu, L.K., Hollinger, D.Y., Richardson, A.D., Stoy, P.C., Siqueira, M.B.S., Monson, R.K., Burns, S.P., and Flanagan, L.B. (2006). Evaluation of Remote Sensing Based Terrestrial Productivity From Modis Using Regional Tower Eddy Flux Network Observations, *Ieee Transactions on Geoscience and Remote Sensing* **44**, 1908-1925.

Holland, E.A., Braswell, B.H., Lamarque, J.F., Townsend, A., Sulzman, J., Muller, J.F., Dentener, F., Brasseur, G., Levy, H., Penner, J.E., and Roelofs, G.J.(1997). Variations in the Predicted Spatial Distribution of Atmospheric Nitrogen Deposition and Their Impact on Carbon Uptake by

Terrestrial Ecosystems, *Journal of Geophysical Research-Atmospheres* **102** , 15849-15866.

Hornberger, G.M., Bencala, K.E., and Mcknight, D.M.(1994). Hydrological Controls on Dissolved Organic-Carbon During Snowmelt in the Snake River Near Montezuma, Colorado, *Biogeochemistry* **25**, 147-165.

Houghton, R.A.(2007). Balancing the Global Carbon Budget, *Annual Review of Earth and Planetary Sciences* **35**, 313-347.

Houghton, R.A. and Hackler, J.L.(2006). Emissions of Carbon From Land Use Change in Sub-Saharan Africa, *Journal of Geophysical Research-Biogeosciences* **111**.

Hutley, L.B., O'grady, A.P., and Eamus, D. (2001). Monsoonal Influences on Evapotranspiration of Savanna Vegetation of Northern Australia, *Oecologia* **126**, 434-443.

IPCC.(2001). Climate Change 2001: The Scientific Basis. Contribution of Working Group I to the Third Assessment Report of the Intergovernmental Panel on Climate Change, Cambridge University Press, Cambridge.

IPCC(2007). Climate Change 2007 : The Physical Science Basis. Summary for Policymakers. *Contribution of working group I to the fourth assessment report of the Intergovernmental panel on climate change.* http://ipcc-wg1.ucar.edu/index.html (April 2007).

Irvine, J., Law, B.E., Anthoni, P.M., and Meinzer, F.C.(2002). Water Limitations to Carbon Exchange in Old-Growth and Young Ponderosa Pine Stands, *Tree Physiology* **22**, 189-196.

Iwata, H., Malhi, Y., and Von Randow, C.(2005). Gap-Filling Measurements of Carbon Dioxide Storage in Tropical Rainforest Canopy Airspace, *Agricultural and Forest Meteorology* **132**, 305-314.

Jackson, R.B., Carpenter, S.R., Dahm, C.N., Mcknight, D.M., Naiman, R.J., Postel, S.L., and Running, S.W.(2001). Water in a Changing World, *Ecological Applications* **11**, 1027-1045.

Janssens, I.A., Freibauer, A., Ciais, P., Smith, P., Nabuurs, G.J., Folberth, G., Schlamadinger, B., Hutjes, R.W.A., Ceulemans, R., Schulze, E.D., Valentini, R., and Dolman, A.J.(2003). Europe's Terrestrial Biosphere Absorbs 7 to 12% of European Anthropogenic CO_2 Emissions, *Science* **300**, 1538-1542.

Jarvis, P.G.(1976). Interpretation of Variations in Leaf Water Potential and Stomatal Conductance Found in Canopies in Field, *Philosophical Transactions of the Royal Society of London Series B-Biological Sciences* **273**, 593-610 .

Jassal, R.S., Black, T.A., Cai, T.B., Morgenstern, K., Li, Z., Gaumont-Guay, D., and Nesic, Z.(2007). Components of Ecosystem Respiration and an Estimate of Net Primary Productivity of an Intermediate-Aged Douglas-Fir Stand, *Agricultural and Forest Meteorology* **144**, 44-57.

Joffre, R., Ourcival, J.M., Rambal, S., and Rocheteau, A.(2003). The Key-Role of Topsoil Moisture on Co2 Efflux From a Mediterranean Quercus Ilex Forest, *Annals of Forest Science* **60**, 519-526.

Jones, M.B. and Humphries, S.W.(2002). Impacts of the C-4 Sedge Cyperus Papyrus L. On Carbon and Water Fluxes in an African Wetland, *Hydrobiologia* **488**, 107-113.

Joos, F., Prentice, I.C., Sitch, S., Meyer, R., Hooss, G., Plattner, G.K., Gerber, S., and Hasselmann, K.(2001b). Global Warming Feedbacks on Terrestrial Carbon Uptake under the Intergovernmental Panel on Climate Change (Ipcc) Emission Scenarios, *Global Biogeochemical Cycles* **15**, 891-907.

Ju, W.M. and Chen, J.M.(2005). Distribution of Soil Carbon Stocks in Canada's Forests and Wetlands Simulated Based on Drainage Class, Topography and Remotely Sensed Vegetation Parameters, *Hydrological Processes* **19**, 77-94.

Ju, W.M., Chen, J.M., Black, T.A., Barr, A.G., Liu, J., and Chen, B.Z.(2006a). Modelling Multi-Year Coupled Carbon and Water Fluxes in a Boreal Aspen Forest, *Agricultural and Forest Meteorology* **140** , 136-151.

Ju, W.M., Chen, J.M., Black, T.A., Barr, A.G., Mccaughey, H., and Roulet, N.T.(2006c). Hydrological Effects on Carbon Cycles of Canada's Forests and Wetlands, *Tellus Series B-Chemical and Physical Meteorology* **58**, 16-30.

Kane, E.S., Valentine, D.W., Michaelson, G.J., Fox, J.D., and Ping, C.L.(2006). Controls over Pathways of Carbon Efflux from Soils along Climate and Black Spruce Productivity Gradients in Interior Alaska, *Soil Biology & Biochemistry* **38**, 1438-1450.

Keeling, C.D., Chin, J.F.S., and Whorf, T.P.(1996). Increased Activity of Northern Vegetation Inferred From Atmospheric Co2 Measurements, *Nature* **382**, 146-149.

Keeling, C.D., Whorf, T.P., Wahlen, M., and Vanderplicht, J.(1995). Interannual Extremes in the Rate of Rise of Atmospheric Carbon-Dioxide Since 1980, *Nature* **375**, 666-670.

Kelliher, F.M., Leuning, R., Raupach, M.R., and Schulze, E.D.(1995). Maximum Conductances for Evaporation From Global Vegetation Types, *Agricultural and Forest Meteorology* **73**, 1-16.

Kielland, K., Olson, K., Ruess, R.W., and Boone, R.D.(2006). Contribution of Winter Processes to Soil Nitrogen Flux in Taiga Forest Ecosystems, *Biogeochemistry* **81**, 349-360.

Kim, J., Guo, Q., Baldocchi, D.D., Leclerc, M., Xu, L., and Schmid, H.P.(2006). Upscaling Fluxes From Tower to Landscape: Overlaying Flux Footprints on High-Resolution (Ikonos) Images of Vegetation Cover, *Agricultural and Forest Meteorology* **136**, 132-146.

Kleynhans, M.T., James, C.S., and Birkhead, A.L.(2007). Hydrologic and Hydraulic Modelling of the Nyl River Floodplain Part 3: Applications to Assess Ecological Impact, *Water Sa* **33**, 21-25.

Knapp, A.K., Fahnestock, J.T., Hamburg, S.P., Statland, L.B., Seastedt, T.R., and Schimel, D.S.(1993). Landscape Patterns in Soil Plant Water Relations and Primary Production in Tallgrass Prairie, *Ecology* **74**, 549-560.

Kolchugina, T.P. and Vinson, T.S.(1993). Equilibrium-Analysis of Carbon Pools and Fluxes of Forest Biomes in the Former Soviet-Union, *Canadian Journal of Forest Research-Revue Canadienne De Recherche Forestiere* **23**, 81-88.

Koster, R.D., Guo, Z.C., Dirmeyer, P.A., Bonan, G., Chan, E., Cox, P., Davies, H., Gordon, C.T., Kanae, S., Kowalczyk, E., Lawrence, D., Liu, P., Lu, C.H., Malyshev, S., Mcavaney, B., Mitchell, K., Mocko, D., Oki, T., Oleson, K.W., Pitman, A., Sud, Y.C., Taylor, C.M., Verseghy, D., Vasic, R., Xue, Y.K., and Yamada, T.(2006). Glace: the Global Land-Atmosphere Coupling Experiment. Part I: Overview, *Journal of Hydrometeorology* **7**, 590-610.

Kowalski, A.S., Loustau, D., Berbigier, P., Manca, G., Tedeschi, V., Borghetti, M., Valentini, R., Kolari, P., Berninger, F., Rannik, U., Hari, P., Rayment, M., Mencuccini, M., Moncrieff, J., and Grace, J.(2004). Paired Comparisons of Carbon Exchange Between Undisturbed and Regenerating Stands in Four Managed Forests in Europe, *Global Change Biology* **10**, 1707-1723.

Kozlowski, T.T.(2000). Responses of Woody Plants to Human-Induced Environmental Stresses: Issues, Problems, and Strategies for Alleviating Stress, *Critical Reviews in Plant Sciences* **19**, 91-170.

Kravchenko, I.K.(2002). Methane Oxidation in Boreal Peat Soils Treated With Various Nitrogen Compounds, *Plant and Soil* **242**, 157-162.

Kuchment, L.S., Demidov, V.N., and Startseva, Z.P.(2006). Coupled Modeling of the Hydrological and Carbon Cycles in the Soil-Vegetation-Atmosphere System, *Journal of Hydrology* **323**, 4-21.

Kumagai, T., Katul, G.G., Saitoh, T.M., Sato, Y., Manfroi, O.J., Morooka, T., Ichie, T., Kuraji, K., Suzuki, M., and Porporato, A.(2004). Water Cycling in a Bornean Tropical Rain Forest Under Current and Projected Precipitation Scenarios, *Water Resources Research* **40**.

Kundzewicz, Z.W.(2002). Ecohydrology - Seeking Consensus on Interpretation of the Notion, *Hydrological Sciences Journal-Journal Des Sciences Hydrologiques* **47**, 799-804.

Lacey, G.C. and Grayson, R.B.(1998). Relating Baseflow to Catchment Properties in South-Eastern Australia, *Journal of Hydrology* **204**, 231-250.

Lafleur, P.M., Moore, T.R., Roulet, N.T., and Frolking, S.(2005). Ecosystem Respiration in a Cool Temperate Bog Depends on Peat Temperature but Not Water Table, *Ecosystems* **8**, 619-629.

Lal, R.(2005). Forest Soils and Carbon Sequestration, *Forest Ecology and Management* **220**, 242-258.

Landsberg, J.J. and Waring, R.H.(1997). A Generalised Model of Forest Productivity Using Simplified Concepts of Radiation-Use Efficiency, Carbon Balance and Partitioning, *Forest Ecology and Management* **95**, 209-228.

Lavigne, M.B., Foster, R.J., and Goodine, G.(2004). Seasonal and Annual Changes in Soil Respiration in Relation to Soil Temperature, Water Potential and Trenching, *Tree Physiology* **24**, 415-424.

Leuning, R., Dunin, F.X., and Wang, Y.P.(1998). A Two-Leaf Model for Canopy Conductance,

Photosynthesis and Partitioning of Available Energy. Comparison With Measurements, *Agricultural and Forest Meteorology* **91**, 113-125.

Linne, H., Hennemuth, B., Bosenberg, J., and Ertel, K.(2007). Water Vapour Flux Profiles in the Convective Boundary Layer, *Theoretical and Applied Climatology* **87**, 201-211.

Liu, J., Chen, J.M., Cihlar, J., and Park, W.M.(1997a). A Process-Based Boreal Ecosystem Productivity Simulator Using Remote Sensing Inputs, *Remote Sensing of Environment* **62**, 158-175.

Luo, Y.Q., White, L.W., Canadell, J.G., Delucia, E.H., Ellsworth, D.S., Finzi, A., Lichter, J., and Schlesinger, W.H.(2003). Sustainability of Terrestrial Carbon Sequestration: a Case Study in Duke Forest With Inversion Approach, *Global Biogeochemical Cycles* **17**.

Manzoni, S. and Porporato, A.(2007). Theoretical Analysis of Nonlinearities and Feedbacks in Soil Carbon and Nitrogen Cycles, *Soil Biology & Biochemistry* **39**, 1542-1556.

Margolis, H.A., Flanagan, L.B., and Amiro, B.D.(2006). The Fluxnet-Canada Research Network: Influence of Climate and Disturbance on Carbon Cycling in Forests and Peatlands, *Agricultural and Forest Meteorology* **140**, 1-5.

Martin, P.H., Valentini, R., Jacques, M., Fabbri, K., Galati, D., Quaratino, R., Moncrieff, J.B., Jarvis, P., Jensen, N.O., Lindroth, A., Grelle, A., Aubinet, M., Ceulemans, R., Kowalski, A.S., Vesala, T., Keronen, P., Matteucci, G., Grainer, A., Berbingier, P., Loustau, D., Grelle, A., Schulze, E.D., Tenhunen, J., Rebman, C., Dolman, A.J., Elbers, J.E., Bernhofer, C., Grunwald, T., Thorgeirsson, H., Kennedy, P., and Folving, S.(1998). New Estimate of the Carbon Sink Strength of Eu Forests Integrating Flux Measurements, Field Surveys, and Space Observations: 0.17-0.35 Gt(C), *Ambio* **27**, 582-584.

Mcguffie, K. and Henderson-Sellers, A.(2001). Forty Years of Numerical Climate Modelling, *International Journal of Climatology* **21**, 1067-1109.

Melillo, J.M., Aber, J.D., Linkins, A.E., Ricca, A., Fry, B., and Nadelhoffer, K.J.(1989). Carbon and Nitrogen Dynamics Along the Decay Continuum - Plant Litter to Soil Organic-Matter, *Plant and Soil* **115**, 189-198.

Miglietta, F., Gioli, B., Hutjes, R.W.A., and Reichstein, M.(2007). Net Regional Ecosystem Co2 Exchange From Airborne and Ground-Based Eddy Covariance, Land-Use Maps and Weather Observations, *Global Change Biology* **13**, 548-560.

Monson, R.K., Burns, S.P., Williams, M.W., Delany, A.C., Weintraub, M., and Lipson, D.A.(2006). The Contribution of Beneath-Snow Soil Respiration to Total Ecosystem Respiration in a High-Elevation, Subalpine Forest, *Global Biogeochemical Cycles* **20**.

Moore, T.R., Bubier, J.L., Frolking, S.E., Lafleur, P.M., and Roulet, N.T.(2002). Plant Biomass and Production and Co2 Exchange in an Ombrotrophic Bog, *Journal of Ecology* **90**, 25-36.

Naeem, S., Thompson, L.J., Lawler, S.P., Lawton, J.H., and Woodfin, R.M.(1995). Empirical-Evidence

That Declining Species-Diversity May Alter the Performance of Terrestrial Ecosystems, *Philosophical Transactions of the Royal Society of London Series B-Biological Sciences* **347** , 249-262.

Neff, J.C. and Asner, G.P.(2001). Dissolved Organic Carbon in Terrestrial Ecosystems: Synthesis and a Model, *Ecosystems* **4**, 29-48.

Nelson, F.E.(2003). (Un)Frozen in Time , *Science* **299**, 1673-1675.

Nemani, R., White, M., Thornton, P., Nishida, K., Reddy, S., Jenkins, J., and Running, S.(2002). Recent Trends in Hydrologic Balance Have Enhanced the Terrestrial Carbon Sink in the United States, *Geophysical Research Letters* **29**.

Nikolov, N.T., Massman, W.J., and Schoettle, A.W.(1995). Coupling Biochemical and Biophysical Processes at the Leaf Level - an Equilibrium Photosynthesis Model for Leaves of C-3 Plants, *Ecological Modelling* **80**, 205-235.

Norby, R.J., Edwards, N.T., Riggs, J.S., Abner, C.H., Wullschleger, S.D., and Gunderson, C.A.(1997). Temperature-Controlled Open-Top Chambers for Global Change Research, *Global Change Biology* **3**, 259-267.

Novick, K.A., Stoy, P.C., Katul, G.G., Ellsworth, D.S., Siqueira, M.B.S., Juang, J., and Oren, R.(2004). Carbon Dioxide and Water Vapor Exchange in a Warm Temperate Grassland, *Oecologia* **138**, 259-274.

Oechel, W.C., Vourlitis, G.L., Verfaillie, J., Crawford, T., Brooks, S., Dumas, E., Hope, A., Stow, D., Boynton, B., Nosov, V., and Zulueta, R.(2000). A Scaling Approach for Quantifying the Net Co2 Flux of the Kuparuk River Basin, Alaska, *Global Change Biology* **6**, 160-173.

Overpeck, J., Hughen, K., Hardy, D., Bradley, R., Case, R., Douglas, M., Finney, B., Gajewski, K., Jacoby, G., Jennings, A., Lamoureux, S., Lasca, A., Macdonald, G., Moore, J., Retelle, M., Smith, S., Wolfe, A., and Zielinski, G.(1997). Arctic Environmental Change of the Last Four Centuries, *Science* **278**, 1251-1256.

Panikova, N.S., Flanaganb, P.W., Oechelc, W.C., Mastepanovd, M.A., and Christensend, T.R.(2006). Microbial Activity in Soils Frozen to Below-39 Degrees C, *Soil Biology & Biochemistry* **38**, 785-794.

Pitman, A.J., Henderson-Sellers, A., Desborough, C.E., Yang, Z.L., Abramopoulos, F., Boone, A., Dickinson, R.E., Gedney, N., Koster, R., Kowalczyk, E., Lettenmaier, D., Liang, X., Mahfouf, J.F., Noilhan, J., Polcher, J., Qu, W., Robock, A., Rosenzweig, C., Schlosser, C.A., Shmakin, A.B., Smith, J., Suarez, M., Verseghy, D., Wetzel, P., Wood, E., and Xue, Y.(1999). Key Results and Implications From Phase 1(C) of the Project for Intercomparison of Land-Surface Parametrization Schemes, *Climate Dynamics* **15**, 673-684.

Porporato, A., D'odorico, P., Laio, F., and Rodriguez-Iturbe, I.(2003). Hydrologic Controls on Soil Carbon and Nitrogen Cycles. I. Modeling Scheme, *Advances in Water Resources* **26**, 45-58.

Porporato, A. and Rodriguez-Iturbe, I.(2002). Ecohydrology - a Challenging Multidisciplinary Research

Perspective, *Hydrological Sciences Journal-Journal Des Sciences Hydrologiques* **47**, 811-821.

Potter, C., Klooster, S., De Carvalho, C.R., Genovese, V.B., Torregrosa, A., Dungan, J., Bobo, M., and Coughlan, J.(2001). Modeling Seasonal and Interannual Variability in Ecosystem Carbon Cycling for the Brazilian Amazon Region, *Journal of Geophysical Research-Atmospheres* **106**, 10423-10446.

Prentice, I.C., Farquhar, G.D., Fasham, M.J.R., Golden, M.L., Heiman, M., Jaramillo, V.J., Kheshgi, H.S., Quere, C.Le., Scholes, R.J., and Wallace, D.W.R. : 2001, 'The carbon cycle nd atmopshere carbon dioixide ', *In* Houghton, J.T., Ding, Y., Griggs, D.J., Noguer, M., Linden, P.J.v.d., Dai, X., Maskell, K., and Johnson, C.A., eds. Climate Change 2001: the scientific basis. Contribution of Working Group I to the Third Assessment Report of the Intergovernmental Panel on Climate Change , Cambridg University Press, Cambridg, UK.

Price, A.G., Dunham, K., Carleton, T., and Band, L.(1997). Variability of Water Fluxes Through the Black Spruce (Picea Mariana) Canopy and Feather Moss (Pleurozium Schreberi) Carpet in the Boreal Forest of Northern Manitoba, *Journal of Hydrology* **196**, 310-323.

Prietofernandez, A., Villar, M.C., Carballas, M., and Carballas, T.(1993). Short-Term Effects of a Wildfire on the Nitrogen Status and Its Mineralization Kinetics in an Atlantic Forest Soil, *Soil Biology & Biochemistry* **25**, 1657-1664.

Prokushkin, A.S., Knorre, A.A., Kirdyanov, A.V., and Schulze, E.D.(2006). Productivity of Mosses and Organic Matter Accumulation in the Litter of Sphagnum Larch Forest in the Permafrost Zone, *Russian Journal of Ecology* **37**, 225-232.

Prueger, J.H., Hatfield, J.L., Kustas, W.P., Hipps, L.E., Macpherson, J.I., Neale, C.M.U., Eichinger, W.E., Cooper, D.I., and Parkin, T.B.(2005). Tower and Aircraft Eddy Covariance Measurements of Water Vapor, Energy, and Carbon Dioxide Fluxes During Smacex, *Journal of Hydrometeorology* **6**, 954-960.

Rannik, U., Kolari, P., Vesala, T., and Hari, P.(2006). Uncertainties in Measurement and Modelling of Net Ecosystem Exchange of a Forest, *Agricultural and Forest Meteorology* **138**, 244-257.

Rinne, J., Riutta, T., Pihlatie, M., Aurela, M., Haapanala, S., Tuovinen, J.P., Tuittila, E.S., and Vesala, T.(2007). Annual Cycle of Methane Emission From a Boreal Fen Measured by the Eddy Covariance Technique, *Tellus Series B-Chemical and Physical Meteorology* **59**, 449-457.

Rodriguez-Iturbe, I., D'odorico, P., Porporato, A., and Ridolfi, L.(1999). On the Spatial and Temporal Links Between Vegetation, Climate, and Soil Moisture, *Water Resources Research* **35**, 3709-3722.

Rodriguez-Iturbe, I., Porporato, A., Laio, F., and Ridolfi, L.(2001). Plants in Water-Controlled Ecosystems: Active Role in Hydrologic Processes and Response to Water Stress - I. Scope and General Outline, *Advances in Water Resources* **24**, 695-705.

Running, S.W.(1994). Testing Forest-Bgc Ecosystem Process Simulations Across a Climatic Gradient in Oregon, *Ecological Applications* **4**, 238-247.

Schilling, K. and Zhang, Y.K.(2004). Baseflow Contribution to Nitrate-Nitrogen Export From a Large, Agricultural Watershed, Usa, *Journal of Hydrology* **295**, 305-316.

Schimel, D.S.(1995). Terrestrial Biogeochemical Cycles - Global Estimates With Remote-Sensing, *Remote Sensing of Environment* **51**, 49-56.

Schlesinger, W.H.(2000). Carbon Sequestration in Soils: Some Cautions Amidst Optimism, *Agriculture Ecosystems & Environment* **82**, 121-127.

Schlesinger, W.H. and Andrews, J.A.(2000). Soil Respiration and the Global Carbon Cycle, *Biogeochemistry* **48**, 7-20.

Schlesinger, W.H. and Lichter, J.(2001). Limited Carbon Storage in Soil and Litter of Experimental Forest Plots Under Increased Atmospheric CO_2, *Nature* **411**, 466-469.

Schroter, D., Wolters, V., and De Ruiter, P.C.(2003). C and N Mineralisation in the Decomposer Food Webs of a European Forest Transect, *Oikos* **102**, 294-308.

Schulze, E.D.(2006). Biological Control of the Terrestrial Carbon Sink, *Biogeosciences* **3**, 147-166.

Schulze, E.D., Kelliher, F.M., Korner, C., Lloyd, J., and Leuning, R.(1994). Relationships Among Maximum Stomatal Conductance, Ecosystem Surface Conductance, Carbon Assimilation Rate, and Plant Nitrogen Nutrition - a Global Ecology Scaling Exercise, *Annual Review of Ecology and Systematics* **25**, 629-&.

Schulze, E.D., Leuning, R., and Kelliher, F.M.(1995). Environmental Regulation of Surface Conductance for Evaporation From Vegetation, *Vegetatio* **121**, 79-87.

Schulze, E.D., Robichaux, R.H., Grace, J., Rundel, P.W., and Ehleringer, J.R.(1987). Plant Water-Balance, *Bioscience* **37**, 30-37.

Sellers, P.J., Hall, F.G., Kelly, R.D., Black, A., Baldocchi, D., Berry, J., Ryan, M., Ranson, K.J., Crill, P.M., Lettenmaier, D.P., Margolis, H., Cihlar, J., Newcomer, J., Fitzjarrald, D., Jarvis, P.G., Gower, S.T., Halliwell, D., Williams, D., Goodison, B., Wickland, D.E., and Guertin, F.E.(1997). Boreas in 1997: Experiment Overview, Scientific Results, and Future Directions, *Journal of Geophysical Research-Atmospheres* **102**, 28731-28769.

Sellers, P.J., Mintz, Y., Sud, Y.C., and Dalcher, A.(1986). A Simple Biosphere Model (SiB) for Use Within General-Circulation Models, *Journal of the Atmospheric Sciences* **43**, 505-531.

Sellers, P.J., Randall, D.A., Collatz, G.J., Berry, J.A., Field, C.B., Dazlich, D.A., Zhang, C., Collelo, G.D., and Bounoua, L.(1996a). A Revised Land Surface Parameterization (Sib2) for Atmospheric Gcms. Part I: Model Formulation, *Journal of Climate* **9**, 676-705.

Shashkov, A., Higuchi, K., and Chan, D.(2007). Aircraft Vertical Profiling of Variation of Co2 Over a Canadian Boreal Forest Site: a Role of Advection in the Changes in the Atmospheric Boundary

Layer Co2 Content, *Tellus Series B-Chemical and Physical Meteorology* **59**, 234-243.

Shibu, M.E., Leffelaar, P.A., Van Keulen, H., and Aggarwal, P.K.(2006). Quantitative Description of Soil Organic Matter Dynamics - a Review of Approaches With Reference to Rice-Based Cropping Systems, *Geoderma* **137**, 1-18.

Sitch, S., Brovkin, V., Von Bloh, W., Van Vuuren, D., Assessment Bene, and Ganopolski, A.(2005). Impacts of Future Land Cover Changes on Atmospheric Co2 and Climate, *Global Biogeochemical Cycles* **19**.

Sivapalan, M., Beven, K., and Wood. E.F(1987). On Hydrologic Similarity, 2. A Scaled Model of Storm Runoff Producton, *Water Resources Research* **23**, 2266-2278.

Soja, A.J., Cofer, W.R., Shugart, H.H., Sukhinin, A.I., Stackhouse, P.W., Mcrae, D.J., and Conard, S.G.(2004). Estimating Fire Emissions and Disparities in Boreal Siberia (1998-2002), *Journal of Geophysical Research-Atmospheres* **109**.

Steinfeld, G., Letzel, M.O., Raasch, S., Kanda, M., and Inagaki, A.(2007). Spatial Representativeness of Single Tower Measurements and the Imbalance Problem With Eddy-Covariance Fluxes: Results of a Large-Eddy Simulation Study, *Boundary-Layer Meteorology* **123**, 77-98.

Su, H.B., Schmid, H.P., Grimmond, C.S.B., Vogel, C.S., and Oliphant, A.J.(2004). Spectral Characteristics and Correction of Long-Term Eddy-Covariance Measurements Over Two Mixed Hardwood Forests in Non-Flat Terrain, *Boundary-Layer Meteorology* **110**, 213-253.

Syed, K.H., Flanagan, L.B., Carlson, P.J., Glenn, A.J., and Van Gaalen, K.E.(2006). Environmental Control of Net Ecosystem Co2 Exchange in a Treed, Moderately Rich Fen in Northern Alberta, *Agricultural and Forest Meteorology* **140**, 97-114.

Szlavecz, K., Placella, S.A., Pouyat, R.V., Groffman, P.M., Csuzdi, C., and Yesilonis, I.(2006). Invasive Earthworm Species and Nitrogen Cycling in Remnant Forest Patches, *Applied Soil Ecology* **32**, 54-62.

Tague, C.L. and Band, L.E.(2004). RHESSys: Regional Hydro-Ecologic Simulation System—An Object-Oriented Approach to Spatially Distributed Modeling of Carbon, Water, and Nutrient Cycling, *Earth Interactions* 1–42.

Tan, X. and Chang, S.X.(2007). Soil Compaction and Forest Litter Amendment Affect Carbon and Net Nitrogen Mineralization in a Boreal Forest Soil, *Soil & Tillage Research* **93**, 77-86.

Tanaka, S., Ando, T., Funakawa, S., Sukhrun, C., Kaewkhongkha, T., and Sakurai, K.(2001). Effect of Burning on Soil Organic Matter Content and N Mineralization Under Shifting Cultivation System of Karen People in Northern Thailand, *Soil Science and Plant Nutrition* **47**, 547-558.

Tardieu, F., Zhang, J., and Davies, W.J.(1992). What Information Is Conveyed by an Aba Signal From Maize Roots in Drying Field Soil, *Plant Cell and Environment* **15**, 185-191.

Thompson, M.V., Randerson, J.T., Malmstrom, C.M., and Field, C.B.(1996). Change in Net Primary

Production and Heterotrophic Respiration: How Much Is Necessary to Sustain the Terrestrial Carbon Sink?, *Global Biogeochemical Cycles* **10**, 711-726.

Throop, H.L., Holland, E.A., Parton, W.J., Ojima, D.S., and Keough, C.A.(2004). Effects of Nitrogen Deposition and Insect Herbivory on Patterns of Ecosystem-Level Carbon and Nitrogen Dynamics: Results From the Century Model, *Global Change Biology* **10**, 1092-1105.

Townsend, A.R., Braswell, B.H., Holland, E.A., and Penner, J.E.(1996). Spatial and Temporal Patterns in Terrestrial Carbon Storage Due to Deposition of Fossil Fuel Nitrogen, *Ecological Applications* **6**, 806-814.

Traore, S., Thiombiano, L., Millogo, J.R., and Guinko, S.(2007). Carbon and Nitrogen Enhancement in Cambisols and Vertisols by Acacia Spp. In Eastern Burkina Faso: Relation to Soil Respiration and Microbial Biomass, *Applied Soil Ecology* **35**, 660-669.

Turnipseed, A.A., Anderson, D.E., Blanken, P.D., Baugh, W.M., and Monson, R.K.(2003). Airflows and Turbulent Flux Measurements in Mountainous Terrain Part 1. Canopy and Local Effects, *Agricultural and Forest Meteorology* **119**, 1-21.

Valentini, R., Matteucci, G., Dolman, A.J., Schulze, E.D., Rebmann, C., Moors, E.J., Granier, A., Gross, P., Jensen, N.O., Pilegaard, K., Lindroth, A., Grelle, A., Bernhofer, C., Grunwald, T., Aubinet, M., Ceulemans, R., Kowalski, A.S., Vesala, T., Rannik, U., Berbigier, P., Loustau, D., Guomundsson, J., Thorgeirsson, H., Ibrom, A., Morgenstern, K., Clement, R., Moncrieff, J., Montagnani, L., Minerbi, S., and Jarvis, P.G.(2000). Respiration As the Main Determinant of Carbon Balance in European Forests, *Nature* **404**, 861-865.

Van Hees, P.A.W., Jones, D.L., Finlay, R., Godbold, D.L., and Lundstomd, U.S.(2005). The Carbon We Do Not See - the Impact of Low Molecular Weight Compounds on Carbon Dynamics and Respiration in Forest Soils: a Review, *Soil Biology & Biochemistry* **37**, 1-13.

Vazquez, R.F. and Feyen, J.(2007). Assessment of the Effects of Dem Gridding on the Predictions of Basin Runoff Using Mike She and a Modelling Resolution of 600 M, *Journal of Hydrology* **334**, 73-87.

Verseghy, D.L.(1991). Class-a Canadian Land Surface Scheme for Gcms .1. Soil Model, *International Journal of Climatology* **11**, 111-133.

Vinuesa, J.F. and De Arellano, J.V.G.(2003). Fluxes and (Co-)Variances of Reacting Scalars in the Convective Boundary Layer, *Tellus Series B-Chemical and Physical Meteorology* **55**, 935-949.

Waelbroeck, C.(1993). Climate Soil Processes in the Presence of Permafrost - a Systems Modeling Approach, *Ecological Modelling* **69**, 185-225.

Wang, W.G., Davis, K.J., Cook, B.D., Butler, M.P., and Ricciuto, D.M.(2006). Decomposing Co2 Fluxes Measured Over a Mixed Ecosystem at a Tall Tower and Extending to a Region: a Case Study, *Journal of Geophysical Research-Biogeosciences* **111**.

Wang, Y.P. and Leuning, R.(1998). A Two-Leaf Model for Canopy Conductance, Photosynthesis and Partitioning of Available Energy I: Model Description and Comparison With a Multi-Layered

Model, *Agricultural and Forest Meteorology* **91**, 89-111.

White, A., Cannell, M.G.R., and Friend, A.D.(2000). The High-Latitude Terrestrial Carbon Sink: a Model Analysis, *Global Change Biology* **6**, 227-245.

Wigmosta, M.S. and Lettenmaier, D.P.(1999). A Comparison of Simplified Methods for Routing Topographically Driven Subsurface Flow, *Water Resources Research* **35**, 255-264.

Wong, S.C., Cowan, I.R., and Farquhar, G.D.(1985). Leaf Conductance in Relation to Rate of Co2 Assimilation .3. Influences of Water-Stress and Photoinhibition, *Plant Physiology* **78**, 830-834.

Woodward, F.I. and Friend, A.D.(1988). Controlled Environment Studies on the Temperature Responses of Leaf Extension in Species of Poa With Diverse Altitudinal Ranges, *Journal of Experimental Botany* **39**, 411-420.

Yi, C., Davis, K.J., Bakwin, P.S., Denning, A.S., Zhang, N., Desai, A., Lin, J.C., and Gerbig, C.(2004). Observed Covariance Between Ecosystem Carbon Exchange and Atmospheric Boundary Layer Dynamics at a Site in Northern Wisconsin, *Journal of Geophysical Research-Atmospheres* **109**.

Zalewski, M.(2002). Ecohydrology - the Use of Ecological and Hydrological Processes for Sustainable Management of Water Resources, *Hydrological Sciences Journal-Journal Des Sciences Hydrologiques* **47**, 823-832.

Zgallai, H., Steppe, K., and Lemeur, R.(2006). Effects of Severe Water Stress on Partitioning of C-14-Assimilates in Tomato Plants, *Journal of Applied Botany and Food Quality-Angewandte Botanik* **80**, 88-92.

Zhang, Y., Grant, R.F., Flanagan, L.B., Wang, S., and Verseghy, D.L.(2005). Modelling Co2 and Energy Exchanges in a Northern Semiarid Grassland Using the Carbon- and Nitrogen-Coupled Canadian Land Surface Scheme (C-Class), *Ecological Modelling* **181**, 591-614.

Zhang, Y.P., Sha, L.Q., Yu, G.R., Song, Q.H., Tang, J.W., Yang, X.D., Wang, Y.S., Zheng, Z., Zhao, S.J., Yang, Z., and Sun, X.M.(2006). Annual Variation of Carbon Flux and Impact Factors in the Tropical Seasonal Rain Forest of Xishuangbanna, Sw China, *Science in China Series D-Earth Sciences* **49**, 150-162.

Zhou, S.Q., Chen, J.M., Peng, G., and Xue, G.Y.(2006). Effects of Heterogeneous Vegetation on the Surface Hydrological Cycle, *Advances in Atmospheric Sciences* **23**, 391-404.

Zhuang, Q., Mcguire, A.D., Melillo, J.M., Clein, J.S., Dargaville, R.J., Kicklighter, D.W., Myneni, R.B., Dong, J., Romanovsky, V.E., Harden, J., and Hobbie, J.E.(2003). Carbon Cycling in Extratropical Terrestrial Ecosystems of the Northern Hemisphere During the 20th Century: a Modeling Analysis of the Influences of Soil Thermal Dynamics, *Tellus Series B-Chemical and Physical Meteorology* **55**, 751-776.

Zimov, S.A., Schuur, E.A.G., and Chapin, F.S.(2006). Permafrost and the Global Carbon Budget, *Science* **312**, 1612-1613.

CHAPTER 2.

Development of a Spatially Explicit Hydro-ecological Modeling Framework, BEPS-Terrainlab V2.0: Model Description and Test in a Boreal Ecosystem.

2.1 Abstract

A spatially explicit, process-based hydro-ecological model, BEPS-TerrainLab V2.0, was developed to improve the representation of ecophysiological, hydro-ecological and biogeochemical processes of boreal ecosystems in a tightly coupled manner. Several processes unique to boreal ecosystems were implemented in this model including the lateral water flow, stratification of vegetation into overstory, understory, and moss layers to calculate various processes. To account for preferential water fluxes through the moss-peat system in the boreal forest floor, a new parameterization scheme was introduced based on laboratory analyses. Upscaling of leaf-scale ecophysiological processes to the canopy scale were carried out while simultaneously considering variations in leaf physiological conditions. Explicit calculation of the aerodynamic resistance for each canopy layer further facilitated adequate representation of turbulent processes for evapotranspiration (ET). The modified model was tested with two years of continuous measurements taken at the Eastern Old Black Spruce Site of the Fluxnet-Canada Research Network located in a boreal watershed in north central Quebec, Canada. The model was tested by comparing the simulated and measured (or measurement-derived) ET, water table depth (WTD), volumetric water content (VSWC) and gross primary productivity (GPP). The model was able to explain 83% of the ET, 92% of the GPP variability and 72% of the WTD dynamics. Simulations indicated that in humid ecosystems such as eastern Canadian boreal watersheds, sub-surface baseflow is the main mechanism of soil water partitioning as opposed

to other processes such as surface overland flow or ET and that local hydrological conditions can have a strong influence on ecosystem physiology.

2.2. Introduction

Hydrological controls on carbon (C) cycles and their implications on global climate change have recently gained recognition (e.g., Gedney et al., 2006). Studies involving high frequency micrometeorological measurements have also demonstrated that there is a tight link between hydrological and C cycling processes, with mechanisms/processes operating differently at various spatio-temporal scales (e.g., Baldocchi et al., 1996; Verstraeten et al., 2006). There are several ecological processes that are highly sensitive to hydrological controls such as photosynthesis, heterotrophic respiration, redox-mediated methane production, and transport of dissolved organic carbon (DOC). Therefore, local hydrological regimes control the fluxes of mass and energy in the soil-plant-atmosphere continuum, although the extent that this is true in different boreal regions is still an open question.

At the landscape scale, topographical differences are the main cause of potential differences (gravitational), which control water movement and, therefore, local-scale water balance. Current regional estimates of biogeochemical cycles overlook the large variations caused by topographic effects on soil water, temperature and nutrient availability (Grant et al., 2004a). Simulation of soil moisture using implicit schemes such as bucket models, or using surrogates such as remote sensing-derived soil moisture products (e.g., radar), might be biased, especially for landscape scale applications, owing to large topographic variability (Soulis et al., 2000). In addition to its role in the redistribution of soil water, topography also has remarkable effects on modulating the microclimate, including temperature, precipitation and absorbed solar radiation (Wigmosta et al., 1994). Modeling studies have mostly focused on point-scale

processes (e.g., Grant et al., 2006; Ju et al., 2006a) or large-scale generalizations (e.g., Ju and Chen, 2005). Point-scale models do not adequately represent processes such as topographically driven lateral water fluxes and are therefore not hydrologically realistic.

Current advances in ecological research conducted at different spatial scales have lead to the development and testing of terrestrial ecosystem models that have various levels of sophistication. These ecosystem models have used different strategies to quantify soil-water controls on plant physiological mechanisms that determine ecosystem response. However, only a few of these models explicitly considered lateral hydrological processes to define local-scale water balance and have most often employed simplified schemes to partition various hydrological processes at the landscape scale. It is quite likely that unrealistic characterization of soil moisture could result in errors in simulated ecophysiological mechanisms due to the erroneous representation of plant physiological conditions. This warrants a more advanced integration of distributed hydrological modeling and ecological modeling to understand biogeochemical processes at the landscape scale more thoroughly.

Therefore, we developed a hydro-ecological model, BEPS-TerrainLab V2.0. The main objective of this paper is to introduce BEPS-TerrainLab V2.0 and test its performance by comparing its hydro-ecological simulations with continuous high precision measurements of various ecophysiological indicators measured on a boreal landscape in eastern Canada. We also document various hydro-ecological concepts and parameterizations that are used within the model.

2.3. Model Description

BEPS-TerrainLab V2.0 originated from the Boreal Ecosystem Productivity Simulator, (BEPS, Liu et al., 1997) that was developed during the Boreal Ecosystem-Atmosphere Study

(BOREAS). BEPS describes several biophysical processes such as canopy radiative transfer and stomatal dynamics; ecophysiological processes such as Gross Primary Productivity (GPP), evapotranspiration (ET) and autotrophic respiration, for a monolayer canopy, with emphasis on boreal forest ecosystems. BEPS represents the ecosystem primary production using a spatially and temporally upscaled version of the leaf-level instantaneous photosynthesis model of Farquhar et al. (1980). Ecosystem ET is calculated using the Penman-Monteith leaf level model that is spatially upscaled to the canopy scale. It uses a simplified parameterization to represent soil hydrological controls on the above-mentioned ecophysiological processes (bucket model), and simulates the fluxes of mass and energy across the soil-biosphere-atmosphere continuum.

BEPS-TerrainLab V1.0 (Chen et al., 2007) was an improvement in that it included a distributed hydrological model, TerrainLab (Chen et al., 2005b) that was coupled to BEPS. TerrainLab adopted concepts from Wigmosta et al. (1994) and it was tested in the Southern Study Area (SSA) of the BOREAS region to study the spatio-temporal variation of ET and soil moisture. El Maayar and Chen (2006) used TerrainLab to develop empirical spatial upscaling algorithms for ET. As a coupled version of BEPS and TerrainLab, Chen et al. (2007) used BEPS-TerrainLab V1.0 as a learning tool to understand the impact of landscape scale topographic variations on primary production in the mountainous areas of China. BEPS-TerrainLab V1.0 was further modified to include peatland specific parameterizations for studying coupled water and C cycling processes of the Mer Bleue bog in southern Ontario by Sonnentag et al. (2007). All of the above-mentioned studies were conducted during the growing season and the strong linkages between local hydrology and C cycling were not studied in detail. Moreover, the existence of many modeling gaps led to further improvements and eventually to the creation of BEPS-TerrainLab V2.0.

Most hydrological processes are explicitly described within the BEPS-TerrainLab V2.0 modeling unit. Furthermore, landscape scale hydrological processes that critically affect the local water balance are described based on topography. This facilitates adequate description of soil water regimes by solving a detailed water balance equation in a spatially explicit manner at daily time steps. The modeling unit (Figure 2-1) was designed initially to match with high-resolution remote sensing datasets, i.e., at 30 m. However, the model may be run at any spatial resolution by resampling the spatial input datasets.

BEPS-TerrainLab V2.0 introduces several modifications to its predecessor with a tighter coupling of hydrological, ecophysiological, C and biogeochemical cycles unique to boreal landscapes. A detailed documentation of various hydro-ecological processes considered in BEPS-TerrainLab V2.0 is given in the appendix section. Key areas of improvement are:

1. Inclusion of a preferential water flow mechanism that occurs within the boreal forest floor moss-peat complex, after characterizing some of the hydraulic properties of moss and peat using laboratory measurements.
2. Improved spatial upscaling of leaf-level photosynthesis and ET to the canopy scale, using fractions of leaf area index (LAI) that represents various levels of illumination (sunlit or shaded) and soil saturation (saturated or unsaturated) that return specific physiological characteristics to a leaf. This procedure mathematically mimics physiological conditions of leaves in a canopy.
3. Explicit calculation of photosynthesis and ET for various canopy layers, i.e., overstory, understory and moss layers, using specific biophysical parameters and upscaling schemes.

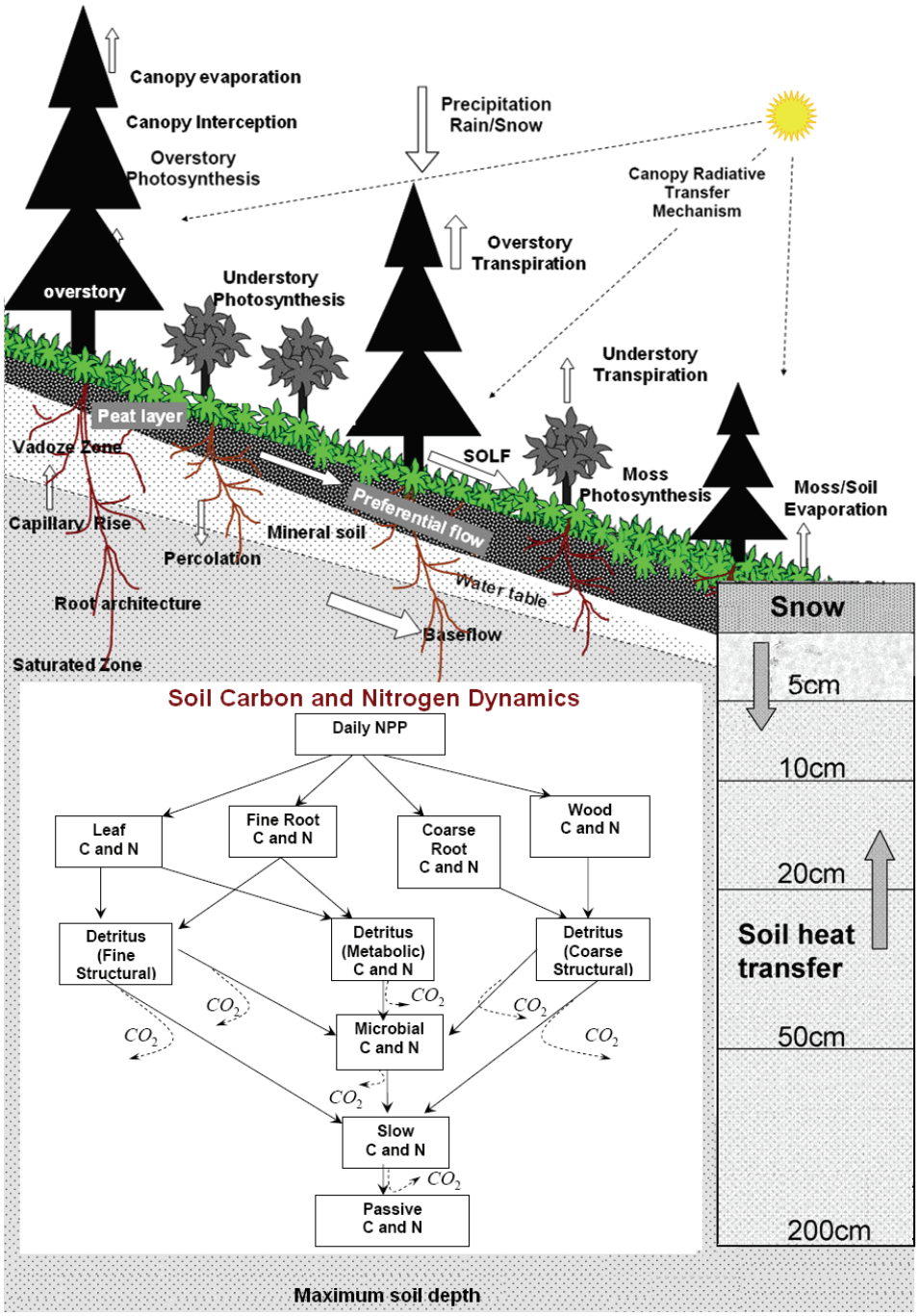

Figure 2-1. A schematic representation of a BEPS-TerrainLab V2.0 modelling unit. Most hydro-ecological processes are represented in this modeling unit. The soil profile is divided into saturated and unsaturated zones by the position of the water table. The lateral water fluxes that link neighboring pixels include sub-surface baseflow and surface overland flow that are topographically driven.

4. Explicit calculation of wind profiles within various canopy levels (overstory, understory and moss layers) leading to realistic representations of turbulent transfer and aerodynamic resistance terms that are adequate for ET calculations.

5. Calculation of topographically driven baseflow based on hydraulic head instead of the conventionally used topographic gradient. This is useful for boreal applications where the topographic differences are subtle.

6. Inclusion of a surface overland flow routing mechanism based on a quasi-physical modified Manning's approach.

In addition to hydro-ecological processes, BEPS-TerrainLab V2.0 also has a biogeochemical module. A detailed description of the biogeochemical module that considers soil C and nitrogen (N) dynamics can be found in Govind et al. (2008d).

2.4. Site Description

The simulation study was conducted on a boreal landscape located near Chibougamau in north-central Quebec, Canada. This landscape encompasses a black spruce-moss dominated boreal ecosystem. The Eastern Old Black Spruce site (EOBS) of the Fluxnet-Canada Research Network (FCRN), is located at 49.69^{o}N and 74.34^{o}W, which is ~50 km southeast of Lake Chibougamau and ~200 km northwest of Lac St. Jean. The climate of this region is cold temperate with a mean annual temperature of 0°C and a mean annual precipitation of 961.3 mm (Environment Canada, 2006). This landscape has a rolling topography with a gentle slope of < 5%, which is typical of the Canadian Shield. This gentle topography often represents eskers and other forms of glacial depositional features. Around 11,000-9,000 yrs B.P., retreat of the ice resulted in the deposition of glacial materials, on which the present soils have developed. Since

the soil is derived from glacio-fluvial deposits, it consists of poorly graded materials. Soil organic matter is composed mainly of moss necromass, which occurs throughout the region in poorly drained depressions or flat areas where black spruce trees dominate.

The vegetation on this boreal landscape is dominated by black spruce (*Picea mariana*) or aspen (*Populus sp.)* and birch (*Betula sp*) in the coniferous or mixed forest stands, respectively. Jack pine (*Pinus banksiana* Lamb.) and tamarack (*Larix larcinia*) also occur sporadically. The understory is mainly dominated by Labrador tea. The forest floor consists of a thick moss layer that is dominated by feather moss or lichens in the moderately dry areas and *Sphagnum sp* in wetter locations. At the landscape scale, vegetation varies across the gentle topographic gradient. On elevated parts of the landscape such as eskers, deciduous to mixed forest stands dominate. On relatively flat and low-lying locations, there is a species transition from dense black spruce–moss dominated stands to wetlands dominated by moss and stunted black spruce trees.

2.5. Spatial Data Set Preparation

Several spatially explicit input datasets are required to run BEPS-TerrainLab V2.0. Most of these spatial datasets were prepared by combining remote sensing, GIS, ground measurements and modeling. The details of the preparation of these datasets specific to this study are given below. Figures 2-2a to 2-2f show various spatial datasets used in this study. Land-cover-specific biophysical parameters are required to simulate ecophysiological and hydrological processes in a spatially explicit manner. For this study, a land-cover map was obtained from the Earth Observation for Sustainable Development of Forests, EOSD, a joint project between the Canadian Forest Service and the Canadian Space Agency. Since land-cover data is qualitative information, resampling a land-cover map is likely to create many errors. The

EOSD land-cover product was available at 25 m resolution, which thus required that all other spatial input datasets be resampled to 25 m resolution and reprojected to UTM zone 18N. In 2005, we conducted a ground truth validation campaign and confirmed that the EOSD land-cover product was of high quality. Table 2-2 shows some of the major land-cover specific biophysical parameters used in this study.

A digital elevation model (DEM) was obtained from the Canadian Council of Geomatics (CCG), which was further processed to make it hydrologically consistent, using the spatial information on lakes and rivulets in the form of vector data. Further to this, a watershed boundary was delineated based on the topography, using the ArcHydro tool in ArcGIS 9.1. Since this boreal landscape has subtle topographic variations, delineation of a watershed based on topography was difficult. We used several of Strahler's stream order thresholds until a watershed boundary was derived that also retained the 1 km^2 footprint area (explained in section 2.6) of the eddy covariance tower at the EOBS site. The watershed boundary is shown in Figures 2-2A to 2F.

Leaf abundance is the key parameter that controls the interception of solar energy by vegetation. The process of photosynthesis uses intercepted solar energy to fix atmospheric CO_2. Conventionally, leaf abundance is quantified using leaf area index, LAI. In BEPS-TerrainLab V2.0, LAI is used to model radiative transfer within plant canopies that govern many processes such as evaporation, transpiration, photosynthesis and snowmelt. As well, upscaling of leaf-scale ecophysiological processes to the canopy scale is carried out using LAI. Therefore, it is quite important to have accurate LAI estimates. Watershed scale spatially explicit LAI data were obtained by combining remote sensing techniques and ground-based LAI measurements. We used a Landsat-TM image (path-16 row-25) to derive a watershed scale NDVI map after adequate atmospheric corrections were carried out with the 6S model using MODIS-derived

atmospheric aerosol data. Further, ground-measured LAI along a designated 400 m transect (Chen et al., 2006) was correlated to satellite-derived NDVI to derive a site-specific LAI-NDVI algorithm (Figure 2-3). We also inverted the watershed scale NDVI using a site-specific algorithm to derive a watershed scale LAI map.

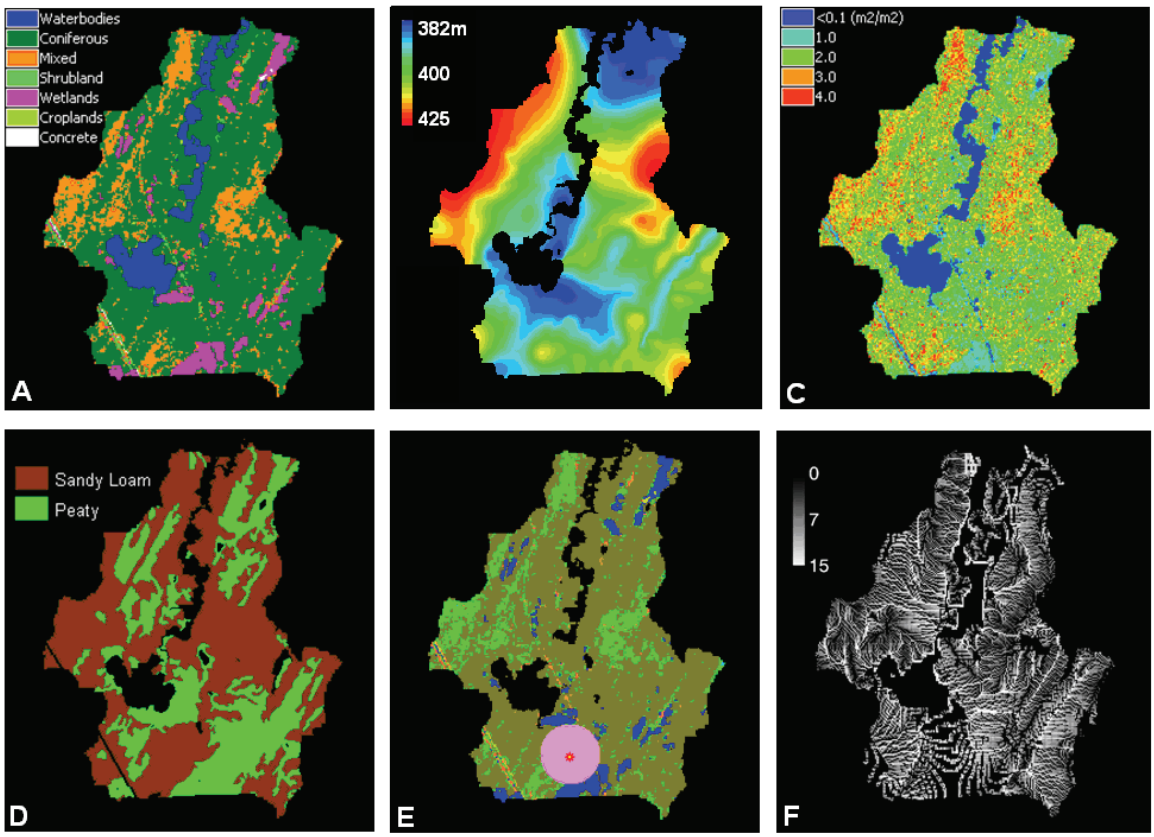

Figure 2-2. Various spatial datasets required to run BEPS-TerrainLabV2.0 at a daily time step. These datasets include (A) A validated land cover map (B) Digital elevation model (DEM) that was further processed to make it hydrologically consistent. Aspect and slope were derived from the DEM. (C) Leaf area index (LAI) map derived using remote sensing and ground based measurements and (D) Soil textural class. All the data sets have a spatial resolution of 25 x 25 m. Projection is UTM Zone 18N; (E) The ~1km^2 foot print region of the tower; and (F) Wetness Index used for a topography-based initialization of WTD.

Soil texture is important information that is essential to parameterize soil hydraulic properties. Currently, there is very little soil information for much of northern boreal regions in Canada at fine spatial resolution. Hence, a watershed scale soil texture map was derived using a look-up table that combined information on plot scale soil textural analysis conducted by Bernier et al. (2005), soil surface-deposit type obtained from the Quebec Ministry of Natural Resources and land-cover. Soil texture was determined according to the USDA textural classification with the inclusion of "peat" predominantly found in boreal ecosystems. Soil texture-specific hydraulic properties were assigned based on Rawls et al. (1982). To parameterize peat saturated hydraulic conductivity, we conducted a laboratory measurement using a constant head permeameter method. Table 2-1 shows the specific soil texture parameters used in this study.

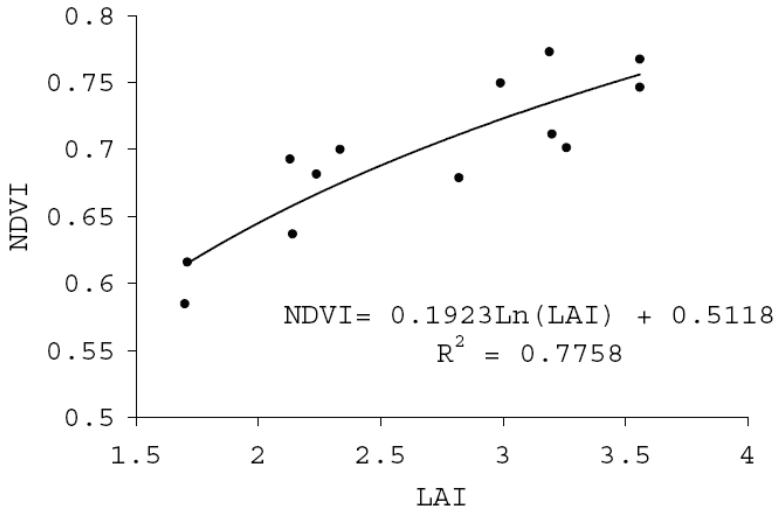

Figure 2-3. NDVI-LAI algorithm developed using ground based LAI measurements (taken along an east – west transect during the 2003 growing season) and remote sensing derived NDVI values. This algorithm was inverted and applied to the entire watershed to derive a watershed scale LAI map.

Table 2-1. Hydraulic properties of various soil types in the watershed

Hydraulic Property	Symbol	Unit	Sandy Loam	Peat
Field Capacity	θ_{330}	%	0.33[a,d]	0.45[b]
Permanent wilting Point	θ_{1500}	%	0.10[c,d]	0.10[b]
Porosity	ϕ	%	0.46[e,d]	0.83[e]
Max. Conductance of Soil Surface	α	$mm\ \sec^{-1}$	1.0[f]	2.0[f]
Saturated Hydraulic Conductivity (Vertical)	$K_{sat,vertical}$	$m\ day^{-1}$	6.0[b]	258[h]
Saturated Hydraulic Conductivity (Horizontal)	$K_{sat,horizontal}$	$m\ day^{-1}$	10.0[b]	258[h]
Ks-decay rate with depth	σ	m^{-1}	0.03[f]	7.50[i]
Exponent of the moisture release equation	b	--	4.9[d,g]	6.0[i]

a=Tombul et al.(2004) ;b=This study; c=Kirchman et al.(1999) ; d=Rawls et al. (1982); e=Shwarzel et al.(2002); f=This study, calibrated; g=Beringer et al. (2001); h=This study, based on laboratory measurements of peat hydraulic properties; i=Letts et al. (2000).

Table 2-2. Landcover specific biophysical parameters used in BEPS-TerrainLab V2.0.

Biological Parameter	Units	Conifer	Mixed	Deciduous	Wetlands
Canopy clumping index	--	0.50[a]	0.70[a]	0.80[a]	0.90[b]
Maximum carboxylation rate at 25°C	$\mu mol.m^{-2}s^{-1}$	33.0[c]	50.0[d]	60.0[d]	33.0[c,e]
Maximum stomatal conductance	mms^{-1}	1.60[a]	3.00[a]	5.00[a]	1.60[f]
Cuticular conductance	mms^{-1}	0.15[g]	0.15[g]	0.15[g]	0.15[g]
Optimum temperature for photosynthesis	^{o}C	20.0[h]	20.0[h]	20.0[h]	20.0[h]
Maximum temperature for photosynthesis	^{o}C	37.0[h]	37.0[h]	37.0[h]	37.0[h]
Vapor pressure deficit at stomatal opening	kPa	0.20[i]	0.20[i]	0.20[i]	0.20[i]
Vapor pressure deficit at stomatal closure	kPa	2.00[i]	2.00[i]	2.00[i]	2.00[i]
Root extinction coefficient	--	0.94[j,k]	0.95[j,k]	0.96[j,k]	0.93[j]
Overstory canopy height,	m	8.0[l,p]	10.0[p]	12.0[p]	3.0[p]
understory canopy height	m	1.0[l,p]	2.0[p]	1.5[p]	0.5[p]
Wind attenuation coefficient, cn	--	2.74[m,n,o]	2.78[m]	2.78[m]	2.74[m]
Moss fraction	%	85[p]	50[p]	75[p]	90[p]
Peat depth criteria	cm	20.0[i,j]	15.0[j]	15.0[j]	50.0[j]
Precipitation interception coefficient	$mmLAI^{-1}day^{-1}$	0.2[q,r]	0.25[q,r]	0.3[q]	0.09[q,r]

a=Liu et al. (2002) ; Liu et al. (1997) and Chen et al. (2006)
b=Sonnentag et al. (2007a) and unpublished measurements at a wetland location near the EOBS site.
c=Bonan et al. (1995) and Chen et al. (1999)
d=after Wilson et al. (2001)
e=wetlands in the study site have stunted black spruce trees.
f=Sonnentag et al. (2008)
g=This study.
h=after Kimball et al. (1997); Chen et al. (1999) and Way and Sage (2008)
i= Dang et al. (1997) ; Kimball et al. (1997) and Chen et al. (1999)
j=after Jackson et al. (1996) for mixed forests, the value is calibrated between conifers and deciduous
k=after Chen et al. (2005).
l= Fluxnet Canada-Data Information System.
m=Amiro et al. (1988)
n= Cionco et al. (1978)
o=Heddeland and Lettenmaier (1995)
p=Calibrated in this study, based on 2004 and 2005 field campaigns.
q=Running and Coughlan (1988); r=adjusted to account for the effects of leaf morphology on interception.

2.6. Flux and Meteorological Measurements

The eddy covariance (EC) technique is being used to make continuous high-frequency measurements of CO_2 and energy fluxes at the EOBS site of FCRN. EC instrumentation at EOBS is comprised of a three-dimensional sonic anemometer and both a closed and an open-path infrared gas analyzers (IRGA), mounted on a scaffold tower 24 m above the ground. Continuous meteorological data are also measured using meteorological instruments mounted on the EC tower. Time domain reflectometers (Campbell Scientific CS615 sensor) are used to measure volumetric soil moisture content (VSWC). These TDR probes are placed below the moss layer at an undisturbed location within the footprint region of the EOBS tower, and measures VSWC at 5, 10, 20 and 50 cm depths. Electronic piezometers (Solinst level-loggers) are used to monitor the water table depth (WTD) fluctuations. Rainfall is measured using a tipping bucket rain gauge near the EOBS tower and the total precipitation is measured using a Geonor T200B rain gauge. More details on the measurements at the EOBS site can be found in Bergeron et al. (2007).

Considering the tower height, prevailing wind direction and the gentle terrain, the tower fetch corresponds to an approximate circular shape having a radius of ~500 m centered on the tower. Using an inverse Lagrangian model, Kljun et al. (2004) conducted a flux footprint analysis and estimated that the site's fetch contributed at least 90% of the measured flux, and therefore, we used a circular area having a radius of 500 m as "the footprint" for our data analyses. Since BEPS-TerrainLab V2.0 runs at a daily time step, we temporally upscaled the half-hourly meteorological ecosystem flux measurements to a daily time step. From the latent heat flux measurements (W m^{-2}), ET (mm day^{-1}) was derived for model comparison. GPP fluxes were obtained from the fluxes of net ecosystem exchange (NEE) of CO_2 at the EC tower. Using

the methodology outlined in Bergeron et al. (2007), an ecosystem respiration algorithm was derived using nighttime NEE fluxes and temperature. This facilitates the calculation of GPP from NEE fluxes. These flux datasets (half-hourly) were supplied through the FCRN *Data Information System*. All the flux and meteorological data were quality controlled.

For the present study, we used the measurements taken between January 2004 and December 2005. All pixels in the watershed were assigned explicit meteorological data that were topographically corrected using a separate sub-routine within BEPS-TerrainLab V2.0, using meteorological measurements at the tower site.

2.7. Initialization of Water Table and Ecosystem Carbon Pools

With initial WTD being a necessary input to BEPS-TerrainLab V2.0, a WTD was spun up before the actual simulation. We ran the model several times using 2004 meteorological data. The initial run for this iterative WTD initialization process used a topography-derived WTD using the TOPMODEL principle of Beven and Kirkby (1979). Subsequently, the model was run iteratively using the WTD from day 365 as the initial WTD, until an acceptable seasonal WTD pattern was obtained. Thereafter, the spun-up WTD was used for subsequent analyses. We used the WTD from day 365 of 2004 as the initial WTD for 2005 simulations.

Apart from the spatial datasets commonly used for hydrological modeling as described above, BEPS-TerrainLab V2.0 also requires explicit information on the current sizes of various ecosystem C-pools (12 in all) and their corresponding current C:N ratios to run the biogeochemical part. The methodology to initialize ecosystem C-pools were carried out using long-term simulations that consider climate change, CO_2 variations, disturbance effects, forest growth and age effects, etc. and are described in Govind et al. (2008b). These initialized C pools are critical for soil nitrogen dynamics.

2.8. Results and Discussion

2.8.1. Spatio-temporal Patterns of ET.

The simulated total ET was compared with the ET derived from the latent heat flux measured by the EC system installed at the EOBS tower. Figures 2-4 a and b show the annual pattern of the measured and the modeled ET in the footprint region for 2004 and 2005, respectively. Five-day moving averages of the simulated and measured ET for 2004 and 2005 are displayed in the time series panel (Figure 2-4a) for added visual clarity. One to one comparisons of the daily values were able to explain 82% (RMSE=0.34 mm day^{-1}) and 84% (RMSE =0.40 mm day^{-1}) of the variability in the ET measured at the EC tower in 2004 and 2005, respectively. Although there is a general tendency of the model to underestimate ET, it seems to perform adequately during most parts of the year for both 2004 and 2005. Discrepancies were found during winter, when the model underestimated the latent heat flux especially in 2004.

One possible explanation for this discrepancy is the underestimation of snow sublimation that might have contributed to higher winter latent heat values sensed by the EC tower. Analysis of meteorological data revealed that the winter of 2004 was much colder and drier than 2005 and this might have resulted in increased sublimation for 2004. There are studies that demonstrate that sublimation of intercepted snow constitutes a significant component of the water balance of boreal ecosystems (Lundberg and Halldin, 1994). Based on EC measurements, Molotosch et al. (2007) demonstrated that intercepted snowfall results in rapid response of above-canopy latent heat fluxes as high as 3.7mm day^{-1}. Another factor that might explain the discrepancies between the simulated and measured ET could be the presence of Lake Inlet situated about 900 m northwest of the EOBS tower. We speculate that this “lake effect” could slightly influence the EC measurements of latent heat flux because advective

process could alter the local humidity, altering the vapour pressure deficit at the tower site, depending on wind patterns. However, the lake was not in the sector of the fottprint from which the predominant winds originated.

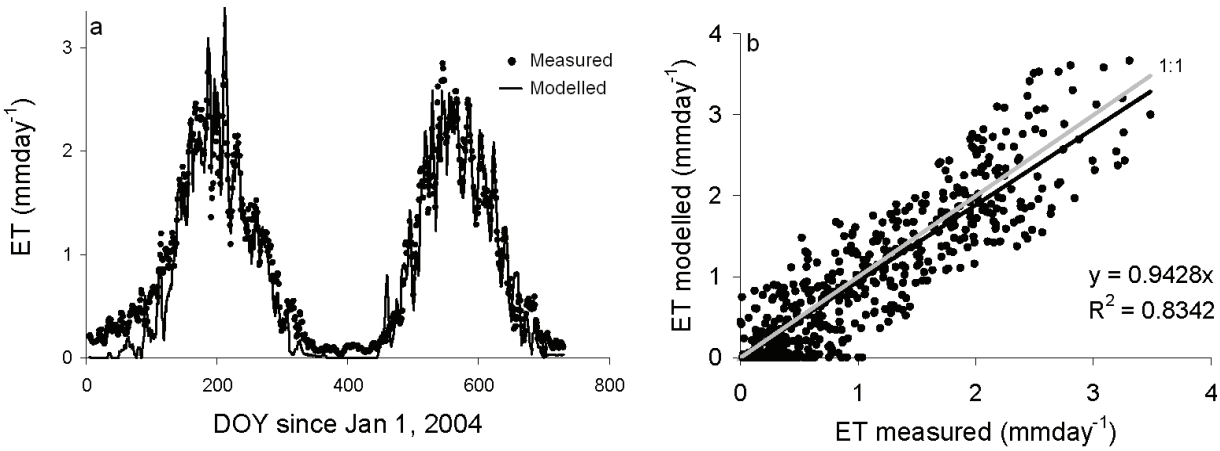

Figure 2-4. Comparison of simulated and measured ET time-series (5-day moving average for visual clarity) for the years 2004 and 2005, at the EOBS tower footprint region. (b)One to one comparison of simulated and measured ET for the years 2004 and 2005 (combined).

The annual total ET loss at the FCRN tower site was simulated to be 330.2 mm (325 mm measured) and 257.67 mm (287 mm measured), in 2004 and 2005, respectively.

Figures 2-5a and 2-5b show the spatial distributions of annual ET simulated for 2004 and 2005 for the watershed around the EOBS flux tower. The spatial distribution of the simulated annual ET reflects the combined effects of physiological variation in plant functional types (land-cover), topographical controls on radiation and soil moisture; soil texture-mediated soil moisture regimes and variations in LAI values. On this boreal landscape, where different land-cover types exist, simulated values of annual ET are highly controlled by plant species that have variations in LAI and g_s. Topography largely controls the distribution of plant functional types (or land-cover types) on this boreal watershed. The coniferous stands had an annual average

simulated ET of 307 and 302 mm, in 2004 and 2005, respectively. Mixed forest stands have an annual average of 441 and 441.5 mm, in 2004 and 2005, respectively. Wetlands, on the other hand, have an annual average of 267 and 278 mm, in 2004 and 2005, respectively.

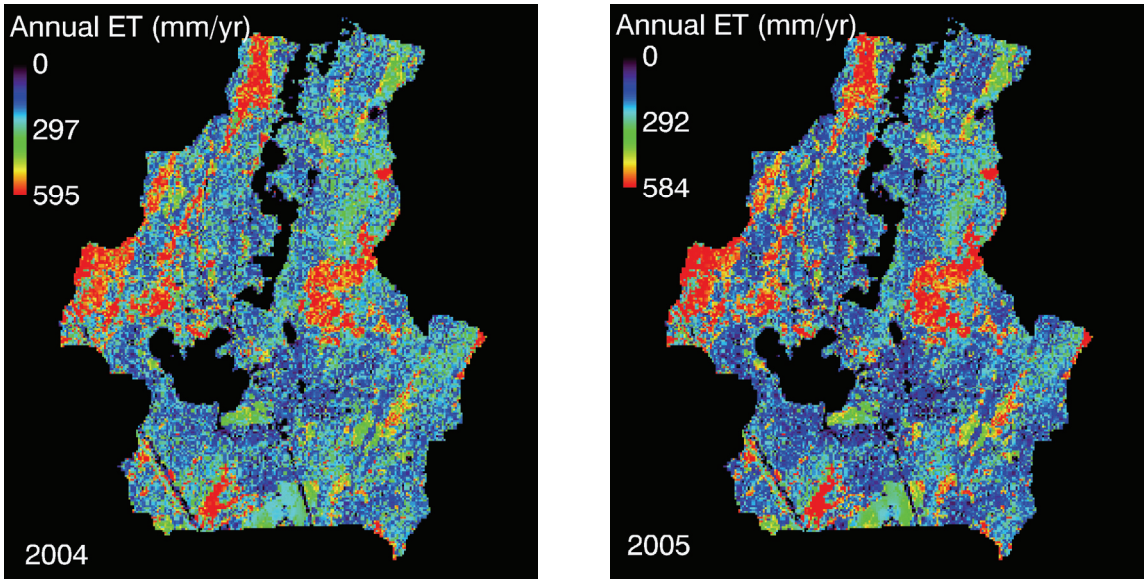

Figure 2-5. Spatial distributions of annual total ET simulated by BEPS-Terrainlab for (a) 2004 and (b) 2005 for the watershed surrounding the EOBS flux tower.

In this humid boreal ecosystem, water is not a scarce resource. Factors that govern the level of resistance imparted by a vegetated land surface on the potential rate of ET were vegetation type, presence of moss layer and soil type. Even under conditions of unlimited water supply, ET may not proceed at rates determined by the available energy and vapour pressure deficits (Roberts, 2007) because ET is highly influenced by transpiration, which is strongly controlled by vegetation characteristics such as LAI, vegetation height, maximum stomatal conductance ($g_{s,\max}$), and the clumping nature of the canopy elements. The $g_{s,\max}$ for deciduous and mixed stands are higher than for conifers (see Table 2-2). Therefore, it is likely that the ambient g_s values in deciduous stands are relatively higher resulting in a greater amount of

water being transpired than evaporated. At lower elevations, where conifers and wetlands dominate, lower values of ET could be attributed not only due to plant characteristics (low g_s and LAI), but also to increased stress as a result of saturated soil conditions. In a measurement study conducted in a boreal forest in Saskatchewan in central Canada (Amiro et al., 2006), it was shown that lower elevation regions, in spite of having shallower WTD conditions, did not show higher ET.

Watershed scale ET is the combination of several sub-component processes that are physical (canopy evaporation, sublimation and soil evaporation) and biological (canopy and moss transpiration) in nature, and occur simultaneously. ET partitioning among various sub-components reflect the characteristic feature of a land-cover. For example, in black spruce stands where the overstory canopy is generally open, the forest floor ET is a significant contributor to the total ET because of lower transpiration from overstory and understory canopies. Since we assume that a moss layer covers 85% of a black spruce forest floor, only 15% is exposed soil surface (see Table 2-2). Therefore, the major contributor of forest floor ET in black spruce stands is moss transpiration, rather than soil evaporation. Deciduous and mixed forests have relatively higher contributions from overstory and understory transpiration rather than forest floor ET.

In addition to vegetation-controlled processes, we also need to understand the contribution of soils to the total ET. Elevated regions of the watershed that represent eskers and glacial deposits have sandy loam soils as opposed to low-lying areas where peat soils are found. Mineral soils, such as sandy loam soils, have a lower value for maximum soil surface conductance ($g_{soil,\max}$) as opposed to peat soils, which further corroborates the fact that forest

floor ET in low lying areas (conifer, wetlands, etc.) is higher than that of upland regions having deciduous species, although the total ET remains lower than upland areas.

In 2004, the annual precipitation was 1,053 mm, whereas in 2005, the annual precipitation was 902 mm. This implies that 31.2% and 31.8% of the annual precipitation was used for the modeled total ET in 2004 and 2005, respectively

2.8.2. Soil Volumetric Water Content (VSWC) and Water Table Depth (WTD).

Conceptually, BEPS-TerrainLab V2.0 has two soil layers: the unsaturated zone and the saturated zone. WTD is calculated as the depth (from the soil surface) down to the point where the soil moisture is less than saturation. On a daily time step, hydrological processes such as percolation of water from the unsaturated zone to the saturated zone, capillary rise from the saturated zone to the unsaturated zone and lateral sub-surface and surface fluxes will all simultaneously affect the net water balance of a pixel, which consequently updates the unsaturated zone storage and WTD. Refer the appendix for details.

Figure 2-6 shows the temporal dynamics of the modeled footprint average VSWC in comparison to the TDR measured VSWC (average of 0-50 cm), which is representative of the EOBS footprint region. The VSWC varied quite rapidly during the course of the year in response to the temporal variation of precipitation and other associated hydrological processes. The model was able to capture the temporal pattern in fair agreement with the measurements for most parts of the growing season. The model adequately captured the steep decline in the VSWC between days 200-230 in 2004 and 200-250 in 2005.

Soil type at EOBS footprint is primarily a podzol with an organic layer having sandy-loam texture. The physical properties of the soil in the footprint region are shown in Table 2-2. We can conclude from Figure 2-6 that VSWC remains near field-capacity during the late spring

and seldom falls below the permanent wilting point even in mid-summer. The VSMC measured at this location is representative of the EOBS tower footprint region and was used by Bergeron et al. (2007) and Bergeron et al. (2008) to make various ecosystem scale generalizations.

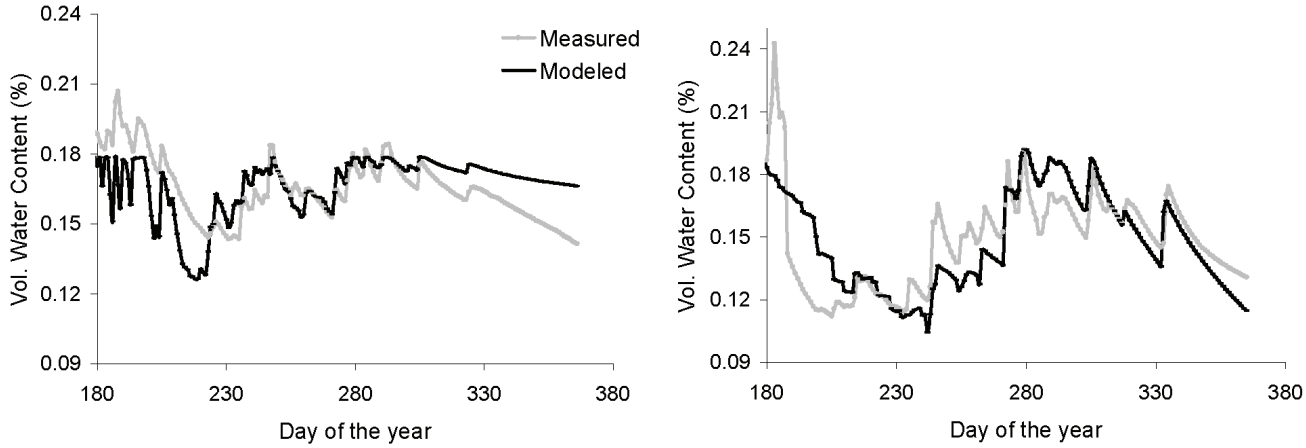

Figure 2-6. Simulated vs. modeled VSWC at the EOBS flux tower footprint for the years (a) 2004 and (b) 2005.

Discrepancies arise because in BEPS-TerrainLab V2.0, VSWC is the average of the entire unsaturated zone (which is highly dynamic). This discrepancy could be reduced only if we incorporate a multi-layer unsaturated zone moisture movement that is solved using Richard's equation. Scale issues that underlie this comparison also need to be considered. Here, a point-scale measurement of VSWC is compared with the footprint average VSWC simulation which makes a quantitative comparison is very difficult.

To test the performance of the model for WTD simulation, the measurements taken by the Solinst level-logger were compared to the simulated WTD (Figure 2-7). Measurements taken at two-hour intervals were converted to daily mean values for comparison. In the saturated zone, the current day WTD is simulated by updating the previous day's WTD using equation

A15 in the appendix. The model was able to explain 69% and 76% of the measured variability between days 120 and 365 for 2004 and 2005, respectively. The comparison showed that the model performance was satisfactory during the growing season, autumn and early winter, and captured the overall trend of measurements in both the years. During the mid-growing season in 2004, between days 200-240 and 241- 271, the WTD declined rapidly due to prolonged dry periods in combination with optimum conditions for ET losses (higher g_s). In 2005 as well, there was a prolonged drought period between days 180 to 270. The model satisfactorily captured this rapid decline as well as the subsequent rise of WTD. This was possible because the magnitudes of various hydrological processes that affected the local water balance were modeled with reasonable accuracy.

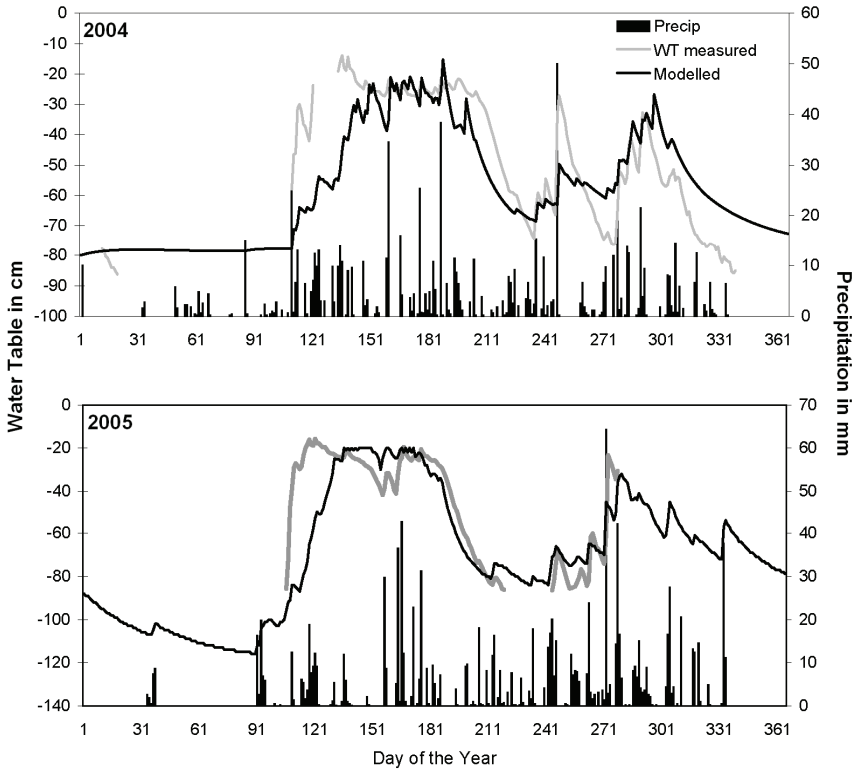

Figure 2-7. Comparison of simulated and measured WTD fluctuations at the EOBS flux tower site for the years (a) 2004 and (b) 2005.

In 2004, on day 247, an intense single day precipitation event made the WTD rise rapidly within a few hours (as inferred from the two-hourly measurement data). Although the model captures this dynamics of the WTD, the simulated magnitude did not agree fully with the measurements. We speculate that this is a scale related issue because we observed a net surface overland flow (SOLF) in the footprint region as a whole. In BEPS-TerrainLab V2.0, SOLF occur only when the soil is saturated, i.e., when WTD=0.

Another discrepancy was seen in the early spring when the model underestimated the simulated WTD. This is probably due to a weaker parameterization of the snowmelt process wherein the contribution of snowmelt in raising the WTD appears to be underestimated. Since we adopted a quasi-physical snowmelt model, it is probable that a higher accuracy in the snow-melt process was not achieved. Again, scale issues must be considered while analyzing various discrepancies between measured and modeled WTDs. Point–scale measurements were compared with the simulated dynamics of the WTD in a pixel that has an area of 625 m^2.

2.8.3. Sub-surface Baseflow, Surface Overland Flow and the Water Balance.

The footprint average sub-surface baseflow, calculated using a modified approach (please see appendix for details) that accommodates the preferential water fluxes within the moss–peat layer, is shown in Figure 2-8 for 2004 and 2005, respectively. The patterns of the baseflow time-series resemble that of the WTD patterns. This is because previous day WTD and slope are the only variables used to calculate baseflow fluxes. The simulated time-series of baseflow looks reasonable because most of the seasonal patterns are captured (i.e., spring season peak discharges and the mid-summer recession). Responses of baseflow toward precipitation events are different for different soil textural types due to differences in their inherent hydraulic properties. Since there was no runoff measurement at the EOBS site, we

were not able to validate the baseflow. In the spring, there is an upsurge in baseflow fluxes due to the rapid saturation of the soil profile with snowmelt water. Since the process of snowmelt affects the level of WTD, soil transmissivity increases correspondingly, leading to large baseflow fluxes.Our simulations show that the baseflow caused 637 mm and 552 mm of water loss from the footprint region, which was 64% and 66% of the annual infiltrated water (through-fall + stem-flow + snowmelt), in 2004 and 2005, respectively.

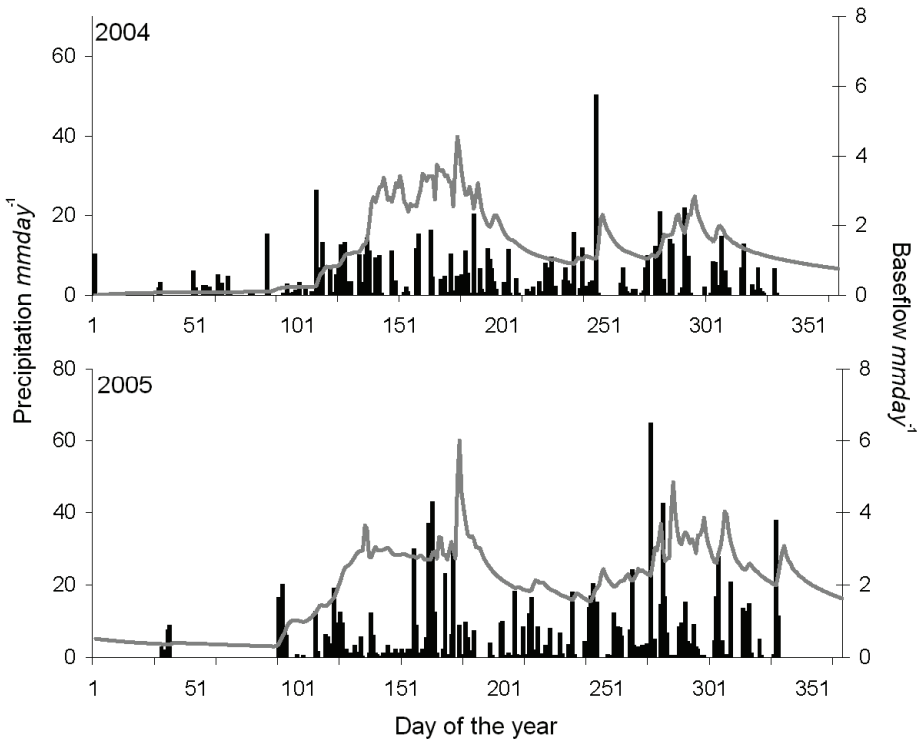

Figure 2-8. Simulated foot print average sub-surface baseflow fluctuations for the years 2004 and 2005.

Surface overland flow (SOLF) is another type of lateral hydrological process. In this model, assuming a Hewlett run-off hypothesis, we further assume that SOLF occurs only due to soil saturation when the WTD reaches the soil surface. Due to very high infiltration capacities of the moss-peat system on the boreal forest floor, SOLF is rarely observed on this boreal

landscape. In humid ecosystems such as boreal forests, precipitation intensities are low and rarely exceed soil surface infiltration capacity. Most of the through-fall or snowmelt profile readily enters the soil. When the WTD reaches the soil surface, excess water "ponds" and drains off laterally as SOLF, which further influences the water balance of neighboring pixels. The simulated footprint average SOLF was 79.4 mm and 69.1 mm in 2004 and 2005, respectively. Most of this occurred between days 134 and 195 in 2004 coinciding with the snowmelt period. On day 247 in 2004, a high intensity precipitation event occurred that lasted only a few hours; most of this water was lost in the form of surface runoff. Similarly, in 2005, the surface runoff mostly occurred during the days before and after the mid growing season drought when high intensity precipitation events occurred. A comparison of the magnitudes of surface and sub-surface baseflow reveals that the latter is the most dominant flow-path of soil water in this humid boreal ecosystem. The presence of macroporous conduits in the moss-peat layer creates preferential pathways for the water to move across the terrain making baseflow a dominant runoff mechanism in this ecosystem.

Analysis of the spatial distribution of WTD is a useful way to test the relative magnitudes of sub-surface baseflow and SOLF and to identify locations of saturation. In this humid boreal watershed, SOLF occurs due to surface saturation rather than infiltration excess. Figures 2-9a and 2-9b show the spatial distribution of WTDs during the spring (DOY=130) and growing season (DOY=260), respectively. These days of the year represent hydrologically distinct time periods within a year (2004). During the spring, snowmelt recharges the soil storage and brings the WTD near the ground surface. In low-lying locations of the watershed where the soil depth is shallow compared to the up-lands, the WTD reaches near the ground surface creating saturated zones. The saturated zones are normally found in locations adjacent to depressions and rivers. In Figure 2-9a, these saturated zones are represented in black tones.

Blue tones represent locations that are very prone to saturation (shallow WTD) while red tones represent locations having deeper WTDs, mostly seen in up-lands.

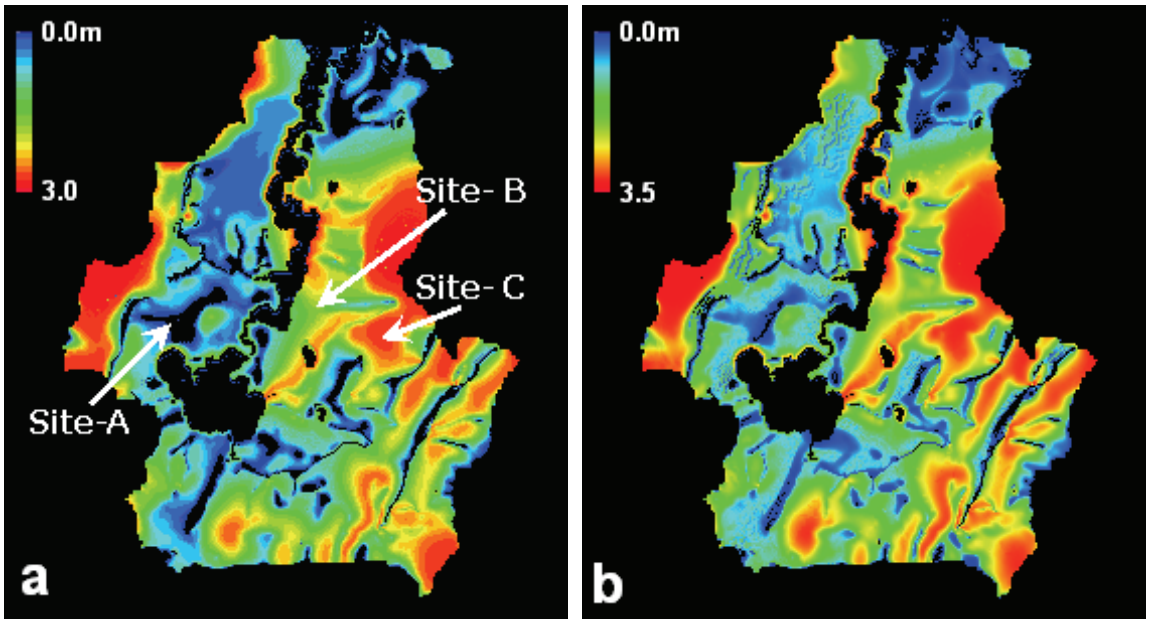

Figure 2-9. Spatial distribution of water table depths (WTD) during (a) spring (DOY=130) and (b) growing season (DOY=260)

In Figure 2-9b, it can be seen that the aerial coverage of saturated zones shrinks in the growing season due to soil water depletion due to lack of precipitation and increased evapotranspiration. From this plot it is clear that the relative magnitudes of saturated areas are small and they are variable in time ("variable source area") in comparison to the total watershed area. Figure 2-10 shows the temporal variation of lateral water flow (both SOLF and sub-surface baseflow) for three topographically distinct locations in the watershed as shown in Figure 2-9a. Site-A (elevation= 390 amsl) is a low-lying area, Site-B (elevation= 390 amsl) is an intermediate location and Site-C (elevation= 415 amsl) lies in the up-land. It is quite clear from the hydrographs that during the spring season, when the soil storage is recharged with snowmelt

water, the major flow-path in Site-A is SOLF whereas in Site-C it is sub-surface baseflow. It is clear that SOLF is only a temporary process (spring) over the course of the year and the dominant flow-path in most parts of this zero-order boreal watershed is the sub-surface baseflow. In perennial streams, however, SOLF is the dominant flow-path.

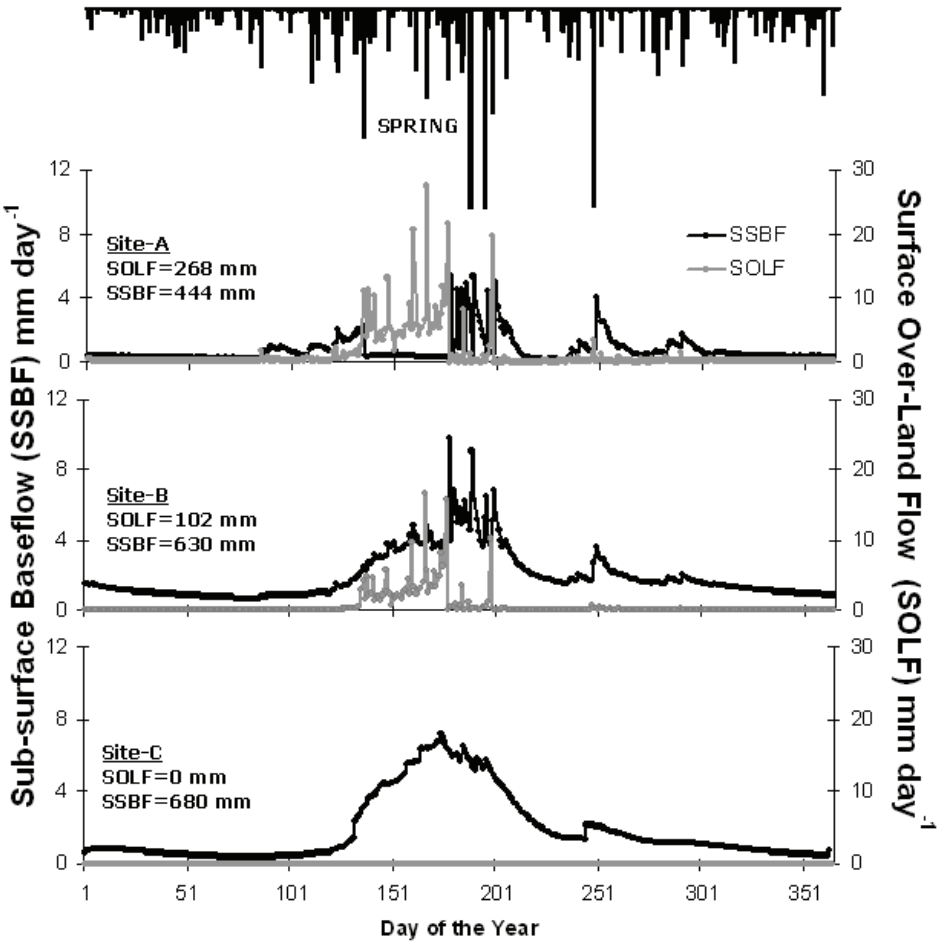

Figure 2-10. Comparison of hydrographs of three representative locations showing the dominant flow-path

An annual water balance analysis in the footprint region reveals the following information. The total annual precipitation was 1,053 mm and 902 mm in 2004 and 2005, respectively. Of this precipitation, 63.7 mm (2004) and 65.2 mm (2005) were intercepted on the

vegetation canopy and some portion of the intercepted precipitation, i.e., 58.2 mm (2004) 40.7 mm (2005) were evaporated directly to the atmosphere. The remaining 5.5 mm (2004) and 24.5 mm (2005) reached the ground as stem-flow and drips. In 2004, since the precipitation was comparatively of lower intensity that was evenly distributed throughout the year, the stem-flow was much less and most of the intercepted water that remained on the canopy directly evaporated or sublimed. The through-fall, which directly reached the ground through canopy gaps, was 732.6 mm (2004) and 661.3 mm (2005). The snowmelt was 256.0 mm in 2004 and 175.7 mm in 2005. The infiltrated water that entered the soil profile consisted of through-fall, stem-flow and snowmelt constituted 989.0 mm and 837.0 mm of water in 2004 and 2005, respectively. The footprint average annual soil water balance shown in Figure 2-9 describes how the soil hydrological processes were partitioned annually. Inputs include the infiltrated water (sum of through-fall, stem-flow and snowmelt), inflowing overland flow and inflowing sub-surface baseflow. The outputs include ET (all sub-components except canopy evaporation or sublimation), outflowing overland flow and outflowing sub-surface baseflow.

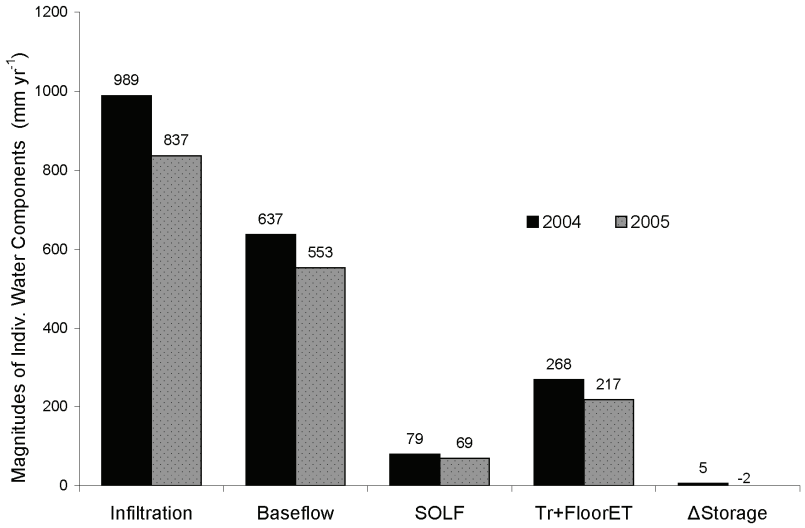

Figure 2-11. Simulated magnitudes of soil water balance components in the EOBS foot print region in 2004 and 2005, between days 1 to 365.

The storage change of soil moisture in the soil profile of the tower footprint equals the difference between the inputs and outputs as shown in Equation A 18.

The bottom line of this analysis reveals that the most dominant form of soil water partitioning in this ecosystem is sub-surface baseflow, which is approximately 65% of the annual infiltrated water into the soil. This is followed by ET losses from the soil water, which is around 26% of the infiltrated water. SOLF is not a dominant mechanism of lateral soil water delivery. This warrants the inclusion of topographically driven mechanism in ecosystem models as a major controller of local water balance for realistic simulation of various ecosystem processes such as GPP or soil C-dynamics.

2.8.4. Spatiotemporal Patterns of GPP

GPP is the first stage of C assimilated by plants from the atmosphere through the process of photosynthesis. Figure 2-10 shows the footprint average comparison of the simulated daily GPP and EC measurement-derived GPP for 2004 and 2005. Our modeling effort explained 91% and 92% of the variability in measured GPP, in 2004 (RMSE= 0.42 gC m^{-2} yr^{-1}) and 2005 (RMSE= 0.51 gC m^{-2} yr^{-1}), respectively. The main discrepancies were observed during the peak growing periods when the model was highly sensitive to soil water status. During the model development phase, we experienced an overestimation of the simulated GPP in spring. We found out that this overestimation was due to an unrealistic representation of the plant physiological status when ambient air temperature was used for photosynthesis calculation. In reality, during the spring, soil temperature remains much lower which keeps the vegetation in a physiologically inactive state. We rectified this problem by introducing two major modifications to the model: (1) we introduced soil nitrogen (N) cycle in conjunction with soil C-dynamics facilitated the realistic simulation of seasonal patterns of N-mineralization in the soil (Govind et

al., 2008 b,d) and (2) we introduced a soil temperature scalar into the Jarvis algorithm (Equation A19 in the appendix) which improved the simulation of g_s.

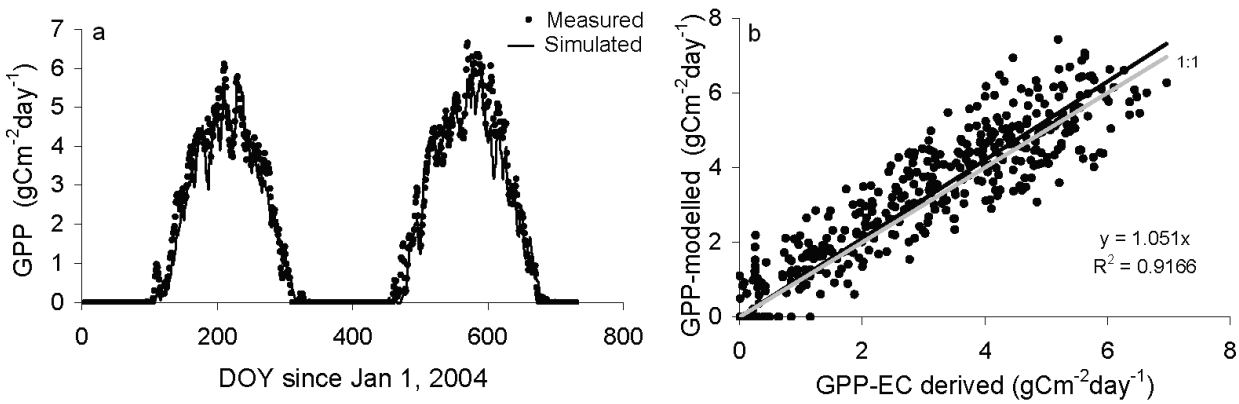

Figure 2-12. (a) Comparison of simulated and measured GPP time-series (5-day moving average) for the years 2004 and 2005, at the EOBS tower footprint region. (b) One-to-one comparison of simulated and measured GPP for the years 2004 and 2005 (combined).

During much of the growing season, the model performance was satisfactory since both modeled and measured GPP values followed similar trends. On every land-cover type, there are unique GPP sub-component contributions to the overall GPP, i.e., overstory, understory and moss. The magnitudes of these fractions greatly depend on various factors particularly g_s, soil moisture, soil temperature and soil N dynamics, which directly or indirectly depend on hydrological processes. Our approach of modeling the total ecosystem GPP as the sum of overstory, understory and moss components and employing a quasi-physiological spatial upscaling strategy is a new contribution (see Appendix for model details). Table 1 shows various land-cover specific physiological parameters used for GPP simulation. The simulated annual average GPP in the footprint region is 613 gC m^{-2} yr^{-1} (592 gC m^{-2} yr^{-1} measured by the EC technique) and 709 gC m^{-2} yr^{-1} (680 gC m^{-2} yr^{-1} measured by the EC technique), in 2004 and 2005, respectively.

The spatial distribution of the simulated annual GPP (Figures 2-11) reveals that deciduous and mixed forests have high annual photosynthesis (annual averages of 1,046 and 1,250 gC m^{-2} yr^{-1}in 2004 and 2005, respectively) as opposed to conifer stands (annual averages of 610 and 704 gC m^{-2} yr^{-1}in 2004 and 2005, respectively) or wetlands (annual average of 457 and 501 gC m^{-2} yr^{-1} in 2004 and 2005, respectively). Deciduous stands have higher stomatal conductance ($g_{s\,max}$ =5 mm sec^{-1}) as opposed to conifer stands ($g_{s\,max}$ =1.6 mm sec^{-1}). Second, leaves in deciduous stands are less clumped (clumping index of 0.8-0.9) than in conifers (clumping index of 0.5-0.6), and this increases the probability of sunlit leaves in the canopy.

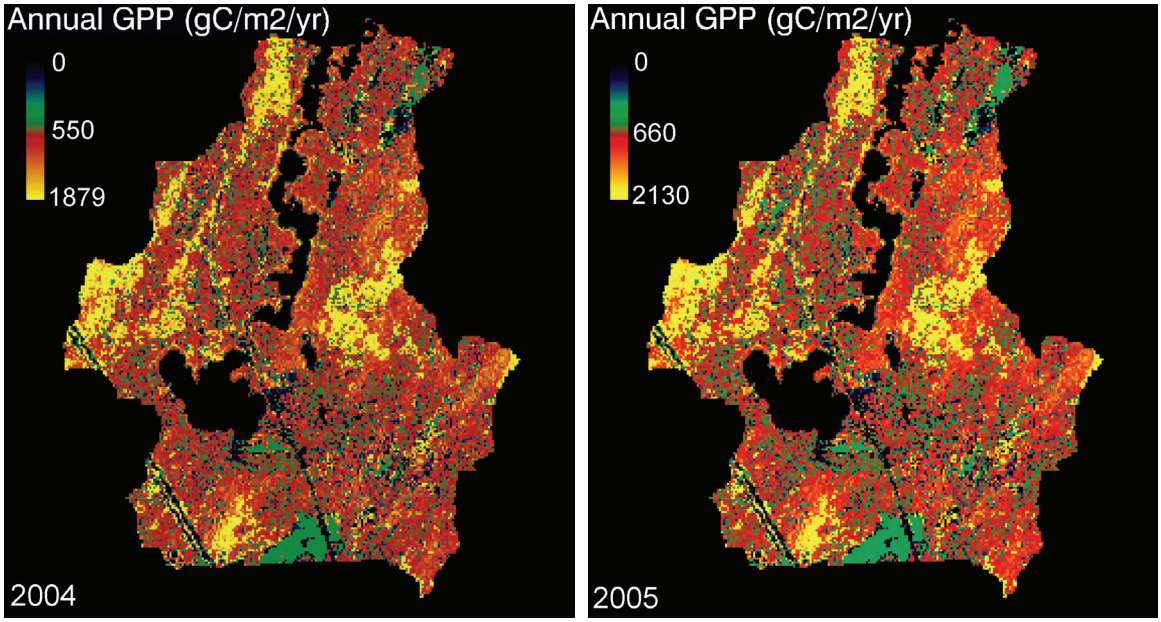

Figure 2-13. Spatial distribution of GPP simulated for the years 2004 and 2005

2.9. Summary and Conclusions

A process-based, spatially distributed, hydro-ecological model, BEPS-TerrainLab V2.0 was further developed to understand the strong links between hydro-ecological, ecophysiological and biogeochemical processes. The performance of this model to simulate

various hydro-ecological parameters was tested using various field measurements taken in a boreal spruce ecosystem in 2004 and 2005. Comparison of the simulations with the measurements reveals that BEPS-TerrainLab V2.0 can adequately simulate various hydro-ecological processes such as ET, dynamics of WTD, VSMC and photosynthesis. Since the processes described in this model are implemented using a systems approach that is mostly physical in nature, it could be extrapolated to any ecosystem with minimal calibration. From the lessons learned during model development and from the model testing phases, we draw the following conclusions:

1. Since boreal forest floors are predominantly covered by a moss-peat layer, lateral water fluxes take preferential pathways through this highly permeable layer. Based on our laboratory measurements, we developed a parameterization for preferential flow, which substantially improved the baseflow simulation for this boreal landscape. More laboratory experiments on peat hydraulic properties and peat specific pedo-transfer functions are required for improved hydrological modeling in boreal ecosystems.

2. Simultaneous consideration of the fractions of LAI corresponding to different moisture and light regimes as weighting factors to upscale leaf-level ecophysiological processes such as transpiration and photosynthesis is a strategy that permits upscaling of plant physiological processes in an effective manner. This strategy also mimics the environmental stress factors affecting the ecophysiological processes such as ET and GPP.

3. Explicit modeling of aerodynamic resistance based on turbulence created within different canopies (height, understory, etc.) is critical for accurate ET modeling, which determines the water balance and therefore C cycling in the boreal landscapes.

4. In humid eastern Canadian boreal ecosystems, sub-surface baseflow is the main mechanism of groundwater redistribution, which is almost 63% of the infiltrated water. Hence, proper accounting of this parameter is critical to improve our understanding of hydro-ecological connectivity. We conclude that the accuracy of the DEM is the most critical factor, which governs the reliability of baseflow simulations.

5. Improved snowmelt modeling is an essential requirement for accurate modeling of hydro-ecological processes in boreal ecosystems.

2.10. Appendix

2.10.1. Hydro-Ecological Processes Considered in BEPS-TerrainLab V2.0

2.10.1.1. Canopy Hydrological Processes

Precipitation is the only form of input of water at the watershed scale. In BEPS-TerrainLab V2.0, precipitation is categorized as rain or snow using a prescribed air temperature threshold of 0°C. The vegetation canopies intercept precipitation as a function of their interception storage capacity (i.e., a function of LAI). Some portion of canopy-intercepted precipitation returns to the atmosphere as canopy sublimation (snow) or canopy evaporation (rain), depending on the meteorological conditions. The only factors affecting evaporation are available energy, dryness of the air and the wind speed and there are no biological controls. The precipitation that is not intercepted, directly reaches the ground surface as through-fall. The remainder of the water after evaporation or sublimation reaches the ground surface as stem-flow.

The most important canopy hydrological process is transpiration. Unlike evaporation, a strong biological control determines the magnitude of transpired water. This is manifested through the ambient stomatal resistance (or conductance, g_s) for water vapour transport. The

transpiration occurs from both overstory and understory canopy layers. However, the ecophysiological conditions of the leaves and the microclimate strongly influence the rates of transpired water within a given canopy. In BEPS-TerrainLab V2.0, the processes of evaporation and transpiration are modeled using the Penman-Monteith (PM) equation using leaf or surface specific net radiation, stomatal (or surface) resistance and aerodynamic resistance values. Canopy evaporation is also computed in a similar way except that the stomatal resistance is replaced by a very low resistance term following Running and Coughlan (1988). The total ecosystem scale ET is expressed as:

$$\begin{aligned} ET = {} & x_1.To_{sun,sat} + x_2.To_{sun,unsat} + x_3.To_{shade,sat} + x_4.To_{shade,unsat} + \\ & y_1.Tu_{sat} + y_2.Tu_{unsat} + S_{floor} + z_1.E_{moss} + z_2.E_{soil} + I_{evap} + I_{sub} \end{aligned} \quad \text{(A1)}$$

ET	Total ecosystem scale evapotranspiration.
$T_{o\,sun,unsat}$	Transpiration from sunlit leaves getting unsaturated soil moisture.
$T_{o\,sun,sat}$	Transpiration from sunlit leaves getting saturated soil moisture.
$T_{o\,shade,unsat}$	Transpiration from shaded leaves getting unsaturated soil moisture.
$T_{o\,shade,sat}$	Transpiration from shaded leaves getting saturated soil moisture.
$T_{u\,unsat}$	Transpiration from understory getting unsaturated soil moisture.
$T_{u\,sat}$	Transpiration from understory getting saturated soil moisture.
S_{floor}	Sublimation of snow from forest floor.
E_{moss}	Moss evaporation.
E_{soil}	Soil evaporation.
I_{evap}	Evaporation of canopy intercepted water.
I_{sub}	Sublimation of canopy intercepted snow.

x_{1-4} Overstory transpiration upscaling factor.

y_{1-2} Understory transpiration weighting factor (0-1).

z_{1-2} Forest-floor evaporation weighting factor (0-1).

Each of the sub-component (except sublimation) is calculated using the Penman Monteith equation expressed in a general form as given below.

$$Ex = \frac{\Delta R_{\mathrm{n}x} + \rho c_{\mathrm{p}} \dfrac{e_{\mathrm{s}} - e}{\alpha}}{\lambda_{\mathrm{v}} (\Delta + \gamma (1 + \dfrac{\beta}{\alpha}))} \delta t \qquad \text{(A2)}$$

Ex is the amount of water evaporated or transpired from a unit surface, x (leaf, moss or a soil patch). R_{nx} is the net radiation of the evaporation or transpiration surface, see Chen et al., (2005a) for equations. ρ is the density of moist air, calculated as a function of air temperature. C_p is the specific heat of air at a constant pressure. e_s and e are the saturated and actual vapor pressures, respectively. λ is the latent heat of vaporization of water, Δ is the slope of the saturated vapor pressure-temperature curve, γ is the psychrometric constant, a weak function of ambient air temperature, α is the aerodynamic resistance for a particular canopy layer; and β is the stomatal resistance for a particular leaf or surface under a given light and moisture regime.

β = 0 when x= I_{evap}

$\beta = r_{s\,sun,unsat}$, the stomatal resistance of sunlit overstory leaves, when x=$T_{o\,sun,unsat}$.

$\beta = r_{s\,sun,sat}$, the stomatal resistance of sunlit overstory leaves, when x=$T_{o\,sun,sat}$.

$\beta = r_{s\,shade,unsat}$ is the stomatal resistance of shaded overstory leaves, when x= $T_{o\,shade,unsat}$.

$\beta = r_{s\,shade,sat}$ is the stomatal resistance of shaded overstory leaves, when x=$T_{o\,shade,sat}$.

$\beta = r_{c\,under\,unsat}$ is the canopy resistance of the understory when x= $T_{u\,unsat}$.

$\beta = r_{c\,undersat}$ is the canopy resistance of the understory when x= $T_{u\,sat}$.

$\beta = r_{soil/moss}$ is the soil or moss resistance as a function of VSWC when x= ET_{floor}

In all cases, stomatal resistance β is calculated as the reciprocal of stomatal conductance, using the Jarvis algorithm (see section 2.4).

Unlike BEPS-TerrainLab V1.0 where a constant value for aerodynamic resistance (α) was used irrespective of the vertical position of the evapotranspiring surface (overstory, understory or forest floor). BEPS-TerrainLab V2.0 calculates explicit α values for different components using the approach given by Tague and Band (2004). A logarithmic wind speed decay profile is assumed for the top of the overstory canopy and an exponential wind speed decay profile is assumed within the canopy (Figure 2-A1). The overstory aerodynamic resistance α_o is calculated as follows:

$$\alpha_o = \frac{\log\left[\frac{(z_{sc} - d_o)}{zo_0}\right] / 0.41^2}{u*} \tag{A3}$$

Where, z_{sc} is the screen height; d_o is the zero plane displacement of the overstory, assumed to be 0.7 z_o, where z_o is the overstory canopy height. z_{oo} is the roughness length, which is assumed to be 0.1 z_o. Friction velocity is $u*$.

For the calculation of understory aerodynamic resistance, α_u an exponential wind profile is assumed. Friction velocity in this case is computed as:

$$u_0 = u* \frac{\log\left(\frac{z_0 - d_0}{z_{o0}}\right)}{\log\left(\frac{z_s - do}{z_{o0}}\right)} \tag{A4}$$

Wind speed within the canopy is allowed to decay in an exponential manner until $0.1z_{0_o}$ is reached, after which a logarithmic wind profile is assumed. The resulting aerodynamic resistance of the understory canopy having a height $z_u > 0.1\,z_0$ is calculated as:

$$\alpha_u = \alpha_0 + \log\frac{(z_s - d_0)}{z_{o0}} z_0 \exp^{-cn} \frac{\left(\exp\left[-cn\frac{(d_u + z_{ou})}{z_0}\right] - \exp\left[-cn\frac{(d_0 + z_{o0})}{z_0}\right]\right)}{u*0.41^2 cn(z_o - d_0)} \tag{A5}$$

cn is a vegetation-specific wind attenuation coefficient and d_u is the zero plane displacement of the understory. For vegetation layers that have a height less than $0.1\,z_0$ (e.g., moss or soil surface), Equation A5 is repeated along with an additional term given below:

$$\alpha_{u'} = \alpha_u + \left[\frac{\log\frac{(0.1z_0)^2}{z_{ou}}}{0.41^2 u*}\right] \tag{A6}$$

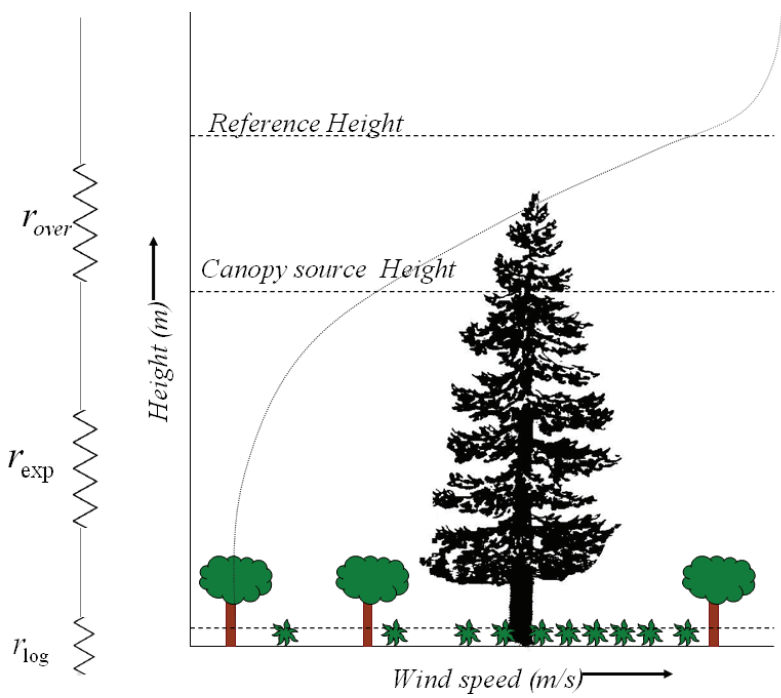

Figure 2-A1. Schematic representation of the vertical wind profile and aerodynamic resistances to the vertical scaler transfer within and above the canopy.

2.10.1.1.1. Spatial Upscaling of Evapotranspiration.

In BEPS-TerrainLab V2.0, we assume that light and soil moisture are the governing factors that distinguish physiological status of the leaves within a canopy that result in variabilities in their stomatal conductances, g_s (or stomatal resistances). Leaf-level processes are spatially upscaled to the canopy scale by weighting with their respective LAI fractions that correspond to a given light (sunlit or shaded) or soil moisture regime (saturated or unsaturated). Unlike the previous version of the model that used a *big-leaf approach* to calculate the ecosystem scale ET, we employ a modified sunlit-shaded leaf strategy and call it a *four-leaf approach.* This approach uses unique g_s specific to physiologically distinct leaves. Under saturated soil moisture conditions, g_s will be substantially lower than in unsaturated soil moisture conditions, provided that VSMC is not below the permanent wilting point. Leaf-level transpiration calculated using specific g_s for different radiation (sunlit or shaded) and moisture regimes (saturated and unsaturated) is upscaled by weighting with their respective LAI fractions.

$$T_o = \left[T_{sun,unsat} LAI_{sun}.\mu + T_{sun,sat} LAI_{sun}(1-\mu)\right] + \left[T_{shade,unsat} LAI_{shade}.\mu + T_{shade,sat}.LAI_{shade}(1-\mu)\right]$$

$$\begin{aligned} T_{sun,sat} &= f(R_{n\,sun} g_{s,sun,sat}, \phi) \\ T_{sun,unsat} &= f(R_{n\,sun} g_{s,sun,sat}, \theta) \\ T_{shade,sat} &= f(R_{n\,shad} g_{s,shade,sat}, \phi) \\ T_{shade,unsat} &= f(R_{n\,shad} g_{s,shade,unsat}, \theta) \end{aligned} \qquad \text{(A7)}$$

Where, T_o is the overstory transpiration and the function f is Penman Monteith equation, which uses surface-specific net radiation (R_n) and g_s (as a function of soil moisture, θ or $\theta_s = \phi$).

However, for the understory canopy, we use a *big-leaf approach* to upscale transpiration, using canopy conductance $g_{c,under}$, which is simply calculated as $g_{s\,under} \times LAI_{under}$. However, the relative understory contribution from the saturated and unsaturated zones is considered in BEPS-TerrainLab V2.0. The understory transpiration can be expressed as given below:

$$T_{under} = (T_{under}.\mu_{under}) + (T_{under}.(1-\mu_{under})) \quad \text{(A8)}$$

2.10.1.1.2. Leaf Fractions in a Canopy Corresponding to Varying Water and Light Regimes

To quantify the fraction of leaves in a canopy that correspond to different soil moisture regimes, we employ the *Pipe Theory* of Shinozaki (1964a and b) and assume that the shoots and roots are proportionally distributed. Fractions of roots lying in the saturated and unsaturated zones are directly used in Equations A7 and A8. We use a simple root decay coefficient χ to determine the proportion of roots that are lying in the saturated and unsaturated zones. Depending on the position of the WTD and root geometry, these fractions are calculated following a simple empirical approach suggested by Gale and Grigal (1987).

$$f(\mu) = \mu_{\mathrm{j}} = 1 - \chi^{z_{\mathrm{j}}} \quad \text{(A9)}$$

where μ_j is the root fraction in the unsaturated zone, and χ is the root distribution coefficient, which is a species specific value and z_i is the WTD (in cm). A high value of χ (e.g., 0.98) indicates a deep root system. A typical χ value for the boreal forest is ~0.943 (Jackson et al., 1996). For the present study, the understory root distribution coefficient χ_{under} was assumed to be 75% of the overstory value, implicitly describing the understory as shallow rooted plants. Refer to Table 1 for specific land-cover root distribution coefficients, which are typical of a boreal ecosystem.

To calculate the sunlit and shaded leaf fractions for a canopy, a function involving the canopy-clumping index and the solar zenith angle is used after Chen et al. (1999). Future improvements can be made by incorporating strategies to differentiate light regimes in understory and forest floors.

2.10.1.1.3. Forest Floor Evapotranspiration

The forest floor ET is the sum of moss transpiration and soil evaporation. Separation of soil evaporation and moss transpiration is complicated because the distribution of moss varies quite rapidly at sub-pixel scales. Creation of a watershed-scale moss distribution map is not practically feasible using the current spatial resolution (25 m), owing to large sub-pixel variability in moss distribution. To circumvent this issue, we prescribe a land-cover specific moss cover fraction, ξ based on our field experience. The soil cover fraction will then be (1- ξ). Since the *area index* of soil and moss together is united, no weighting term is necessary for upscaling it.

$$E_{floor} = \left(E_{moss}.\xi\right) + \left(E_{soil}.(1-\xi)\right) \tag{A10}$$

$$E_{moss/soil} = f\left(R_{n\,floor}, g_{soil} : g_{moss}\right)$$

For ET_{moss}, the moss conductance is calculated using Williams and Flanagan (1998). For soil evaporation, soil conductance is calculated as a function of VSWC and is described in section 2.4.

2.10.1.2. Unsaturated Zone Hydrological Processes

The unsaturated zone is the region above the WTD, where the VSWC is below saturation. Infiltration of throughfall, stemflow and snowmelt water occurs into the underlying

soil. The process of infiltration continues until the infiltration capacity, $I_{\max}$ is reached. $I_{\max}$ is calculated based on the Green and Ampt (1911) approximation as shown below.

$$I_{\max} = \mathrm{K}_{\mathrm{surf}} * \left(1 + \frac{(\phi - \theta_{\mathrm{t-1}}).\mathrm{S}_{\mathrm{f}}}{\mathrm{I}_{\mathrm{cum}}}\right) \tag{A11}$$

where K_{surf} ground surface is the hydraulic conductivity, which is equivalent to the moss saturated hydraulic conductivity, and K_{peat} is around 280 mm day^{-1}, ϕ is porosity, θ_{t-1} is the previous day VSWC of the unsaturated zone, S_f is the wetting front suction calculated according to Beckers and Alila (2004) , and I_{cum} is the cumulative infiltration, which is assumed to be the sum of through-fall, stem-flow and snowmelt that reaches the soil surface Water above the infiltration capacity becomes surface runoff (saturation excess flow). However, surface runoff is rare in boreal forests unless saturation is attained.

Percolation and Capillary rise are the vertical movements of water between the unsaturated and saturated zones. Percolation happens in the unsaturated zone when the VSWC in the unsaturated zone exceeds the field capacity. Water in the unsaturated zone having energy status above the field capacity moves vertically downward under the influence of gravity and reaches the saturated zone. In BEPS-TerrainLab V2.0, percolation is calculated similar to Wigmosta et al. (1994) or Chen et al. (2005). On a daily basis, capillary rise of water is possible from the saturated zone to the unsaturated zone under conditions of excessive surface dryness. These upward fluxes of water occur against gravity under conditions when unsaturated water content is below saturation. This creates a positive matric potential gradient in the upward direction. This process is modeled according to Eagleson (1978) similar to Chen et al. (2005). The unsaturated hydraulic conductivity and matric potential used for percolation and capillary rise are calculated using the closed form pedo-transfer function following Campbell et al. (1998).

Other forms of hydrological processes that govern the hydrological process in unsaturated zones include transpiration losses through overstory and understory roots that capture water. Forest floor evapotranspiration that includes moss transpiration and soil evaporation also reduces water from the unsaturated zone.

2.10.1.3. Saturated Zone Hydrological Processes

At a daily time step, one of the inputs of water into the saturated zone includes percolation. Another important process that determines the gain or loss of water to the saturated zone is the topographically driven sub-surface baseflow, which is a lateral phenomenon. In BEPS-TerrainLab V2.0, baseflow is modeled similar to Wigmosta et al. (1994), which is analogous to a depth-integrated Darcy's equation.

$$Q_{baseflow} = \sum_{i=1}^{8} T.\beta.w \qquad \text{(A12)}$$

where $Q_{baseflow}$ is the baseflow in m^3 day^{-1}; β is the local water table slope (analogous to hydraulic gradient) and T_{ij} is the hydraulic transmissivity (m^2 day^{-1}), which is calculated as shown below.

$$T_{ij} = K_{sat\,ij}.\frac{\left(\exp^{-f.z_{ij}} - \exp^{-f.d_{ij}}\right)}{f_{ij}} \qquad \text{(A13)}$$

Where, f is the $K_{sat} - depth$ decay constant, which is a soil texture specific value for a given pixel, ij the effective width of flow, w is the contour width in the k direction, and is assumed to be $0.5x$ in the cardinal direction of water flow and $0.398x$ in the diagonal direction (Quinn et al., 1991), and x is the grid size. The net sub-surface baseflow of a given pixel $_{ij}$ to its down-slope or up-slope neighbor is the difference between the total sub-surface inflow and total sub-surface outflow (Figure 2-A2).

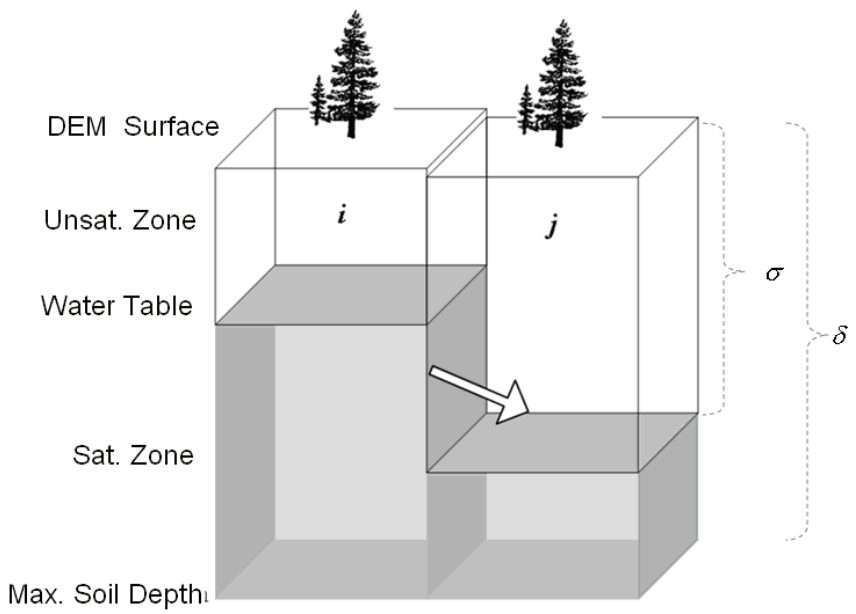

Figure 2-A2. Calculation of hydraulic head gradient using water-table slope. This approach seems to work well in boreal landscapes where the topographic differences are subtle.

The sub-surface geology of the landscape has a critical role in governing the lateral movement of sub-surface water (ground water). In the Canadian Shield, where the study site is located, shallow soils underlain by impermeable crystalline bedrock represents the dominant sub-surface geology and thus, the confining layer often mimics the surface topography (Price et al., 2005). In this situation, WTD dynamics is a direct function of localized recharge, sub-surface fluxes and ET losses resulting in predictable and relatively simpler effects related to shorter term variation in weather (precipitation and ET). Thus, the dynamics of WTD and flow rates in these types of settings are simply a reflection of bedrock geomorphology consequent of shallow soils. However, application of this model to other regions where the soil is very deep (e.g. tropical regions where laterite soils predominate), the sub-surface geology is quite complex and topography induced ground water fluxes are more difficult to predict. Unique conditions such as "perched" ground water or "pseudo ground water" can further complicate the WTD and

sub-surface lateral water dynamics. Therefore, applicability of this model to such systems needs rigorous site-specific parameterizations or calibrations. However, in such locations where the WTD is very deep, the rooting zone mostly lies in the unsaturated zone and vadoze zone hydrological processes are likely to be the major controls on vegetation.

Using the above mentioned parameterization alone, our initial efforts did not yield realistic baseflow values because we ignored the effects of the moss-peat complex that dominates boreal forest floors (Price et al., 1997). Moss-peat systems create a unique hydrological regime owing to its very high surface infiltration capacity, its ability to facilitate preferential flow and its very high water holding capacity. Moss-peat systems have unique hydraulic behaviors under extreme wetness conditions, i.e., hydrophilic versus hydrophobic. Moreover, the porosity of this substrate is near 80-85% and the water-holding capacity is five times greater than its dry weight (laboratory estimation, results not shown).

The importance of preferential flow in humid forest floors and along topographic gradients has been recently recognized (e.g., Beckers and Alila, 2004; Weiler and Mcdonnell, 2007). In BEPS-TerrainLab V2.0, we assume that as long as the WTD is below the moss-peat layer, i.e., in the mineral soil, no preferential flow occurs, and baseflow through the mineral soil is calculated in the conventional manner as given in Equation A15. However, when the WTD remains within the peat layer, the baseflow occurs through preferential pathways. To represent preferential flow in the moss-peat layer, we allocate a peat layer specific transmissivity, T_{peat} employing a peat-specific $Ks_{peat} - depth$ decay scheme. When the WTD is above a "*peat depth criterion,*" baseflow occurs using T_{peat}, which is defined as a function of the peat saturated hydraulic conductivity, K_{speat}, as shown below.

$$T_{peat_{ij}} = \frac{Ks_{peat}\left(\exp^{-7.5048 z_{ij}} - \exp^{-7.5048 z_p}\right)}{7.5048} \tag{A14}$$

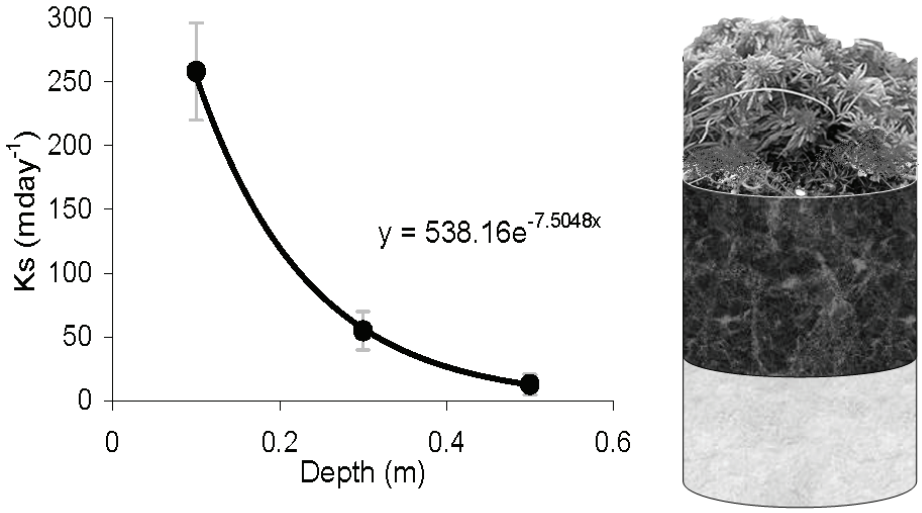

Figure 2-A3. Variation of saturated hydraulic conductivity (Ks_{peat}) with soil-depth for a moss-peat system. This decay scheme is used to parameterize baseflow once the WTD reaches a land-cover specific "*peat layer criteria*". This procedure implicitly captures the preferential flow of water on boreal landscapes. Values displayed here (each points) represent the average for five treatments for each depth. A constant head permeameter approach was used to measure Ks_{peat} in the laboratory.

We developed this parameterization based on laboratory measurements of saturated hydraulic conductivity for several moss-peat columns. In the summer of 2004, we collected peat cores from 5 locations around the EOBS tower, at three depths, i.e., 0-15 cm; 15-30 cm and 30-50 cm using aluminum cores 10 cm in diameter and 35 cm long. Saturated hydraulic conductivity was estimated using the constant head permeameter method. From this data, a curve was fit to explain the variation of Ks_{peat} with depth, as shown in Figure 2-A3. We derived two important points from this exercise. Surface Ks_{peat} was measured as 258 $\pm$ 5 m day^{-1}and the $Ks_{peat} - depth$ decay constant obtained was 7.5048.

Similar to the unsaturated zone, transpiration losses also occur from the saturated zone mediated through overstory and understory roots fractions. Once the saturated zone

hydrological processes are considered, the current day WTD is modified using an updating mechanism as shown below.

$$z^{t+1} = z^{t} - \frac{\Delta S}{(\phi - \theta)} \tag{A15}$$

where, z^{t+1} is the WTD in the current time step, z_{ij}^{t} is the WTD at the previous time step, ϕ is the soil porosity and θ_{t+1} is the current day VSWC in the unsaturated zone and ΔS is the change in the unsaturated zone storage (m).

Under conditions of excessive soil profile saturation, WTD can reach the surface and thereafter any water that is added to the soil profile "ponds" and drains off laterally as surface overland flow, SOLF ($R_{surface}$). Although $R_{surface}$ is generally considered a rare process in boreal landscapes due to high infiltration capacities associated with the moss-peat layer, from our field experience we know the existence of ephemeral surface water, especially in low lying areas of the watershed. To explicitly describe this process, we adopted a quasi-physical representation using a modified Manning's approach proposed by Voinov et al. (1998) to route this ponded water laterally over the surface of the ground. Hortonian surface overland flow is often non-existent in boreal landscapes and sub-surface baseflow is the dominant form of lateral water movement. From our field and modeling experience, we believe that a Hewlett type of run-off mechanism is most suited for hydrological modeling of zero-order forested boreal watersheds. The net water balance for a pixel can be summarized as:

In the unsaturated zone, $\Delta W_{\text{unsat}} = P - S - I_{\text{evap}} - R_{surface} + W_{\text{cr}} - W_{pe} - T_{\text{sat}} - E_{floor}$ (A16)

In the saturated zone, $\Delta W_{sat} = W_{\text{pe}} - R_{base\ flow} - T_{\text{sat}} - W_{\text{cr}}$ (A17)

Net water balance of the soil profile (pixel) as a whole is the sum of the storage change in the unsaturated and saturated zones, which is determined by adding Equations A16 and A17,

$$\Delta W = P - S - I_{evap} - R_{surface} - R_{baseflow} - T_{unsat} - T_{sat} - ET_{floor} \quad \text{(A 18)}$$

Here ΔW is the storage change of a soil profile.

P Precipitation

S All forms of sublimation

I_{evap} All forms of canopy evaporation.

$R_{baseflow}$ Surface overland flow

$R_{surface}$ Sub-surface baseflow

T_{unsat} Transpiration loss from the unsaturated zone (overstory + understory)

T_{sat} Transpiration loss from the saturated zone (overstory + understory)

E_{floor} Evaporation from the forest floor (moss+soil)

W_{pe} Percolation from the unsaturated to saturated zone

W_{cr} Capillary rise from the saturated to unsaturated zone

2.10.1.4. Stomatal Conductance, Moss Conductance and Soil Conductance

Stomatal dynamics play a key role in most of the ecophysiological processes because it is one of the primary links in the soil-plant-atmosphere continuum of mass and energy. A number of factors influence g_s (Jarvis, 1976). These factors include meteorological variables (solar radiation, temperature, vapour pressure deficit, and CO_2 concentration), plant parameters (leaf water potential, leaf stomatal density) and soil properties (soil water content or soil water potential). In BEPS-TerrainLab V2.0, we use the multiplicative approach proposed by Jarvis (1976) to constrain a maximum potential stomatal conductance, $g_{s,\max}$, for water vapour

transport. $g_{s,\max}$ is a land-cover specific value (see Table 2-1). In this approach, various scalars (ranging from a minimum value of 0 to a maximum value of 1) that represent the dynamics of environmental factors are used to constrain $g_{s,\max}$ to provide the g_s.

Although more sophisticated models of stomatal dynamics are available in the literature (e.g., Ball et al., 1987 or Leuning, 1997), we chose to adopt this approach for two reasons. Unlike other models that operate at finer temporal resolutions (e.g., half-hourly), BEPS-TerrainLab V2.0 runs at a daily time step. Therefore, application of an elegant method for calculating g_s is impractical unless a sound temporal upscaling mechanism is developed for plant physiological behavior from instantaneous to daily time steps. Although it is possible to use daily mean values as inputs for mechanistic models of g_s, we believe that it may not completely represent real plant physiological processes. The second issue relates to the spatial resolution of the modeling domain. On a distributed modeling scenario, employing a mechanistic stomatal conductance model is computationally challenging. A mechanistic g_s model requires iterative calculations in order to update the ambient g_s for CO_2 by equilibrating it with photosynthesis at the previous time step. This procedure is not practically feasible for distributed modeling where time-consuming iterations need to be avoided. Although one analytical solution was developed by Baldocchi (1994) to circumvent iterations, much effort is still needed to modify this solution for daily applications.

Moreover, mechanistic g_s models do not realistically relate the effects of soil water content. For example, Ball et al. (1987) utilize a scalar for soil moisture status, similar to the Jarvis' multiplicative approach we adopt. Since the focus of the present study is to investigate the links between soil moisture status and its effect on C assimilation, we believe that the Jarvis algorithm is best suited for spatially explicit hydro-ecological modeling considering our current

computational constraints. We made a further modification to the Jarvis method by including a new scalar that represents the effect of another environmental factor, i.e., soil temperature following Heddeland and Lettenmaier (1995). In boreal regions, during spring or in the early summer, soil temperature remains much lower than air temperature. This condition makes the plant physiologically inactive and therefore, limits water uptake and growth (Bonan and Shugart, 1989). The modified Jarvis algorithm after the inclusion of a scalar $f(T_s)$ for soil temperature can be summarized as shown below:

$$g_{\mathrm{s}} = g_{s\max} . \left\lfloor f(F_{\mathrm{p}}) \times f(T_a) \times f(D_{\mathrm{v}}) \times f(\theta_{\mathrm{sw}}) \times f(T_s) \right\rfloor \tag{A19}$$

In Equation A19, $g_{s\max}$ is land-cover specific maximum stomatal pore conductance (see Table 2-1). F_p is the photosynthetic photon flux density (PPFD), T_a is the mean temperature, D_v is vapour pressure deficit and θ_{sw} is the VSMC or saturated VSMC (assumed as porosity) depending on the physiological nature of leaves as described in section 2.10.1.1.1. The method for calculating these scalars can be found in Chen et al. (2005). The new scalar $f(T_s)$ is calculated as shown in Figure 2-A4a. Soil temperature, T_s, is calculated by solving the Fourier heat transfer equation using a semi-implicit Crank-Nicholson solution for a 5-layered soil (Govind et al., 2008d).

Finally, the total conductance is calculated by considering the cuticular conductance $g_{cuticle}$ and stomatal conductance g_s in parallel and boundary layer conductance $g_{boundary}$ in series. Such that the total stomatal conductance (often simply referred as stomatal conductance, g_s) for water vapor exchange becomes:

$$g_{total} = \frac{g_{boundary} \times \left(g_{cuticle} + g_s\right)}{g_{boundary} + g_{cuticle} + g_s} \tag{A20}$$

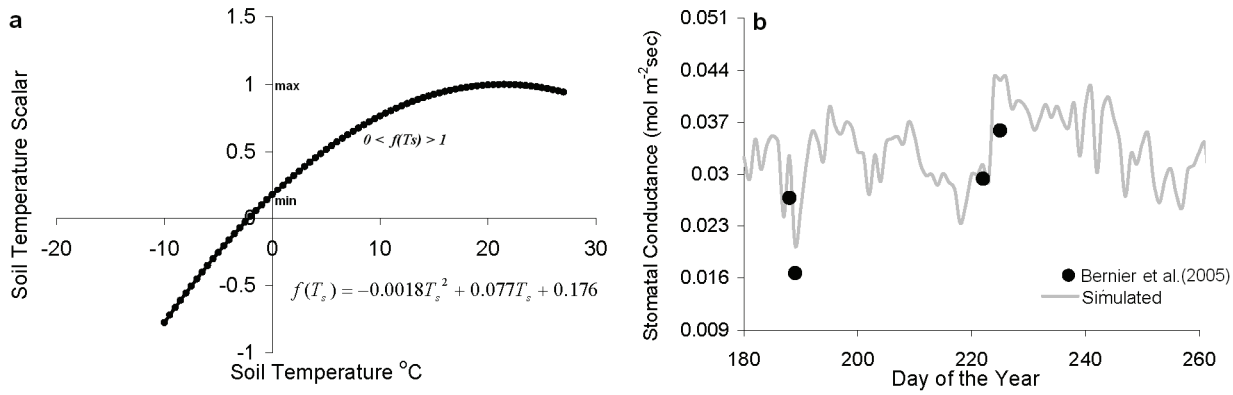

Figure 2-A4 (a) The soil temperature scalar $f(T_s)$ used to constrain $g_{\max}$ for a wide range of soil temperature values. (b) Footprint average (all leaf types) simulated g_s in comparison to measurements taken using an ADC LC-Pro-photosynthesis system in the growing season of 2004.

The reciprocal of *stomatal conductance,* i.e., *stomatal resistance* calculated in this manner (m s^{-1}) is directly used in equation A1 for ET calculations whereas for photosynthesis, the stomatal conductance (m s^{-1}) is reduced by a factor of 0.625 to account for CO_2 exchange. Figure 2-A4b shows a qualitative comparison of the simulated g_s (average for all leaf-types) with the measurements (Bernier et al., 2005) taken at the footprint region using an ADC LC-Pro photosynthesis system in the growing season of 2004.

However, for the moss layer, the conductance is calculated using a least squares regression after Williams and Flanagan (1998).

$$g_{s,moss} = -0.195 + 0.134W_{moss} - 0.256W_{moss}^2 - 2.28\times10^{-3}W_{moss}^3 - 9.84\times10^{-5}W_{moss}^4 + 1.68\times10^{-6}W_{moss}^5 \quad \text{(A21)}$$

Where W_{moss} is the water content of moss (ratio of fresh weight to dry weight), which is calculated empirically as a function of WTD, z using the approach of Frolking et al. (2002).

$$W_{moss} = 8.8 - 12.5 \times z \tag{A22}$$

The moss conductance for CO_2 and water is differentiated according to Sonnentag et al. (2008) with a threshold W_{moss} value of 5.0.

Soil surface conductance is calculated as.

$$g_{soil} = \begin{cases} 0.0001 & if, \theta < \theta_{wp} \\ \left[\dfrac{\theta - \theta_{wp}}{\theta_{fc} - \theta_{wp}}\right] \times \left[\left(g_{soil,\max} - 0.0001\right) + 0.0001\right] & if, \theta > \theta_{wp} and, \theta < \theta_{fc} \end{cases} \tag{A23}$$

where θ is the ambient VSWC, θ_{wp} and θ_{fc} are the permanent wilting point and field capacity, respectively.

2.10.1.5. Photosynthesis

According to Farquhar et al. (1980), the process of photosynthesis of a C3 leaf at a given instant can be approximated as the minimum of Rubisco-limited and light-limited gross photosynthesis rates as shown below.

$$A = \min(W_c, W_j) - R_d \tag{A24}$$

$$W_c = V_m \frac{C_i - \Gamma}{C_i + K} \quad \text{and} \quad W_j = J \frac{C_i - \Gamma}{4.5C_i + 10.5\Gamma} \tag{A25}$$

where, A is the net photosynthesis, W_c and W_j are Rubisco-limited and light-limited gross photosynthesis rates in μmol m^{-2} s^{-1}, respectively. R_d is the dark respiration. V_m is the maximum carboxylation rate in μmol m^{-2} s^{-1}. C_i is the intercellular CO_2 concentration; K is a function of enzyme kinetics. Γ is the CO_2 compensation point without the effects of dark respiration. Both

Γ and K are temperature-dependent parameters (Chen et al., 1999). V_m in Equation A25 can be expressed as a function of both temperature and leaf nitrogen content Bonan (1995).

$$V_m = V_{m25}.2.4^{\frac{(T-25)}{10}}.f(T).f(N) \tag{A26}$$

In BEPS-TerrainLab V2.0, we temporally vary N dynamics based on explicit modeling of soil C dynamics and the resultant nitrogen mineralization. This necessitates a comprehensive initialization procedure to spin up current soil (simulation year) C-pools using a long-term modeling framework such as InTEC (Chen et al., 2000). Because of its distinct scope, soil C and N dynamics and its relationship to the local hydrological regime will be discussed elsewhere (Govind et al., 2008d).

Chen et al. (1999a) developed an analytical solution to upscale temporally this instantaneous model by equating Equation A24 with $g(C_i - C)$, another form of a photosynthesis equation (Leuning et al., 1990) for daily applications. Here, g is the conductance of CO_2 through the pathway from the atmosphere outside of the leaf boundary layer (μmolmol^{-2}s^{1}Pa^{-1}) and C_i and C_a are the intercellular and atmospheric CO_2 concentrations, respectively. After accounting for the diurnal variation in g as a function of several diurnally varying environmental controls, two equations result, which can be integrated further using the extreme values of g as the boundary conditions.

$$A_c = \frac{\eta}{2(g_n - g_{\min})} \int_{g_{\min}}^{g_n} \left[(C_a + K)g + V_m - R_d - \sqrt{\left((C_a + K)g + V_m - R_d\right)^2 - 4\left(V_m(C_a - \Gamma) - (C_a + K)R_d\right)g} \right] dg$$

$$A_j = \frac{\eta}{2(g_n - g_{\min})} \int_{g_{\min}}^{g_n} \left[(C_a + 2.3\Gamma)g + 0.2J - R_d - \sqrt{\left((C_a + 2.3\Gamma)g + 0.2J - R_d\right)^2 - 4\left(0.2J(C_a - \Gamma) - (C_a + 2.3\Gamma)R_d\right)g} \right] dg \tag{A27}$$

In these equations, η (≈1.27) is the correction factor that is applied to account for the assumption that the diurnal pattern of g varies in a similar way to the solar zenith angle, SZA, which is a reasonable assumption because most of the environmental variables vary in accordance with SZA. For a complete derivation of this analytical solution, refer to Chen et al. (1999b).This temporally integrated model is adequate for daily calculations by simultaneously preserving the physiological meaning of photosynthesis as well as mathematical consistency. This temporally upscaled leaf level model is spatially upscaled in BEPS-TerrainLab V2.0 using a modification for the LAI fractions that correspond to different leaf physiological status in a manner similar to the spatial upscaling strategy adopted for ET upscaling (*four-leaf approach*) for overstory canopy and *big-leaf approach* for understory and moss.

$$A = \left[A_{sun,unsat} LAI_{sun}.\mu + A_{sun,sat} LAI_{sun}(1-\mu)\right] + \left[A_{shade,unsat} LAI_{shade}.\mu + A_{shade,sat}.LAI_{shade}(1-\mu)\right]$$

$$\begin{aligned} A_{sun,sat} &= f(g_{s,sun,sat}, \phi) \\ A_{sun,unsat} &= f(g_{s,sun,sat}, \theta) \\ A_{shade,sat} &= f(g_{s,shade,sat}, \phi) \\ A_{shade,unsat} &= f(g_{s,shade,unsat}, \theta) \end{aligned} \qquad \text{(A 28)}$$

A, for each radiation and hydrologic regime within a canopy layer is calculated based on the function, f , which is shown Equation A24.

References

Amiro, B.D., Barr, A.G., Black, T.A., Iwashita, H., Kljun, N., Mccaughey, J.H., Morgenstern, K., Murayama, S., Nesic, Z., Orchansky, A.L., and Saigusa, N.(2006). Carbon, Energy and Water Fluxes at Mature and Disturbed Forest Sites, Saskatchewan, Canada, *Agricultural and Forest Meteorology* **136**, 237-251.

Amiro, B.D. and Davis, P.A.(1988). Statistics of Atmospheric-Turbulence Within a Natural Black Spruce Forest Canopy, *Boundary-Layer Meteorology* **44**, 267-283.

Baldocchi, D.(1994). An Analytical Solution for Coupled Leaf Photosynthesis and Stomatal Conductance Models, *Tree Physiology* **14**, 1069-107.

Baldocchi, D., Valentini, R., Running, S., Oechel, W., and Dahlman, R.(1996). Strategies for Measuring and Modelling Carbon Dioxide and Water Vapour Fluxes Over Terrestrial Ecosystems, *Global Change Biology* **2**, 159-168.

Ball, J.T., Woodrow, I.E., and Berry, J.A.: 1987, 'A model predicting stomatal conductnance amd its contribution to the control of photosynthesis under different environmental conditions', *In*Progress in Photosynthesis Research, Martinus Nijhoff Publishers, Dordrecht, pp 221-224.

Beckers, J. and Alila, Y.(2004). A Model of Rapid Preferential Hillslope Runoff Contributions to Peak Flow Generation in a Temperate Rain Forest Watershed, *Water Resources Research* **40**.

Bergeron, O., Margolis, H.A., Black, T.A., Coursolle, C., Dunn, A.L., Barr, A.G., and Wofsy, S.C.(2007). Comparison of Carbon Dioxide Fluxes Over Three Boreal Black Spruce Forests in Canada, *Global Change Biology* **13**, 89-107.

Bergeron, O., Margolis, H., Coursolle, C., and Giasson, MA.(2008). How Does Forest Harvest Influence Carbon Dioxide and Water Fluxes of Black Spruce Ecosystems in Eastern North America?, *Agricultual and Forest Meteorology*. (in press).

Bernier, P.Y., Boivin-Chabot, S., and Dagnault, S. Gas exchange in Black Spruce at Fluxnet Mature Site, Chibougamau, Québec, Canada.. 2005. ECOLEAP project, Canadian Forest Service, Natural Resources Canada.

Beringer, J., Lynch, A.H., Chapin, F.S., Mack, M., and Bonan, G.B.(2001). The Representation of Arctic Soils in the Land Surface Model: the Importance of Mosses, *Journal of Climate* **14**, 3324-3335.

Beven, K.J. and Kirkby, M.J.(1979). A Physically Based Variable Contributing Model of Basin Hydrology, *Hydrological Science Bulletin* **24**, 43-69.

Bonan, G.B.(1995). Land Atmosphere Co2 Exchange Simulated by a Land-Surface Process Model Coupled to an Atmospheric General-Circulation Model, *Journal of Geophysical Research-Atmospheres* **100**, 2817-2831.

Bonan, G.B. and Shugart, H.H.(1989). Environmental-Factors and Ecological Processes in Boreal

Forests, *Annual Review of Ecology and Systematics* **20**, 1-28.

Campbell, G.S. and Norman, J.M.: 1998, 'An Introduction to Environmental Biophysics', *In* Springer-Verlag, New York, pp 1291-144.

Chen, J., Chen, W.J., Liu, J., Cihlar, J., and Gray, S.(2000). Annual Carbon Balance of Canada's Forests During 1895-1996, *Global Biogeochemical Cycles* **14**, 839-849.

Chen, J.M., Chen, X.Y., Ju, W.M., and Geng, X.Y.(2005). Distributed Hydrological Model for Mapping Evapotranspiration Using Remote Sensing Inputs, *Journal of Hydrology* **305**, 15-39.

Chen, J.M., Govind, A., Sonnentag, O., Zhang, Y.Q., Barr, A., and Amiro, B.(2006). Leaf Area Index Measurements at Fluxnet-Canada Forest Sites, *Agricultural and Forest Meteorology* **140**, 257-268.

Chen, J.M., Liu, J., Cihlar, J., and Goulden, M.L.(1999). Daily Canopy Photosynthesis Model Through Temporal and Spatial Scaling for Remote Sensing Applications, *Ecological Modelling* **124**, 99-119.

Chen, X., Chen, Y.D., and Xu, C.Y.(2007). A Distributed Monthly Hydrological Model for Integrating Spatial Variations of Basin Topography and Rainfall, *Hydrological Processes* **21**, 242-252.

Cionco, R.M.(1978). Analysis of Canopy Index Values for Different Canopy Densities, *Bulletin of the American Meteorological Society* **59**, 1507.

Dang, Q.L., Margolis, H.A., Coyea, M.R., Sy, M., and Collatz, G.J.(1997). Regulation of Branch-Level Gas Exchange of Boreal Trees: Roles of Shoot Water Potential and Vapor Pressure Difference, *Tree Physiology* **17**, 521-535.

Eagleson, P.S.(1978). Climate, Soil, and Vegetation .3. Simplified Model of Soil-Moisture Movement in Liquid-Phase, *Water Resources Research* **14**, 722-730.

El Maayar, M. and Chen, J.M.(2006). Spatial Scaling of Evapotranspiration As Affected by Heterogeneities in Vegetation, Topography, and Soil Texture, *Remote Sensing of Environment* **102**, 33-51.

Environment Canada . Canadian Climate Normals or Averages 1971-2000. 2006. 2007-05-15.

Farquhar, G.D., Caemmerer, S.V., and Berry, J.A.(1980). A Biochemical-Model of Photosynthetic Co2 Assimilation in Leaves of C-3 Species, *Planta* **149**, 78-90.

Frolking, S., Roulet, N.T., Moore, T.R., Lafleur, P.M., Bubier, J.L., and Crill, P.M.(2002). Modeling Seasonal to Annual Carbon Balance of Mer Bleue Bog, Ontario, Canada, *Global Biogeochemical Cycles* **16**.

Gale, M.R. and Grigal, D.F.(1987). Vertical Root Distributions of Northern Tree Species in Relation to Successional Status, *Canadian Journal of Forest Research-Revue Canadienne De Recherche Forestiere* **17**, 829-834.

Gedney, N., Cox, P.M., Betts, R.A., Boucher, O., Huntingford, C., and Stott, P.A.(2006). Detection of a Direct Carbon Dioxide Effect in Continental River Runoff Records, *Nature* **439**, 835-838.

Govind, A., Chen, J.M., Ju, W., and Sonnentag, O.(2008b). A Spatially Explicit Hydro-ecological Modeling Framework (BEPS-TerrainLab V2.0) Part 2: Effect of Lateral Hydrological Processes on Photosynthesis and Evapotranspiration., *Journal of Hydrology*. Submitted.

Govind, A., Chen, J.M., Bernier, P.Y., Guindon, L., Margolis, H., and Beaudoin, A. (2008c). Reconstructing the Carbon Balance of a Boreal Ecosystem under Climate Change, CO2 Fertilization, Nitrogen Deposition and Disturbance Effects., *Geoderma*. Submitted.

Govind, A., Chen, J.M., and Ju, W.(2008d). Spatially Explicit Simulation of Hydrologically Controlled Carbon and Nitrogen Cycles and Associated Feedback Mechanisms in a Boreal Ecosystem. *Journal of Geophysical Research-Biogeosciences*. Submitted.

Grant, R.F.(2004a). Modeling Topographic Effects on Net Ecosystem Productivity of Boreal Black Spruce Forests, *Tree Physiology* **24**, 1-18.

Grant, R.F., Zhang, Y., Yuan, F., Wang, S., Hanson, P.J., Gaumont-Guay, D., Chen, J., Black, T.A., Barr, A., Baldocchi, D.D., and Arain, A.(2006). Intercomparison of Techniques to Model Water Stress Effects on Co2 and Energy Exchange in Temperate and Boreal Deciduous Forests , *Ecological Modelling* **196**, 289-312 .

Green, W. A., and G. A. Ampt (1911), Studies on soil physics I: the flow of air and water, *J. Agr. Sci.* **4**, 1-24.

Heddeland, I. and Lettenmaier, D. Hydrological modeling of boreal forest ecosystems (1995). Dept of Civil Engineering,U of Washington. Water Resource Series .

Jackson, R.B., Canadell, J., Ehleringer, J.R., Mooney, H.A., Sala, O.E., and Schulze, E.D.(1996). A Global Analysis of Root Distributions for Terrestrial Biomes, *Oecologia* **108**, 389-411.

Jarvis, P.G.(1976). Interpretation of Variations in Leaf Water Potential and Stomatal Conductance Found in Canopies in Field, *Philosophical Transactions of the Royal Society of London Series B-Biological Sciences* **273**, 593-610 .

Ju, W.M. and Chen, J.M.(2005). Distribution of Soil Carbon Stocks in Canada's Forests and Wetlands Simulated Based on Drainage Class, Topography and Remotely Sensed Vegetation Parameters, *Hydrological Processes* **19**, 77-94.

Ju, W.M., Chen, J.M., Black, T.A., Barr, A.G., Liu, J., and Chen, B.Z.(2006a). Modelling Multi-Year Coupled Carbon and Water Fluxes in a Boreal Aspen Forest, *Agricultural and Forest Meteorology* **140** , 136-151.

Kimball, J.S., White, M.A., and Running, S.W.(1997). Biome-Bgc Simulations of Stand Hydrologic Processes for Boreas, *Journal of Geophysical Research-Atmospheres* **102**, 29043-29051.

Kirchmann, H., Snall, S., Eriksson, J., and Mattsson, L.(2005). Properties and Classification of Soils of the Swedish Long-Term Fertility Experiments: V. Sites at Vreta Kloster and Hogasa, *Acta Agriculturae Scandinavica Section B-Soil and Plant Science* **55**, 98-110.

Kljun, N., Calanca, P., Rotachhi, M.W., and Schmid, H.P.(2004). A Simple Parameterisation for Flux Footprint Predictions, *Boundary-Layer Meteorology* **112**, 503-523.

Letts, M.G., Roulet, N.T., Comer, N.T., Skarupa, M.R., and Verseghy, D.L.(2000). Parametrization of Peatland Hydraulic Properties for the Canadian Land Surface Scheme, *Atmosphere-Ocean* **38**, 141-160.

Leuning, R.(1990). Modeling Stomatal Behavior and Photosynthesis of Eucalyptus-Grandis, *Australian Journal of Plant Physiology* **17**, 159-175.

Leuning, R.(1997). Scaling to a Common Temperature Improves the Correlation Between the Photosynthesis Parameters J(Max) and V-Cmax, *Journal of Experimental Botany* **48**, 345-347.

Liu, J., Chen, J.M., Cihlar, J., and Park, W.M.(1997). A Process-Based Boreal Ecosystem Productivity Simulator Using Remote Sensing Inputs, *Remote Sensing of Environment* **62**, 158-175.

Liu, J., Chen, J.M., Cihlar, J., and Chen, W.(2002). Net Primary Productivity Mapped for Canada at 1-Km Resolution, *Global Ecology and Biogeography* **11**, 115-129.

Lundberg, A. and Halldin, S.(1994). Evaporation of Intercepted Snow - Analysis of Governing Factors, *Water Resources Research* **30**, 2587-2598.

Molotch, N.P., Blanken, P.D., Williams, M.W., Turnipseed, A.A., Monson, R.K., and Margulis, S.A.(2007). Estimating Sublimation of Intercepted and Sub-Canopy Snow Using Eddy Covariance Systems, *Hydrological Processes* **21**, 1567-1575.

Price, A.G., Dunham, K., Carleton, T., and Band, L.(1997). Variability of Water Fluxes Through the Black Spruce (Picea Mariana) Canopy and Feather Moss (Pleurozium Schreberi) Carpet in the Boreal Forest of Northern Manitoba, *Journal of Hydrology* **196**, 310-323.

Price, J.S., Branfireun, B.A., Waddington, J.M., and Devito, K.J.(2005). Advances in Canadian Wetland Hydrology, 1999-2003, *Hydrological Processes* **19**, 201-214.

Quinn, P., Beven, K., Chevallier, P., and Planchon, O.(1991). The Prediction of Hillslope Flow Paths for Distributed Hydrological Modeling Using Digital Terrain Models, *Hydrological Processes* **5**, 59-79.

Rawls, W.J., Brakensiek, D.L., and Saxton, K.E.(1982). Estimation of Soil-Water Properties, *Transactions of the Asae* **25**, 1316-&.

Roberts, J.(2007). The Role of Plant Physiology in Hydrology: Looking Backwards and Forwards, *Hydrology and Earth System Sciences* **11**, 256-269.

Running, S.W. and Coughlan, J.C.(1988). A General Model of Forest Ecossytem Processes for Regional Applications I. Hydrological Balance, Canopy Gas Exchange and Primay Production Processes , *Ecological Modelling* **42**, 125-154.

Shinozaki, K., Yoda, K., Hozumi, K., and and Kira, T.(1964a). A Quantitative Analysis of Plant Form. Pipe Model Theory. II. Further Evidences of the Theory and Its Application in Forest Ecology., *Jpn. J. Ecol.* 133–139.

Shinozaki, K., Yoda, K., Hozumi, K., and and Kira, T. (1964b). A Quantitative Analysis of Plant Form. Pipe Model Theory. I. Basic Analysis., *Jpn. J. Ecol.* 97–105.

Schwarzel, K., Renger, M., Sauerbrey, R., and Wessolek, G.(2002). Soil Physical Characteristics of Peat Soils, *Journal of Plant Nutrition and Soil Science-Zeitschrift Fur Pflanzenernahrung Und Bodenkunde* **165**, 479-486.

Sonnentag, O., Chen, J.M., Roulet, N.T., Ju, W., and Govind, A.(2008). Spatially Explicit Simulation of Peatland Hydrology and Carbon Dioxide Exchange: Influence of Mesoscale Topography, *Journal of Geophysical Research-Biogeosciences* **113**.

Sonnentag, O., Talbot, J., Chen, J.M., and Roulet, N.T.(2007). Using Direct and Indirect Measurements of Leaf Area Index to Characterize the Shrub Canopy in an Ombrotrophic Peatland, *Agricultural and Forest Meteorology* **144**, 200-212 .

Soulis, E.D., Snelgrove, K.R., Kouwen, N., Seglenieks, F., and Verseghy, D.L.(2000). Towards Closing the Vertical Water Balance in Canadian Atmospheric Models: Coupling of the Land Surface Scheme Class With the Distributed Hydrological Model Watflood, *Atmosphere-Ocean* **38**, 251-269.

Tague, C.L. and Band, L.E.(2001). Evaluating Explicit and Implicit Routing for Watershed Hydro-Ecological Models of Forest Hydrology at the Small Catchment Scale, *Hydrological Processes* **15**, 1415-1439.

Tague, C.L. and Band, L.E.(2004). RHESSys: Regional Hydro-Ecologic Simulation System—An Object-Oriented Approach to Spatially Distributed Modeling of Carbon, Water, and Nutrient Cycling, *Earth Interactions* 1–42.

Tombul, M., Akyurek, Z., and Sorman, A.U.(2004). Determination of Soil Hydraulic Properties Using Pedotransfer Functions in a Semi-Arid Basin, Turkey, *Hydrology and Earth System Sciences* **8**, 1200-1209.

Verstraeten, W.W., Veroustraete, F., and Feyen, J.(2006). On Temperature and Water Limitation of Net Ecosystem Productivity: Implementation in the C-Fix Model, *Ecological Modelling* **199**, 4-22.

Voinov, A.A., Fitz, H.C., and Costanza, R. (1998). Surface Water Flow in Landscape Models: I. Everglades Case Study, *Ecological Modelling* **108**, 131-144.

Way D.A. & Sage R.F. (2008) Elevated growth temperatures reduce the carbon gain of black spruce (*Picea mariana* (Mill.) B.S.P.). *Global Change Biology*, **14**, 624-636.

Weiler, M. and Mcdonnell, J.J.(2007). Conceptualizing Lateral Preferential Flow and Flow Networks and Simulating the Effects on Gauged and Ungauged Hillslopes, *Water Resources Research* **43**.

Wigmosta, M.S., Vail, L.W., and Lettenmaier, D.P.(1994). A Distributed Hydrology-Vegetation Model for Complex Terrain, *Water Resources Research* **30**, 1665-1679.

Williams, T.G. and Flanagan, L.B.(1998). Measuring and Modelling Environmental Influences on Photosynthetic Gas Exchange in Sphagnum and Pleurozium, *Plant Cell and Environment* **21**, 555-564.

Wilson, K.B., Baldocchi, D.D., and Hanson, P.J.(2001). Leaf Age Affects the Seasonal Pattern of Photosynthetic Capacity and Net Ecosystem Exchange of Carbon in a Deciduous Forest, *Plant Cell and Environment* **24**, 571-583.

CHAPTER 3

Effects of Sub-surface Baseflow on Photosynthesis and Evapotranspiration.

3.1. Abstract

Landscape scale hydrological processes can greatly alter the local-scale water balance and many ecological processes linked to it. We hypothesize that in humid forest ecosystems, sub-surface baseflow has significant influence on the spatial distribution of ecophysiological processes such as gross primary productivity (GPP) or evapotranspiration (ET). To investigate this further, we conducted a numerical experiment using a further developed spatially explicit hydro-ecological model, BEPS-TerrainLab V2.0. We constructed three modeling scenarios 1) *Explicit*, where a realistic calculation of baseflow was employed considering topographic controls 2) *Implict,* where the baseflow calculations were based on a bucket modeling approach 3) *NoFlow*, where the lateral water flow was turned off in the model. The results show large differences among the three scenarios for the simulated GPP and ET. The *NoFlow* generally underestimated GPP and ET while the *Implicit* scenario overestimated them. GPP was more sensitive to baseflow fluxes than ET because of the presence of compensatory mechanisms in the total ET. The key mechanisms controlling GPP and ET were manifested through changes in stomatal conductance (g_s), nitrogen (N) availability, unique contributions from the forest floor and also due to an alteration in the spatial upscaling mechanisms. Further, we conducted a sensitivity analysis using 14 parameters that are common to both GPP and ET simulation. The sensitivity analysis revealed that the magnitudes of errors due to inaccurate hydrological representation are more serious than parameter inaccuracies. We conclude that current large

scale GPP and ET estimates that ignore hydrological controls could have significant errors because of the large topographic variations on the Earth's surface.

3.2. Introduction

Terrestrial carbon (C) dynamics under climate change is a matter of speculation due to various uncertainties in the coupling of biogeochemical cycles that are not very well understood. The majority of terrestrial fresh water resources (including ice and snow) and soil C-stocks are distributed at high latitude boreal forests that have a major role in global climate change (Van Hees et al., 2005). Although on a long-term basis, C cycling in boreal forests is driven by climate and disturbances (Kurz and Apps, 1995), on a short-term basis, the inter-annual variability of boreal forest biogeochemical processes is determined by variations in hydrological processes (Metcalfe and Buttle, 1999; Devito et al.,2005). Hydrological effects on boreal ecosystem productivity have been highlighted only quite recently (e.g., Ju et al., 2006; Pauwels and Wood 2000).

Although at local scales, mostly matric and osmotic potentials govern soil-water flow, at landscape or watershed scales, topographical differences are the main cause for potential gradients (gravitational) that control water movement. In humid forested watersheds where the infiltration capacity is several times higher than the precipitation intensity, sub-surface baseflow is the most common form of lateral water transport. Considering the importance of sub-surface baseflow in humid forest ecosystems that generally have non-Hortonian run-off generation mechanisms, it is possible that simulation of soil-moisture using simplified schemes such as *bucket modeling*, or using surrogates such as remote sensing-derived soil-moisture products may not comprehensively explain the hydrologically-controlled ecophysiological and biogeochemical processes. The nature of the soil-water partitioning and the spatial and

temporal dynamics of ecophysiological processes in these ecosystems are determined by the manner in which lateral hydrological processes are conceptualized in modeling domains.

To investigate the errors associated with spatially explicit ecophysiological simulations that ignore explicit modeling of soil water partitioning and sub-surface baseflow fluxes, we conducted a numerical experiment using a better-developed and validated hydro-ecological model, BEPS-TerrainLab V2.0 (Govind et al.,2008a). We analyzed the influence of baseflow on two main ecophysiological processes, gross primary productivity (GPP) and evapotranspiration (ET) using various hydrological scenarios that differ in the mechanism of soil water partitioning consequent of the differences in the conceptualization of baseflow fluxes. These scenarios represent the current forms of hydrological representations that are used directly or indirectly in many ecosystem models. Specific objectives of this study are:

1) To investigate the effects of unrealistic hydrological regimes on the spatial and temporal distribution of GPP and ET through a simple modeling experiment.
2) To identify the dominant mechanisms that create variations in the simulated GPP and ET.
3) To analyze the sensitivity of some selected parameters used within BEPS-TerrainLab V2.0 to understand the potential error contribution associated with them vis-à-vis the errors created due to improper hydrological representation.

3.3. Model Description

BEPS-TerrainLab V2.0 is a spatially explicit hydro-ecological model that simulates C , N and hydrological cycles and the related feedback relationships in a tightly coupled manner. A detailed description of this model can be found in Govind et al. (2008a, this issue) and Govind et al. (2008d). This model employs a temporally and spatially upscaled photosynthesis sub-model (Chen et al., 1999) to simulate daily GPP as a function of hydrologically controlled

stomatal conductance (g_s) and plant N status in addition to comprehensive calculation of canopy radiation regimes. Most of the hydrological processes are explicitly modeled in BEPS-TerrainLab V2.0 by solving a detailed water balance equation that considers lateral water fluxes, saturated and unsaturated zone hydrological processes, snow dynamics and ET, at a daily time step. ET is explicitly calculated as evaporation and transpiration using the Penman-Monteith equation for different canopy layers, moss or soil surfaces, in the modeling domain using surface specific radiation, and resistance terms. Soil temperature at various depths is calculated by numerically solving the Fourier heat transfer process. Explicit modeling soil C dynamics as a function of soil-water, soil temperature and variable CN ratios facilitates the modeling of biogeochemical processes such as N-mineralization (Govind et al., 2008d). This model was tested using two years of measurements of GPP, ET, water table depth (WTD), volumetric soil moisture content (Govind et al., 2008a, this issue), snow depth, soil temperature and net ecosystem exchange (Govind et al., 2008d).

3.4. Site Description

The numerical experiment was conducted in a boreal watershed located in north Quebec, Canada. This region falls under humid continental sub-arctic or boreal (taiga) climatic type. Vegetation in this boreal landscape consists of black spruce(*Picea mariana*) as the dominant tree species. Paper birch (*Betula papyrifera Marsh.*) and aspen (*Populus balsamifera L.*) can also be found in locations where a fire event has occurred in the recent past or along watercourses.Black spruce forest are often characterized by a thick moss ground cover comprising feather moss or lichens in the moderately drier areas and *Sphagnum* moss in wetter locations. Landscape vegetation composition varies across the gentle topographic gradient. The Eastern Old Black Spruce site (EOBS) of the Fluxnet-Canada Research Network (FCRN), is

located in the watershed at 49.69°N and 74.34°W, which is ~50 km southeast of Lake Chibougamau and ~200 km northwest of the Lac St. Jean. Since mid-2003, an eddy covariance tower at EOBS has been making continuous high precision measurements of the fluxes of mass and energy between the landscape and the atmosphere. The fetch of the tower extends to 500m in all directions. Therefore, we used a circular area subtended by a 500m radius centered on the tower as "the footprint" for our data analyses (Govind et al., 2008a). The soil at this site is derived from glacio-fluvial deposits, and thus consists of poorly graded materials. The soil is predominantly a podzol, covered by an organic layer with an average depth of 26-30 cm and in humid areas, the soil is organic with an average organic layer of 125 cm (Giasson et al., 2006).

3.5. Datasets Used

In order to perform this numerical experiment, we used various spatial and meteorological datasets used in Govind et al. (2008a) for the year 2004. These spatial datasets include: 1. a land-cover map, 2. a leaf area index (LAI) map, 3. a hydrologically consistent digital elevation model (DEM), 4. soil texture map and, 5. an initial WTD map . All of these spatial datasets have a spatial resolution of 25 m with a UTM Zone 18N projection. Land-cover-specific biophysical parameters and soil texture-specific hydraulic parameters were assigned based on Table 1 and Table 2 in Govind et al. (2008a), respectively. Daily meteorological variables such as maximum temperature, minimum temperature, dew point temperature, incoming shortwave radiation, wind speed, and precipitation (rain or snow) collected at one point (EOBS tower site) were uniquely assigned for all pixels in the modeling domain after correcting for the effects of elevation and slope on temperature and solar radiation, respectively.

3.6. Water Balance of a BEPS-TerrainLab V2.0 Modeling Unit (Pixel)

Since the present study investigates the ecophysiological effects based on the nature of soil water partitioning as a result of variations in sub-surface baseflow, it is important to understand how the local-scale water balance is conceptualized in a BEPS-TerrainLab V2.0 modeling unit. This distributed eco-hydrological model performs calculations on a pixel-to-pixel basis. The net water balance for a pixel at a daily time step can be summarized as shown below:

In the unsaturated zone, $\Delta W_{\text{unsat}} = I - R_{surface} + W_{\text{cr}} - W_{pe} - T_{\text{o,unsat}} - T_{\text{u,unsat}} - E_{floor}$ (1)

Where, ΔW_{unsat} is the storage change in the unsaturated zone

I Net precipitation that reaches the soil surface and is composed of throughfall, stemflow, and snowmelt. This quantity is not affected by the type of scenario.

$R_{surface}$ Saturation overland flow (SOLF)

W_{cr} Capillary rise from the saturated zone to the unsaturated zone.

W_{pe} Percolation from the unsaturated zone to the saturated zone.

$T_{o,unsat}$ Overstory transpiration (water consumed by roots lying in the saturated zone).

$T_{u,unsat}$ Understory transpiration (water consumed by roots lying in the saturated zone).

E_{floor} Forest floor evaporation (weighted sum of soil and moss evaporation) or sublimation from forest floor snow.

In the saturated zone, $\Delta W_{sat} = W_{\text{pe}} - R_{base\ flow} - T_{\text{o,sat}} - T_{\text{u,sat}} - W_{\text{cr}}$ (2)

Where, ΔW_{sat} Storage change in the saturated zone.

$R_{baseflow}$ Sub-surface baseflow.

$T_{o,sat}$ Overstory transpiration (water consumed by roots lying in the saturated zone).

$T_{u,unsat}$ Understory transpiration (water consumed by roots lying in the saturated zone).

The net water balance of the modeling unit as a whole is the sum of the storage change in the unsaturated and the saturated zones, ΔW i.e., Equations 1+2.

$$\Delta W = I - R_{surface} - R_{baseflow} - T_{o,unsat} - T_{o,sat} - T_{u,unsat} - T_{u,sat} - E_{floor} \quad (3)$$

3.7. Numerical Experiment

At watershed scale, lateral hydrological processes could be either due to sub-surface baseflow or SOLF. Since non-Hortonian runoff generation mechanisms are more probable in boreal ecosystems, it is quite intuitive that in humid forested ecosystems when the annual precipitation is much larger than the annual evapotranspiration and the SOLF is rare, topographically driven baseflow play significant role in modifying the local-scale water balance. To investigate the differences in the simulated ecophysiological processes due to variations in soil hydrological regimes, we designed three modeling scenarios that only differed in the manner in which sub-surface baseflow calculations were conceptualized. All spatial and meteorological datasets and initialization procedures were kept constant. The scenarios were:

1) *Explicit* – This is a realistic scenario that includes both forms of lateral water movement, i.e., sub-surface baseflow and SOLF that are calculated using topography and realistic run-off generation mechanisms as outlined in Govind et al. (2008a). This means that baseflow is calculated as a function of the slope of WTD (updated on a daily basis) using a depth integrated Darcy's approach using peat or mineral soil specific transmissivity schemes. The baseflow calculated in this manner is exchanged with the neighboring pixels. When WTD reaches the ground surface, water gets "ponded" and is routed laterally on the ground surface

as SOLF, which enters the water balance calculation of neighboring pixels. This *Explicit* scenario represents the simulation made in Govind et al. (2008a) that represents the "reality". Since this scenario explicitly calculates various hydrological processes similar to what happens in the field, we call it "*Explicit*".

2) *Implicit*-In this scenario, the baseflow is "accounted" assuming a bucket modeling scheme. Theoretically, when the soil-water potential lies between saturation (0 kPa) and field capacity (-330 kPa), its energy status is adequate for gravitational flow. In the *Implicit* scenario, we assume that when the soil water exceeds field capacity, water is prone to lateral movement in the form of sub-surface baseflow. This assumption is currently used directly or indirectly in ecological models that employ "available water content" to constrain ecophysiological processes. The baseflow in the *Implicit* scenario is calculated as:

$$Q_{b\,implicit} = \lfloor \phi - \theta_{fc} \rfloor d \tag{4}$$

where ϕ is the porosity of the soil and θ_{fc} is the volumetric soil water content at the field capacity, d is the depth of the saturated zone, which is the difference between the maximum soil depth and WTD, measured from the soil surface. $Q_{implicit}$ (mm) is the baseflow calculated using the *Implicit* scenario. The baseflow calculated in this way is directly used for daily water balance without being *distributed to* or being *contributed from* the neighboring pixels. Since there is no topographic constrain in this scenario, baseflow occurs freely and the soil always tends to maintain water status below the field capacity and it seldom saturates the whole soil profile unless a very heavy precipitation event occur and the soil storage capacity is much less (e.g. a very shallow soil profile). Thus, the probability of getting SOLF is almost negligible in this scenario.

3) *NoFlow* - This scenario assumes that there no topographically driven sub-surface baseflow between the pixels in the modeling domain. The infiltrated soil water either evaporates or transpires. When WTD reaches the soil surface, "ponding" occurs and thereafter topographically driven SOLF is initiated. SOLF further enters the water balance calculation of neighbouring pixels. Although sub-surface baseflow is "turned-off" in the *NoFlow* scenario, lateral exchange of water among the neighbouring pixels occurs through SOLF. The point to be noted is that in the *NoFlow* scenario, SOLF occurs only after the entire soil profile is saturated. The increased soil saturation could create stress conditions to the vegetation leading to variations in the magnitude of ecophysiological processes. This is the type of hydrological representation that exists in ecological models that consider topographically driven water-flow but ignore the physiological effects of water partitioning within the soil profile.

In this paper, occasionally the *Implicit* and the *NoFlow* scenarios are collectively referred to as "non-explicit scenarios". Currently, regional scale ecological models mostly abstract hydrological controls using either form of non-explicit scenarios or their variants. Table 3-1 shows the characteristic features of the three hydrological scenarios considered in this numerical experiment. Three unique model runs were conducted using the hydrological scenarios and the daily values of GPP and ET were summed to get annual GPP and annual ET. In this study, to investigate hydrological influence on GPP and ET, annual values were used for spatial analysis while EC-tower footprint average values were used for temporal analysis. We chose to use the average values simulated at the footprint of the EC tower to compare the variations among the scenarios because in a previous study (Govind et al., 2008a) the footprint average simulations (the *Explicit* scenario) were validated using eddy covariance data for two years, which provide additional confidence in the comparative analysis.

Table 3-1 Characteristic Features of the Three Hydrological Scenarios Considered in This Numerical Experiment

Features	Scenarios		
	Explicit	***Implicit***	***NoFlow***
Baseflow (BF)	Realistic	Accounted	NA‡
Occurrence of SOLF	Possible	Rare	Dominant
Profile saturation	Realistic	Overly drained	Overly wet
Routing of BF	Present	Absent	Absent
Routing of SOLF	Present	Absent	Present
Effect of topography	Considered	Ignored	Considered§
Direction of BF	Inflow -Outflow	Outflow	NA‡
Pixels involved	9	1	9
Root saturation*	$0< \mu <1$	$\sim \mu =1$	$\sim \mu =0$
Nutrient availability	Accurate	Intensified	Suppressed
Ecological models	Not yet common	Common**	Not common#

‡ Not at all produced in this scenario

§ SOLF drains off based on topography after soil storage is filled up.

* Fraction of root saturation is quantified using the parameter $(1-\mu)$ as a function of root geometry and WTD (see section 3.9.3)

**e.g. Liu et al. (1997a) ; Potter et al. (2001); Heinsch et al. (2006); Coops et al. (2007)

e.g. Some Land Surface Schemes in GCMs that consider topographically driven SOLF but not BF.

3.8. Results

3.8.1 Variation of ET and GPP Sub-components under Hydrological Scenarios

Ecosystem ET and GPP are composed of various sub-components representing vegetation (overstory and understory) and forest floor (soil and moss). These sub-component contributions are likely to vary under different hydrological scenarios. Knowledge of the dynamics of ET and GPP sub-component contributions improve our understanding of the underlying hydro-ecological mechanisms. We analyzed the relative variations of these components using the simulated footprint average values for different scenarios.

In all scenarios, canopy evaporation was simulated to be 58.2 mm, which was 5.5% of the annual precipitation (1,053 mm). This component did not change in any of the scenarios because canopy evaporation is not affected by soil water. Overstory transpiration (as the sum of *sunlit-saturated, sunlit-unsaturated, shaded-saturated and shaded-unsaturated*) showed pronounced differences among scenarios. In the *Explicit* scenario, overstory transpiration was simulated to be 118.6 mm whereas in the *Implicit* scenario, it increased to 125.8 mm and in the *NoFlow* scenario, it decreased to 98.3 mm. There were also significant differences in the simulated understory transpiration (more than overstory). Understory transpiration was 63.1 mm in the *Explicit* scenario, 85.4 mm in the *Implicit* scenario, and 77.6 mm in the *NoFlow* scenario, showing the high sensitivity of understory transpiration to soil moisture fluctuations. Forest floor evaporation varied quite differently as opposed to transpiration because of the combined effects of soil evaporation and moss transpiration. Forest floor evaporation was highest in the *NoFlow* scenario (100.7 mm) and lowest in the *Implicit* scenario (62.7 mm). Figures 3-1a and 3-1b show the relative magnitude of these differences. Simulations also suggest that transpiration is the major contributor to the total ET in real world situations followed by forest floor ET.

GPP sub-components also showed pronounced variations under different hydrological scenarios. The overstory GPP is comprised of *sunlit-saturated*, *sunlit-unsaturated*, *shaded-saturated* and *shaded-unsaturated* GPP sub-components, while the understory GPP is comprised of *understory saturated* and *understory unsaturated* sub-components (Govind et al., 2008a).

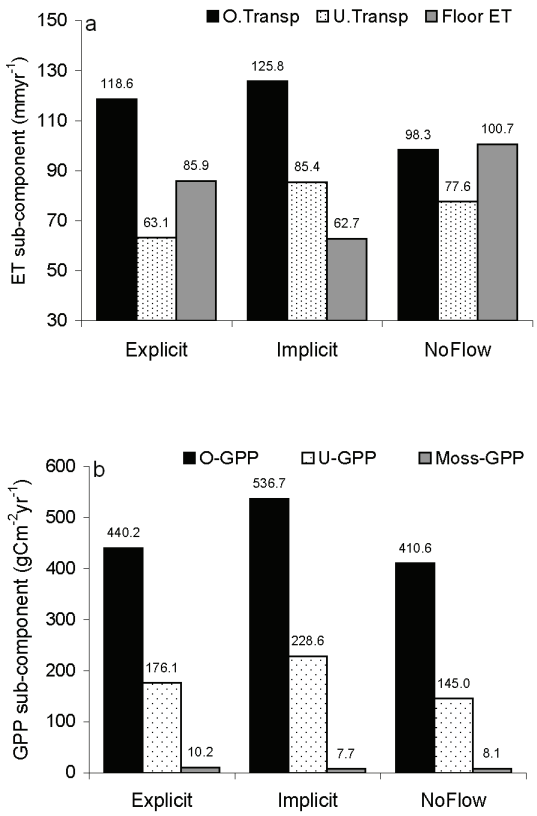

Figure 3-1. Variations among ET and GPP sub-component partitioning under various scenarios of baseflow calculations: (a) Differences in ET sub-component partitioning; and (b) Differences in GPP sub-component partitioning.

The footprint-averaged annual overstory GPP was 440, 536 and 410 $gCm^{-2}yr^{-1}$ under the *Explicit*, *Implicit* and the *NoFlow* scenarios, respectively. The contribution of understory GPP was 176, 228 and 143 $gCm^{-2}yr^{-1}$, under the *Explicit*, *Implicit* and the *NoFlow* scenarios, respectively. There was a striking reduction in the understory GPP in the *NoFlow* scenario and a

drastic increase in the *Implicit* scenario. Since the understory roots are shallower than the overstory roots, they are more sensitive to frequent root zone moisture fluctuations, under different scenarios. In the *Explicit* scenario, the moss GPP was 10.2 $gCm^{-2}yr^{-1}$, under the *Implicit* scenario it was 7.7, and in the *NoFlow* scenario it was 8.1 $gCm^{-2}yr^{-1}$, implying a subtle change in moss GPP.

3.8.2. Temporal Dynamics of GPP and ET under Various Scenarios

The seasonal patterns of GPP and ET simulated under the three scenarios are shown in the Figures 3-2a and 3-2b. In general, GPP was overestimated in the *Implicit* scenario and underestimated in the *NoFlow* scenario, in comparison to the *Explicit* scenario. The overestimation by the *Implicit* scenario was intense between days 150 to 200 coinciding with spring when the soil was generally saturated due to recharging of the soil profile by snowmelt water rapidly bringing the WTD closer to the soil surface. All the scenarios showed a decrease in GPP between the days 210 and 240. This was a dry period in 2004 and consequently the WTD declined in all the scenarios. This decline in soil moisture below the field capacity slightly reduced g_s and hence GPP. It is clear that the decline in GPP was smaller and slower in the *NoFlow* scenario and faster and pronounced for the *Implicit* scenario.

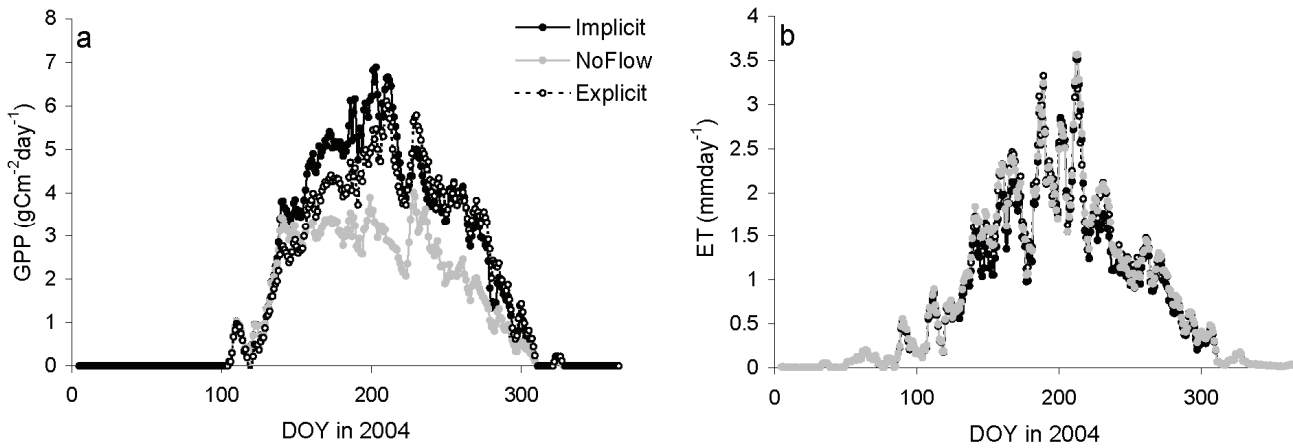

Figure 3-2 Annual variations of GPP and Total ET in the footpint area of the EOBS tower, under various hydrological scenarios.

Figure 3-1b shows the temporal pattern of the footprint average total ET (as the sum of overstory and understory transpiration; canopy evaporation, sublimation and forest floor evaporation). Unlike GPP, all scenarios showed more or less similar magnitudes and trends for the total ET. In a strict sense, the *NoFlow* scenario slightly overestimated total ET during the spring and in the late summer in comparison to the *Explicit* scenario. We should consider that evapotranspiration has many sub-component processes (both physical and biological) that behave differently under various soil moisture conditions (Govind et al., 2008a). Although it can be generalized that the simulated total ET under the *Implicit* scenario is slightly higher than that of the *Explicit* scenario throughout the year, however in the spring, the *Implicit* scenario slightly underestimated total ET in comparison to the *Explicit* scenario. Although these temporal comparisons reflect some of the first-order differences in the footprint region, other regions of the watershed should be analyzed to clarify the underlying hydro-ecological responses.

A comparison of the simulated ET and GPP under the different scenarios against the EC-tower measurements reveals that the *Explicit* scenario is superior in comparison to either the

Implicit or the *NoFlow* scenarios (Table 3-2). The slopes of the simulations reveal that the *NoFlow* scenario slightly underestimates and the *Implicit* scenario overestimates ET. Statistically, the slopes of the simulated ET under the *Explicit* (1.04; *p=0.062)* and the *NoFlow* (0.97; *p=0.257)* scenarios are not significantly different from 1 (EC-measurements). However, in the *Implicit* scenario (1.05; *p=0.041*), the slope being significantly different from 1, the overestimation of ET by this scenario can be further justified. The RMSE was highest for the *NoFlow* scenario (0.387 mm day^{-1}) and lowest for the *Explicit* scenario (0.365 mm day^{-1}) with the *Implicit* scenario having an intermediate level of error (0.363 mm day^{-1}). The Nash-Shutcliffe Efficiency (NF-Effi.) was highest for the *Explicit* scenario (0.80) and lowest for the *NoFlow* (0.69) scenario with the *Implicit* scenario having an intermediate level of efficiency (0.76).

Table 3-2. Statistical measures of model performance under the three hydrological scenarios.

Scenarios	***Explicit***		***NoFlow***		***Implicit***	
Criteria	**ET**	**GPP**	**ET**	**GPP**	**ET**	**GPP**
Slope (b1)	1.046	1.001	0.971	0.640	1.052	1.087
p-value1	*0.062*	*0.951*	*0.257*	*<0.001*	*0.041*	*<0.001*
R^2	0.842	0.924	0.804	0.767	0.832	0.856
p-value	*<0.001*	*<0.001*	*<0.001*	*<0.001*	*<0.001*	*<0.001*
RMSE	0.365	0.559	0.387	0.686	0.383	0.869
NS-Effi.	0.80	0.91	0.69	0.58	0.73	0.76

Regression Model	$y = b_o + b_1 x$
Null Hypothesis	$H_o : b_1 = 1$
Alternative Hypothesis	$H_1 : b_1 \neq 1$
Significance Level	0.05

A comparison of the simulated GPP under the different scenarios against the EC-tower measurements reveals that the GPP is highly sensitive to hydrology than ET. The slopes of the

simulations reveal that the *NoFlow* scenario (0.64) underestimates and the *Implicit* scenario (1.09) slightly overestimates the seasonal GPP. Statistically, the slopes of the simulated GPP under the *Explicit* (1.00; *p=0.951)* is not significantly different from 1 (EC-measurements). However, for the *NoFlow* (0.64; *p=<0.001*) and the *Implicit* scenario (1.09; *p=<0.001*), the slope being significantly different from 1, the underestimation or overestimation of GPP under non-explicit hydrological scenarios is statistically justified. The RMSE was highest for the *Implicit* scenario (0.869 gC m^{-2} day^{-1}) and lowest for the *Explicit* scenario (0.559 gC m^{-2} day^{-1}) with the *Implicit* scenario having an intermediate level of accuracy (0.689 gC m^{-2} day^{-1}). The NF-Effi. was highest for the *Explicit* scenario (0.91) and lowest for the *NoFlow* (0.58) scenario with the *Implicit* scenario having an intermediate level of accuracy (0.76).

3.8.3. Spatial Variability of GPP under Hydrological Scenarios

A pixel-to-pixel comparison of the annual GPP simulated under the three scenarios (*Explicit* vs. *NoFlow* or *Implicit*) for the whole watershed (number of pixels n= 35,426) are shown in the Figures 3-3a and 3-3b, respectively. These plots demonstrate that the simulated GPP varied significantly under the three scenarios (deviation from the 1:1 line). Note that one unit on x or y-axis corresponds to a 200 $gCm^{-2}yr^{-2}$, which is a substantial amount of C. Variations in the annual GPP suggest that the *NoFlow* scenario greatly underestimated GPP as opposed to the *Explicit* scenario (Figure 3-3a). The magnitude of underestimation was as high as -35%. There were also cases of overestimation of GPP as much as 10% of the realistic values. On an average for the whole watershed, GPP was underestimated by 1.5% in the *NoFlow* scenario.

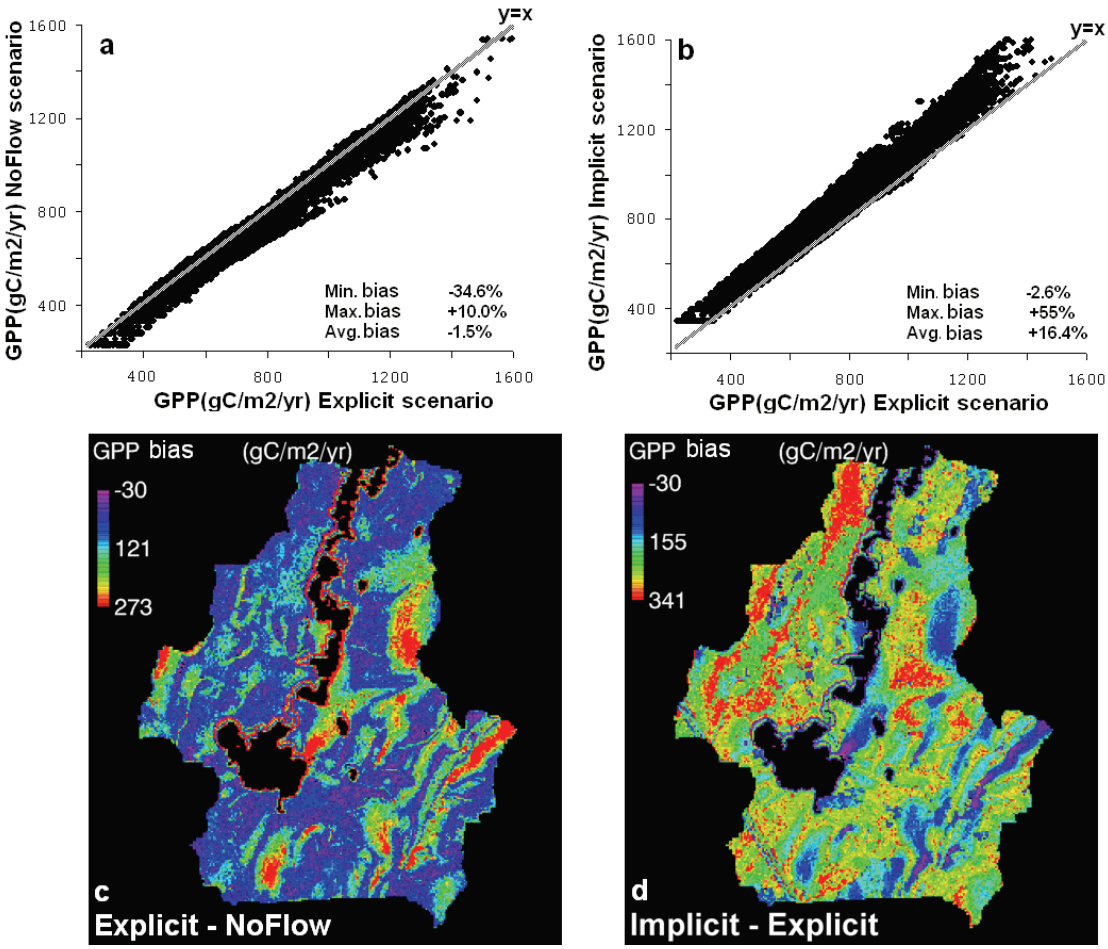

Figure 3-3. A pixel to pixel comparison of annual GPP for the entire watershed under (a) the *Explicit* and the *NoFlow* scenarios and (b) the *Explicit* and the *Implicit* scenarios. (c) Spatial variation of the GPP difference between the *Explicit* and the *NoFlow* scenarios (*Explicit- NoFlow*). Note that the maximum positive difference (underestimation by the *NoFlow* scenario) is seen on the hillslopes where the baseflow is intense. (d) Spatial variation of the GPP difference between the *Implicit and* the *Explicit* scenarios (*Implicit-Explicit*). Note that the maximum positive difference is seen in most parts of the watershed where the surface is near flat.

Comparison between *Implicit* vs. *Explicit* scenarios revealed an opposite trend. Figure 3-3b shows a pixel-to-pixel plot of annual GPP simulated by the *Implicit* vs. *Explicit* scenarios. The *Implicit* scenario overestimated annual GPP by as much as 55% and the watershed average overestimation was as high as 16.4%, which is a large difference.

The spatial variability of these differences is better understood by visually interpreting a difference map using the annual GPP simulated under the *Explicit* and a "non-explicit" scenario. Figure 3-3c shows the difference between the annual GPP simulated using *Explicit* and *NoFlow* scenarios. Differences were large on the hill-slope locations of the watershed where the influence of sub-surface baseflow is quite high (red tones). On flatter locations, GPP differences were minimal owing to subtle topographic differences (blue tones). "Turning-off" sub-surface baseflow would not make much difference to the soil water status of flatter locations, and hence plant physiological conditions were not affected greatly.

Annual GPP on hillslopes were generally underestimated under the *Implicit* scenario (blue tones) due to "less than normal" baseflow fluxes due to the absence of topographic control. In Figure 3-3d it can be seen that the overestimation under the *Implicit* scenario was as high as 341 $gCm^{-2}yr^{-1}$. The *Implicit* scenario generally overestimated annual GPP on flatter areas (red tones) because this scenario unrealistically maintained the soil moisture status at hyper-optimal levels which facilitated proper stomatal functioning and plant growth which resulted in higher annual GPP. Locations having a dominance of mixed or deciduous species showed a striking overestimation. For example, in the northwestern parts of the watershed where mixed forests are found on esker ridges, there is a significant overestimation of annual GPP because water was always maintained at optimal conditions that created hyper-optimal conditions for plant growth resulting in an overestimation of as much as 341 $gCm^{-2}yr^{-1}$. We believe that in this humid boreal ecosystem in eastern North America (annual precipitation=1053mm) where the annual precipitation is greater than annual evapotranspiration soil water seldom falls below the permanent wilting point and plant stress conditions are more likely created due to water abundance than water scarcity.

On hill-slope locations (Figure 3-3d, blue tones) annual GPP was underestimated because the implicitly simulated baseflow fluxes were less than reality (*Explicit*) and this lead to conditions of slight soil saturation and a small reduction in annual GPP (30 $gCm^{-2}yr^{-1}$).

From these results it can be deduced that the errors created due to the *Implicit* scenario on GPP are more intense on flat areas and elevated-flat areas than on hillslopes and vice versa for the *NoFlow* scenario. We postulate that soil hydraulic properties (e.g., Ksat, field capacity, wilting point, etc.); the nature of the vegetation (LAI, clumping index, maximum stomatal conductance) and the mechanisms of biogeochemical cycling (soil C-pool dynamics and consequent N release) simultaneously govern the hydro-ecological response within a given topographic location.

3.8.4. Spatial variability of ET under Various Scenarios

A pixel-to-pixel comparison of the simulated annual total ET calculated under the *Explicit* and the *NoFlow* scenarios revealed that the deviation could be either positively or negatively biased (see Figure 3-4a). Annual total ET is the sum of annual overstory transpiration; annual understory transpiration; annual forest floor evaporation (moss and soil evaporation); annual canopy evaporation (not altered under various scenarios) and annual sublimation (not altered under various scenarios). Transpiration sub-components generally decline under soil saturation due to stomatal regulation whereas forest floor evaporation increase due to increase in soil saturation (a behavior distinct from vascular plants).

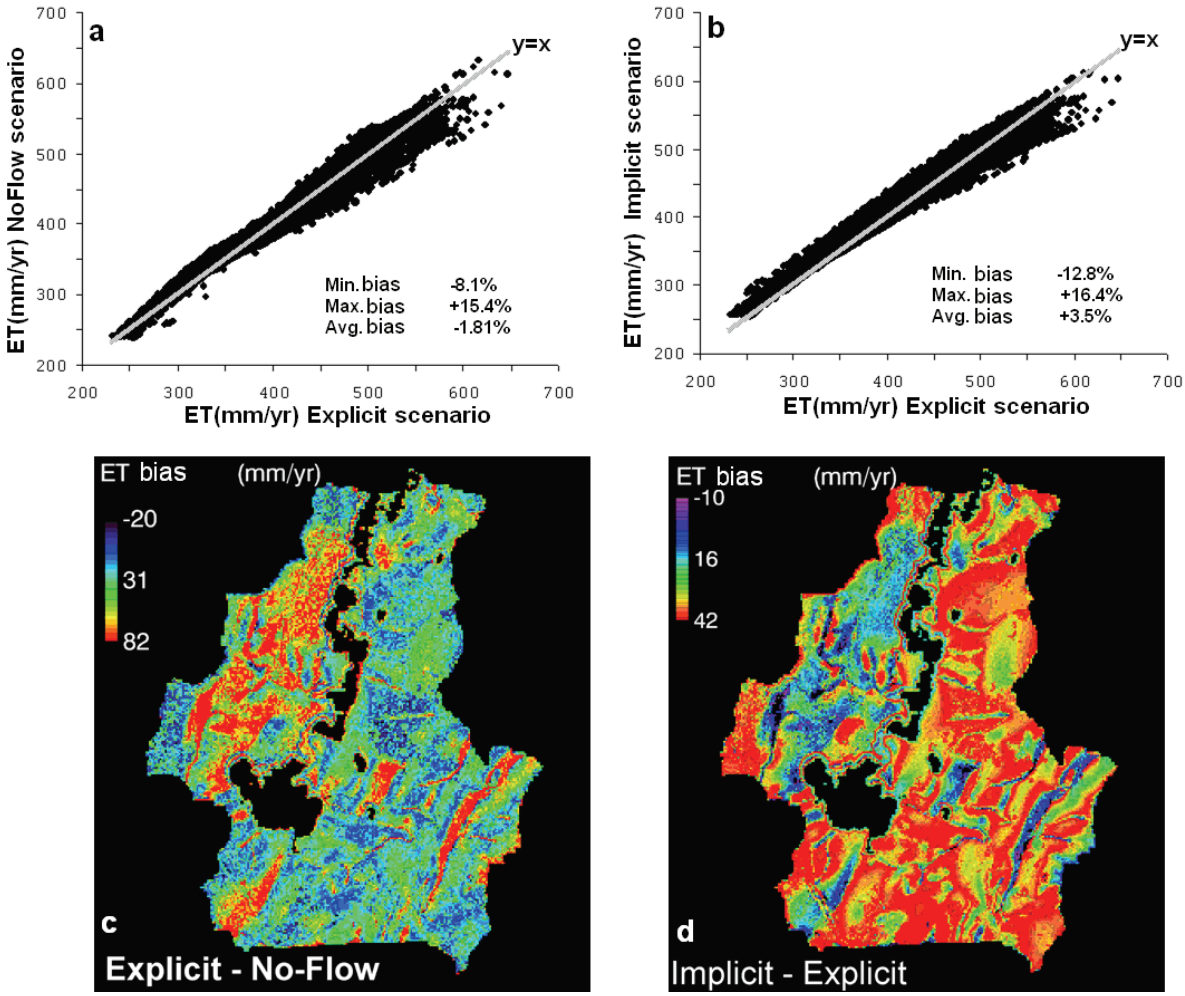

Figure 3-4. A pixel to pixel comparison of annual ET for the entire watershed under (a) *Explicit* and *NoFlow* scenarios and (b) *Explicit* and *Implicit* scenarios. (c) Spatial variation of the ET difference between the *Explicit* and *NoFlow* scenarios. Note that the maximum positive difference (underestimation by the *NoFlow* scenario) is seen on the depressions that are otherwise saturated with water. This is due to rapid reduction in soil and moss evaporation. (d) Spatial variation of the ET difference between *Implicit and Explicit* scenarios. Note that the maximum positive difference is seen in most flat parts of the watershed because of "more than normal" unrealistically created baseflow under the *Implicit* scenario that lowers soil water content to the field capacity.

Under the *NoFlow* scenario, since the soil profile was generally saturated and WTD reaches the surface of the soil, forest floor evaporation increases, which compensates (or sometimes increases the magnitudes) for the reduction in transpiration on the annual total ET.

Due to these mutual compensating effects between the vascular plants and the forest floor, annual total ET simulated under the *NoFlow* scenario was only slightly lower (watershed average underestimation was 1.81%) in comparison to the *Explicit* scenario. Under the *Implicit* scenario, however, the annual total ET generally increased due to enhancements in plant transpiration. On locations such as depressions and streams, where unrealistically high baseflow was simulated, the soil moisture sharply declined which substantially reduced the forest floor evaporation which reduced the annual total ET (the transpiration component in the locations are lower). However, the overall effect of the *Implicit* scenario on the annual total ET is a slight overestimation of 3.5% in comparison to the *Explicit* scenario.

The spatial distribution of the differences in the simulated annual total ET under various scenarios is shown in Figures 3-4 c and d, respectively. Under the *NoFlow* scenario (Figure 3-4c), annual total ET was generally underestimated in comparison to the *Explicit* scenario (red or green tones). The most prominent differences were seen on the northwestern part of the watershed and in low-lying locations. These locations represent meso-scale topographic features formed due to glacial activity e.g. drumlins or eskers that have parallel ridges and depressions that exist side by side. These depressions normally accumulate water from the nearby ridges and the total annual ET mostly contributed by forest floor evaporation. Under the *NoFlow* scenario, these locations dried out due to the absence of baseflow contributions from surrounding regions (a "decoupling effect") and total annual ET is reduced. A similar situation exists in depressions located in the southern part of the region near streams and rivulets.

The *Implicit* scenario (Figure 3-4d) generally overestimated the annual total ET especially on flatter locations of the watershed, in comparison to the *Explicit* scenario (red tones). However, on locations where there are depressions (in the northwestern part) and rivulets (southeastern part), the overestimation is weaker. The soils at these locations become "drier

than usual" because of the combined effects of excessive baseflow fluxes and the absence of water from the surrounding areas ("a decoupling effect" analogous to what Devito et al. (2005) observed during dry periods in a similar environment). This decoupling effect resulted in a decreased soil saturation and low forest-floor evaporation. This condition resulted only in a weak increase in total annual ET even though there was a slight increase in transpiration (blue tones).

From the magnitude of these differences, we can reason that unrealistic hydrological representations affect GPP more severely than ET. This is because GPP is affected by three hydro-ecologically controlled mechanisms: (1) Soil moisture controlled dynamics of ambient g_s, (2) Soil moisture controlled alteration in plant N status as a function of soil organic matter decomposition; and (3) Soil moisture controlled modification in the proportion of roots that lie in saturated or unsaturated zones which proportionately affect the leaf physiological status. Hydro-ecological effects on the total ET are comparatively less intense because a decrease in transpiration would be compensated by an increase in forest floor evaporation and vice versa. Moreover, no biochemical controls (e.g., plant N) exists in the Penman-Monteith equation, which is used to calculate ET.

3.8.5. Variation of Soil Water Balance under Hydrological Scenarios

The mechanism of soil water balance under various scenarios considered in this study is unique, resulting in variations in rhizosphere hydrological regimes that affect ecophysiological mechanisms such as ET and GPP. Figure 3-5 shows the partitioning of soil-water (footprint average) during the modeling period of one year, for different scenarios. It is obvious that under the *NoFlow* scenario, where the sub-surface baseflow is "turned-off", the main mechanism of lateral water flow is SOLF, which is almost 66% of the infiltrated water. In the

current model set up, SOLF occurs only after the soil profile is saturated up to the soil surface and the excess water that is ponded is subjected to topographically driven surface runoff (Hewlett's hypothesis). This mechanism of profile saturation resulted in a positive change in soil water storage as much as 9.4% of the annual infiltrated water. The increased saturation of the soil profile causes a large fraction root to remain in the saturated zone (where $\theta = \phi$, porosity), for most parts of the year.

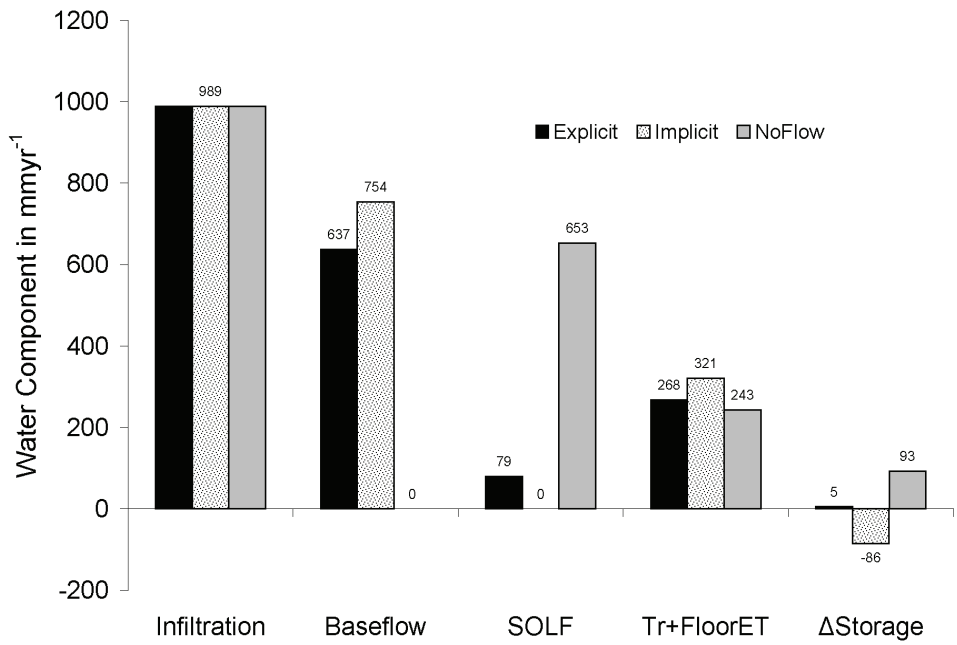

Figure 3-5. Nature of water balance under various hydrological scenarios in the footprint region of the EOBS tower in 2004.

Since the soil remained saturated in the *NoFlow* scenario, g_s declines and consequently the transpiration was reduced with a simultaneous increase in soil and moss surface conductance resulting in increased forest floor evaporation, in comparison to the *Explicit* scenario. However, the sum of transpiration and forest floor evaporation (24.5% of infiltrated water) is slightly lower than that in the *Explicit* scenario.

The *Implicit* scenario simulated baseflow without any topographical control. Soil water having energy status above the field capacity was allowed to "drain-off" which results in excessive draining even in flatter areas. Hence, the simulated baseflow was greater than that of the *Explicit* scenario. Since the soil profile is drained excessively, the WTD never rose to the soil surface, and therefore, no SOLF occured. The soil profile remained unsaturated for most parts of the year, creating conducive conditions for plant growth due to increased g_s and plant N availability. This results in excessive transpiration although forest floor evaporation is reduced. However, the sum of transpiration and soil evaporation remains higher than that of the *Explicit* scenario. Excessive baseflow combined with excessive transpiration loss created a negative storage in the *Implicit* scenario of about -8.6% of the infiltrated water during the modeling time period of 365 days.

Having seen that total runoff (SOLF+Baseflow) is more or less the same in all three scenarios, we speculate that the nature of soil-water partitioning controls biogeochemical and plant physiological mechanisms that greatly alter ecophysiological processes, even if we consider the lateral water fluxes on the lanfscape in a non-explicit manner.

3.9. Discussion

Physiologically, soil water status influences g_s either by altering leaf-water potential or by changing the level of phytohormones produced by roots in response to soil-water status. There are several studies that demonstrate the effect of soil water-induced stress factors (excess or deficiency) that decreases the potential rate of g_s. At one extreme, excess water reduces oxygen and elevates CO_2 in the root zone, limiting water uptake and resulting in leaf-water deficits that cause stomatal closure. On the other, drought reduces the soil-water potential,

which affects the plant water relationship. At larger spatial scales, topography determines the hydrologic response and the spatio-temporal distribution of locations of soil saturation and unsaturation . Topography-governed lateral water fluxes could result in either sub-surface baseflow or SOLF. Of these, baseflow is a continuous and less interrupted phenomenon, which is several times more important than SOLF in boreal forests. Hence, sub-surface baseflow can play a significant role in altering the local-scale water balance.

3.9.1. Stomatal Dynamics

The magnitude of the ambient g_s governs the amount of C-that enters the plant for photosynthesis and the amount of water that leaves the plant as transpiration. The difference in simulated GPP and ET under various scenarios can be mainly attributed to stomatal dynamics that is affected by several environmental controls, of which soil water status is one of the most influential and dynamic one.

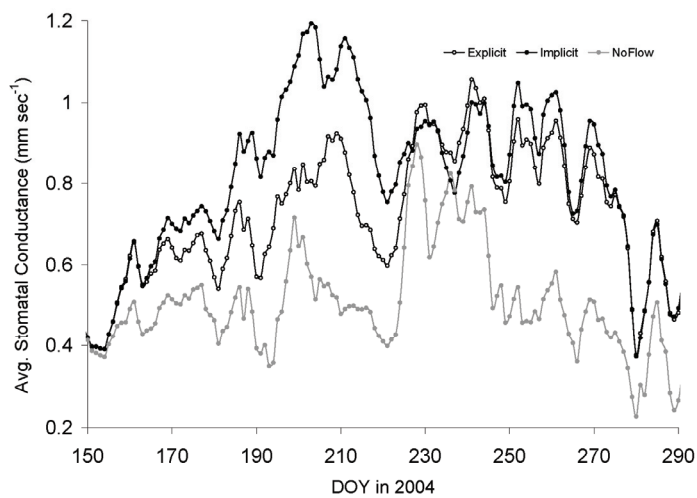

Figure 3-6. Seasonal dynamics of the average g_s in the footprint region, under different scenarios. Note the pronounced underestimation by the *NoFlow* scenario and overestimation by the *Implicit* scenario in comparison to the *Explicit* scenario.

In BEPS-TerrainLab V2.0, there are four types of leaves within a given canopy (Govind et al., 2008a). They are *sunlit-saturated*, *sunlit-unsaturated*, *shaded-saturated*, and *shaded-unsaturated*. All of these, depending on their light and soil moisture regimes, have different magnitudes of g_s. Also, there are different plant species in the boreal landscape that have a wide range of maximum stomatal conductance values ($g_{s,\max}$).

Various environmental controls such as light and water stress can constrain $g_{s,\max}$, resulting in a wide range of ambient g_s values. For example, g_s of a healthy black spruce leaf may be similar to the g_s of a stressed leaf of a deciduous species. Figure 3-6 shows the dynamics of the average g_s in the footprint area under different scenarios. In general, the g_s simulated by the *NoFlow* scenario is lower than that of the *Explicit* scenario while the *Implicit* scenario had higher values. These differences were large in the spring when the soil is saturated and baseflow fluxes are intense due to recharging of soil profile due to snow melt water.

3.9.2. Nitrogen Mineralization

Another factor that is responsible for creating variations in simulated GPP can be attributed to leaf N concentration. In this pristine ecosystem, differences in the leaf N concentration occurs due to changes in soil C-pool decomposition, which is influenced by various hydrological scenarios. This directly affects photosynthesis. Various soil C-pools, when they decompose (mainly due to heterotrophic respiration), release N that is available to plants for uptake. The rates of C-pool decomposition are mediated by many biotic and abiotic factors that are linked to the local hydrological regime. Leaf N concentration directly affects photosynthesis by altering the Vcmax , the maximum carboxylation rate in the temporally integrated Farquhar's model used within BEPS-TerrainLab V2.0. Heterotrophic respiration was

unrealistically increased under the *Implicit* scenario as opposed to the *NoFlow* scenario due to conducive soil moisture and temperature conditions for microbial proliferation and soil organic pool decomposition. The detailed mechanism behind the modeling of soil C-pool decomposition and N mineralization under various hydrological scenarios is addressed in Govind et al. (2008d).

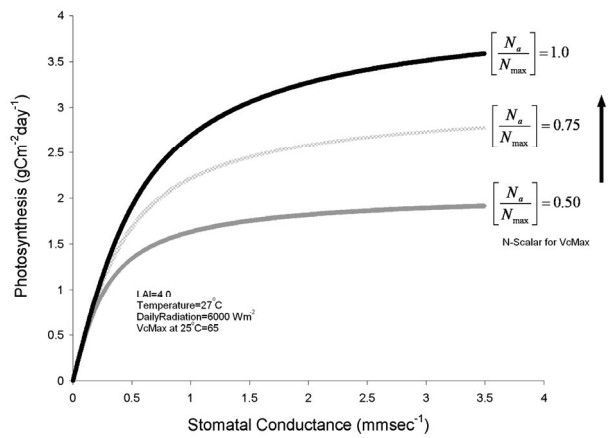

Figure 3-7. Relationship between stomatal conductance and GPP simulated using the temporally integrated Farquhar model (Chen et al.,1999), at various levels of plant N, for a given set of conditions. Both stomatal conductance and N availability are affected under various hydrological scenarios.

The conceptual relationship between g_s, N status and photosynthesis operating within the BEPS-TerrainLab V2.0 modeling domain is shown in the Figure 3-7. This relationship was plotted based on a set of hypothetical conditions with only g_s and N as variables. Note the close synergism between g_s and plant N status in affecting photosynthesis. Both of these parameters are highly dependent on the local hydrological status. The scalar $N_a / N_{\max}$ is the ratio of ambient plant N (%) to the maximum plant N (%). In BEPS-TerrainLab V2.0, soil N is calculated as shown in a generalized form below.

$$N_a = f(T_s, \theta, \sum_1^9 C, N_{fix}, N_{dep}) \quad (5)$$

Where, T_s is the soil temperature, θ is the volumetric soil water content, C is the size of a soil C pool (9 in total), N_{fix} is N fixation by biological or physical processes (lightning induced or biological N fixation), N_{dep} is the dry and wet deposition. All of these parameters are determined by soil water status, except N_{dep}.

3.9.3. Dynamics of Root Fractions within a Soil Saturation Regime

Differences in the input and output components of soil-water balance result in variation of the WTD in a given pixel, which demarcates the separation of saturated and unsaturated zones. Unlike the unsaturated zone, in the saturated zone, all the soil pores are filled with water ($\theta = \phi$). Different hydrological scenarios simulated unique combinations of soil saturated and unsaturated zones.

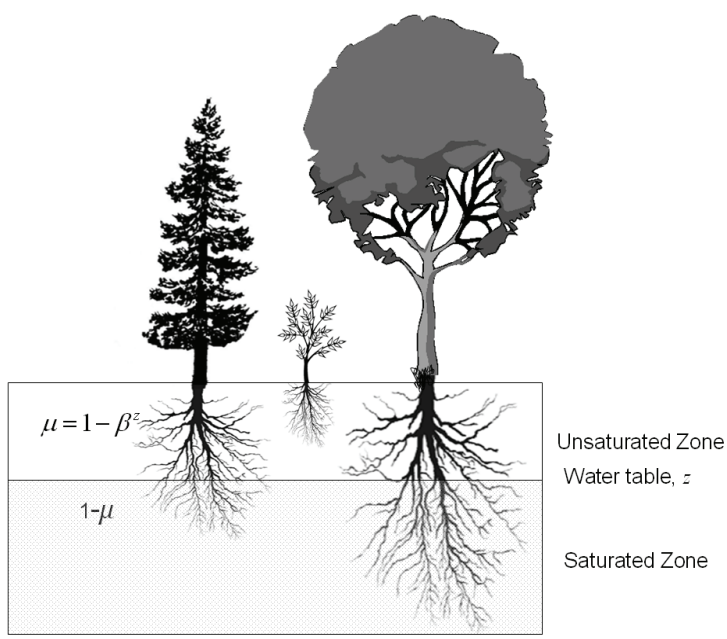

Figure 3-8. A schematic representation of the separation of roots into unsaturated and saturated fractions as a function of root geometry factor, β, and water table, z. These fractions are used to constrain the ecophysiology of leafs in a proportionate manner, in order to calculate the stomatal conductance g_s.

The root geometry as modeled by the method outlined by Gale and Grigal (1987) and the position of WTD determines the fractions of roots lying in the saturated and unsaturated zone (see the conceptual sketch in Figure 3-8).Figure 3-9 b shows the variation of unsaturated root fraction, μ with WTD for different types of root geometries. As the water table rises (value decreases), the unsaturated fraction (μ) decreases and the saturated root fraction $(1-\mu)$ increases. For shallow-rooted plants such as understory shrubs (e.g., β =0.88), the unsaturated root fraction μ reaches 100% for a WTD as shallow as 35 cm, and for deep-rooted plants such as the overstory trees (e.g. β =0.945) μ reaches 100% only when WTD is as deep as 80 cm. This mechanism has major implications for ecophysiological processes, which determine the magnitude of ET and GPP manifested through alterations in g_s .

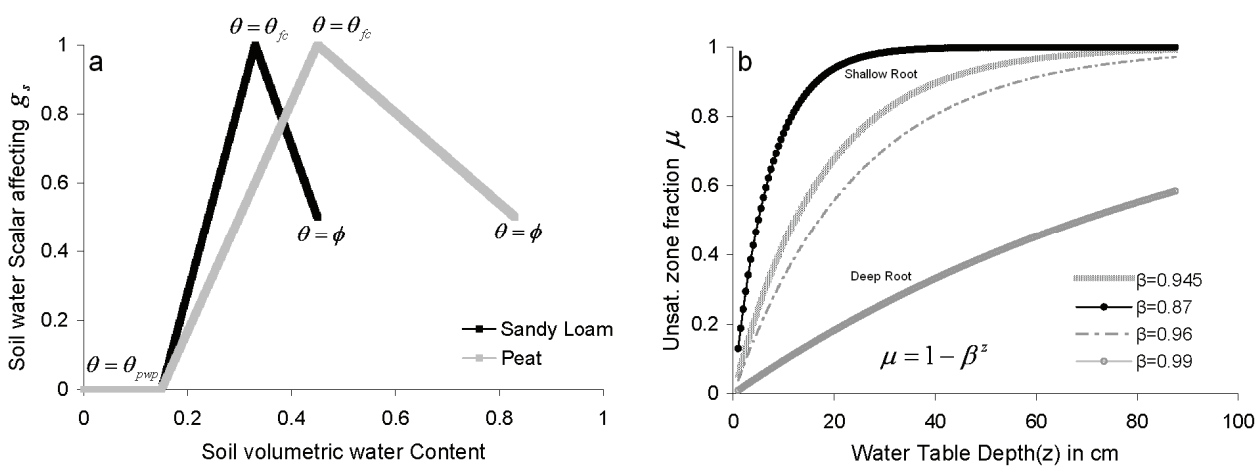

Figure 3-9. (a). Nature of the soil water scalar for a wide range of soil moisture conditions , for different soil texture types. This scalar is used to constrain the maximum stomatal conductance $g_{s,\max}$. (b). Nature of partitioning of the unsaturated (μ) and saturated (1- μ) root fractions as a function of water table position (z cm from the surface) and the root decay constant (β), a land cover specific parameter describing the root geometry.

Under the *NoFlow* scenario, since the soil profile becomes excessively saturated, the unsaturated root fraction μ declines, resulting in an increase in the saturated root fraction $(1-\mu)$. On the other hand, under the *Implicit* scenario, the opposite is true, i.e., μ increases (see Figure 3-8). We assume that these differences in root-wetting under various scenarios influence the leaf physiology in a proportionate manner based on the pipe theory (Shinozaki et al., 1964). The total LAI of a canopy can be divided into leaves that get water from the saturated zone (LAI_{sat}) and those that get water from the unsaturated zone (LAI_{unsat}). The soil water scalar $f(\theta)$, that governs ambient g_s using the Jarvis' multiplicative algorithm (Jarvis, 1976), is a function of the volumetric water content (θ) of the unsaturated zone and porosity in the saturated zone. The application of this scalar results in higher stomatal conductance ($g_{s,unsat}$) in leaves corresponding to unsaturated water content than in leaves that correspond to saturated water content ($g_{s,sat}$). Figure 3-9a shows the variation of $f(\theta)$ for a wide range of soil moisture conditions. Note nature of this scalar which linearly increases between the permanent wilting point and the field capacity and the reduction beyond the field capacity.

Apart from soil water regimes, radiation regimes (sunlit and shaded) could also govern stomatal dynamics. However, the proportion of sunlit and shaded leaves does not change under various hydrological scenarios considered here. Therefore, various scenarios show differences in simulated ecophysiological processes mainly due to the magnitude of μ and $1-\mu$ that are used as weighting parameters to upscale leaf-level processes to the canopy scale. This upscaling mechanism is a unique function of root geometry and these effects are implemented in the model in the following manner (especially the overstory canopy):

$$T = \left[T_{sun,unsat} LAI_{sun}.\mu + T_{sun,sat} LAI_{sun}(1-\mu)\right] + \left[T_{shade,unsat} LAI_{shade}.\mu + T_{shade,sat}.LAI_{shade}(1-\mu)\right]$$

$$A = \left[A_{sun,unsat} LAI_{sun}.\mu + A_{sun,sat} LAI_{sun}(1-\mu)\right] + \left[A_{shade,unsat} LAI_{shade}.\mu + A_{shade,sat}.LAI_{shade}(1-\mu)\right]$$

T = Canopy scale transpiration

A = Canopy scale photosynthesis, GPP.

LAI = Total Leaf Area Index

$$LAI_{sun} = 2.Cos\theta.\left(1 - \exp\left[-\frac{0.5.\Omega.LAI}{Cos\theta}\right]\right) \quad (8)$$

LAI_{sun} is the sunlit LAI, θ =Solar Zenith Angle, Ω is Canopy Clumping Index.

$$LAI_{shade} = LAI - LAI_{sun} \quad (9)$$

LAI_{shade} is the shaded LAI

3.10. Model Sensitivity to different Parameters for GPP and ET Simulations

GPP and ET are the two main ecophysiological indicators that determine the characteristic features of a vegetated land surface in terms of surface energy balance and C dynamics. Although BEPS-TerrainLab V2.0 can simulate various ecological and hydrological processes with reasonable accuracy as demonstrated by two years of simulation study in Govind et al. (2008a), the model might still be vulnerable to uncertainties attributed to certain model parameters. Considering the non-linear effects of model parameters under various scenarios, and to reinforce the numerical experiment, we performed a sensitivity analysis of various parameters used within the model. Moreover, this also provides an opportunity to compare the errors in simulated ecophysiological processes because of hydrological

misrepresentation vis-à-vis the errors caused by the model parameters themselves. Having selected fourteen parameters that are common to both ET and GPP calculations, we performed a simple sensitivity analysis by altering their magnitudes by a fixed percentage (increase or decrease) and quantified their sensitivity to GPP and ET in terms of percentage change from realistic simulations.

Table 3-3 shows the sensitivity of different parameters for the ET and GPP simulations. Each value shown in Table 3-3 is a unique model run that has the same inputs and parameter-values except for the parameter under consideration. It is clear that ET and GPP are quite sensitive to a small error in LAI. A 25% decrease in LAI could underestimate annual ET and GPP by 5% and 7%, respectively. Whereas, a 25% increase in LAI could create an error of 11% and 12% overestimation of annual ET and GPP, respectively. The reason for the high sensitivity of LAI is that it is critical to a number of hydro-ecological processes that directly or indirectly affects ET and GPP. Considering its high sensitivity, it is highly recommended that reliable LAI data be used that is derived using remote sensing techniques in conjunction with ground measurements. Our strategy of deriving a watershed scale LAI map is quite comprehensive and involved remote sensing, ground measurements and laboratory analysis as outlined in Govind et al. (2008a) and Chen et al. (2006). We suggest eco-hydrologists or hydro-ecologists devote much attention to reliably quantifying LAI because this parameter is used in a number of eco-hydrological processes (see Table 3-3).

Errors in the clumping index (Ω) can have a substantial influence on the magnitudes of simulated ET and GPP. The proportion of sunlit and shaded leaf fractions in a canopy is primarily governed by canopy architecture quantified using Ω. A highly clumped canopy (such as in conifers) have more shaded leaves than sunlit leaves, at a given solar zenith angle, SZA.

Since the proportion of shaded leaves (LAI_{sun}) increases in canopies with higher Ω, GPP increases due to increased contributions from direct radiation penetrating the canopy, and vice versa. However, since ET is mainly governed by net radiation, Ω could have the opposite effect. Therefore, it is highly recommended to have accurate estimates of Ω for hydro-ecological simulations of different land-cover types using ground measurements and laboratory analyses in tandem (e.g., Chen et al., 2006).

Maximum stomatal conductance ($g_{s\max}$) is another parameter that could considerably affect the ET and GPP simulations. In addition to various environmental controls, $g_{s\max}$ is the primary biological parameter that determines the magnitude of the ambient g_s. Another parameter that goes into the calculation of ambient g_s is cuticular conductance $g_{cuticle}$. It may also introduce significant error in the ecophysiological simulations because the total stomatal conductance is the combination of g_s, $g_{cuticle}$ and $g_{boundary}$. Although the magnitude of $g_{cuticle}$ is very small, since $g_{cuticle}$ is conceptualized to be parallel to g_s, the total stomatal conductance is affected linearly.

From our simple comparison, most of the parameters that we investigated significantly affected ET and GPP and GPP is more sensitive to these parameters than the ET. The smaller sensitivity for ET is because it has many sub-component processes that are either biological or physical in nature with unique mechanisms. However, for GPP, all sub-components that are highly regulated by hydrological controls are biological in nature.

These results also point out that the maximum error caused by highly sensitive parameters such as LAI, $g_{s,\max}$, Ω is less than the errors caused by hydrological misrepresentation (e.g., 16.4% overestimation in the *Implicit* scenario).

Table 3-3. Sensitivity of various parameters considered in BEPS-TerrainLab V2.0 for ET and GPP simulations.

Parameter	Symbol	Process	Range	Low		High	
				%ET	%GPP	%ET	%GPP
Leaf Area Index	LAI	RT,ST,SC,CH	±25%	- 6.02	- 11.02	+5.43	+10.10
Canopy Clumping Index	Ω	RT,CH,	±25%	+1.82	-3.69	-2.32	+5.72
Max. Stomatal Conduc.	$g_{s\max}$	ST	±25%	- 5.84	-12.31	+5.29	+9.90
Cuticular Conductance	$g_{cuticle}$	ST	±25%	- 0.76	- 2.80	+0.74	+2.65
Ratio of $g_{s\max}$ over/under	ς	ST(under)	±25%	+2.89	+3.96	-1.91	-3.12
Peat depth criteria	δ	CH,VSH	±2cm	+0.12	+0.16	-0.13	-0.20
Soil Porosity	ϕ	SSH	±10%	-1.62	-2.14	+0.89	+0.69
K_s -depth decay coeff.	α	SSH	±25%	+0.004	+0.013	-0.004	-0.011
Vertical Sat. Hydr. Cond.	$K_{s,vertical}$	SSH	±25%	+0.05	+0.10	-0.05	-0.10
Horiz. Sat. Hydr. Cond.	$K_{s,horizontal}$	SSH	±25%	-0.29	-0.76	+0.29	+0.70
Moisture release parameter	b	VSH	±25%	-0.73	-1.38	+0.20	+0.41
Max. Soil Conduc.	λ	VSH	±25%	-0.90	+0.05	+0.73	-0.05
Root extinction coeff.	β	CH,SSH, SC	±10%	-1.15	+0.05	+1.12	-0.07
Moss fraction	λ	CH,VSH	±15%	+0.43	+0.06	-0.43	-0.08

RT=Radiative Transfer Process; ST=Stomatal Conductance; SC=Scaling up; CH=Canopy Hydrological Process; SSH= Saturated Zone; VSH=Vadoze Zone Hydrological Process

3.11. Summary and Conclusions

Among modelers and experimentalists, there is a growing interest in comprehending the relationships between hydrological and biological processes in ecosystems. To advance our understanding of landscape-scale C cycling in conjunction with climate change, we need to couple hydrological and ecophysiological processes in our models. In this context, we carried out a modeling experiment to demonstrate the importance of hydrological processes in C cycling in a boreal ecosystem. Based on our modeling experience, we draw the following conclusions:

1. Generally, GPP calculated under the assumptions of no lateral baseflow underestimated values in comparison to reality. The highest underestimations are seen on hill slopes, as opposed to flat areas and low lands. On the other hand, simplified bucket model representations of hydrological processes overestimate GPP due to the rapid increase in g_s and nutrient availability due to optimal soil moisture conditions. The overestimations are intense on flat regions where excessive drainage conditions are simulated as opposed to hill-slopes.
2. The dynamics of ET are quite different from those of GPP under different hydrological representations. This is because of the presence of sub-component processes that behave differently under various soil moisture conditions and are compensatory in nature.
3. Various hydrological representations result in differences in the position of the WTD and therefore, in variations in the proportions of rhizosphere saturation. This proportionately alters g_s and the upscaling mechanism of leaf-level processes to the canopy scale. Consequently, large differences in canopy scale transpiration and photosynthesis are seen under various hydrological representations.

4. The sensitivity analysis reveals that some parameters used for eco-hydrological modeling are highly sensitive for ecophysiological simulations justifying the importance of the creation of these datasets with rigorous ground and laboratory measurements.

5. Since a misrepresentation of model parameters creates smaller errors in GPP and ET in comparison to hydrological misrepresentation, the importance of explicit hydrological representations in process-based ecological modeling efforts is highlighted.

These conclusions reinforces that explicit modeling of hydrological processes is a critical requirement to realistically simulate ecophysiological and biogeochemical processes.

References

Chen, J.M., Govind, A., Sonnentag, O., Zhang, Y.Q., Barr, A., and Amiro, B.(2006). Leaf Area Index Measurements at Fluxnet-Canada Forest Sites, *Agricultural and Forest Meteorology* **140**, 257-268.

Chen, J.M., Liu, J., Cihlar, J., and Goulden, M.L.(1999). Daily Canopy Photosynthesis Model Through Temporal and Spatial Scaling for Remote Sensing Applications, *Ecological Modelling* **124**, 99-119.

Coops, N.C., Black, T.A., Jassal, R.P.S., Trofymow, J.A.T., and Morgenstern, K.(2007). Comparison of Modis, Eddy Covariance Determined and Physiologically Modelled Gross Primary Production (Gpp) in a Douglas-Fir Forest Stand, *Remote Sensing of Environment* **107**, 385-401.

Devito, K.J., Creed, I.F., and Fraser, C.J.D.(2005). Controls on Runoff From a Partially Harvested Aspen-Forested Headwater Catchment, Boreal Plain, Canada, *Hydrological Processes* **19**, 3-25.

Environment Canada . Canadian Climate Normals or Averages 1971-2000. 2006. 2007-05-15.

Gale, M.R. and Grigal, D.F.(1987). Vertical Root Distributions of Northern Tree Species in Relation to Successional Status, *Canadian Journal of Forest Research-Revue Canadienne De Recherche Forestiere* **17**, 829-834.

Giasson, M.A., Coursolle, C., and Margolis, H.A.(2006). Ecosystem-Level Co2 Fluxes From a Boreal Cutover in Eastern Canada Before and After Scarification, *Agricultural and Forest Meteorology* **140**, 23-40.

Govind, A., Chen, J.M., Margolis, H., Ju, W., Sonnentag, O., and Giasson, M.(2008a). A Spatially Explicit Hydro-Ecological Modeling Framework (BEPS-TerrainLab V2.0) Part 1: Model Description and Test in a Boreal Ecosystem in Eastern North America., *Journal of Hydrology*. Submitted.

Govind, A., Chen, J.M., Bernier, P.Y., Guindon, L., Margolis, H., and Beaudoin, A. (2008c). Reconstructing the Carbon Balance of a Boreal Ecosystem under Climate Change, CO2 Fertilization, Nitrogen Deposition and Disturbance Effects., *Geoderma*. Submitted.

Grant, R.F., Zhang, Y., Yuan., F., Wang, S., Gaumont-Guay, D., Hanson, P.J., Chen, J.M., Black, T.A., Barr, A., Baldocchi, D.D., and Arain, A.(2005). Modelling Water Stress Effects on CO2 and Energy Exchange in Temperate and Boreal Deciduous Forests, *Global Biogeochemical Cycles(accepted)* .

Heinsch, F.A., Zhao, M.S., Running, S.W., Kimball, J.S., Nemani, R.R., Davis, K.J., Bolstad, P.V., Cook, B.D., Desai, A.R., Ricciuto, D.M., Law, B.E., Oechel, W.C., Kwon, H., Luo, H.Y., Wofsy, S.C., Dunn, A.L., Munger, J.W., Baldocchi, D.D., Xu, L.K., Hollinger, D.Y., Richardson, A.D., Stoy, P.C., Siqueira, M.B.S., Monson, R.K., Burns, S.P., and Flanagan, L.B. (2006). Evaluation of Remote Sensing Based Terrestrial Productivity From Modis Using Regional Tower Eddy Flux Network Observations, *Ieee Transactions on Geoscience and Remote Sensing* **44**, 1908-1925.

Ju, W.M., Chen, J.M., Black, T.A., Barr, A.G., Liu, J., and Chen, B.Z.(2006a). Modelling Multi-Year Coupled Carbon and Water Fluxes in a Boreal Aspen Forest, *Agricultural and Forest Meteorology* **140** , 136-151.

Kurz, W.A. and Apps, M.J.(1995). An Analysis of Future Carbon Budgets of Canadian Boreal Forests, *Water Air and Soil Pollution* **82**, 321-331.

Liu, J., Chen, J.M., Cihlar, J., and Park, W.M.(1997). A Process-Based Boreal Ecosystem Productivity Simulator Using Remote Sensing Inputs, *Remote Sensing of Environment* **62**, 158-175.

Pauwels, V.R.N. and Wood, E.F.(2000). The Importance of Classification Differences and Spatial Resolution of Land Cover Data in the Uncertainty in Model Results Over Boreal Ecosystems, *Journal of Hydrometeorology* **1**, 255-266.

Porporato, A., Laio, F., Ridolfi, L., and Rodriguez-Iturbe, I.(2001). Plants in Water-Controlled Ecosystems: Active Role in Hydrologic Processes and Response to Water Stress - Iii. Vegetation Water Stress, *Advances in Water Resources* **24**, 725-744.

Potter, C., Klooster, S., De Carvalho, C.R., Genovese, V.B., Torregrosa, A., Dungan, J., Bobo, M., and Coughlan, J.(2001). Modeling Seasonal and Interannual Variability in Ecosystem Carbon Cycling for the Brazilian Amazon Region, *Journal of Geophysical Research-Atmospheres* **106**, 10423-10446.

Shinozaki, K., Yoda, K., Hozumi, K., and and Kira, T.(1964). A Quantitative Analysis of Plant Form. Pipe Model Theory. II. Further Evidences of the Theory and Its Application in Forest Ecology., *Jpn. J. Ecol.* 133–139.

Van Hees, P.A.W., Jones, D.L., Finlay, R., Godbold, D.L., and Lundstomd, U.S.(2005). The Carbon We Do Not See - the Impact of Low Molecular Weight Compounds on Carbon Dynamics and Respiration in Forest Soils: a Review, *Soil Biology & Biochemistry* **37**, 1-13.

CHAPTER 4.

Reconstruction of Carbon Pools of a Boreal Ecosystem under the Influence of Climate Change, CO_2 Fertilization, N Deposition and Disturbance.

4.1. Abstract

Spatially explicit simulation of biogeochemical processes is imperative to better understand landscape scale patterns of terrestrial carbon (C) cycle. However, these simulations require explicit information on the spatial distribution of current sizes of various C-pools. Current sizes of ecosystem C-pools result from the integrated effects of historical events such as climate change, CO_2 fertilization, N deposition and various disturbances. In this study, we use a long-term carbon balance model, InTEC, to reconstruct the historical C-balance in a mature black spruce ecosystem in central Quebec, Canada. The simulation showed that in this boreal landscape mature black spruce stands have stabilized in terms of their productivity and are currently oscillating in its status as a weak C-sink to weak C-source depending on the inter-annual variation of the hydro-meteorological conditions. However, stands that were disturbed in the recent decades, comprising mostly of deciduous species, act as significant C-sinks. The simulated magnitudes of C-pools in the aboveground biomass and soils generally compared well with the measurements taken at 12 inventory plots located in the watershed in 2003. The largest discrepancies were found in recently disturbed stands (for aboveground C-pools) or where moss necro-mass was abundant (for soil C-pools). The reconstructed C-pools serve as valuable datasets for spatially explicit biogeochemical modeling at finer time-steps using intensive process based hydro-ecological models which could reduce the current uncertainties in terrestrial C-balance.

4.2. Introduction

Studies have shown that the effects of global warming may change the status of the terrestrial biosphere from a C-sink to a C-source by the middle of this century (Cox et al., 2000; Cramer et al., 2001). Many studies suggest that disturbance history has large effects on the current dynamics of terrestrial C along with inter-annual differences in climate and changes in atmospheric CO_2 concentration (Thornton et al., 2002). Inter-annual variations in the balance between photosynthesis and ecosystem respiration can result in large changes in net C-exchange between the biosphere and the atmosphere. This is especially true in mature forest stands where the systems are often close to C-neutral condition. On a long term basis, the sizes of C-pools present in the vegetation biomass and soil of an ecosystem depend on the disturbance history (Sun et al., 2004a; Sun et al., 2004b), atmospheric CO_2 concentration (Chen et al., 2000a; Johnson et al., 2000; Alexandrov et al., 2003), nitrogen (N) deposition rate (Turunen et al., 2004), stand age (Gower et al., 1996; Peltoniemi et al., 2004), soil texture (Torn et al., 1997), drainage class (Rapalee et al., 1998), and climate (Apps et al., 2000; Black et al., 2000; Barr et al., 2002; Griffis et al., 2003).

Inter-annual dynamics of terrestrial biomes can be studied using coordinated measurements and modeling that operate at various spatial and temporal scales and resolutions. Although temporally precise flux measurements are available for some sites, extrapolating this information to landscape or regional scales requires the use of models that can simulate C-balance for wide ranges of spatial and temporal scales with various degrees of sophistication. However, there are many inconsistencies existing among the simulations conducted by various models, even though the fundamental physics that describe biophysical processes are similar. The first major inconsistency lies in how well various ecosystem C-pools are initialized prior to running the model because they are the substrates for various biogeochemical processes. Since most of the soil organic transformations do not necessarily follow zero-order kinetics, we need to assume

Monod kinetics (first order kinetics) that warrants accurate sizes of various C-pools (Shibu et al. 2006). It is therefore quite intuitive that differences in the sizes of C-substrates could explain the differences in model simulations. This warrants the need for accurate sizes of current C-pools that are reconstructed based on long-term effects of climate change, disturbance history (natural or anthropogenic), changes in atmospheric CO_2 concentration, effects of N-deposition and the associated synergistic effects (feedback relationships).

Most of the point-scale (or lumped) ecological models initialize the current sizes of C-pools by running the model for centuries until all C-pool sizes become stabilized. This strategy overlooks the historical trends in the disturbance and non-disturbance factors, resulting in unrealistic C-pool sizes. Furthermore, many point scale models that are sophisticated in conceptualizing various processes fail to represent the spatial heterogeneity necessary for accurate landscape-level simulations because of computational challenges. A spatially explicit reconstruction of various components of the C-cycle is therefore a necessary step for increasing the confidence in regional or global C balance estimation (Chen et al., 2003). The use of remote sensing is an alternative way to obtain the spatial distribution of current sizes of above ground C-stocks of an ecosystem especially using LIDAR or RADAR technology. However, these techniques cannot provide detailed information on the magnitudes of soil C-pools which is the more important considering its role in heterotrophic respiration, which has more uncertainties than autotrophic respiration. Moreover, remote sensing based approaches mostly relate signals to ground based estimates using empirical relationships which may not necessarily work well in a wide range of spatial and temporal domains.

In this study, first we use a long-term ecosystem C balance model, the Integrated Terrestrial Ecosystem Carbon Balance Model (InTEC, Chen et al., 2000), to reconstruct the terrestrial C-balance of a mature black spruce ecosystem in a spatially explicit manner,

considering the combined effects of disturbance and non-disturbance factors (climate change, CO_2 fertilization and N deposition). Further, we validate and analyze the reconstructed C-pools (biomass and soil) with different measurements made in the recent years (eddy covariance, indirect measurements of plant area index (PAI), and forest inventory-plot measurements).

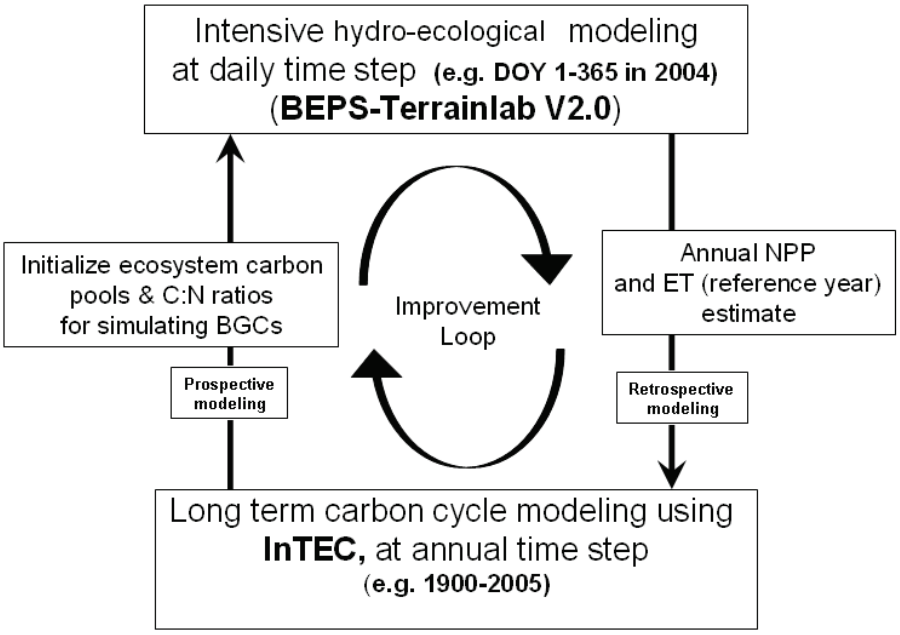

Figure 4-1. Strategy adopted for spatially explicit short-term modeling of biogeochemical cycles using BEPS-TerrainLab V2.0 with C- pools initialized through long-term modeling using InTEC.

We believe that C-pools reconstructed in this manner could further be used as precursors for intensive, spatially-explicit simulation of biogeochemical cycles at finer time-steps using coupled process based hydro-ecological models such as BEPS-TerrainLab V2.0 (Govind et al., 2008a; Govind et al., 2008d). A synergistic combination of a short-term intensive modeling (having a tight coupling of ecophysiological, hydrological and biogeochemical processes) on one hand and a long-term modeling that considers disturbance (natural and anthropogenic) and non-disturbance (climate change, atmospheric CO_2 concentration and N-deposition) factors (Figure 4-

1),in tandem, is likely to reduce the current uncertainties associated with terrestrial C cycling processes and could further improve our bottom-up modeling strategies.

4.3. Model and Theory

The present study employs the Integrated Terrestrial Ecosystem Carbon Balance Model (InTEC, Chen et al., 2000) for the spatially-explicit simulation of long-term ecosystem C cycling processes at an annual time step under a combined climate change and disturbance scenario. Previously, InTEC was used to simulate regional scale (Canadian landmass) historical C-cycling (Chen et al., 2000; Chen et al., 2000a; Chen et al., 2000b; Ju and Chen, 2005; Ju et al., 2006b). Its ability to reconstruct ecosystem C-pools along with their C:N ratios has not been fully exploited. This model simulates the gross primary productivity (GPP) employing a leaf-level biochemical model (Farquhar et al., 1980) and simulates the soil C and N cycles using a modified version of the CENTURY model (Parton et al., 1993). Since InTEC runs at an annual time step at large spatial scales, rigorous mathematical upscaling strategies are adopted to upscale biophysical processes in space (canopy scale) and time (annual). InTEC considers the long term changes in the atmospheric CO_2 concentration and N-deposition which affects annual photosynthesis by processes such as CO_2 fertilization and soil N cycling which affect plant physiological status. Disturbances are considered explicitly in this model as processes that directly release C into the atmosphere and modify the terrestrial C balance. The net C budget of a forest ecosystem is modeled based on the inter-annual variability in the disturbance and non-disturbance factors. C-fluxes in the form of dissolved organic carbon (DOC) and methane fluxes are not considered in the InTEC model. Since these fluxes are very small compared to the C fluxes due to photosynthesis, respiration or due to disturbance events, DOC fluxes are not generally considered (Schimmel 1995). Moreover, since DOC fluxes are small compared to the total C stocks present in

the ecosystem is often not considered in the annual net ecosystem productivity (NEP) calculations (Janssens et al. 2003). (Figure 4-2).

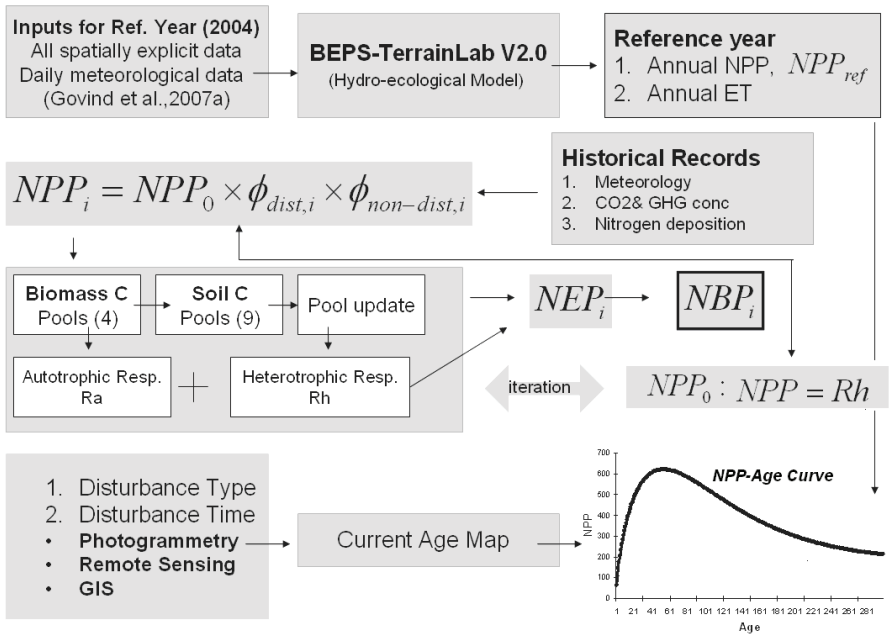

Figure 4-2.A schematic representation of the InTEC modeling framework (Chen et al., 2000).

Since InTEC's modeling philosophy is quite different from conventional models, it is important to briefly describe some of the important steps involved in this modeling procedure, in a sequential manner. More details can be found in Chen et al. (2003). The uniqueness of this model is the inclusion of a strategy to reduce the errors in net ecosystem productivity (NEP) simulations by assuming a dynamic equilibrium between NPP and R_h in the pre-industrial period. This assumption ensures that the C balance estimated for the recent years is the accumulated effects of all the factors that affect terrestrial C-cycle since the pre-industrial period (Chen et al., 2003).

Before running InTEC, reference year NPP and evapotranspiration (ET) maps are created based on the spatially explicit biophysical and meteorological data sets collected in the current time (e.g. 2004 in this study), using a rigorous process based modelling approach that runs at

finer time-steps. Many methods are available to simulate the reference year NPP or ET. Some common methods include the use of a remote sensing -based ecological model such as BEPS (Liu et al., 1997), hydro-ecological model such as BEPS-TerrainLab (Chen et al., 2005; Chen et al., 2007) or hydro-ecological model with biogeochemical processes such as BEPS-TerrainLab V2.0 (Govind et al., 2008a).The simulation of the reference year NPP is an important step that determinines the accuracy of the long-term C cycle modeling using InTEC. Chen et al. (2003) demonstrate that a small error in the reference year NPP (NPP_{ref}) can introduce significant errors in the reconstructed annual NPP or NBP and thus the accuracy of the reconstructed C-pool sizes. Therefore, qualities of reference year NPP and ET maps are critical for simulations using InTEC.

Further, a historical baseline NPP time series is reconstructed for each pixel in the modeling domain based on the NPP-stand age relationship. The coefficients of the NPP-stand age relationship are determined using historical mean annual temperature (a surrogate of the "site index" used in forestry), as shown below.

$$NPP_{age} = a.\left[1 + \frac{b.\left(\frac{age}{c}\right)^{d} - 1}{\exp\left(\frac{age}{c}\right)}\right] \tag{1}$$

$$a = \bar{a} + \left[5.2468 \times T_{avg}\right] \tag{2}$$

$$b = \bar{b} + \left[\left(0.2076 \times T_{avg}{}^{2} \times 0.85\right) + \left(\left(1.6891 \times T_{avg} \times 0.75\right)\right)\right] \tag{3}$$

$$c = \bar{c} + \left[\left(0.993 \times T_{avg}{}^{2}\right) + \left(6.8412 \times T_{avg} \times 0.75\right)\right] \tag{4}$$

$$d = \bar{d} + \left[\left(0.046 \times T_{avg}{}^{2} \times 0.4\right) - \left(0.6878 \times T_{avg} \times 0.42\right)\right] \tag{5}$$

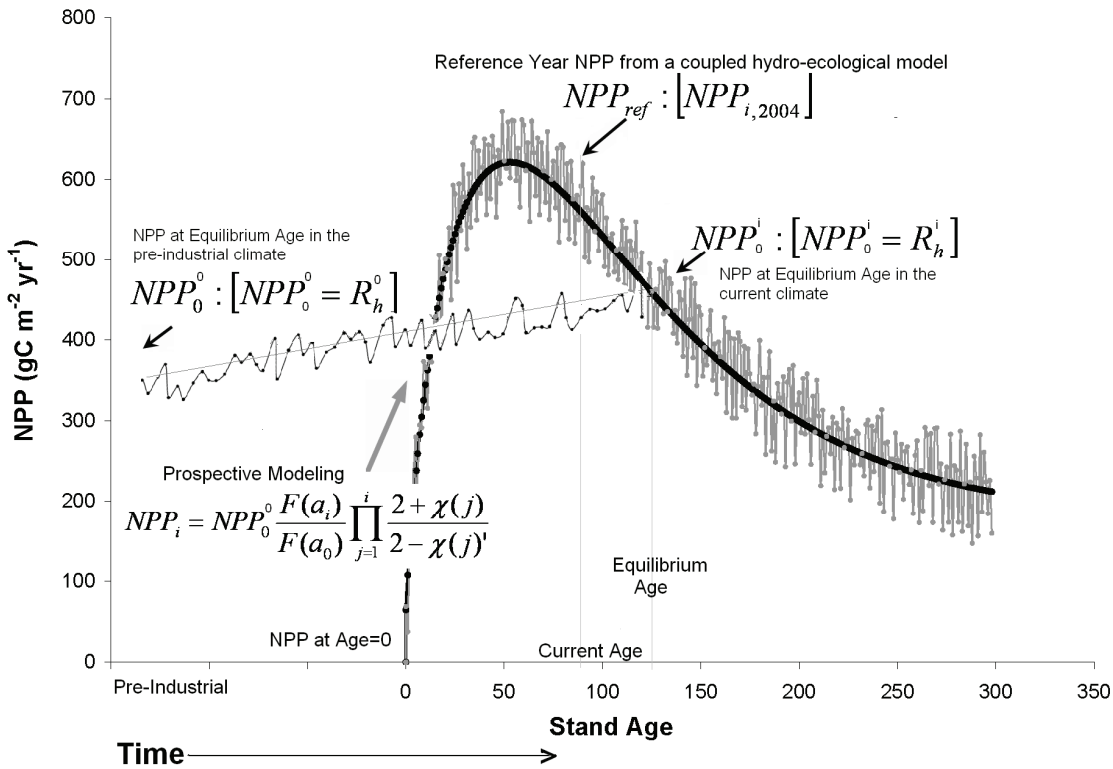

Figure 4-3. A conceptual diagram showing the long-term C-balance modeling strategy adopted within InTEC. Note how the current estimates of NPP (NPP_{ref}) is used to retrospectively estimate NPP at the *equilibrium age* (NPP= Rh) under pre-industrial climate, which is further used for prospective modeling. The sketch shown here is applicable for an undisturbed forest stand. For disturbed stands, re-growth is considered. However NPP is assumed to be NPP at equilibrium age with effects only of climate change.

Further, a historical NPP modification curve is constructed for each pixel based on meteorological forcing, N-deposition and historical variations of CO_2 concentration. Combining the historical NPP and its modification functions, a "realistic" NPP (NPP_i) time-series is created. This is accomplished by satisfying the criteria that the reconstructed NPP agree with NPP_{ref} using an iterative procedure. From this iteration, NPP_0, the NPP at the equilibrium age is determined. At the equilibrium age, it is assumed that NPP(NPP_0) is at dynamic equilibrium with heterotrophic respiration (R_h) i.e. all the C in the ecosystem is used for R_h (Figure 4-3).

Using NPP_0, the sizes of pre-initial soil C-pools are estimated through a spin-up procedure under the equilibrium assumption.

NPP_i is prospectively calculated using response functions for disturbance (ϕ_{dist}), non-disturbance factors ($\phi_{non-dist}$) and NPP_0. During prospective modeling, the stand age increases progressively affecting the forest productivity and the overall ecosystem C-balance. In the years when a disturbance event occurs, the stand age is reduced to 0 and in the following years the vegetation regenerates in the above mentioned manner. The prospective simulation methodology can be summarized as

$$NPP_i = NPP_0 \times \phi_{dist} \times \phi_{non_dist} \,. \tag{6}$$

$$NPP_i = NPP_0 \frac{F(a_i)}{F(a_0)} \prod_{j=1}^{i} \frac{2+\chi(i)}{2-\chi(i)} \tag{7}$$

In the above equation NPP_i is the NPP in the ith year; NPP_0 is the NPP at equilibrium age, $F(a_i)$ and $F(a_o)$ are normalized productivity of a forest at ages a_0 (the starting year) and a_i (the ith year), respectively(Chen et al., 2003) and this ratio represents the response function, ϕ_{dist}. $\chi(i)$ is the integrated effects of non-disturbance factors on NPP. These non-disturbance factors include effect of climate, CO_2 fertilization and N availability (Chen et al., 2000a).

Annually NPP_i is partitioned into four biomass C-pools (wood, foliage, fine-root and coarse root) which further get decomposed into nine soil C-pools updating the existing sizes of C-pools. Autotrophic and R_h are calculated as a function of the existing C-pool sizes and abiotic factors such as temperature, moisture and the influence of soil texture causing decomposition of C-pools. In the process of C-pool decomposition, N is mineralized and consequently the C:N ratios of individual C-pools change. From the reconstructed annual NPP_i, annual net ecosystem

Productivity NEP and net biome productivity NBP are obtained by deducting R_h and losses of C due to disturbance events, respectively.

Table 4-1. Description of various conceptual carbon pools considered in the InTEC model.

Pool No	Ecosystem C-pool	Symbol	Fate	Remarks
	Biomass C-pools			
	Above Ground Biomass C-pools			
1	Wood C-pool	C_w	C_{cd}	Tree trunk, stems, twigs.
2	Foliage C-pool	C_l	C_{ssd}	Leaves, flowers, cones
	Below Ground Biomass C-pools			
3	Fine-root C-pool	C_{fr}	C_{fsd}	Dynamic.
4	Coarse-root C-pool	C_{cr}	C_{cd}	Large Roots.
	Soil C-pools			
	Surface Soil C-pools			
6	Surface Structural C-pool	C_{ssd}	$C_s, C_{sm}, free\ CO_2$	Dead leaves.
7	Surface Metabolic C-pool	C_{smd}	$C_{sm}, free\ CO_2$	Mostly Surface organic acids.
8	Surface Microbial C-pool	C_{sm}	$C_s, free\ CO_2$	Surface Fungi and Bacteria.
9	Coarse & Dead wood detritus C-pool	C_{cd}	$C_s, C_{sm}, free\ CO_2$	Both surface and sub-surface soil C-pool.
	Sub-surface Soil C-pools			
10	Soil Microbial C-pool	C_m	$C_p, C_s, free\ CO_2$	Bacteria, Fungi, VAM.
11	Fine-root structural litter C-pool	C_{fsd}	$C_s, C_m, free\ CO_2$	Fine-root Detritus.
11	Fine-root metabolic C-pool	C_{fmd}	$C_m, free\ CO_2$	Soil enzymes, metabolites.
12	Slow C-pool	C_s	$C_p, C_m, free\ CO_2$	Part of Humus, Humic and Fulvic acids.
13	Passive C-pool	C_p	$C_m, free\ CO_2$	Mostly recalcitrant Humus.

The C-pools spun up in this manner can be further used by detailed process-based hydro-ecological models such as BEPS-Terrainlab V2.0 that runs at finer temporal resolutions to either simulate seasonal biogeochemical processes or to generate a further improved annual NPP

(NPP_{ref}) for further refining InTEC simulations as shown in Figure 4-1. Table 4-1 shows the description of various C-pools (biomass and soil) conceptualized in the InTEC modeling domain.

4.4. Site Description

This long term simulation was conducted for a boreal watershed located in north-central Quebec, Canada. The climate of this region is cold temperate with a mean annual temperature of 0°C and a mean annual precipitation of 961.3 mm (Environment Canada, 2006). The soil is a ferro-humic to humic podzol, covered by an organic layer with an average depth of ~30 cm. In humid areas, the soil is predominantly organic with an average depth of 125 cm (Giasson et al., 2006). Drainage is good to moderate and the water table is usually below 50 cm deep. This region has an average growing degree-days of around 1800-2000 °C.

At the landscape scale, vegetation species compositions vary across the gentle topographic gradient. On elevated parts of the landscape such as eskers, deciduous to mixed forest stands are found. On flatter locations to low lands, there is a species transition from black spruce–moss dominated stands to wetlands dominated by different moss species and stunted black spruce trees. Currently, the vegetation of the study site consists of an overstorey dominated by black spruce (*Picea mariana*) in coniferous sites, aspen (*Poplus sp.)* or birch (*Betula sp*) in deciduous and mixed forests, and sporadic occurrence of jack pine (*Pinus banksiana* Lamb.), tamarack (*Larix larandicina* Du Roi) and balsam fir (*Abies balsamea*). The understory is mostly dominated by Labrador tea, Salix *sp.*. The forest floor in coniferous stands consists of a thick moss layer (Bergeron et al., 2007), dominated by feather moss or lichens in moderately dry areas and *Sphagum sp.* in relatively wetter locations.

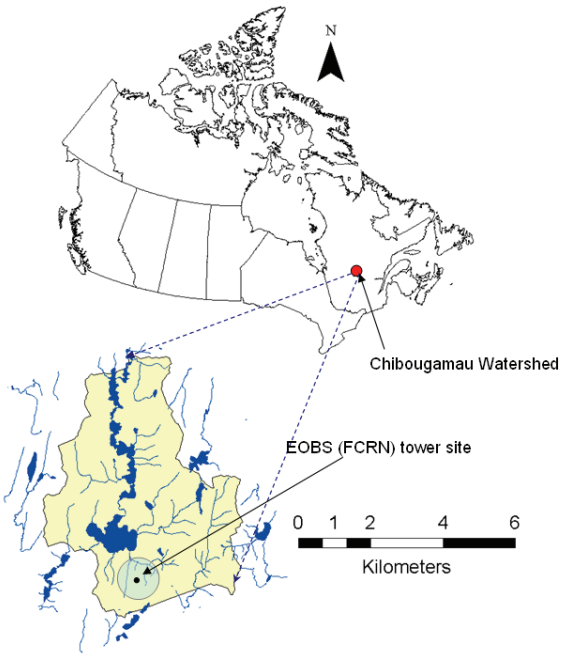

Figure 4-4. Location of the study site, Chibougamau watershed, which includes the Eastern Old Black Spruce (EOBS) tower site of FCRN where near-continuous high-frequency measurements of carbon, water and energy fluxes are being made using the eddy covariance technique. The scale shown in the figure applies to the watershed.

The Eastern Old Black Spruce (EOBS) eddy covariance flux tower site of Fluxnet-Canada Research Network (FCRN) is located at 49.69°N and 74.342°W in the southwestern part of this boreal watershed (Figure 4-4). The eddy covariance (EC) technique is being used at the EOBS site, and near-continuous 30-minute CO_2, water and energy fluxes measurements have been made since June 2003. Predominant wind comes from the S-SW, both during day and night. The footprint of the EC tower is a circular area with 500m radius centered on the tower (Kljun et al., 2004). In the footprint region, the vegetation is mostly mature black spruce trees.

4.5. Spatial Data Set Preparation

Several spatially explicit datasets are required to run the InTEC model. These datasets include a current land-cover map, current leaf are index (LAI) map, soil texture, current stand age map, reference year NPP and reference year ET maps, and a N deposition map. The details of the preparation of these datasets are given below.

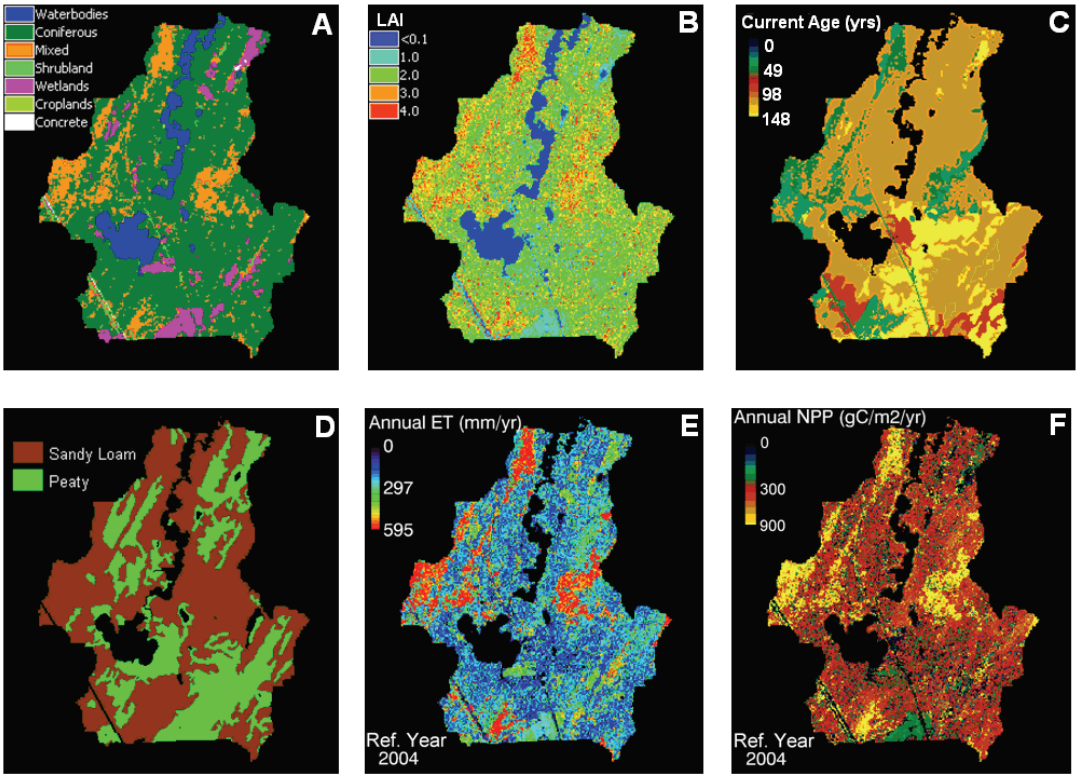

Figure 4-5. Various spatial datasets required to drive InTEC at annual time steps. These datasets include (A) Validated reference year land cover map, obtained from the Canadian Forest Service (EOSD project); (B) Reference year leaf area index (LAI) map derived from remote sensing imagery using an algorithm derived from ground based LAI measurements;(C) Current forest stand age map derived using photogrammetry, satellite remote sensing and GIS; (D) Soil texture derived from soil deposit dataset (Quebec Ministry of Natural Resources), land cover type (CFS-LFC) and intensive point analysis; (E) Reference year evapotranspiration from Govind et al. (2008 a); and (F) Reference year NPP from the hydro-ecological simulation conducted by Govind et al. (2008a). All the data sets have a spatial resolution of 25 x 25 m. Projection is UTM Zone 18N. The scale of the ~40km^2 watershed is shown in Figure 4-4.

4.5.1. Land Cover Map

A land cover map is required to apply land-cover-specific coefficients for various biogeochemical cycling processes in the InTEC model. A land cover map was obtained from the Earth Observation for Sustainable Development of Forests (EOSD) project, a collaborative effort between the Canadian Forest Service, (Laurentian Forestry Centre, Sainte Foy, Quebec) and the Canadian Space Agency. This land cover product was available at 25 m resolution (Figure 4-5A), which necessitates that all the other spatial input datasets be resampled to 25 m resolution and reprojected to UTM zone 18N.

4.5.2. Reference Year Leaf Area Index Map

Within InTEC, LAI in each year is simulated as the ratio of C content of foliage biomass and specific leaf area. The role of the reference year LAI is to constrain the historical changes in LAI simulated by the model. A reference year LAI at watershed scale was derived by inverting a site specific LAI-NDVI algorithm over a high resolution NDVI product obtained using Landsat imagery subjected to various corrections. In the summer of 2003 and 2004, we measured LAI using indirect techniques along a 400 m east-west transect in the EOBS footprint. Following the procedures given in Chen et al. (2002) and Chen et al. (2006), LAI values measured along the transect were correlated with satellite-derived NDVI values to determine a site specific LAI-NDVI algorithm. A watershed scale LAI product (Figure 4-5B) was derived by inverting this algorithm based on remote sensing derived NDVI.

4.5.3. Disturbance History and Current Stand Age Map

The spatial distribution of *current age* of stands in the modeling domain is an important factor that determines the long term trends in the ecosystem C dynamics simulated by the InTEC model (Chen et al., 2003). *Current age* implies current productivity and time when the last disturbance occurred. With a known NPP-age relationship, it is possible to create a baseline NPP history. In the model, all forms of disturbances that remove significant amounts of biomass are assumed to be caused by forest fire (refer appendix for details). For disturbance events such as clear-cuts or infrastructure development, this assumption is reasonable because all these disturbance-types are associated with the complete removal of living biomass. However, for disturbances such as partial cutting or insect damage, we followed a different strategy by proportionately weighting the NPP simulated under completely disturbed and undisturbed conditions.

The *current age* of disturbed stands is the age since the last disturbance event. However, for undisturbed stands, it is the sum of the age in 1920 and the time period between initial year (1920) and current year (2005). For the present study, stand ages were interpreted from a collection of aerial photos archived at the Ministère des Ressources Naturelles et de la Faune du Québec (since 1928). The year, extent and the type of subsequent disturbances were also interpreted from later sets of aerial photographs. The disturbance types were classified as clear-cut, partial cut, insect defoliation or infrastructure. Unfortunately, aerial photographs were available only for the southern half of the watershed. However, the availability of a detailed GIS forestry database (covering the whole modeling domain) from the Canadian Forest Service Laurentian Forestry Centre (hereafter, CFS-LFC) that have information on disturbance type and the availability of high a resolution land cover product (section 4.5.1) facilitated the identification of forest stands that faced similar disturbance time in the northern portion of the watershed using

a look-up table procedure. In areas where disturbance polygons were absent, it was assumed to be undisturbed. A *current age* map was thus created (Figure 4-5C).

4.5.4. Reference Year NPP and ET Maps

A reference year (2004) NPP and ET are required to run the InTEC model. Reference year (2004) NPP and ET maps were produced using a spatially explicit model that considers various hydrological, ecophysiological and biogeochemical processes in a tightly coupled manner, BEPS-TerrainLab V2.0 (Govind et al., 2008a). The BEPS-TerrainLab V2.0 model runs at daily time-steps. In BEPS-TerrainLab V2.0, photosysnthesis (GPP) is calculated as the sum of overstory, understory and the moss layer using a leaf-level instantaneous biogeochemical model that is temporally and spatially upscaled to canopy scale at a daily time-step. Explicit hydrology and biogeochemical representations control plant physiological status through alterations in daily stomatal conductance and plant nutrition (N). The canopy radiative transfer mechanism also determines the plant physiological status. Daily autrotrophic respiration is deducted from GPP to derive daily NPP. Ecosystem scale ET is calculated as the sum of soil evaporation, moss transpiration, understory and overstory transpiration and canopy evaporation and sublimation of snow using surface specific resistances and net radiation that go into the Penman-Monteith equation.

These leaf level processes are spatially upscaled to canopy scales using fractions of LAI that are physiologically different. The simulation that produced reference year NPP model was extensively tested for its performance by comparing the seasonal dynamics of several ecophysiological parameters such as gross primary productivity, ET, ecosystem respiration, water-table, snow-depth, and volumetric water content for two years at daily time steps (GPP r^2=0.91, RMSE=0.45gC m^2 day^{-1} and ET r^2=0.83, RMSE=0.35 mm day^{-1}). We computed annual

NPP by summing up simulations made at daily time steps using BEPS-TerrainLab V2.0. Figure 4-5E and Figure 4-5F show the reference year ET and NPP, respectively.

4.5.5. Soil Texture Map

Soil texture is an important variable for terrestrial C cycle modeling since it governs the hydraulic properties, a critical input for hydro-ecological modeling of the reference year NPP and a highly sensitive parameter used in InTEC. Soil texture plays a critical role in determining the decomposition rates of various soil C-pools, including the soil microbial C-pool (C_m), slow soil organic C-pool (C_s) and passive C-pools (C_p). See Table 4-A1 for details. A watershed scale soil texture map was derived based on a look-up table procedure that combines information on land cover type (EOSD product), intensive soil textural analysis at the various locations in the footprint region and surficial deposit data (Quebec Ministry of Natural Resources).

4.5.6. Data on N-Deposition

Information regarding N deposition (sum of wet and dry deposition) is required to realistically calculate terrestrial C cycle processes because soil N plays a critical role in biogeochemical processes. Since spatially explicit information on N deposition is absent for the study area at fine spatial resolution and N deposition is likely to be less variable in this forest ecosystem, we used an average N deposition value for the whole modeling domain (0.3 g m^{-2} y^{-1}). This average value was obtained from a Canada-wide interpolated N deposition map created by Chen et al. (2003) using the measured N deposition data collected by Ro et al. (1995) for 29 stations spread across the Canadian landmass. Assuming this value as the reference year N deposition in 2004, we temporally interpolated N deposition for each modeling year with respect

to the reference year N deposition value according to the temporal pattern of Canada's greenhouse gas emission rate, as shown below:

$$Ndep_i = Ndep_0 + \frac{\lfloor G_i - G_{i,0} \rfloor \times \lfloor Ndep_{i,ref} - Ndep_{i,0} \rfloor}{G_{i,ref} - G_{i,0}} \quad (8)$$

where $Ndep$ (g N m^{-2} y^{-1}).) is the N deposition rate in year i, G (Tg C y^{-1}).) is the greenhouse gas emission rate. The values i_0, i_{ref} and i represent the initial, the reference, and the year in consideration, respectively.

4.5.7. Meteorological Data

Long term hydro-meteorological data are required to run InTEC between 1920 and 2005 because they form the primary controls on the inter-annual variability of the terrestrial C cycle, in addition to vegetation and controls. In this study, we used the annual average temperature and precipitation collected from the Chapais meteorological observatory that meets the WMO standards (Lat. /Long. 49°47' N; 74°51' W; elevation 396 amsl), which is located near the EOBS tower site. Since InTEC simulation needs specific meteorological parameters such as spring and growing season temperatures, daily hydro-meteorological values are required to calculate them.

To this end, stochastic simulations of daily air temperature and precipitation from monthly values were made according to Régnière and St-Amant (2007). Annual spring temperature for each year was calculated as the mean of DOY 85 to 145 (Figure 4-6C). For annual growing season temperature, for each year, the mean temperature between DOY 85 and 240 was taken (Figure 4-6E). The annual precipitation was the sum of the daily mean precipitation data (Figure 4-6F). The historical trend in the variation in CO_2 concentration is required to run the process model of photosynthesis. To this end, the historical CO_2 concentration was assumed to be

that of SRES-A2 emission scenario of the IPCC. We used a CO_2 concentration between 1920 and 2005 from this emission scenario (Figure 6A).

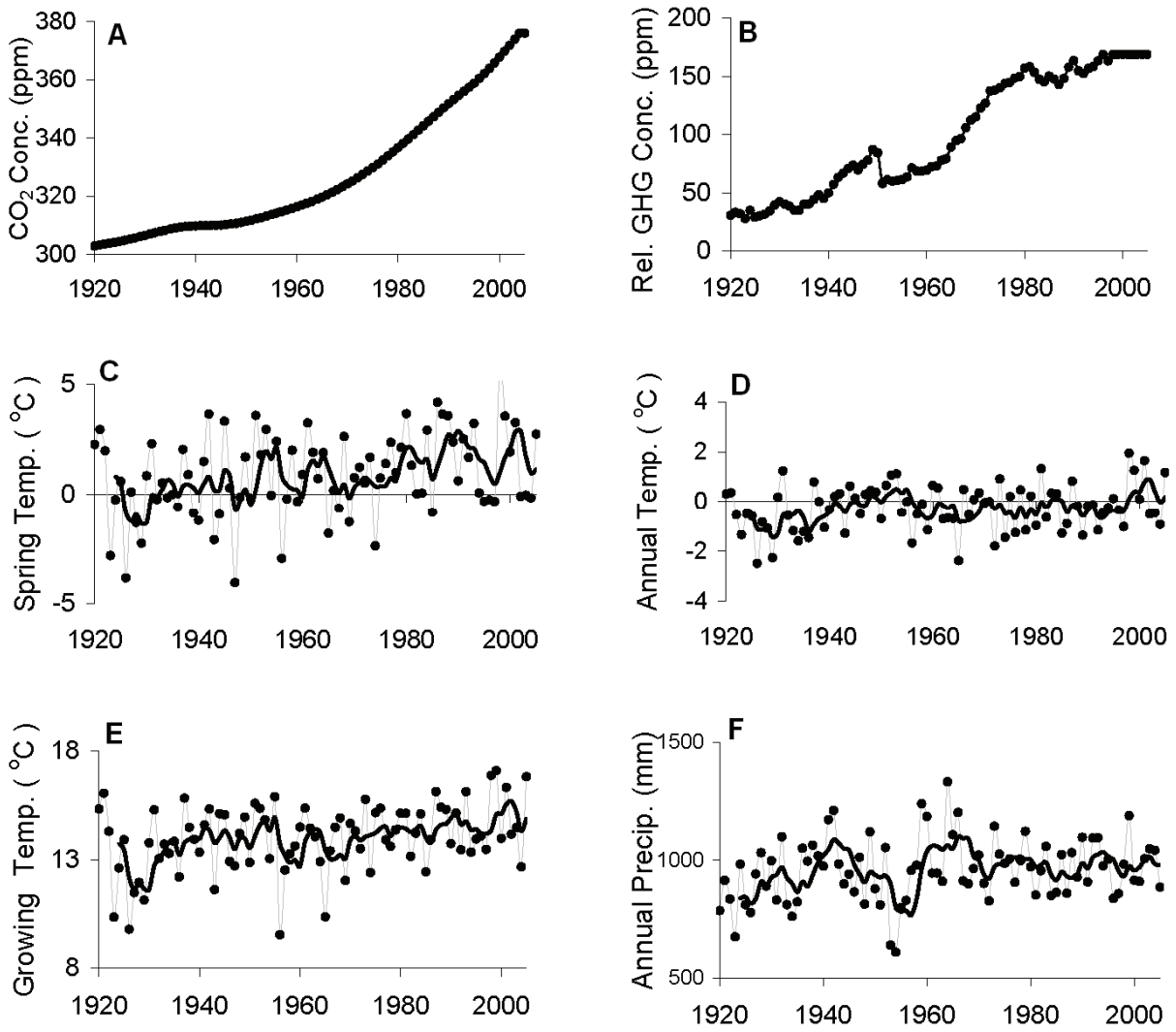

Figure 4-6. Temporal patterns of the non disturbance factors used for reconstructing the C balance using the InTEC model. (a) Temporal pattern of CO_2 concentration according to SRES-A2 emission scenario. (b) Rate of green house gas emission. (c) Mean annual spring temperature as the average of daily mean temperatures between DOY 85 to 125. (d) Mean annual temperature as the average of daily mean temperatures between DOY 1 to 365. (e) Mean annual growing season temperature as the average of daily mean temperatures between DOY 85 to 240.(f) Mean annual precipitation as the sum of daily sum of precipitation between DOY 1 to 365.

4.6. Measurement of Ecosystem C-Stocks.

4.6.1. Measurement of Biomass C-Stocks.

In 2003, C-stock measurements were made by the CFS-LFC at several inventory plots spread around the EC tower at EOBS (Figure 4-7). The establishment of inventory plots was conducted using aerial photography and high a resolution land-cover map employing a randomized sampling scheme, using a GIS. In the field, the distribution of the ground-plot locations was made in such a way that every significant stand type in the footprint region was properly represented. Thus, 12 inventory plots each having an area of 400 m^2 were demarcated in a 78 hectare area as shown in the Figure 4-7.

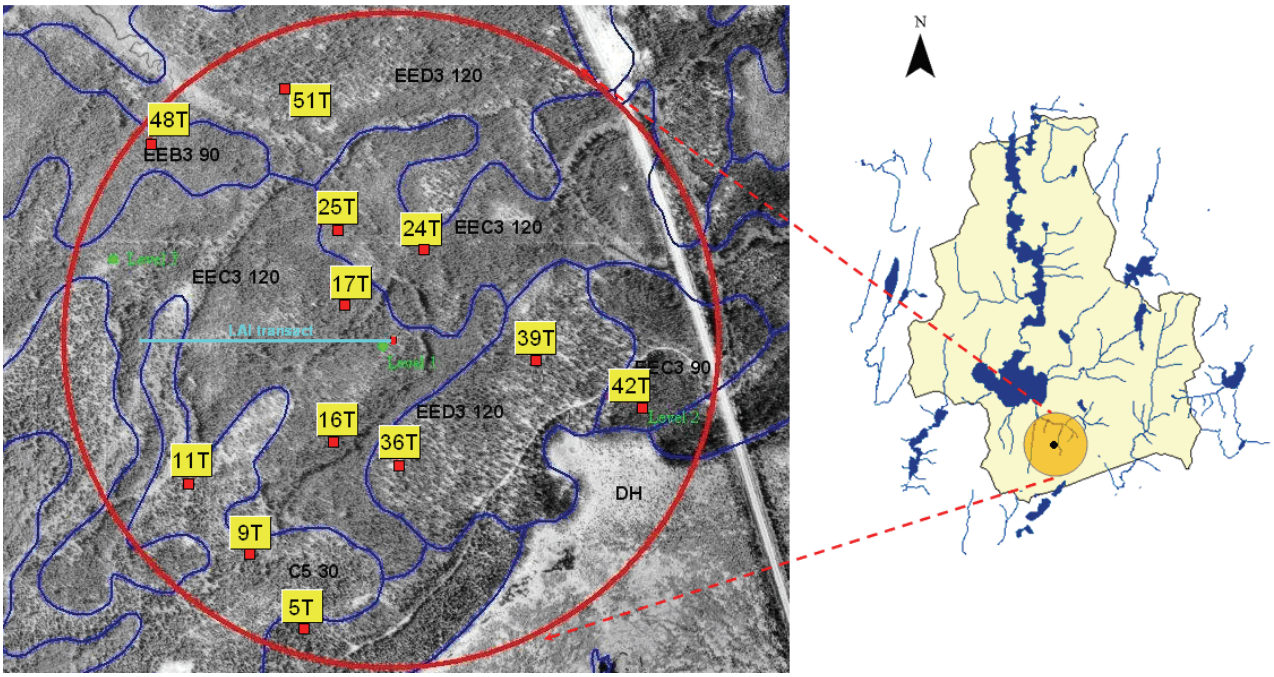

Figure 4-7. Locations of the CFS inventory plots in the footprint region of the FCRN's EOBS tower site

In each plot, complete tree inventories were made by measuring the diameter at breast height (DBH) and several other parameters. Further, C contents in the biomasses of trees were computed using local species-specific allometric equations (Table 4-2) assuming a C content of

50%. The InTEC simulated aboveground C-pools were compared to the inventory plot-based biomass C-stocks for the year 2003.

Table 4-2. Species specific allometric equations used to convert DBH to tree biomass

Species		Allometric Equation (kg/tree)	Source
Black Spruce	*Picea mariana*	$Biomass = DBH^{(2.42887 \times 0.096332)}$	Lambert et al. (2005)
Jack Pine	*Pinus banksiana*	$Biomass = DBH^{(2.2037314 \times 0.195698)}$	Lambert et al. (2005)
White Birch	*Betula papyrifera*	$Biomass = DBH^{(2.3304 \times 0.16024)}$	Lambert et al. (2005)
Aspen	*Pinus banksiana*	$Biomass = DBH^{(2.35102 \times 0.13263)}$	Lambert et al. (2005)
Balsam fir	*Abies balsamia*	$Biomass = DBH^{(2.33184 \times 0.10372)}$	Lambert et al. (2005)
Speckled Alder	*Alnus incana*	$Biomass = DBH^{(2.2087 \times 0.2612)}$	Ter-Mikaelan (1997)
Salix sp.	*Salix sp*	$Biomass = \frac{[(\exp(Ln(DBH))0.3937) \times 1.4392] + 7.2314}{1000}$	Jenkins et al. (2003)

4.6.2. Measurement of Soil C-Stocks.

In 2003, the CFS-LFC measured soil C stocks at four selected inventory plots located in the foot print region of the EOBS tower(in 17T, 24T, 36T, and 39T). For a representative spatial coverage, soil horizons were sampled at four to eight points within each inventory plot. The soil samples were analyzed in the laboratory for organic, mineral soil C and soil surface detritus C, using a LECO CR12 Total C analyzer. The soil C stocks thus analyzed did not include C contained in the living root biomass. We used this measured soil C-stock data to validate the simulated soil C-pools.

4.7. Indirect Measurements of PAI as a Surrogate of Above Ground Biomass

Plant Area Index (PAI) represents the coverage of above ground biomass per unit area and thus includes information on the amount of foliage and wood biomass. To further ascertain the accuracy of the simulated aboveground biomass C, we planned to correlate the simulated aboveground biomass in 2003 with the measurements of PAI were taken along an east-west transect from the EOBS tower and at all the CFS-LFC inventory plots. PAI was indirectly estimated using a combination of digital hemispherical photography and a plant canopy analyzer (LAI-2000) in the growing season of 2003 (Chen et al., 2006). The transect measurements were made at 10 m intervals on a westbound 400 m transect starting from the EOBS tower location (see the cyan-colored line in Figure 4-7) and also at all the inventory plots. To correlate the PAI measurements with the above ground biomass C-pools of an InTEC pixel having a 25m resolution, the 10 m measurements were averaged to match with the modeling domain's spatial resolution (25 m).

4.8. Results and Discussion

4.8.1. Dynamics of Ecosystem C Processes

Figure 4-8 shows the historical trend of the three main ecosystem parameters (NPP, NBP and AGB) simulated at the EOBS footprint region in comparison to a disturbed site that is located in another part of the landscape (at 74°19′ 54.5″ W and 49° 42′ 38.2″N). Panels A, C and E show the historical trend in the EOBS footprint average values whereas Panels B, D and F illustrate the reconstructed ecosystem parameters for a disturbed site(clear-cut in 1963) for NPP, NBP and above ground biomass (AGB), respectively. The modeled NPP, NBP and AGB time-series suggest that in the recent years, the productivity of the EOBS stand has stabilized, an age related effect of

these mature black spruce stands. Our results are consistent with some of the measurement studies conducted in a similar ecosystem that used a chrononosequence-based approach demonstrating the saturation of productivity in mature black spruce stands (e.g. Bond-Lamberty et al., 2004; Wang et al., 2003). Age effect on NPP is an important aspect for long-term terrestrial C-cycling and has been studied quite extensively in several field measurements (Gower et al., 1997; Ryan et al., 1997). Panels B, D show how InTEC simulates the re-growth and C-balance following a disturbance event. It can be seen that although the regeneration of the stand occurred rapidly, the system remained a C-source for at least 20 years and then turned into a C-sink because the soil C-pools continue to decompose at much greater rates than photosynthetic C fixation.

In the recent years (e.g. 2004), the annual NPP at the EOBS site was simulated to be 288.1 gC m^{-2}. To test the accuracy of this annual NPP estimate, we used the EC measurements available in the recent years assuming NPP to be 47% of GPP derived from the flux measurements. Landsberg and Waring (1997) advocate that the errors created as a result of simplifying the autotrophic respiration term (as 47% of GPP) are smaller than errors that result from the calculation of autotrophic respiration under a wide range of environmental conditions. Recent studies also suggested that the NPP to GPP ratio may not be affected by an increased temperature and elevated CO_2 concentration (Cheng et al., 2000; Peng et al. 2002). Comparison of annual NPP simulated (288.1 gC m^{-2}) and EC-derived NPP (278.2 gC m^{-2}) shows that InTEC captures the 2004 footprint average NPP quite reasonably. These values are also consistent with the field measurements taken in a similar ecosystem (Bond-Lamberty et al., 2004; Wang et al., 2003).

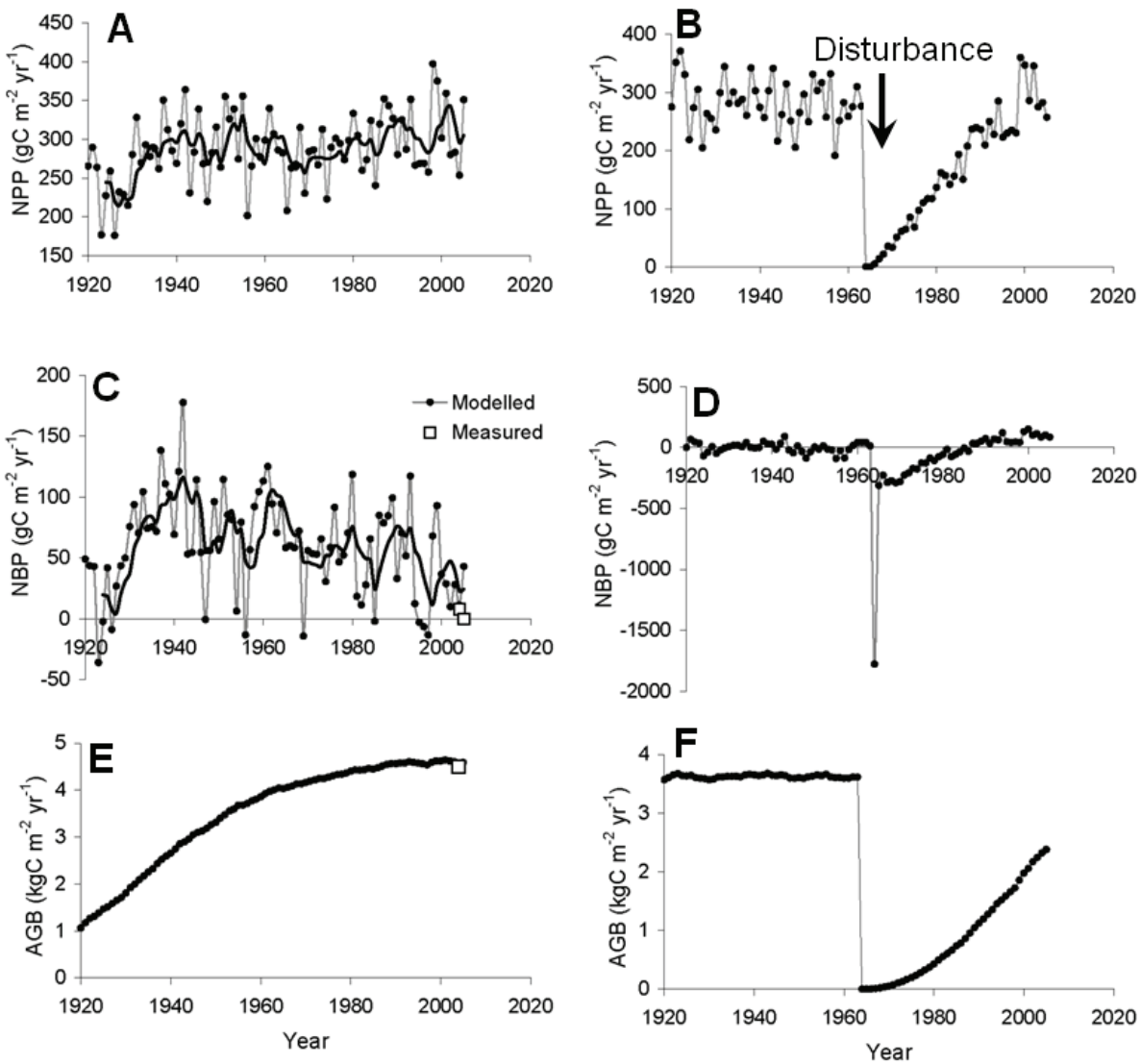

Figure 4-8 Reconstructed ecosystem C fluxes and biomass simulated by the InTEC model. (A) EOBS tower footprint-averaged historical NPP. (B) Footprint average historical NPP of a disturbed (1963) site at 74°19′ 54.5″ W and 49° 42′ 38.2″N. (C) EOBS tower footprint-averaged historical NBP. (E) EOBS tower footprint-averaged aboveground biomass C. (D) Average historical NBP of a disturbed (1963) site. (F) Average aboveground biomass C of the disturbed (1963) site, demonstrating the model's ability to reproduce the disturbance effects on C balance.

Year 2005 is a prospective simulation year, i.e. a year beyond the reference year. For the year 2005, NPP was simulated to be of 335 gC m^{-2} yr^{-1} whereas EC measurements suggested 320 gC m^{-2} yr^{-1}. Although the comparison reveals some discrepancy, it should be noted that the 2005

primary productivity was much higher than 2004. A similar trend of higher primary production (GPP) was observed in 2005 using a hydro-ecological simulation study conducted by Govind et al. (2007a) at a daily time step. A higher GPP was observed in this year because the ecosystem began to dry up in late June and lasted until late September which resulted in soil moisture remaining below field capacity but still well above the permanent wilting point creating conducive growth conditions. In this humid boreal ecosystem, water is not limiting and drying enhances the physiological status resulting in increased stomatal conductance due to less saturated soil conditions and also due to increased N availability (due to increased decomposition of soil C stocks). This explains the higher primary production in 2005.

With regard to NEP (specifically NBP), this ecosystem is near C-neutral for mature conifer stands. Inter-annual variability in temperature, light, precipitation, duration of growing season, etc., made the annual NEP values oscillate between a weak C-source and a weak C-sink. For the year 2004, InTEC simulated a footprint-averaged NEP value of 8 gC m^{-2} as against 6 ± 12 gC m^{-2} from the measured values. However in 2005, our simulation showed a footprint average NEP value of 30 gC m^{-2} as opposed to the EC-measured value of 0 ± 3 gC m^{-2}. We speculate that this discrepancy was mainly due to an underestimation of ecosystem respiration ($R_h + R_a$) on an annual basis. Since 2005 was relatively dry, the soil moisture remained conducive for heterotrophic metabolism resulting in a higher R_h that brought down the ecosystem to a C-neutral state even though the primary production remained high. The underestimation of R_h by the model could be mainly attributed to the temporal resolution (annual) adopted by the InTEC model which is too coarse to capture extreme conditions that happen at finer temporal resolution (e.g. daily or sub-daily). For example, while analyzing daily simulations of NEP in a hydro-ecological modeling study conducted for the same site (Govind et al., 2008d), it was noted that

even during the mid-growing season, on some days, the ecosystem behaved as a strong C-source. These were warm-dry days when the total ecosystem respiration was much higher than photosynthesis. Thus, it seems that models such as InTEC that runs at an annual time-step, although adequate for long-term modeling of C-balance of an ecosystem, it could have some uncertainties while simulating the C-balance of C-neutral ecosystems (old-forests) where the inter-annual variations in hydro-meteorological conditions that strongly influence the ecosystem's status between a weak C-source or a weak C-sink.

Despite the discrepancies that arise due to differences in the temporal resolutions in both the approaches (modeling and EC-measurements), we should consider the fact that the main purpose of InTEC was to reconstruct the long-term ecosystem C balance and get a reasonable estimate of the magnitudes of different C-pools in a spatially explicit manner.

4.8.2. Dynamics of Ecosystem C-Pools

4.8.2.1. Temporal Dynamics of Ecosystem C-Pools

Figure 4-9 shows the temporal dynamics of various ecosystem C-pools in the EOBS footprint region simulated by the model. It is obvious that over the years, the sizes of different C-pools had a different dynamic. Temporal variation of biomass C-pools such as wood (C_w), coarse-root (C_{cr}), fine-root (C_{fr}) and foliage (C_l) are displayed in panels A, B, C and D, respectively. All of the biomass C-pools showed a general increase with time. Since the *current age* of the footprint region is around 120 years, the biomass C-pool sizes showed a general saturation effect. A saturation of biomass C-pool was observed because a major portion of the C assimilated by photosynthesis was used for growth and maintenance respiration as the stands matured, similar to the saturation of NPP discussed in section 4.6.1.

A similarity in the temporal variations can be observed among all the biomass C-pools because they were all derived from annual NPP using constant allocation coefficients that vary for each land-cover types (refer Table 4-A1). Among the biomass C-pools, C_{fr} showed a higher inter-annual variability followed by C_l. Kalyn and Van Rees (2006) using a minirhizoctron demonstrated that in boreal ecosystems, fine root dynamics is greatly influential because of rapid decomposition of fine roots relative to aboveground counterparts. There are many studies that demonstrate that the inter-annual dynamics of fine-root and leaf biomasses are strongly linked to the inter-annual variability of environmental controls (Nadelhoffer et al., 1985; Kurz and Kimmins, 1987; Yin et al., 1989; Gower and Vitousek, 1989). The large inter-annual variability of foliage C-pool is mainly attributed to the presence of deciduous stands. There are studies that demonstrate higher inter-annual variability of LAI (Barr et al., 2004) and fine root biomass for deciduous species (Steele et al., 1997 ; King et al., 2001). The EOBS footprint region has both deciduous and conifer stands and this could explain the large inter-annual variability seen in panels C and D. The turnover coefficients for C_{fr} and C_l are almost 10 times larger than that of C_w and C_{cr} (see Table 4-A1).

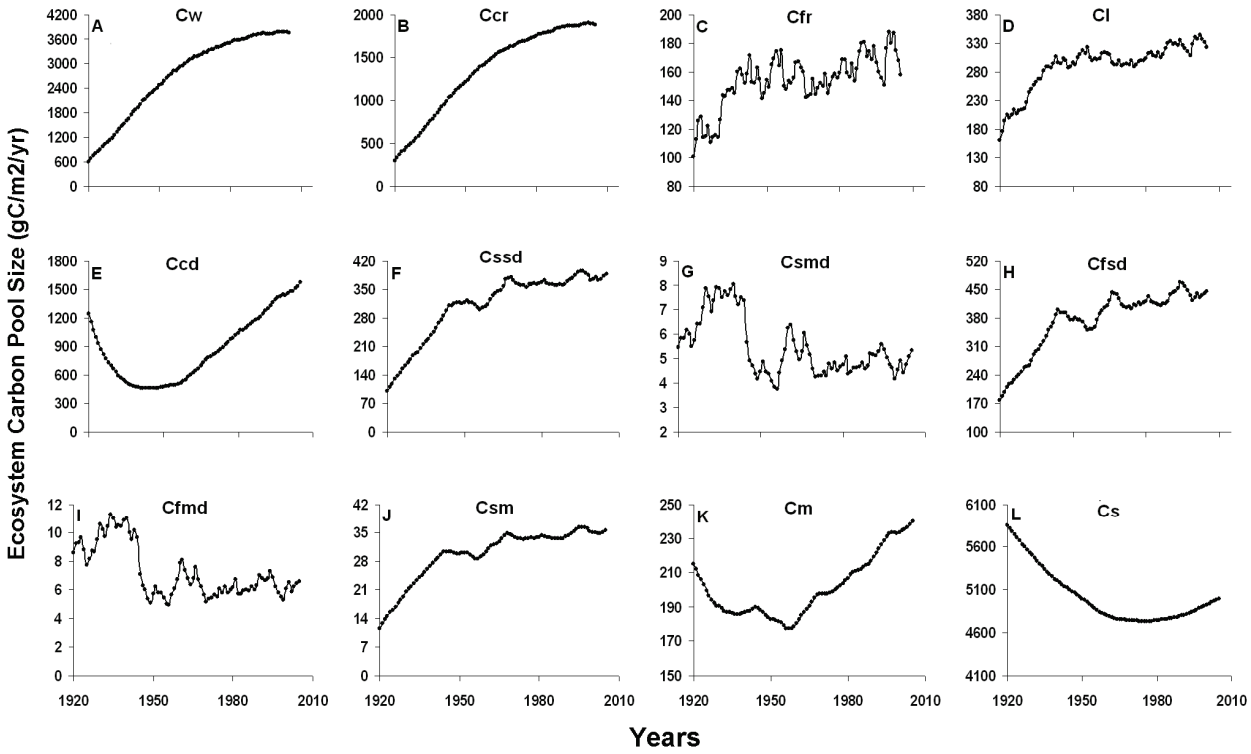

Figure 4-9. Temporal variation of the footprint averaged (A) woody biomass C-pool, C_w; (B) coarse root biomass C-pool, C_{cr}; (C) fine root biomass C-pool, C_{fr}; (D) foliage biomass C-pool, C_l; (E) coarse and dead wood detritus C-pool, C_{cd}; (F) surface structural C-pool, C_{ssd}; (G) surface metabolic C-pool, C_{smd}; (H) fine root structural litter C-pool, C_{fsd}; (I) fine root metabolic C-pool, C_{fmd}; (J) surface microbial C-pool, C_{sm}; (K) soil microbial C-pool, C_m; and (L) Slow C-pool, C_s.

The reconstruction showed that in the initial years of EOBS stand growth, C_w and C_{cr} progressively increased at increasing rates with lesser inter-annual variability in comparison to C_{fr} and C_l (panels A and B in Figure 4-9). Lesser inter-annual variability of C_w and C_{cr} compared to other biomass C-pools is due to small decomposition and constant rate of allocation that builds their sizes in a steady manner. The smaller decomposition rates are mainly due to increased lignin and cellulose contents that are relatively less susceptible to decomposition. One source of uncertainty to this reconstruction is the assumption of constant allocation coefficients

used to partition NPP into leafs, wood, coarse-root and fine-root. With climate change, age, and CO_2 fertilization effects, these allocation coefficients should alter and are likely to influence the current levels of ecosystem C stock sizes. Many studies (Dickson, 1989; Gaudinski et al., 2001; Gower et al., 2001) have shown that with age, the NPP allocation patterns can change.

The soil C-pools followed somewhat different trends as opposed to biomass C-pools. For example, the dead wood and coarse-root detritus C-pool, C_{cd} readily depleted in the initial years of stand establishment .This is because the majority of C_{cd} decomposed into its intermediate products, the slow soil organic matter pool, C_s, and surface microbial pool, C_m along with the liberation of free CO_2 due to heterotrophic respiration. In the initial stages of stand establishment, C_{cd} production was smaller compared to its decomposition rate which explains the decrease of C_{cd} in the initial years. As the age of these black spruce stands increased, C_{cd} accumulated on the forest floor due to mortality of various plant parts such as the snags and coarse wood. The current size of C_{cd} pool was about 1500 gC m^{-2} in 2003. Since there was a continuous production and mortality of foliage and fine roots even during the initial years, there was a steady increase in the surface structural C-pool, C_{ssd}, and the fine-root structural C-pool, C_{fsd} that were derived from C_l and C_{fr}, respectively (panels F and H in Figure 4-9). It can be seen that inter-annual variability of C_{fsd} was more than C_{ssd} which further implies the dynamic nature of its precursor C-pool, C_{fr} (mortality and re-growth). Depending on the lignin contents and abiotic decomposition factors, C_{ssd} and C_{fsd}, got partly transformed to their metabolic counter parts, C_{smd} and C_{fmd} and microbial C-pools, C_{sm} and C_m, respectively. The current magnitudes of C_{fsd} and C_{ssd} was about 450 and 375 gC m^{-2}. The sum of all the soil surface detritus C-pools C_{cd} C_{ssd} C_{fsd} combined

together accounted as much as 23.25 tC ha^{-1} which is comparable to the measurements taken on a black spruce chronosequence by Wang et al. (2003) in a very similar context.

In the InTEC model, metabolic C-pools refer to C present in active bio-molecules such as enzymes, root exudates, etc. Influences of abiotic factors such as soil temperature and soil moisture were the main controls that govern the dynamic nature of these metabolic C-pools (panels G and I in Figure 4-9). Metabolic C-pools form the major portion of the dynamic portion of the C balance due to small residence times. However, studies on the dynamics of the ecosystem-scale metabolic C-fraction is very little. These C-pools also play a significant role in the dynamics of Dissolved Organic Carbon (DOC) and Dissolved Organic Carbon (DON). The sizes of the simulated metabolic C-pools, C_{smd} and C_{fmd}, were rather small and were in the order of only 5-10 gC m^{-2} which are plausible magnitudes under natural conditions (Landgraf et al., 2005; Kielland et al., 2007).

The magnitudes of the microbial C-pools that exist on soil surface (C_{sm}) and within the soil profile (C_m) showed trends similar to their precursor C-pools, C_{sm} and C_m. While C_{sm} was mostly derived from C_{ssd} and C_{smd}, C_m was derived from several precursor C-pools (refer Table A1 for the decomposition products of each C-pool). Multiple-sources of C_m explains its large built up in the soil in comparison to C_{sm}. The higher values of C_m is possible in boreal ecosystems where the growing season is short. In the non-growing season, the near-surface soil temperature is not conducive for microbial proliferation and it is quite probable that microbial population thrives in the sub-soil. There are studies that demonstrate that much of the winter-time soil respiration originates from deeper layers of the soil rather than at the soil surface, which implies higher microbial proliferation in the deeper layers in boreal ecosystems.

The slow (C_s) and passive (C_p) soil C-pools represent the inert forms of soil C. Among these two C-pools, C_p is more recalcitrant than C_s. These C-pools represent humus and humic substances, the most significant and recalcitrant portion of the soil organic matter. At the EOBS site, C_s showed a slight decrease until the mid sixties after which it began to build up in the soil. This continuous increase in C_s could be explained by the simultaneous increase in mean annual temperature and atmospheric CO_2 concentration (Figure 4-6) that had increased photosynthesis and NPP that are the precursors for all the ecosystem C-pools. A higher NPP have resulted in greater amounts of C inputs to the soil. Increased soil temperature during this period had increased soil C decomposition that resulted in an increased C-pool turnover and increased C transfer to the recalcitrant form, which resulted in the built up of C_s. From the Table 4-A1, it can be identified that C_s is formed as an intermediate decomposition product of a number of other soil C-pools such as C_{cd}, C_{ssd}, C_{fsd} and C_m, that are positively related to the annual variations in NPP. Despite its large size C_p changed only very slightly over this temporal span (~9 gC m^{-2} yr^{-1} in 86 years). This implies its (C_p) high stability in comparison to all other soil C-pools (C_p time series not displayed). Currently, the size of C_p is around 1453 gC m^{-2} yr^{-1}. There was a slight decrease in C_p during the time period because its precursor C-pool, C_s decomposed more into the soil microbial C-pool, C_m which also showed an increase since the mid sixties. Table 4-1 and Table 4-A1 show the nature and dynamics of various ecosystem C-pools and rates of decomposition. This table is useful to interpret the long term dynamics of these C-pools under climate change considering the fate of various C-pools in the ecosystem.

From the discussion so far, it is plausible to link the effects of climate change on the long-term C-balance as simulated by InTEC. Under climate change and the consequent amplification of

high latitude temperatures, it is currently believed that boreal ecosystem will sequester larger amounts of C due to enhancement in photosynthesis. However, some recent studies indicate a negative relationship between increasing growing season temperatures and C-assimilation in many spruce species (Brooks et al., 1998, D'Arrigo et al., 2004, Dang & Lieffers, 1989). Tjoelker et al. (1999a) and Way & Sage (2008) postulate that the inhibition of growth at high temperatures is associated with reduced net CO_2 assimilation and high respiration rates. This modification of photosynthesis and respiration in high latitude forest ecosystems under elevated temperatures could have great implications for the accuracies of long-term simulations of C-cycle using models such as InTEC. Piao et al. (2008) proposed that the changes in the seasonal C-cycling in the northern hemisphere are mainly due to warmer autumn temperatures (rather than the extended spring) which enhance respiration in comparison to photosynthesis. Considering the anomalous nature of the influence of elevated temperature (or increased growing season) on terrestrial C-cycling, there is a great need to improve our understanding of the mechanistic controls on the predicted photosynthetic and respiratory fluxes (Miller, 2008) owing to the uncertainty regarding the physiological mechanisms controlling photosynthesis above the thermal optimum (Way & Sage 2008). It is hence essential to incorporate such mechanisms into the InTEC model especially when it is employed to simulate terrestrial C-dynamics under future climates.

4.8.2.2. Spatial Distribution of Ecosystem C-Pools

The spatial distributions of various ecosystem C-pools spun up using InTEC (for the year 2003 are displayed in the Figure 4-10). For simplicity, we display the sum of C-pools that fall under a particular category, i.e. aboveground biomass; belowground biomass; surface soil and sub-soil C-pools, respectively. The spatial distributions of the C-pools reflect factors such as forest growth, age-effects, disturbance and non-disturbance factors all of which affect the current (2003)

magnitudes (sizes) and nature (C:N ratio) of individual C-pool in an integrated manner. From the spatial distributions of both aboveground and belowground biomass C-pools, we can generalize that in the mixed forest stands, biomass C-pools that comprise of wood, foliage, coarse-root, and fine-root, are generally higher than that of coniferous stands or wetlands. Currently, mixed forest stands in this boreal landscape are dominated by aspen or sometimes jack pine trees that were established quickly following a disturbance event such as fire or clear-cut. Predominantly deciduous or mixed stands generally have high NPP (average= 440 gC m^{-2}) compared to black spruce stands (average= 220 gC m^{-2}) due to a variety of reasons (physiological, morphological, edaphic, hydrological and topographic) that contribute to higher values of above and below-ground biomass C-pools. Aspen dominated stands have higher biomass C-pools due to their higher photosynthetic efficiency, LAI and other plant physiological parameters such as maximum stomatal conductance, higher leaf N concentration. Deciduous species have more dynamic C-cycling in comparison to coniferous or wetlands. This C-cycling nature is represented in the modeling domain through higher values of C-pool allocation and decomposition coefficients in comparison to coniferous or wetland stands. Since biomass C-pools build up due to annual NPP increments (if no disturbance occur), the differences of above ground biomass among the land-cover types increase with time. This is the reason for the large range of biomass variability on this boreal landscape. This points out the fact that the quality of spatial datasets such as land-cover, LAI, soil-type will all affect the accuracy of the spatial distribution of the simulated biomass. Moreover, the errors propagate exponentially with time (or age) because biomass is accumulative in nature. Although mixed forest stands are younger, they show higher biomass implying higher annual primary production in the deciduous forest stands as opposed to coniferous stands.

Current age is another factor that can critically determine the spatial patterns of C stocks. Current age in the InTEC model implies the productivity of a stand through the response

function (ϕ_{dist}). This determines the timing of disturbance in the recent past. The accuracy of the current age map is therefore critical to the simulated results. We therefore believe that efforts to map stand age and disturbance regimes of terrestrial ecosystems should be given higher priority by employing a fusion of remote sensing techniques, field studies and modeling, in various research networks.

Wetlands, in general, showed lower C-pools in comparison to upland forested regions. This is primarily because of the lower annual NPP production in wetlands (150-200 gC m^{-2} yr^{-1}). However, the unique aspect of wetlands is that it showed lower, but a consistent accumulation of C stocks over time. There is little age-related effects on wetland productivity. Because soils C-pools are primarily derived from biomass C-pools, the spatial distributions of soil C-pools resemble that of biomass C-pools, especially the surface-soil C-pools. Due to high moisture conditions that curb soil C-decomposition in wetlands, these locations have higher magnitudes of undecomposed surface soil C-pools (sum of C_{cd}, C_{ssd} C_{smd}, C_{sm}). The simulated spatial distributions show that sizes of surface soil C-pools in wetlands are almost as high as that of deciduous forests even though biomass production in the former was far less than the latter. Increased soil saturation in wetlands greatly reduces the decomposition of biomass C-pools that lead to accumulation of C-pools on the surface soil. Many measurement studies have demonstrated that lack of oxygen limits the decomposition of soil organic carbon in poorly drained soils due to microbial activity (Davidson and Lefebvre, 1993, Schuur and Trumbore, 2006, Sun et al., 2004) leading to accumulation of soil C-pools on the surface soil. The surface accumulation of C in wetlands results in reduced sizes of sub-soil C-pools as opposed to other land-cover types where sub-soil C-pools are generally high because of humus production.

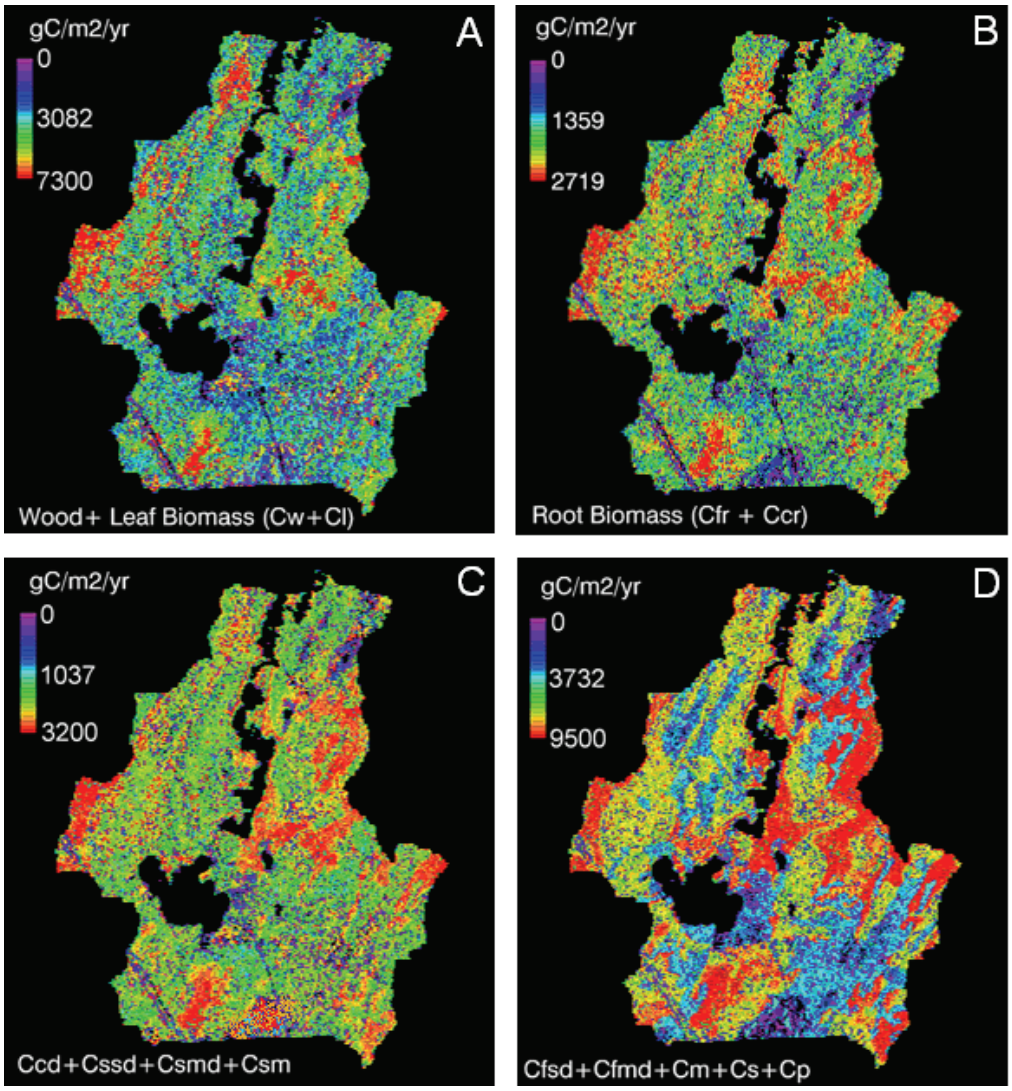

Figure 4-10. (A) Aboveground biomass as the sum of woody biomass C-pool (C_w) and foliage biomass C-pool(C_l); (B) Belowground biomass as the sum of coarse root biomass C-pool (C_{cr}) and fine root biomass C-pool (C_{fr}); (C) soil surface C-pools as the sum of coarse and dead wood detritus C-pool (C_{cd}), surface structural C-pool (C_{ssd}), surface metabolic C-pool(C_{smd}), and surface microbial C-pool (C_{sm}); and (D) Soil C-pools as the sum of fine root structural litter C-pool (C_{fsd}), fine root metabolic C-pool (C_{fmd}), soil microbial C-pool (C_m), slow C pool (C_s), and passive C-pool (C_p).

Although we captured the first order trends of C-pool distribution in wetlands, we believe that there is room for improvement because of the unique wetland-specific biogeochemical processes such as DOC fluxes, methane production and anoxia-based biogeochemistry. Lowering the decomposition coefficients alone will not comprehensively explain the unique C-dynamics of wetlands (peatlands). Future works should incorporate wetland specific biogeochemical processes within the InTEC framework. Work in this direction has already been started (e.g.Ju et al., 2006a). This warrants the need for spatially explicit hydro-thermal considerations in order to improve our long-term terrestrial C-modelling endeavours that incorporates geomorphologic information (e.g. topography and bed rock geology) and landscape scale hydrological processes that determines local-scale hydrological regimes and biogeochemical processes.

4.8.3. Validation of Current Biomass C-Pools

Table 4-3 shows the comparison between the InTEC simulated aboveground biomass C with the measurements taken at the CFS-LFC inventory plots. Overall, the aboveground biomass simulated by InTEC agrees reasonably with the inventory plot measurements (R^2=0.78 and RMSE=0.96 kgC m^{-2} yr^{-1}).The scale at which these comparisons were made are not far apart. The inventory plots have an area of 400 m^2 which is comparable with the pixel size (625 m^2) of an InTEC modeling unit (pixel). There is a general tendency for the model to underestimate the aboveground biomass C. This is especially true in plots 16T, 17T and 51T, where the underestimation was almost 2 kgC m^{-2} yr^{-1}.

Table 4-3. Comparison of InTEC simulated above ground biomass (2003) with inventory plot measurements

NFI_Plot ID	Latitude	Longitude	Species	Measured kgC m^{-2}	Modeled kgC m^{-2}
5T	49°41′17.90′′	74°20′38.07′′	*Pm, Bp, Pt, Ssp*	3.32	4.27
9T	49°41′21.49′′	74°20′41.86′′	*Pm, Ai, Pt, Ssp*	3.21	2.47
11T	49°41′24.99′′	74°20′47.01′′	*Pm, Pib, Ai, Ssp*	1.68	1.48
16T	49°41′27.33′′	74°20′35.83′′	*Pm, Pib*	8.31	6.20
17T	49°41′33.66′′	74°20′34.61′′	*Pm, Pib*	6.59	5.35
24T	49°41′36.29′′	74°20′28.70′′	*Pm, Pib*	4.52	4.71
25T	49°41′37.49′′	74°20′35.31′′	*Pm*	3.41	3.21
36T	49°41′25.98′′	74°20′30.79′′	*Pm, Pib*	2.45	2.97
39T	49°41′30.75′′	74°20′20.19′′	*Pm, Pib*	3.56	2.80
42T	49°41′28.64′′	74°20′11.86′′	*Pm, Ssp*	3.90	2.67
48T	49°41′41.93′′	74°20′49.27′′	*Pm, Pib*	5.75	5.88
51T	49°41′44.36′′	74°20′39.11′′	*Pm, Pib*	4.94	3.83

Pm=*Picea mariana;* ***Pib***=*Pinus banksiana;* ***Bp***= *Betula papyrifera;* ***Pt***= *Populus tremula ;* ***Ssp***= *Salix sp.*

Ai= *Alnus incana*

These discrepancies can be attributed to several reasons. The biomass equations that are used to calculate biomass in the inventory plots have a general tendency to overestimate, especially for the hardwood species (Lambert et al., 2005). This could explain the model's underestimation in plots 16T, 17T and 51T where significant fraction of deciduous species are found. Secondly, the assumption that C-content of biomass is 50% may not be fully valid under field conditions. The C-fraction of biomass could vary depending on plant nutrition and site characteristics. Some studies show that C-content in wood ranges between 47-50% (Thomas and Malczewski, 2007) while others show that C-content of wood and leaves are 50% and 45%,

respectively (Ajtay et al., 1977). Therefore, an assumption of 50% C in biomass can sometimes overestimate C-content, especially in locations where the foliage contributions are high. Nevertheless, many measurement studies have been using this as a fundamental assumption to do terrestrial C-budgeting from biomass estimates. Another factor that can cause discrepancy is the mismatch of spatial scales involved. The inventory plot size is 400 m^2 and the area covered by a pixel in the modeling domain is 625 m^2. This means that more averaging-out occurs within a given InTEC pixel as opposed to an inventory plot to which comparisons were made.

During 2004 and 2005 field campaigns, we visited the plots 16T and 17T, and observed that these locations have very high stand density and prominent understory growth that consisted mainly of deciduous species. The height of understory trees were almost half of that of overstory. In the EOSD land cover classification; these locations are classified as "dense coniferous stands". In the land-cover input dataset used to run the InTEC model, we do not consider stand density as additional information, which could further explain the underestimation in plots 16T and 17T. Future long-term modeling endeavors should incorporate attributes such as stand density for realistic simulation of terrestrial C-cycle. The inventory plots that lie in the southwestern part of the footprint (5T, 9T and 11T) lie close to locations that experienced a disturbance event (clear-cut) in 1963. During our field campaigns we observed that these three plots predominantly comprise of young regenerating black spruce. Regenerating black spruce stands generally show very slow growth as opposed to other plant species and that is why lower aboveground biomass C was noted in these locations

Figure 4-11 shows a linear relationship between the simulated aboveground biomass and the measured PAI, indicating that the spatial variability of aboveground biomass in the field was reasonably captured by the model. We opted to use PAI instead of the LAI because it is indicative of the amount of both foliage and wood per unit ground area rather than LAI, which is indicative

only of the leaf area. The moderate correlation could be attributed partly due to variability in woody and foliage fractions that affect the PAI at each point.

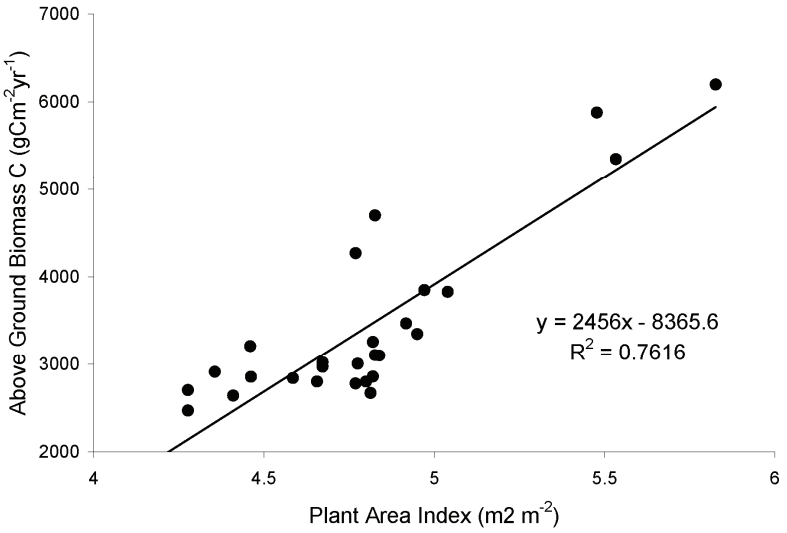

Figure 4-11. Correlation between the simulated aboveground biomass C and the average plant area index measured by digital hemispherical photography and plant canopy analyzer (LAI 2000) in 2003 along a westbound transact from the EOBS tower and at the 12 NFI plots.

Figure 4-12 shows the digital hemispherical photographs taken at the inventory plots. It is obvious that location 16T has the largest amount of biomass and canopy closure as opposed to 11T, which has a relatively open canopy and a greater contribution from foliage biomass than from woody biomass (young stand). Plot 36T also has a lower biomass as opposed to 16T. Similar to 11T, this plot also has an open canopy. However, the difference between 36T and 11T is with respect to their ages. In 36T, even if the PAI was lower, there is greater contribution of the woody biomass in comparison to foliage biomass which makes the total aboveground biomass higher than that of 11T.

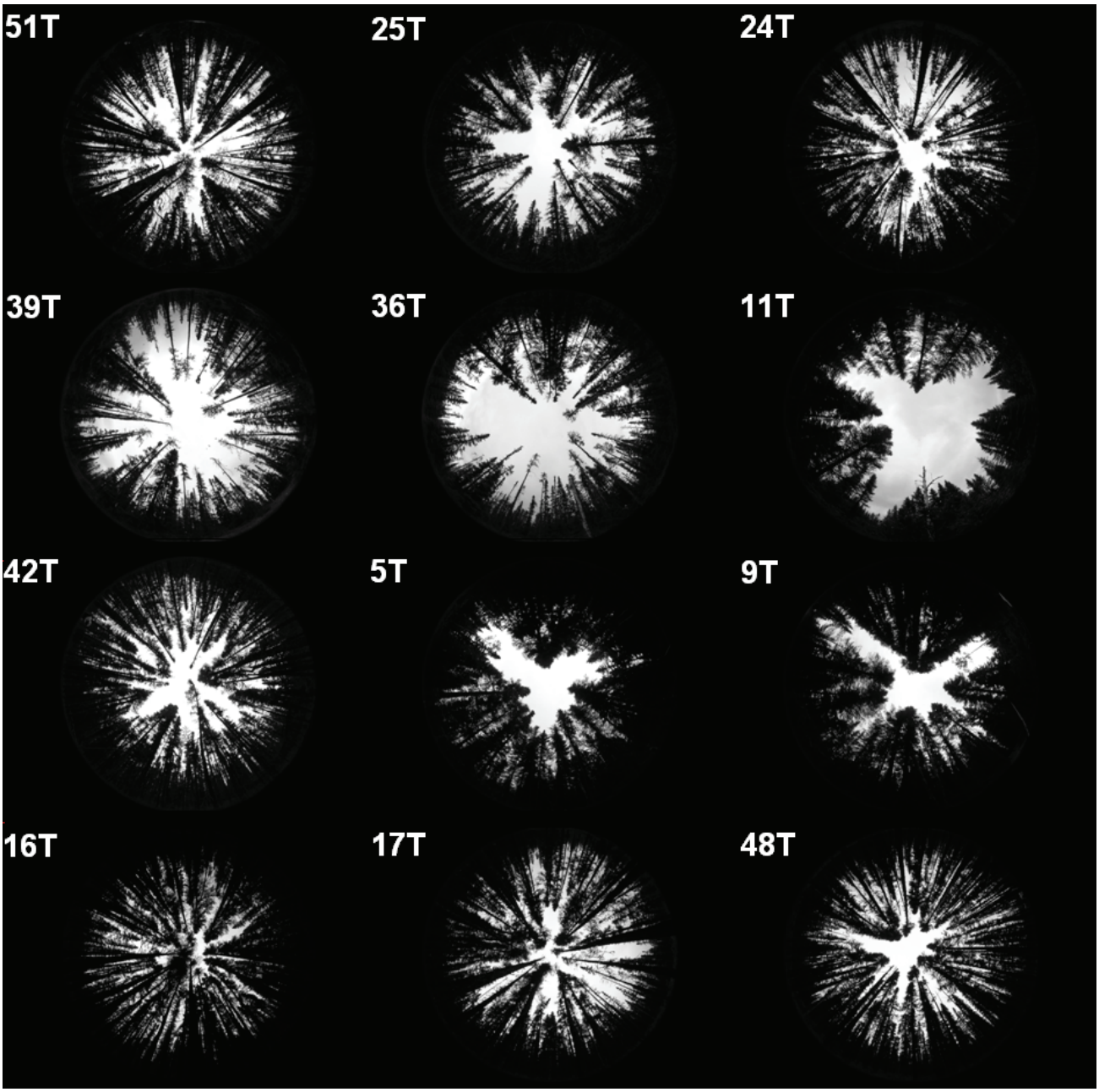

Figure 4-12. Digital hemispherical photographs taken at the 12 NFI plots for calculating plant area index in conjunction with plant canopy analyzer (LAI-2000). Note the relatively high biomass in 16T and 17T as opposed to relatively open canopy in 11T.

4.8.4. Validation of Current Soil C-Pool Sizes

A comparison of the simulated soil C in 2003 (as the sum of all the non-vegetation biomass soil C-pools, C_{cd}, C_{ssd}, C_{smd}, C_{sm}, C_{fmd} C_{fsd}, C_m, C_s and C_p) with the measured soil C-stocks in 2003 is shown in the Table 4-4. The simulated soil C-pools agree quite well with the measurements. The EOBS footprint average soil C-pool was simulated to be 10.01 kgC m^{-2} as against 10.40 kgC m^{-2} measured for the year 2003. There was an underestimation in the plots 17T and 24T and an overestimation in the plots 36T and 39T. This discrepancy can be explained by errors involved while upscaling point measurements to the plot scale, even though the measurements are representative of a 400 m^2 area.

During our 2004 and 2005 field campaigns, we visited these sites and noted that the forest floors at 17T and 24T have a predominant moss-layer along with its necro-mass. We speculate that the moss necro-mass might contribute to a large amount of soil C in the organic layer. There are studies that demonstrate the importance of bryophyte NPP in high latitude boreal ecosystems (Frolking, 1997; Bisbee et al., 2001 and Bond-Lamberty et al., 2004). Although our reference year NPP map that was simulated using BEPS-TerrainLab V2.0 (Govind et al., 2008 a) describes the contribution of moss towards stand level C, this information alone is insufficient to describe the current accumulation of soil C contributed by moss layer because in the InTEC model, the stand level annual NPP is not partitioned into moss biomass. The historical trends in moss growth could be different from that of vascular plants such as the lack of age-effects, influence of forest floor radiation regime as a function of overstory growth etc. In boreal ecosystems, unique characteristics of moss could create some discrepancy in the historical soil C dynamics while using models such as InTEC. Another explanation for the discrepancies in soil C-pools could be because of ignoring forms of C fluxes such as import and export of DOC and methane fluxes.

Sizable quantities of DOC could be exchanged between soil complexes along with topographically driven lateral water fluxes (Hornberger et al., 1994; Aitkenhead-Peterson et al., 2007)

Table 4-4 Comparison of modeled and measured soil C-pools in the foot print region of EOBS tower site

NFI-Plot ID	Latitude	Longitude	Measured kgC m^{-2}	Modeled kgC m^{-2}
17T	49°41′33.66′′	74°20′34.61′′	11.22	10.06
24T	49°41′36.29′′	74°20′28.70′′	14.44	12.68
36T	49°41′25.98′′	74°20′30.79′′	8.93	9.81
39T	49°41′30.75′′	74°20′20.19′′	6.98	7.51

4.9. Summary and Conclusions

Intensive biogeochemical modeling at fine spatial and temporal resolutions requires accurate information on current ecosystem C-pools because their sizes and C:N ratios govern the substrate quality for many biogeochemical processes. C-pools have to be accurate both in terms of their sizes (quantity) and C:N ratios (quality). Incorrectly initialized ecosystem C-pools and their C:N ratios could create errors in the simulated ecological and biogeochemical processes. Although measured values are the best estimates, it is not practical to measure ecosystem C-pools in a spatially distributed manner at high spatial resolutions. Moreover, since temporally fine inventory plot measurements are almost inexistent, chronosequence studies are useful for understanding the forest C-dynamics (Law et al. 2003; Law et al. 2001; Law et al. 2004) and is a good strategy to use space in lieu of time (Baldocchi, 2008) to understand long-term C-dynamics of terrestrial ecosystems. However, secondary site characteristics (characteristics other than stand

age) can influence the site productivity could complicate our understanding of forest productivity in time. The best strategy therefore is to integrate long-term simulation models that uses information from detailed process based short-term models and site and chronosequence measurements, in tandem. In this study, a reconstruction of the ecosystem C balance under the influence of climate and atmospheric (CO_2 and N deposition) changes and disturbances was undertaken using a process model that ran for very long temporal spans.

Historical trends of the C balance along with other ecosystem parameters such as NPP, NEP, aboveground biomass, etc., were simulated by the InTEC model for a boreal landscape. This study showed that in mature stands where black spruce trees dominate, the current productivity is rather low and the ecosystem is almost C neutral. In recent years, the EOBS site was oscillating between being a weak C-sink to weak C-source depending on the inter-annual variation of the hydro-meteorological conditions. Mid-aged stands dominated by aspen stands currently behave as C-sinks. This study also reconstructed most of the ecosystem C-pools in the vegetation and soil. The comparison of the aboveground biomass (as the sum of foliage and wood) as simulated in 2003 with the biomass estimated at the 12 CFS-LFC inventory plots located in the footprint region revealed that the aboveground C simulated by the InTEC model were reasonably accurate. In relatively dense stands there was a slight underestimation in comparison to the allometry-derived stand biomass. Simulated aboveground C was found to be linearly related to the measured plant area index. Similarly, the model was able to simulate the soil C-pools with reasonable accuracy.

There was a trend of slight underestimation of the soil C simulated by the model. We speculate that this underestimation was either due to the scale mismatch between the model and measurements or due to the contribution of moss necro-mass, which is currently not included in the model in terms of its turnover to soil organic matter.

Various cohorts of vegetation can co-exist within a given forest stand creating the possibility of the occurrence of a wide range of growth patterns within a given stand (Wang et al., 2003). Moreover, on a long-term basis, the contribution of moss and minor understory species in the black spruce forest stand can affect the C balance in a different manner than the overstory due to various controls such as canopy radiative transfer and canopy hydrological processes. Despite these short comings, the importance of this work lies in the reconstruction of the historical C balance and spinning up the current sizes of ecosystem C-pools in a spatially explicit manner. These serve as requisite datasets for intensive process-based distributed hydrological and biogeochemical models running at finer time-steps.

4.10. Appendix 1

CN_x CN ratio of C-pool x, e.g. CN_{cr} is the CN ratio of coarse-root biomass C-pool

Cx C content in C-pool x in gCm^{-2}, e.g. C_{cr} is the carbon content of coarse-root biomass pool

F_m Partitioning coefficient for the decomposition of leaf and fine-root litters into their corresponding metabolic C-pools.

f_y Fraction of NPP allocated to a particular biomass pool y

Sub-scripts denoting various C-pools.

a	C released to the atmosphere
cr	Coarse-root biomass pool
fr	Fine-root biomass pool
l	Leaf biomass pool
w	Wood biomass pool
cd	Coarse structural detritus pool

fd	Fine structural detritus pool
md	Metabolic detritus pool
m	Microbial pool
p	Passive soil C-carbon pool
s	Slow soil C-pool

$k_{x,y}$ Transfer coefficient of C from pool x to y in a year

ξ_x C loss from pool x due to fire (gC/m2/yr)

Ratio of foliage burnt	ξ_l =1
Ratio of wood/stem burnt	ξ_w =0.25
Ratio of root burnt	ξ_r =0
Ratio of surface litter burnt	ξ_{slb} =1
Ratio of woody litter burnt	ξ_{cd} =0.02

Equations of carbon pool decomposition at annual time steps. Under conditions of no disturbance, such as fire or clear-cutting, the biomass pools change in the following manner.

$$\Delta C_{w,i} = \frac{\left[f_w.NPP_i - k_{w,cd}.C_{w\,i-1}\right]}{\left[1 + k_{w,cd}\right]} \quad \text{(A1)}$$

$$\Delta C_{cr,i} = \frac{\left[f_{cr}.NPP_i - k_{cr,cd}.C_{cr\,i-1}\right]}{\left[1 + k_{cr,cd}\right]} \quad \text{(A2)}$$

$$\Delta C_{l,i} = \frac{\left[f_l.NPP_i - k_{l,fmd}.C_{l\,i-1}\right]}{\left[1 + k_{l,fmd}\right]} \quad \text{(A3)}$$

$$\Delta C_{fr,i} = \frac{\left[f_{fr}.NPP_i - k_{fr,fmd}.C_{fr\,i-1}\right]}{\left[1 + k_{fr,fmd}\right]} \quad \text{(A4)}$$

When disturbance occurs, these are estimated as the sum of 100% foliage C and 25% of woody C. The remaining biomass C is transferred to the corresponding soil C-pools via the pathways built in the model. The following equations show the dynamics of soil C-pools under undisturbed and disturbed scenarios.

Change in the dead wood and coarse detritus (undisturbed case)

$$\Delta C_{cd\,i} = \frac{\left[k_{w,cd}.C_{wi} + k_{cr,cd}.C_{cr\,i} - \left(k_{cd,a} + k_{cd,m} + k_{cd,s}\right)C_{cd\,i-1}\right]}{\left[1 + \left(k_{cd,a} + k_{cd,m} + k_{cd,s}\right)\right]} \tag{A5}$$

Change in the dead wood and coarse detritus (disturbed case)

$$\Delta C_{cd\,i} = \frac{\left[\left((1-\xi_w).C_{w\,i-1}\right) + \left((1-\xi_r).C_{cr\,i-1}\right) - (\xi_{cd}.C_{cd\,i-1}) - \left(1-\xi_{cd}\right).\left(k_{cd,a} + k_{cd,m} + k_{cd,s}\right)C_{cd\,i-1}\right]}{\left[1 + \left(k_{cd,a} + k_{cd,m} + k_{cd,s}\right)\right]} \tag{A6}$$

Change in the surface structural pool (undisturbed case)

$$\Delta C_{ssd\,i} = \frac{\left[\left(1-F_m\right).k_{l,sl}.C_{l\,i} - \left(k_{ssd,sm} + k_{ssd,s} + k_{ssd,a}\right)C_{ssd\,i-1}\right]}{\left[1 + \left(k_{ssd,sm} + k_{ssd,s} + k_{ssd,a}\right)\right]} \tag{A7}$$

Change in the surface structural pool (disturbed case)

$$\Delta C_{ssd\,i} = \frac{\left[\left(1-F_m\right).(1-\xi_l).C_{l\,i-1} - \left((1-\xi_{slb}).C_{ssd\,i-1}\right) - \left(1-\xi_{slb}\right).\left(k_{ssd,sm} + k_{ssd,s} + k_{ssd,a}\right)C_{ssd\,i-1}\right]}{\left[1 + \left(k_{ssd,sm} + k_{ssd,s} + k_{ssd,a}\right)\right]} \tag{A8}$$

Change in the surface metabolic pool (undisturbed case)

$$\Delta C_{smd\,i} = \frac{\left[\left(F_{m\,i}\right)\left[k_{l,sl}.C_{l\,i} - \left(k_{fd,a} + k_{fd,m} + k_{fd,s}\right)C_{smd\,i-1}\right]\right]}{\left[1 + \left(k_{smd,a} + k_{smd,sm}\right)\right]} \tag{A9}$$

Change in the surface metabolic pool (disturbed case)

$$\Delta C_{smd\,i} = \frac{\left[\left(F_{m\,i}\right)\left[\left(1-\xi_l\right).C_{l\,i} - \left(\xi_{slb}.C_{smd\,i-1}\right) - \left(1-\xi_{slb}\right).\left(k_{fd,a} + k_{fd,m} + k_{fd,s}\right)C_{smd\,i-1}\right]\right]}{\left[1 + \left(k_{smd,a} + k_{smd,sm}\right)\right]} \tag{A10}$$

Change in the fine-root structural pool (undisturbed case)

$$\Delta C_{fsd_i} = \frac{\left[\left(1-F_m\right).k_{fr,fl}.C_{fr_i} - \left(k_{fsd,m} + k_{fsd,s} + k_{fsd,a}\right)C_{fsd_{i-1}}\right]}{\left[1 + \left(k_{fsd,m} + k_{fsd,s} + k_{fsd,a}\right)\right]} \tag{A11}$$

Change in the fine-root structural pool (disturbed case)

$$\Delta C_{fsd_i} = \frac{\left[(1-F_m).(1-\xi_{frb}).C_{fr_{i-1}} - \left(k_{fsd,sm} + k_{fsd,s} + k_{fsd,a}\right)C_{fsd_{i-1}}\right]}{\left[1+\left(k_{fsd,sm} + k_{fsd,s} + k_{fsd,a}\right)\right]} \quad \text{(A12)}$$

Change in the fine-root metabolic pool (undisturbed case)

$$\Delta C_{fmd_i} = \frac{\left[(F_{mi})\left[k_{fr,fl}.C_{fr_i} - \left(k_{fmd,a} + k_{fmd,m}\right)C_{fmd_{i-1}}\right]\right]}{\left[1+\left(k_{fmd,a} + k_{fmd,m}\right)\right]} \quad \text{(A13)}$$

Change in the fine-root metabolic pool (disturbed case)

$$\Delta C_{smd_i} = \frac{\left[(F_{mi})\left[(1-\xi_{frlb}).C_{fr_i} - \left(k_{fmd,a} + k_{fmd,m}\right)C_{fmd_{i-1}}\right]\right]}{\left[1+\left(k_{fmd,a} + k_{fmd,m}\right)\right]} \quad \text{(A14)}$$

Disturbance does not directly affect the remaining C-pools because they are in the soil.

Change in the surface microbial pool

$$\Delta C_{sm_i} = \frac{\left[\left(k_{ssd,sm}.C_{ssd_i} + k_{smd,sm}.C_{smd_{ii}}\right) - .C_{sm_{i-1}}\left(k_{sm,a} + k_{sm,s}\right)\right]}{\left[1+\left(k_{sm,a} + k_{sm,s}\right)\right]} \quad \text{(A15)}$$

Change in the soil microbial pool

$$\Delta C_{m_i} = \frac{\left[\left(k_{fsd,m}.C_{fsd_i} + k_{fmd,m}.C_{fmd_i} + k_{cd,m}.C_{cd_i} + k_{s,m}.C_{s_{i-1}} + k_{p,m}.C_{p_{i-1}}\right) - \left(k_{m,a} + k_{m,s} + k_{m,p}\right).C_{m_{i-1}}\right]}{\left[1+\left(k_{m,a} + k_{m,s} + k_{m,p}\right)\right]} \quad \text{(A16)}$$

Change in the slow carbon pool

$$\Delta C_{s_i} = \frac{\left[\left(k_{cd,s}.C_{cd_i} + k_{fd,s}.C_{fd_i} + k_{m,s}C_{m_i}\right) - \left(k_{s,a} + k_{s,p}.C_{s_{i-1}}\right)\right]}{\left[1+\left(k_{s,a} + k_{s,p} + k_{s,m}\right)\right]} \quad \text{(A17)}$$

Change in the passive carbon pool

$$\Delta C_{p_i} = \frac{\left[\left(k_{m,p}.C_{m_i} + k_{s,p}.C_{s_i}\right) - C_{p_{i-1}}\left(k_{p,m} + k_{p,a}\right)\right]}{\left[1+\left(k_{p,m} + k_{p,a}\right)\right]} \quad \text{(A19)}$$

Table 4-A1 Ecosystem C-pools and their decomposition products and rates of decomposition

Ecosystem Carbon Pool	Symbol	Product of Decomposition	Rate (yr^{-1})
Wood	C_w	C_{cd}	$k_{w,cd}$ =0.0279(C) 0.0280 (D) 0.027(M) 0.013(W)
Coarse Root	C_{cr}	C_{cd}	$k_{cr,cd}$ =0.0269(C) 0.0288(D) 0.027 (M) 0.0139(W)
Fine Root	C_{fr}	C_{fsd}	$k_{fr,fl}$ =0.1925(C) 1.0000(D) 0.3945(M) 0.3945(W)
Leafs	C_l	C_{ssd}	$k_{l,sl}$ =0.5948(C) 0.5948(D) 0.5948(M) 0.3000(W)
Leaf Litter (Structural and Cellulose)	C_{ssd}	C_s C_{sm} $Free-CO_2$	$k_{ssd,s} = 0.4 \times \alpha$ $k_{ssd,sm} = 0.7 \times \beta$ $k_{ssd,a} = 0.6\alpha + 0.3\beta$ $\alpha = [f_1(L_l), A], \quad \beta = [f_2(L_l), A]$
Leaf Litter (Metabolic	C_{smd}	C_{sm} $Free-CO_2$	$k_{smd,sm} = 0.4 \times 14.8 \times A$ $k_{smd,a} = 0.6 \times 14.8 \times A$
Fine Root Litter (Structural and Cellulose)	C_{fsd}	C_s C_m $Free-CO_2$	$k_{fsd,s} = 0.7 \times \alpha$ $k_{fsd,m} = 0.45 \times \beta$ $k_{fsd,a} = 0.3\alpha + 0.55\beta$ $\alpha = 4.8[f_3(L_{fr}).A], \ \beta = 4.8[f_4(L_{fr}).A]$
Fine Root Litter (Metabolic)	C_{fmd}	C_m $Free-CO_2$	$k_{fmd,m} = 0.5 \times 18.5.A$ $k_{fmd,a} = 0.5 \times 18.5.A$
Dead Wood and Coarse Root	C_{cd}	C_s C_m $Free-CO_2$	$k_{cd,s} = 0.55 \times \alpha$ $k_{cd,m} = 0.45 \times \beta$ $k_{cd,a} = 0.45\alpha + 0.55\beta$ $\alpha = 2.8[f_5(L_w).A], \ \beta = 2.8[f_5(L_w).A]$
Surface Microbial	C_{sm}	C_s $Free-CO_2$	$k_{sm,s} = 0.4 \times 6.0 \times A$ $k_{sm,a} = 0.6 \times 6.0 \times A$
Soil Microbial	C_m	C_p C_s $Free-CO_2$	$k_{m,p} = 7.3[f_6(T_s) \times f_8(T_c) - f_7(T_s) - f_9(T_c)].A$ $k_{m,s} = 7.3[f_6(T_s) \times f_8(T_c)].A$ $k_{m,a} = 7.3[f_6(T_s) \times f_7(T_c)].A$
Slow Soil Organic Matter	C_s	C_p C_m $Free-CO_2$	$k_{s,p} = 0.25 \times f_{10}(T_c).A$ $k_{s,m} = 0.25 \times f_{11}(T_c).A$ $k_{s,a} = 0.55 \times 0.25.A$
Passive Soil Organic Matter	C_p	C_m $Free-CO_2$	$k_{p,m} = 0.0045 \times 0.5 \times 1.25 \times A$ $k_{p,a} = 0.0045 \times 0.5 \times 1.25 \times A$

A is a factor that represents the influence of soil temperature and soil moisture in a combined manner. L_l is the lignin fraction of leafs. L_{fr} is the lignin fraction of fine roots. L_w is the lignin fraction of dead wood and coarse root. T_s is the fraction of sand and silt. T_c is the fraction of clay . Functions (f_{1-11}) represents various pool or decomposition specific coefficients.(C)Coniferous forests; (D) Decidous forests; (M) Mixed forests and (W) Wetlands.

References

Aitkenhead-Peterson, J.A., Smart, R.P., Aitkenhead, M.J., Cresser, M.S., and Mcdowell, W.H.(2007). Spatial and Temporal Variation of Dissolved Organic Carbon Export From Gauged and Ungauged Watersheds of Dee Valley, Scotland: Effect of Land Cover and C : N, *Water Resources Research* **43**.

Ajtay, G.L., Ketner, P., and Duvigneaud, P.: 1977, 'Terrestrial primary production and phytomass.', *In*:The Global Carbon Cycle, John Wiley, New York., pp 129–181.

Alexandrov, G.A., Oikawa, T., and Yamagata, Y.(2003). Climate Dependence of the Co2 Fertilization Effect on Terrestrial Net Primary Production, *Tellus Series B-Chemical and Physical Meteorology* **55** , 669-675.

Apps, M.J., Bahatti, J.S., Halliwell, D., and Jiang, H.: 2000, 'Influence of uniform versus random disturbance regime on carbon dynamics in the boreal forest of central Canada', *In* Lal, R., Kimble, J., Eswarn, H., and Stewart, B.A., eds. Global Chnage and Cold Ecosystems, CRC Press, Boca Raton, pp 413-426

Baldocchi D(2008) Breathing of the Terrestrial Biosphere: Lessons Learned From a Global Network of Carbon Dioxide Flux Measurement Systems. *Australian Journal of Botany* **56** 1-26.

Barr, A.G., Griffis, T.J., Black, T.A., Lee, X., Staebler, R.M., Fuentes, J.D., Chen, Z., and Morgenstern, K.(2002). Comparing the Carbon Budgets of Boreal and Temperate Deciduous Forest Stands, *Canadian Journal of Forest Research-Revue Canadienne De Recherche Forestiere* **32**, 813-822.

Barr, A.G., Black, T.A., Hogg, E.H., Kljun, N., Morgenstern, K., and Nesic, Z.(2004). Inter-Annual Variability in the Leaf Area Index of a Boreal Aspen-Hazelnut Forest in Relation to Net Ecosystem Production, *Agricultural and Forest Meteorology* **126**, 237-255.

Bergeron, O., Margolis, H.A., Black, T.A., Coursolle, C., Dunn, A.L., Barr, A.G., and Wofsy, S.C.(2007). Comparison of Carbon Dioxide Fluxes Over Three Boreal Black Spruce Forests in Canada, *Global Change Biology* **13**, 89-107.

Bisbee, K.E., Gower, S.T., Norman, J.M., and Nordheim, E.V.(2001). Environmental Controls on Ground Cover Species Composition and Productivity in a Boreal Black Spruce Forest, *Oecologia* **129**, 261-270.

Black, T.A., Chen, W.J., Barr, A.G., Arain, M.A., Chen, Z., Nesic, Z., Hogg, E.H., Neumann, H.H., and Yang, P.C.(2000). Increased Carbon Sequestration by a Boreal Deciduous Forest in Years With a Warm Spring, *Geophysical Research Letters* **27**, 1271-1274.

Bond-Lamberty, B., Wang, C.K., and Gower, S.T.(2004a). Net Primary Production and Net Ecosystem Production of a Boreal Black Spruce Wildfire Chronosequence, *Global Change Biology* **10**, 473-487.

Brooks J.R., Flanagan L.B. & Ehleringer J.R. (1998) Responses of boreal conifers to climate fluctuations: indications from tree-ring widths and carbon isotope analyses. *Canadian Journal of Forest Research-Revue Canadienne De Recherche Forestiere*, **28**, 524-533.

Chen, J.M., Govind, A., Sonnentag, O., Zhang, Y.Q., Barr, A., and Amiro, B.(2006). Leaf Area Index Measurements at Fluxnet-Canada Forest Sites, *Agricultural and Forest Meteorology* **140**, 257-268.

Chen, J.M., Ju, W.M., Cihlar, J., Price, D., Liu, J., Chen, W.J., Pan, J.J., Black, A., and Barr, A.(2003). Spatial Distribution of Carbon Sources and Sinks in Canada's Forests, *Tellus Series B-Chemical and Physical Meteorology* **55**, 622-641.

Chen, J.M., Chen, X.Y., Ju, W.M., and Geng, X.Y.(2005a). Distributed Hydrological Model for Mapping Evapotranspiration Using Remote Sensing Inputs, *Journal of Hydrology* **305**, 15-39.

Chen, X.F., Chen, J.M., An, S.Q., and Ju, W.M.(2007). Effects of topography on simulated net primary productivity at landscape scale: Carbon Sequestration In China's Forest Ecosystems. *Journal of Environmental Management* 85[3], 585-596.

Chen, J.M., Pavlic, G., Brown, L., Cihlar, J., Leblanc, S.G., White, H.P., Hall, R.J., Peddle, D.R., King, D.J., Trofymow, J.A., Swift, E., Van Der Sanden, J., and Pellikka, P.K.E.(2002). Derivation and Validation of Canada-Wide Coarse-Resolution Leaf Area Index Maps Using High-Resolution Satellite Imagery and Ground Measurements, *Remote Sensing of Environment* **80**, 165-184.

Chen, J.M., Rich, P.M., Gower, S.T., Norman, J.M., and Plummer, S.(1997). Leaf Area Index of Boreal Forests: Theory, Techniques, and Measurements, *Journal of Geophysical Research-Atmospheres* **102**, 29429-29443.

Chen, W.J., Chen, J., and Cihlar, J.(2000a). An Integrated Terrestrial Ecosystem Carbon-Budget Model Based on Changes in Disturbance, Climate, and Atmospheric Chemistry, *Ecological Modelling* **135**, 55-79.

Chen, W.J., Chen, J., Liu, J., and Cihlar, J.(2000b). Approaches for Reducing Uncertainties in Regional Forest Carbon Balance, *Global Biogeochemical Cycles* **14**, 827-838.

Cox, P.M., Betts, R.A., Jones, C.D., Spall, S.A., and Totterdell, I.J.(2000). Acceleration of Global Warming Due to Carbon-Cycle Feedbacks in a Coupled Climate Model (Vol 408, Pg 184, 2000), *Nature* **408**, 750.

Dang Q.L. & Lieffers V.J. (1989) Climate and Annual Ring Growth of Black Spruce in Some Alberta Peatlands. *Canadian Journal of Botany-Revue Canadienne De Botanique*, **67**, 1885-1889.

D'Arrigo R.D., Kaufmann R.K., Davi N., Jacoby G.C., Laskowski C., Myneni R.B. & Cherubini P. (2004) Thresholds for warming-induced growth decline at elevational tree line in the Yukon Territory, Canada. *Global Biogeochemical Cycles*, **18**, -.

Dale, V.H., Joyce, L.A., Mcnulty, S., and Neilson, R.P.(2000). The Interplay Between Climate Change, Forests, and Disturbances, *Science of the Total Environment* **262**, 201-204.

Davidson, E.A. and Lefebvre, P.A.(1993). Estimating Regional Carbon Stocks and Spatially Covarying Edaphic Factors Using Soil Maps at 3 Scales, *Biogeochemistry* **22**, 107-131.

Dickson, R.E.(1989). Carbon and Nitrogen Allocation in Trees, *Annales Des Sciences Forestieres* **46**, S631-S647.

Dixon, R.K., Brown, S.R., Houghton, A., Solonmon, A.M., Trexler, M.C., and Wisniewski, J.(1994). Carbon Pools and Flux of Global Forests, *Science* **263**, 185-190.

Environment Canada . Canadian Climate Normals or Averages 1971-2000. 2006. 2007-05-15.

Fang, J.Y., Piao, S.L., Tang, Z.Y., Peng, C.H., and Wei, J.(2001). Interannual Variability in Net Primary Production and Precipitation, *Science* **293**, U1-U2.

Farquhar, G.D., Caemmerer, S.V., and Berry, J.A.(1980). A Biochemical-Model of Photosynthetic Co2 Assimilation in Leaves of C-3 Species, *Planta* **149**, 78-90.

Frolking, S., Goulden, M.L., Wofsy, S.C., Fan, S.M., Sutton, D.J., Munger, J.W., Bazzaz, A.M., Daube, B.C., Crill, P.M., Aber, J.D., Band, L.E., Wang, X., Savage, K., Moore, T., and Harriss, R.C.(1996). Modelling Temporal Variability in the Carbon Balance of a Spruce/Moss Boreal Forest, *Global Change Biology* **2**, 343-366.

Gaudinski, J.B., Trumbore, S.E., Davidson, E.A., Cook, A.C., Markewitz, D., and Richter, D.D.(2001). The Age of Fine-Root Carbon in Three Forests of the Eastern United States Measured by Radiocarbon, *Oecologia* **129**, 420-429.

Giasson, M.A., Coursolle, C., and Margolis, H.A.(2006). Ecosystem-Level Co2 Fluxes From a Boreal Cutover in Eastern Canada Before and After Scarification, *Agricultural and Forest Meteorology* **140**, 23-40.

Govind, A., Chen, J.M., Margolis, H., Ju, W., and Sonnentag, O.(2008a). A Spatially Explicit Hydroecological Modeling Framework (BEPS-TerrainLab V2.0) Part 1: Model Description and Testing., *Journal of Hydrology*. Submitted.

Govind, A., Chen, J.M., and Ju, W. (2008d). Spatially Explicit Simulation of Hydrologically Controlled Carbon and Nitrogen Cycles and Associated Feedback Mechanisms in a Boreal Ecosystem. *Journal of Geophysical Research-Biogeosciences.* Submitted.

Gower, S.T., Krankina, O., Olson, R.J., Apps, M., Linder, S., and Wang, C.(2001). Net Primary Production and Carbon Allocation Patterns of Boreal Forest Ecosystems, *Ecological Applications* **11**, 1395-1411.

Gower, S.T., Mcmurtrie, R.E., and Murty, D.(1996). Aboveground Net Primary Production

Decline With Stand Age: Potential Causes, *Trends in Ecology & Evolution* **11**, 378-382.

Gower, S.T. and Vitousek, P.M.(1989). Effects of Nutrient Amendments on Fine Root Biomass in a Primary Successional Forest in Hawaii, *Oecologia* **81**, 566-568.

Griffis, T.J., Black, T.A., Morgenstern, K., Barr, A.G., Nesic, Z., Drewitt, G.B., Gaumont-Guay, D., and Mccaughey, J.H.(2003). Ecophysiological Controls on the Carbon Balances of Three Southern Boreal Forests, *Agricultural and Forest Meteorology* **117**, 53-71.

Gower, S.T., Vogel, J.G., Norman, J.M., Kucharik, C.J., Steele, S.J., and Stow, T.K.(1997). Carbon Distribution and Aboveground Net Primary Production in Aspen, Jack Pine, and Black Spruce Stands in Saskatchewan and Manitoba, Canada, *Journal of Geophysical Research-Atmospheres* **102**, 29029-29041.

Hornberger, G.M., Bencala, K.E., and Mcknight, D.M.(1994). Hydrological Controls on Dissolved Organic-Carbon During Snowmelt in the Snake River Near Montezuma, Colorado, *Biogeochemistry* **25**, 147-165.

Janssens, I.A., Freibauer, A., Ciais, P., Smith, P., Nabuurs, G.J., Folberth, G., Schlamadinger, B., Hutjes, R.W.A., Ceulemans, R., Schulze, E.D., Valentini, R., and Dolman, A.J.(2003). Europe's Terrestrial Biosphere Absorbs 7 to 12% of European Anthropogenic CO_2 Emissions, *Science* **300**, 1538-1542.

Jenkins, Jennifer C.; Chojnacky, David C.; Heath, Linda S.; Birdsey, Richard A. (2004). Comprehensive database of diameter-based biomass regressions for North American tree species. Gen. Tech. Rep. NE-319. Newtown Square, PA: U.S. Department of Agriculture, Forest Service, Northeastern Research Station. 45 p.

Johnson, D.W., Cheng, W., and Ball, J.T.(2000). Effects of Co2 and N Fertilization on Decomposition and N Immobilization in Ponderosa Pine Litter, *Plant and Soil* **224**, 115-122.

Ju, W.M. and Chen, J.M.(2005). Distribution of Soil Carbon Stocks in Canada's Forests and Wetlands Simulated Based on Drainage Class, Topography and Remotely Sensed Vegetation Parameters, *Hydrological Processes* **19**, 77-94.

Ju, W.M., Chen, J.M., Black, T.A., Barr, A.G., Mccaughey, H., and Roulet, N.T.(2006a). Hydrological Effects on Carbon Cycles of Canada's Forests and Wetlands, *Tellus Series B-Chemical and Physical Meteorology* **58**, 16-30.

Kalyn, A.L. and Van Rees, K.C.J.(2006). Contribution of Fine Roots to Ecosystem Biomass and Net Primary Production in Black Spruce, Aspen, and Jack Pine Forests in Saskatchewan, *Agricultural and Forest Meteorology* **140**, 236-243.

Kielland, K., Mcfarland, J.W., Ruess, R.W., and Olson, K.(2007). Rapid Cycling of Organic Nitrogen in Taiga Forest Ecosystems, *Ecosystems* **10**, 360-368.

King, J.S., Pregitzer, K.S., Zak, D.R., Sober, J., Isebrands, J.G., Dickson, R.E., Hendrey, G.R., and Karnosky, D.F.(2001). Fine-Root Biomass and Fluxes of Soil Carbon in Young Stands of Paper Birch and Trembling Aspen As Affected by Elevated Atmospheric Co-2 and Tropospheric O-3, *Oecologia* **128**, 237-250.

Kljun, N., Calanca, P., Rotachhi, M.W., and Schmid, H.P.(2004). A Simple Parameterisation for Flux Footprint Predictions, *Boundary-Layer Meteorology* **112**, 503-523.

Kurz, W.A. and Kimmins, J.P.(1987). Analysis of Some Sources of Error in Methods Used to Determine Fine Root Production in Forest Ecosystems - a Simulation Approach, *Canadian Journal of Forest Research-Revue Canadienne De Recherche Forestiere* **17**, 909-912.

Lafleur, P.M., Roulet, N.T., Bubier, J.L., Frolking, S., and Moore, T.R.(2003). Interannual Variability in the Peatland-Atmosphere Carbon Dioxide Exchange at an Ombrotrophic Bog, *Global Biogeochemical Cycles* **17**.

Lambert, M.C., Ung, C.H., and Raulier, F.(2005). Canadian National Tree Aboveground Biomass Equations, *Canadian Journal of Forest Research-Revue Canadienne De Recherche Forestiere* **35**, 1996-2018.

Landsberg, J.J. and Waring, R.H.(1997). A Generalised Model of Forest Productivity Using Simplified Concepts of Radiation-Use Efficiency, Carbon Balance and Partitioning, *Forest Ecology and Management* **95**, 209-228.

Landgraf, D., Wedig, S., and Klose, S.(2005). Medium- and Short-Term Available Organic Matter, Microbial Biomass, and Enzyme Activities in Soils Under Pinus Sylvestris L. And Robinia Pseudoacacia L. In a Sandy Soil in Ne Saxony, Germany, *Journal of Plant Nutrition and Soil Science-Zeitschrift Fur Pflanzenernahrung Und Bodenkunde* **168**, 193-201.

Law BE, Sun OJ, Campbell J, Van Tuyl S, Thornton PE(2003) Changes in Carbon Storage and Fluxes in a Chronosequence of Ponderosa Pine. *Global Change Biology* **9** 510-524.

Law BE, Thornton PE, Irvine J, Anthoni PM, Van Tuyl S(2001) Carbon Storage and Fluxes in Ponderosa Pine Forests at Different Developmental Stages. *Global Change Biology* **7** 755-777.

Law BE, Turner D, Campbell J, Sun OJ, Van Tuyl S, Ritts WD, Cohen WB(2004) Disturbance and Climate Effects on Carbon Stocks and Fluxes Across Western Oregon Usa. *Global Change Biology* **10** 1429-1444.

Miller J.B. (2008) Carbon cycle: Sources, sinks and seasons. *Nature*, **451**, 26.

Nadelhoffer, K.J., Aber, J.D., and Melillo, J.M.(1985). Fine Roots, Net Primary Production, and Soil-Nitrogen Availability - a New Hypothesis, *Ecology* **66**, 1377-1390.

Parton, W.J., Scurlock, J.M.O., Ojima, D.S., Gilmanov, T.G., Scholes, R.J., Schimel, D.S., Kirchner,

T., Menaut, J.C., Seastedt, T., Moya, E.G., Kamnalrut, A., and Kinyamario, J.I.(1993). Observations and Modeling of Biomass and Soil Organic-Matter Dynamics for the Grassland Biome Worldwide, *Global Biogeochemical Cycles* **7**, 785-809.

Peltoniemi, M., Makipaa, R., Liski, J., and Tamminen, P.(2004). Changes in Soil Carbon With Stand Age - an Evaluation of a Modelling Method With Empirical Data, *Global Change Biology* **10**, 2078-2091.

Peng, C.H., Liu, J.X., Dang, Q.L., Apps, M.J., and Jiang, H.(2002). Triplex: a Generic Hybrid Model for Predicting Forest Growth and Carbon and Nitrogen Dynamics, *Ecological Modelling* **153**, 109-130.

Piao S., Ciais P., Friedlingstein P., Peylin P., Reichstein M., Luyssaert S., Margolis H., Fang J., Barr A., Chen A., Grelle A., Hollinger D.Y., Laurila T., Lindroth A., Richardson A.D. & Vesala T. (2008) Net carbon dioxide losses of northern ecosystems in response to autumn warming. *Nature*, **451**, 49-53.

Rapalee, G., Trumbore, S.E., Davidson, E.A., Harden, J.W., and Veldhuis, H.(1998). Soil Carbon Stocks and Their Rates of Accumulation and Loss in a Boreal Forest Landscape, *Global Biogeochemical Cycles* **12**, 687-701.

Ryan, M.G., Lavigne, M.B., and Gower, S.T. (1997). Annual Carbon Cost of Autotrophic Respiration in Boreal Forest Ecosystems in Relation to Species and Climate, *Journal of Geophysical Research-Atmospheres* **102**, 28871-28883.

Regniere, J. and St-Amant, R.(2007). Stochastic Simulation of Daily Air Temperature and Precipitation From Monthly Normals in North America North of Mexico, *International Journal of Biometeorology* **51**, 415-430.

Ro, C., Vet, R., Ord, D., and Holloway, A.. (1995). Canadian Air and Precipitation Monitoring Network (CAPMoN) Annual Summary Reports (1983–1994). *National Atmospheric Chemistry Database (NAtChem)*, Atmospheric Environment Service, Environment Canada.

Schuur, E.A.G. and Trumbore, S.E.(2006). Partitioning Sources of Soil Respiration in Boreal Black Spruce Forest Using Radiocarbon, *Global Change Biology* **12**, 165-176.

Shibu, M.E., Leffelaar, P.A., Van Keulen, H., and Aggarwal, P.K.(2006). Quantitative Description of Soil Organic Matter Dynamics - a Review of Approaches With Reference to Rice-Based Cropping Systems, *Geoderma* **137**, 1-18.

Schimel, D.S.(1995). Terrestrial Biogeochemical Cycles - Global Estimates With Remote-Sensing, *Remote Sensing of Environment* **51**, 49-56.

Steele, S.J., Gower, S.T., Vogel, J.G., and Norman, J.M.(1997). Root Mass, Net Primary Production and Turnover in Aspen, Jack Pine and Black Spruce Forests in Saskatchewan and Manitoba, Canada , *Tree Physiology* **17**, 577-587.

Sun, O.J., Campbell, J., Law, B.E., and Wolf, V.(2004). Dynamics of Carbon Stocks in Soils and Detritus Across Chronosequences of Different Forest Types in the Pacific Northwest, Usa, *Global Change Biology* **10**, 1470-1481.

Sun, R., Chen, J.M., Zhu, Q.J., Zhou, Y.Y., Liu, J., Li, J.T., Liu, S.H., Yan, G.J., and Tang, S.H.(2004b). Spatial Distribution of Net Primary Productivity and Evapotranspiration in Changbaishan Natural Reserve, China, Using Landsat Etm Plus Data, *Canadian Journal of Remote Sensing* **30**, 731-742.

Ter-Mikaelian, M.T., and Korzukhin, M.D. (1997). Biomass equations for sixty-five North American tree species. *For. Ecol. Manage*. 97: 1–24.

Tjoelker M.G., Oleksyn J. & Reich P.B. (1999a) Acclimation of respiration to temperature and CO_2 in seedlings of boreal tree species in relation to plant size and relative growth rate. *Global Change Biology*, **5**, 679-691.

Torn, M.S., Trumbore, S.E., Chadwick, O.A., Vitousek, P.M., and Hendricks, D.M.(1997). Mineral Control of Soil Organic Carbon Storage and Turnover, *Nature* **389**, 170-173.

Thomas, S.C. and Malczewski, G. (2007) Wood carbon content of tree species in Eastern China: Interspecific variability and the importance of the volatile fraction: Carbon Sequestration In China's Forest Ecosystems. *Journal of Environmental Management* 85(3), 659-662.

Thornton, P.E., Law, B.E., Gholz, H.L., Clark, K.L., Falge, E., Ellsworth, D.S., Golstein, A.H., Monson, R.K., Hollinger, D., Falk, M., Chen, J., and Sparks, J.P.(2002). Modeling and Measuring the Effects of Disturbance History and Climate on Carbon and Water Budgets in Evergreen Needleleaf Forests, *Agricultural and Forest Meteorology* **113**, 185-222.

Turunen, J., Roulet, N.T., Moore, T.R., and Richard, P.J.H.(2004). Nitrogen Deposition and Increased Carbon Accumulation in Ombrotrophic Peatlands in Eastern Canada, *Global Biogeochemical Cycles* **18**.

Wang, C.K., Bond-Lamberty, B., and Gower, S.T.(2003). Carbon Distribution of a Well- and Poorly-Drained Black Spruce Fire Chronosequence, *Global Change Biology* **9**, 1066-1079.

Way D.A. & Sage R.F. (2008) Elevated growth temperatures reduce the carbon gain of black spruce (*Picea mariana* (Mill.) B.S.P.). *Global Change Biology*, **14**, 624-636.

CHAPTER-5

Spatially Explicit Simulation of Hydrologically Controlled Carbon and Nitrogen Cycles and Associated Feedback Mechanisms in a Boreal Ecosystem.

5.1. Abstract

Ecosystem models that simulate terrestrial carbon (C) dynamics usually ignore the effects of hydrological controls that govern biogeochemical processes. It is quite possible that topographically-driven, sub-surface baseflow fluxes significantly influence the spatial distribution of C-sources and sinks because of their large contribution to the local water balance that affect many biogeochemical processes. To investigate this, we simulated the biogeochemical processes along with the associated feedback mechanisms in a boreal forest ecosystem using a spatially explicit hydro-ecological model, BEPS-TerrainLab V2.0. The simulated the net ecosystem productivity (NEP) and ecosystem respiration were validated with high frequency eddy covariance measurements for two years. The model was able to explain 80% of the variability in NEP and 84% of the variability in total ecosystem respiration. This was achieved mainly because the model was able to adequately simulate the dynamics of snowpack, the resultant winter-summer soil temperature patterns, the dynamics of soil and vegetation C and nitrogen (N) cycling, and various ecophysiological and hydrological processes. Once we felt confident in the model's ability, we investigated the influence of topographically driven sub-surface baseflow on soil C and N cycling and on the spatiotemporal patterns of terrestrial C-sources and sinks using three hydrological modeling scenarios: 1) *Explicit*, where a realistic calculation of baseflow is employed considering topographic controls 2) *Implict,* where the baseflow calculations were based on a bucket modeling approach 3) *NoFlow*, where the lateral water flow was turned off in the model.In general, the *Implicit* and the *NoFlow* scenarios overestimated NEP, as opposed to the

Explicit scenario. The key processes controlling the NEP differences were attributed to the combined effects of variations in photosynthesis (due to changes in stomatal conductance and nitrogen (N) availability), heterotrophic respiration, and autotrophic respiration, all of which occur simultaneously and affect the NEP. Feedback relationships were also found to exacerbate the differences. We identified six types of NEP-differences (biases), of which the most commonly found was due to *an underestimation of the existing C sources*. Our results indicate that lateral water flow does play a significant role in the terrestrial C source sink distribution due to its direct and indirect effects on biogeochemical processes.

5.2. Introduction

The global C-cycle is closely linked to climate, hydrology, and nutrient cycles because of their effects on terrestrial primary production (Porporato et al., 2003). However, the interactions between these environmental conditions at various spatio-temporal scales are quite variable creating uncertainties in their behavior under future climate. There are many environmental factors that control the interaction between the biogeochemical cycles and the associated feedback mechanisms among them. Of these, hydrological controls on terrestrial C-cycling processes are likely to be the most dominant because these controls are multi-faceted and range widely in the form of plant water stress (excess or deficit), effects on soil chemistry , heterotrophic respiration, controls on methane production, and transport of dissolved organic C (DOC) etc., to name a few. Thus, a simultaneous and realistic representation of all these mechanisms is required to describe the non-linear relationships among various processes.

Surface topography creates hydraulic head differences, which control the lateral water movement over a landscape. Currently, topographic effects on surface or sub-surface hydrological processes are often not explicitly represented to model regional scale C-balance of

ecosystems (Grant, 2004). A study conducted by Govind et al. (2008b) demonstrated that topographically–driven, lateral sub-surface baseflow can significantly alter photosynthesis by mediating through the differences in stomatal dynamics and N availability. Therefore, models that overlook topographic effects on soil water, nutrient, and temperature are likely to have several types of systematic errors in their terrestrial C-source or sink estimates. Despite the proclivity for these models to include errors, a number of regional studies have been performed using abstract representations of soil moisture to predict complex ecosystem processes such as terrestrial C-cycling. These approaches might have pronounced bias compared to reality.

Many measurement and modeling studies have demonstrated that northern boreal forests, which cover about 11% of the earth's land surface, are a terrestrial C-sink. (Thompson et al., 1996; Chen et al., 2003). In order to investigate the hydrological effects on ecosystem C and N cycling and the associated feedback relationships in boreal ecosystems, we developed a spatially-explicit hydro-ecological model, BEPS-TerrainLab V2.0 (Govind et al., 2008a). To represent realistically the hydrological regime within each modeling unit (pixel), a detailed water balance equation is solved in a spatially explicit manner, with inter-pixel connectivity using surface and sub-surface lateral water fluxes. After testing the model's performance for predicting ecophysiological and hydrological processes, Govind et al. (2008a) demonstrated that the most important hydrological process in boreal ecosystems is topographically-driven, sub-surface baseflow, which is almost 60-65% of the infiltrated water, followed by evapotranspiration (ET).

Terrestrial C sources and sinks are not only determined by primary production, but also by other processes such as respiration and the dynamics of soil C and N that are much more complex than gross primary productivity (GPP) or ET. In this paper, we introduce the biogeochemical aspects of BEPS-TerrainLab V2.0 and test its ability to simulate various biogeochemical processes in a boreal ecosystem in eastern Canada. In the current model set up,

we assume that no C is lost from the ecosystem as dissolved organic C or methane. Thus, the difference between the GPP and the daily total ecosystem respiration results in net ecosystem productivity (NEP). Further, we investigate the influence of sub-surface baseflow on soil C and N cycles and its implications for the simulated NEP, soil organic matter decomposition, and N availability, by using three scenarios that represent the existing hydrological representations in ecological models.

5.3. Model Description

BEPS-TerrainLab V2.0 is a hydro-ecological model that simulates the coupled hydrological, eco-physiological, and biogeochemical processes and the associated feedback mechanisms in a spatially explicit manner (Figure 5-1). A complete description of the hydrological and ecophysiological processes simulated by BEPS-TerrainLab V2.0 can be found in Govind et al. (2008a). Details of various ecosystem C and N cycles as affected by various environmental controls are described in this paper. This model runs at a daily time step and the modeling period is generally one or two years. Therefore, it used for simulating short-term ecosystem (soil and biomass) C-dynamics as controlled by abiotic factors such as soil temperature and moisture.

Most of the hydro-ecological processes such as ET, canopy interception, root control on soil water uptake, snowmelt, soil water transport, percolation, capillary rise, and topography-induced lateral water distribution across the terrain are used to solve the local scale water balance. GPP is modeled by the process-based Farquhar model that employs a spatial and temporal upscaling strategy (Chen et al.,1999).

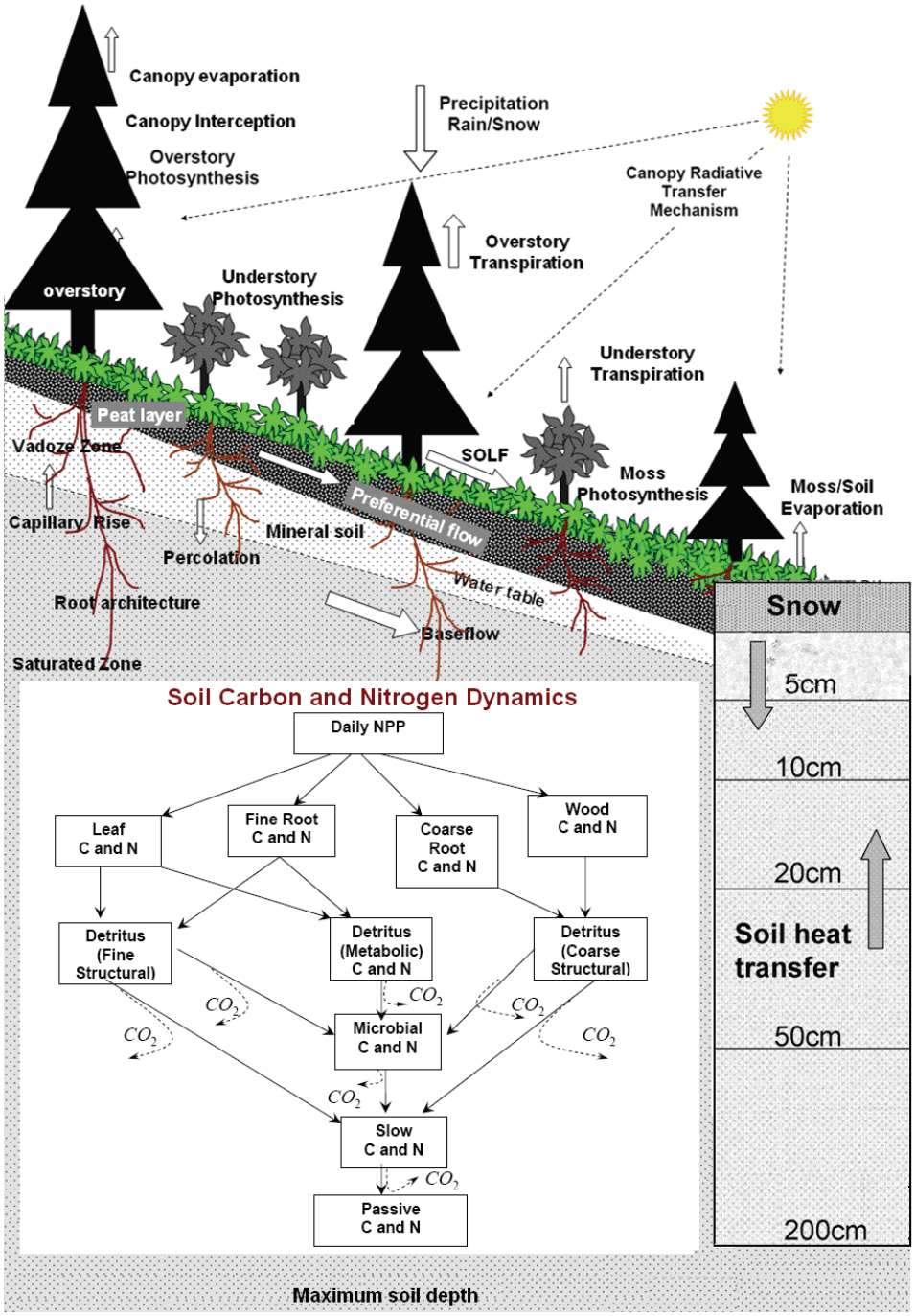

Figure 5-1. Schematic representation of a BEPS-TerrainLab V2.0 modeling unit adopted from Govind et al. (2008a).The belowground biogeochemical processes and their feedback relationships as influenced by hydrology and soil temperature is the focus of this paper.

A Penman-Monteith formulation is used to used to calculate leaf or surface scale ET. Spatial upscaling of leaf level ecophysiological processes are carried out using a *four leaf scheme* that uses leaf area index fractions as weighting factors that correspond to different leaf illuminations (sunlit or shaded) and soil moisture regimes (saturated and unsaturated). Parameters (net radiation, stomatal conductance etc.) specific to different radiation and soil water regimes are used to simulate leaf-level ET and GPP for multi layer canopies (overstory, understory, and moss layer).

5.3.1. Carbon Cycling Processes within BEPS-Terrainlab V2.0

5.3.1.1. Autotrophic Respiration

A part of the C assimilated in the form of GPP is used daily by plants for growth (R_g) and maintenance respiration (R_m), which are known together as autotrophic respiration (R_a).Various components of the vegetation (leaf, stem, and root) at various levels (overstory, understory, and moss) has R_a losses. In BEPS-TerrainLab V2.0, R_g is assumed to be 25% of the GPP for all land cover types (Chen et al., 1999; Liu et al., 1999 Ju et al., 2006). R_m is temperature-dependent for each of the plant components (leaf, stem, and root) which is modeled as

$$R_m = \sum_{i=1}^{4} R_{m,i} = \sum_{i=1}^{4} M_i . r_{m,i} . Q_{10}^{\frac{(T-T_b)}{10}} \quad (1)$$

Here i refers to different plant-parts such as leaf, stem, coarse-root, or fine-root; M is the biomass C-pool size associated with a biomass type; $r_{m,i}$ is the biomass C-pool specific respiration rate at base temperature T_b (^oC); and T is the ambient air temperature for leaves and stems or soil temperature for fine-roots and coarse-roots. In BEPS-TerrainLab V2.0, R_a is explicitly calculated as the sum of overstory, understory, and moss components within each land cover

type. The remainder of the C residing after accounting for R_a is the net primary productivity, NPP, which is further partitioned into leaf, wood, coarse root, and fine root biomass C-pools.

5.3.1.2. Heterotrophic Respiration

In BEPS-TerrainLab V2.0, heterotrophic respiration is comprehensively calculated in a manner similar to the CENTURY model of Parton et al. (1993) with several modifications as suggested by Ju and Chen, (2005) and Ju et al., (2007). Unlike other models, the soil C-cycling processes in BEPS-TerrainLab V2.0 run at a daily time step. The soils C-dynamics in an ecosystem are based on various conceptual C-pools. The biomass C-pools as described in the previous section are decomposed directly or indirectly to nine soil C-pools, i.e., (1) Surface Structural Litter, C_{ssd} (2) Soil Structural Litter, C_{fsd} (3) Woody Litter, C_{cd} (4) Surface Metabolic Litter, C_{smd} (5) Soil Metabolic Litter, C_{fmd} (6) Surface Microbial, C_{sm} (7) Soil Microbial, C_m (8) Slow C-pool, C_s and (9) Passive C-pool, C_p. Based on various environmental controls such as soil moisture and temperature and the inherent physico-chemical nature of individual C-pools that define their decomposition rates and C:N ratios, the sizes of individual soil C-pools are updated on a daily basis due to heterotrophic respiration or inter-conversion between various soil C-pools. The total heterotrophic respiration is the sum of C released to the atmosphere as CO_2 from all the soil C-pools during their decomposition as shown below.

$$R_{hi} = \sum_{j=1}^{9} k_{j_i} . C_{j_i} \qquad (2)$$

where k_{j_i} (day^{-1}) is the rate of C released from the jth soil C-pool on the day i to the atmosphere, and C_{j_i} is the size of the jth C-pool. The actual decomposition rates of individual soil C-pools are determined by constraining the potential decomposition rates using scalars that

correspond to various environmental controls such as soil temperature, moisture, soil texture, N availability, and lignin contents as summarized below.

$$k_{j_i} = \begin{cases} K_j \xi_{j_i} A_i L_j & j = Pools - 1,2,3 \\ K_j \xi_{j_i} A_i & j = Pools - 4,5,8,9 \\ K_j A_i \eta & j = Pool - 7 \\ K_j A_i L_j & j = Pool - 6 \end{cases} \tag{3}$$

In the above equation, K_j is the maximum decomposition rate of the jth pool, which is a landcover-specific parameter (refer Table 5-1). Various scalars that represent environmental controls on the maximum decomposition rate include: A_i, the combined abiotic effect of soil temperature and moisture on soil C decomposition; η, the effect of soil texture on soil microbial turnover; L, the impact of lignin content for structural litter decomposition and ξ, the modifier for the effect of N availability on C decomposition of various pools. A_i is calculated as shown below as the product of soil moisture (M_{si}) and soil temperature (T_{mi}) effects. Figure 5-2 shows the nature of M_{si} and T_{mi}.

$$A_i = M_{si} \times T_{mi} \tag{4}$$

The soil moisture effect M_{si}, is calculated as a function of volumetric soil moisture content, θ.

$$M_{si} = 5.44\left[\frac{\theta_i}{\theta_s}\right] - 5.03\left[\frac{\theta_i}{\theta_s}\right]^2 - 0.472 \tag{5}$$

In BEPS-TerrainLab V2.0, θ_i is simulated using a comprehensive hydrological modeling strategy by solving a detailed water balance equation in a spatially explicit manner. Most of the hydro-ecological processes are considered in this water balance equation, including the topographically-driven, sub-surface baseflow that contributes or distributes water to or from neighboring pixels

Table 5-1. Various landcover specific parameters used for biogeochemical modeling within BEPS-TerrainLab V2.0

Parameters	Unit	Conifers	Mixed	Deciduous	Wetlands	Reference
Temp. sensitivity factor						
Leaf maintenance respiration coefficient	--	0.002	0.002	0.002	0.002	1
Stem maintenance respiration coefficient	--	0.001	0.001	0.001	0.001	1
Coarse root maintenance respiration coefficient	--	0.001	0.001	0.001	0.001	1
Fine root maintenance respiration coefficient	--	0.002	0.002	0.002	0.002	1
Atmospheric nitrogen deposition	$gNm^{-2}day^{-1}$	$8.2x10^{-4}$	$8.2x10^{-4}$	$8.2x10^{-4}$	$8.2x10^{-4}$	2
Wood turn over rate	$gCm^{2}day-1$	7.64E-05	7.64E-05	7.89E-05	1.97E-05	2
Leaf Turn over rate	$gCm^{2}day-1$	7.37E-05	7.34E-05	1.23E-04	3.07E-05	2
Coarse root turn over rate	$gCm^{2}day-1$	5.27E-04	1.08E-03	2.74E-03	6.85E-04	2
Fine root turn over rate	$gCm^{2}day-1$	1.63E-03	1.63E-03	1.63E-03	4.07E-04	2
Surface structural leaf litter decomposition rate	$gCm^{2}day-1$	(3.9x LxAxξ)/365				3
Surface metabolic leaf litter decomposition rate	$gCm^{2}day-1$	(14.8xAxξ)/365				3
Soil structural leaf litter decomposition rate	$gCm^{2}day-1$	(4.8xLxAxξ)/365				3
Soil metabolic leaf litter decomposition rate	$gCm^{2}day-1$	(18.5xAxξ)/365				3
Woody litter decomposition rate	$gCm^{2}day-1$	(2.88xLxAxξ)/365				3
Surface microbial decomposition rate	$gCm^{2}day-1$	(6.0xA)/365				3
Soil microbial decomposition rate	$gCm^{2}day-1$	(7.3xAxη)/365				3
Slow carbon decomposition rate	$gCm^{2}day-1$	(0.2xAxξ)/365				3
Passive carbon decomposition rate	$gCm^{2}day-1$	(0.0045xAxξ)/365				3
NPP allocation coefficient to wood	--	0.3010	0.3817	0.4624	0.4624	2
NPP allocation coefficient to leaf	--	0.2128	0.2077	0.2226	0.2226	2
NPP allocation coefficient to coarse root	--	0.1483	0.1536	0.1190	0.1190	2
NPP allocation coefficient to fine root	--	0.3479	0.2570	0.1960	0.1960	2

Coefficients similar for all land-cover types

A = Abiotic decomposition factor =f(Soil Temperature, Soil Moisture)

ξ =A function of Nitrogen availability

L =A function of lignin content

η =A function of soil-texture

The values shown here are maximum decomposition rates for a specific C-pool

1=Chen et al. (1999) **2**=Chen et al. (2003) **3**= Ju et al. (2007) at annual time steps. In this study original coefficients (annual) are divided by 365 for daily applications. The coefficients for Wetlands are half of the values of "Open Lands" in Chen et al. (2003).

a pixel in consideration ensuring that landscape scale hydrological processes affect local scale water balance. The soil temperature effect is described as shown below:

$$T_{mi} = e^{308.56.\left[\left(\frac{1}{35+46.02}\right)-\left(\frac{1}{T_{si}+46.02}\right)\right]} \tag{6}$$

Here, Ts_i is the soil temperature, which plays a critical role in determining the rate of decomposition of the soil C-pools (Parton et al., 1993).

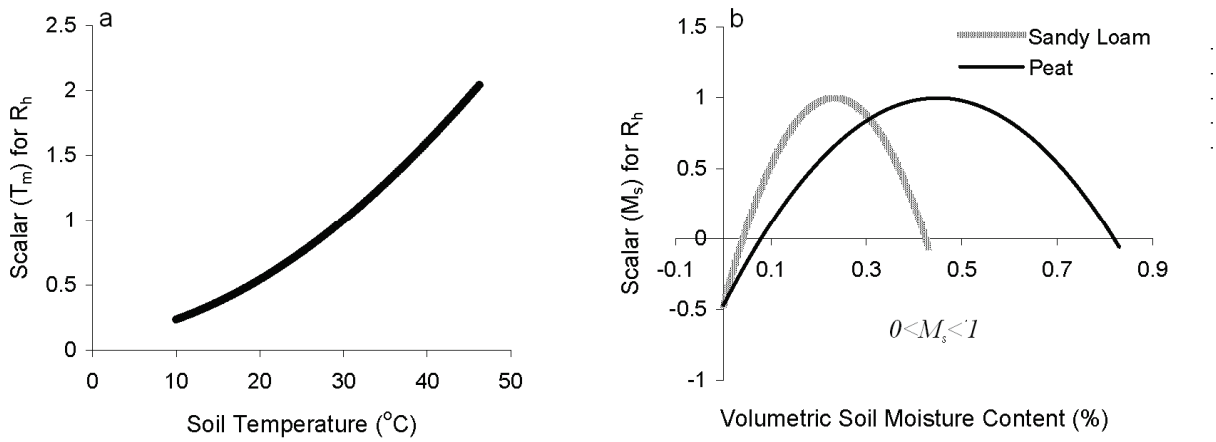

Figure 5-2. Nature of (a) Soil temperature scalar for heterotrophic respiration. (b) Soil moisture scalar for heterotrophic respiration.

Since soil temperature is a critical parameter in simulating biogeochemical processes, in BEPS-TerrainLab v2.0., Ts_i is comprehensively calculated employing a semi-implicit solution of Fourier's one-dimensional heat transfer equation. We consider 6 layers (one snow layer and 5 soil layers) for the heat transfer process. The Fourier's heat transfer equation shown below is solved using an implicit solution, as shown in equation 8.

$$C_i \frac{\partial Ts}{\partial t} = \lambda_i \frac{\partial^2 Ts}{\partial d^2} \tag{7}$$

$$\frac{C_i h_i \left[Ts_{i,t+1} - Ts_{i,t} \right]}{86400 \Delta t} = 2(1-f) \left[\frac{Ts_{i-1,t} - Ts_{i,t}}{\frac{d_{i-1}}{\lambda_{i-1}} + \frac{d_i}{\lambda_i}} - \frac{Ts_{i,t} - Ts_{i,t+1}}{\frac{d_i}{\lambda_i} + \frac{d_{i+1}}{\lambda_{i+1}}} \right] + f \left[\frac{Ts_{i-1,t+1} - Ts_{i,t+1}}{\frac{d_{i-1}}{\lambda_{i-1}} + \frac{d_i}{\lambda_i}} - \frac{Ts_{i,t+1} - Ts_{i,t+1}}{\frac{d_i}{\lambda_i} + \frac{d_{i+1}}{\lambda_{i+1}}} \right] \quad (8)$$

In these equations (7 and 8), C_i is the volumetric soil heat capacity ($Jm^{-3^o}C^{-1}$), and λ is the thermal conductivity ($Wm^{-1^o}C^{-1}$). These two variables vary spatially and temporally and are calculated on a daily basis. d is the vertical depth of a layer and t is the time step and f is the weight associated with the implicit solution. Snow depth plays an important role in determining the winter soil temperature in boreal ecosystems. The snow depth is modeled by temporally varying the snow density and snow water equivalent, as affected by the physical processes of snowmelt (radiation melt or temperature melt) and snow sublimation.

On a daily basis, a small fraction of C is lost (decomposed) or added (from other C-pools). These processes alter the size of a soil C-pools as shown below

$$Cx_i = Cx_{i-1} + \Delta Cx_i \quad (9)$$

where Cx_{i-1} is the size of the C-pool x on the previous day, $i-1$. ΔCx_i is the change in the pool x on a daily basis. The procedure to calculate ΔCx_i for each soil C-pool is different and depends on various environmental constraints and precursors. The equations for calculating ΔCx_i are shown in the Appendix 1. For the first day in 2004, Cx_{i-1} will be the ecosystem C-pool sizes in 2003.

5.3.2. Soil Nitrogen Cycle within BEPS-TerrainLab V2.0

Soil N dynamics and the availability of N to plants are determined by three processes as shown below.

$$N_{avail} = N_{dep} + N_{fix} + N_{\min} \tag{10}$$

These processes are: 1. Dry and wet deposition of N from the atmosphere (N_{dep}); 2. Biological N-fixation by certain microorganisms present in the rhizosphere (N_{fix}); and 3. N-mineralization due to soil C-pool decomposition that is controlled by factors such as soil moisture and temperature ($N_{\min}$). In BEPS-TerrainLab V 2.0, N_{fix} (atmospheric and biological combined) is empirically calculated as a function of daily precipitation and the current size of the soil and surface microbial C-pools. This method is analogous to Ju et al. (2007), where N-fixation is parameterized at annual time steps. In order to downscale temporally and use it for daily calculations, we replaced the annual precipitation and annual mean temperature in the original equation with the daily precipitation and temperature.

$$N_{fix_i} = \left[\frac{c1 \times 2.0^{\frac{T_{s_i}}{10}} \times P_i}{0.45} \right] \times \left(\frac{C_{sm_i} + C_{m_i}}{200} \right) \tag{11}$$

Here, N_{fix_i} is the N-fixation in gN m^{-2} day^{-1}. The coefficient $c1$ determines the fixation rate (in this study we used a value of 4.10x10^{-4} gN m^{-2} day^{-1}). The variable T_{s_i} is the daily mean soil temperature, P_i is daily precipitation (in m), and C_{sm_i} and C_{m_i} are the sizes of surface and soil microbial C-pools, respectively, on the day, i.

Based on various environmental controls, the nine soil C-pools change their size and C:N ratios as a result of heterotrophic respiration and inter-pool conversions. During their decomposition process, N-mineralization occurs, which increases the available N in the soil affecting the plant N status and photosynthesis. This source of available soil N is important for plant growth. Although inorganic forms of N (from the primary or secondary minerals) can also

contribute towards the total available N, it is not a significant factor in humid pristine boreal ecosystems.

5.3.3. Feedback Relationships within BEPS-TerrainLab V2.0

There are a number of feedback mechanisms in nature that make it difficult to comprehend various natural phenomena based on empirical studies alone. In BEPS-TerrainLab V2.0, a number of feedback relationships operate. Some of the important feedback relationships that directly relate to this work are given below.

1. Increase in plant-N increases photosynthesis, which increases soil C through biomass C-inputs. This increases soil C mineralization and, hence, more plant-N (positive feedback).
2. Increase in soil water decreases transpiration. This further increases soil water, resulting in a further decrease of transpiration(positive feedback).
3. Decrease in respiration increases biomass C, which leads to an increase in respiration (negative feedback).

5.4. Site Description

The simulation of the coupled biogeochemical and the related feedback mechanisms was conducted on a boreal landscape located southeast of Lake Chibougamau in north-central Quebec, Canada (Figure 5-3). Biogeographically, this region falls under the *Dfc* Köppen climate classification with a mean annual temperature of 0°C and a mean annual precipitation of 961.3 mm (Environment Canada, 2006). The vegetation of the study site consists of an overstorey, dominated by black spruce (*Picea mariana*), aspen (*Poplus sp.)*, and birch (*Betula sp*). Jack pine (*Pinus banksiana* Lamb.) and tamarack (*Larix larandicina*) are sporadically distributed. The understorey is mostly dominated by Labrador tea or *Salix sp.* The forest floor consists of a thick

moss layer, dominated by feather moss and *Sphagnum sp.* in wetter areas and lichens in moderately drier areas (Bergeron et al., 2007). This landscape has a gentle slope of < 5%, which is typical of the Canadian Shield. The vegetation species composition varies across the gentle topographic gradient with deciduous and mixed forests in the elevated locations such as eskers and coniferous species in flatter locations.

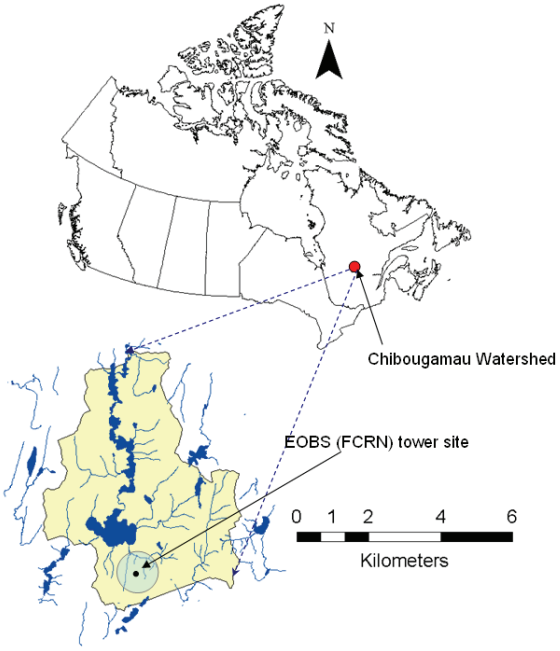

Figure 5-3. Location of the study site, Chibougamau watershed, which includes the Eastern Old Black Spruce (EOBS) tower site of FCRN where continuous high precision measurements of fluxes of mass and energy are being made using eddy covariance technique.

Since the soil is derived from glacio-fluvial deposits, they are mostly ferro-humic to humic podzol having a prominent organic layer with an average depth of 30 cm. In humid areas, the soil is predominantly organic with an average organic layer thickness of ~125 cm (Giasson et al., 2006).

5.5. Flux Measurements

The Eastern Old Black Spruce (EOBS) tower site of Fluxnet-Canada Research Network (FCRN) is located at 49.69°N and 74.342°W in the southwestern part of this boreal watershed. The eddy covariance (EC) technique is being used at EOBS site to make continuous measurements of CO_2 and energy fluxes since mid-2003. These datasets serve for the validation of various ecosystem model simulations. EC instrumentation comprises of a three-dimensional sonic anemometer and a closed and an open-path infrared gas analyzer (IRGA) that are mounted on a 24m scaffold tower. Along with continuous half hourly flux measurements of energy and CO_2, the tower also supports several instruments for measuring continuous meteorological data. Rainfall is measured using tipping bucket rain gauges, and total precipitation is measured using a Geonor T200B rain gauge. WTD is monitored using electronic piezometers. More details on flux and meteorological measurements can be found in Bergeron et al. (2007).

Wind comes predominantly from the south and northwest, both during the day and night. The fetch extends to 500m in all directions. Using an inverse Lagrangian model, Kljun et al. (2004) conducted a flux footprint analysis and estimated that the site's fetch contributed at least 90% of the measured flux in the dominant wind directions. Therefore, we used a circular area subtended by a 500m radius centered on the tower as "the footprint" for our data analyses. Since BEPS-TerrinLab V 2.0 runs at daily time steps, we temporally upscaled the meteorological forcing and ecosystem flux measurements taken at half hourly intervals to a daily time-step between January 2004 and December 2005.

5.6. Spatial and Meteorological Input Dataset and Initialization of C-Pools

For this study, we used the spatial and meteorological datasets of Govind et al. (2008a). The spatial datasets include: 1. Land cover, 2. Leaf area index (LAI), 3. Digital elevation model (DEM), 4. Soil texture 5. Initial water table depth (WTD), 6. Initialized ecosystem C-pools and their C:N ratios(four biomass C-pools and nine soil C-pools i.e. 26 maps) and 7. A watershed boundary derived using DEM. All of these spatial data sets have a spatial resolution of 25m with an UTM Zone 18N projection. Daily meteorological variables such as maximum temperature, minimum temperature, dew point temperature, incoming shortwave radiation, windspeed, and precipitation (rain or snow) collected at one point (EOBS tower site) were assigned for all the pixels in the modeling domain after correcting for the effects of elevation and slope on temperature and solar radiation, respectively. Daily meteorological measurements taken at half hourly intervals were temporally integrated over a 24 hr period. Since this boreal landscape has large heterogeneity with respect to land cover and soil, biophysical and hydraulic parameters were assigned in a spatially explicit manner. Tables 1 and 2 of Govind et al. (2008a) i.e. Tables 2-2 and 2-1 of Chapter 1 show the land cover and soil texture specific parameters for hydro-ecological modeling, respectively. Parameters used for biogeochemical modeling are shown in Table 5-1.

To initialize the size and C:N ratios of C-pools in 2003, a comprehensive initialization procedure was employed assuming that the current sizes and C:N ratios of various ecosystem C-pools result from long-term accumulation of plants and soil C as a function of both natural and human-induced disturbance factors (fire, deforestation, land use change, infrastructure development, insect, and disease) and non-disturbance factors (climate change, CO_2 fertilization, N deposition). To this end, we used a comprehensive C-pool initialization procedure using a long-term C cycle model, InTEC (Chen et a., 2000) under conditions of climate change, CO_2

change, and N-deposition, with consideration of disturbance effect on forest age, from 1920 to 2005 and spun up all the ecosystem C-pools (biomass and soil C-pools) in a spatially explicit manner (see Govind et al., 2008c). These spun-up C-pools were validated with inventory plot measurements taken by the Canadian Forest Service in 2003. This initialization procedure is a necessary step for modeling biogeochemical processes in this forest boreal ecosystem, even though the simulation period extended only for two years.

5.7. Modeling Experiments

We hypothesize that since the lateral sub-surface baseflow is the most predominant hydrological process (~65% of annual precipitation) that redistributes the infiltrated water in a humid boreal landscape, it can significantly affect the local scale hydrological regime and consequently biogeochemical processes along with associated feedback mechanisms. In order to investigate the effect of topographically driven sub-surface baseflow on the spatial distribution of C-sources and sinks (NEP), we conducted a numerical experiment using three modeling scenarios that differ in the manner in which baseflow is represented. Different scenarios used for this numerical experiment are denoted as "*Explicit*","*Implicit*"and"*NoFlow*". A detailed description of these scenarios is given in Govind et al. (2008b).

The *Explicit* scenario has baseflow calculated using topographic controls and has a realistic soil water balance. The *Implicit* scenario calculates baseflow using a *bucket-modeling* approach assuming that soil water above the field capacity drains-off as lateral flow. This scenario neither has topographical control nor has interaction between the neighboring pixels. This methodology is commonly used in most of the existing ecological models where explicit hydrological description is absent. The third scenario, i.e. the *NoFlow*, completely ignores the topographically-driven lateral sub-surface baseflow. The only possible pathway of lateral water movement is

surface overland flow (SOLF). However, SOLF occurs only after the entire soil profile is saturated with water. This method is employed in those models that consider topography driven lateral water flow but ignores the physiological and biogeochemical impacts of soil saturation. In all the three scenarios, we used the same spatial datasets, meteorological forcing and land cover-specific coefficients for hydrological, ecological, or biogeochemical processes. In this paper, the *Implicit* and *NoFlow* scenarios are generally referred to as *Non-Explicit* scenario.

5.8. Results and Discussion

5.8.1. Snow Depth and Soil Temperature

At the EOBS site, around 25% of the annual precipitation is in the form of snowfall, creating an average snowpack thickness of up to 80cm in the month of March. Snowpack, depending on its density, acts as an efficient insulator that favors edaphic life in the long boreal winter.

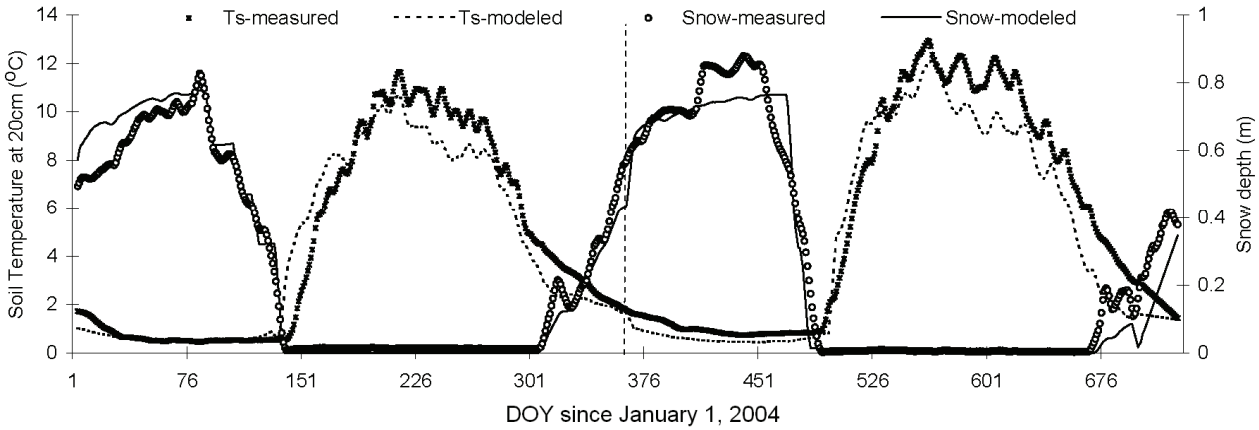

Figure 5-4. Temporal dynamics of the snow depth and near-surface (20 cm) soil temperature measured and modeled.

The simulated dynamics of snowpack thickness and the consequent soil temperature is shown in Figure 5-4 for the years 2004 and 2005. Although we used a quasi-physical approach to

model snow dynamics at daily time steps, we were able to capture the seasonal pattern. Much of the discrepancies in the simulated snow depth were seen towards the spring season, especially in 2005 when the model was highly sensitive to air temperature, rain or radiation, which causes rapid snow ablation. However in reality during this time, there was a large snowpack built-up. The model captured the annual trend of the dynamics of snow depth with reasonable accuracy (r^2=0.90, RMSE = 0.07 m day^{-1}, 2 years). Simulation of snow depth facilitated adequate calculation of winter soil temperature which subsequently affected the simulation of biogeochemical processes. It can be seen from the Figure 5-4 that soil temperature was more or less constant throughout the winter season when the snowpack was present over the soil surface as an insulating layer.

With the inclusion of the multi-layer, one dimensional heat transfer procedure that is solved using a numerical solution, the model was able to capture the annual trend of the near-surface soil temperature (20cm) with reasonable accuracy (R^2=0.92 RMSE 0.5 ^oC day^{-1}, 2 years). The inclusion of one snow layer and five soil layers to implement this numerical solution that utilises temporally, spatially, and vertically varying thermal properties for a modeling domain that consists of ~60,000 pixels is computationally pragmatic. However, for large modeling domains having finer spatial resolutions, the number of soil layers needs to be reduced or the spatial resolution should be made coarser.

5.8.2. Spatio-temporal Patterns of NEP and Respiration

The spatial distributions of the watershed scale annual NEP for the years 2004 and 2005 are shown in Figure 5-5. The spatial distributions demonstrate that locations that generally are dominated with mixed forest act as C-sinks (positive NEP values), whereas mature black spruce stands act as a weak C-source, weak C-sink, or C-neutral. Wetlands behave as a very small C-

sink, similar to mature forest stands. The spatial distribution of annual NEP reveals that middle aged mixed-forest stands are currently acting as significant C-sinks (locations with red tone), while mature coniferous stands (mostly black spruce) exhibit an almost C-neutral behavior. The range of the modeled NEP on this boreal landscape was quite large, i.e., -100 to +375 gC m^{-2} yr^{-1}, implying a large spatial variability in biogeochemical processes.

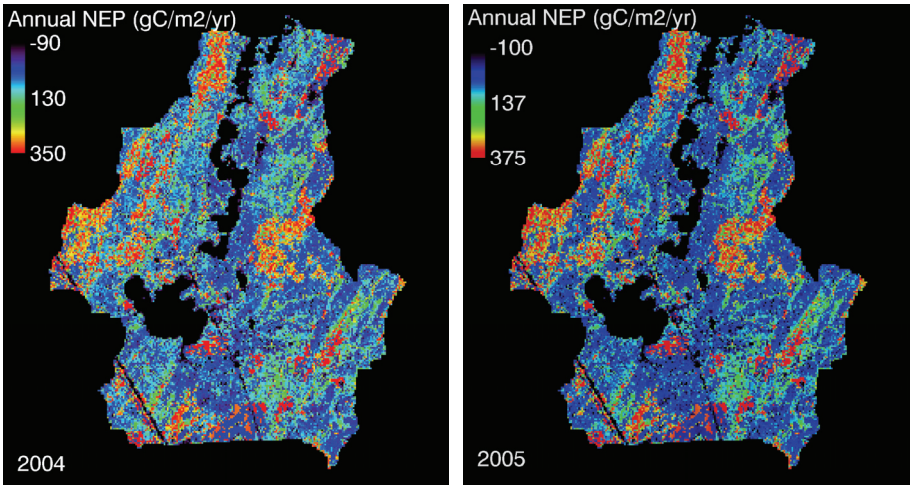

Figure 5-5. Spatial distribution of the annual NEP simulated for the years, 2004 and 2005

Unlike the spatial distribution of the annual GPP as shown in Govind et al. (2008a), annual NEP show only a weak congruence with the LAI or land-cover distribution. Age of a stand has a great influence in determining the magnitude of annual NEP. We identified that comparatively younger, fast-growing, middle-aged stands with positive values of annual NEP are generally associated with aspen-dominated locations that were established after a disturbance event in the recent past. The spatial distribution of annual NEP suggests that C-cycling is strongly dependent on a variety of environmental factors thst are antagonistically or synergistically linked. The simulated temporal pattern of the NEP at the EOBS tower footprint is shown in Figure 5-6 in comparison to the eddy covariance measurements of net ecosystem exchange made in 2004 and

2005. The model is able to capture the temporal pattern of NEP with reasonable accuracy (R^2=0.80, RMSE =0.63 gC m^{-2} day^{-1}, 2 years). The temporal pattern reveals that the ecosystem behaved as a C-source in the winter and a C-sink in the growing season. In 2004, the annual NEP in the footprint region was simulated to be 11 gC m^{-2} yr^{-1} (6±12 gC m^{-2} yr^{-1}, measured by EC technique), and in 2005, it was simulated to be -2.0 gC m^{-2} yr^{-1} (0± 3 gC m^{-2} yr^{-1}, measured).

During the growing season, on some days, the ecosystem behaved as a strong C-source. This indicates that the total respiration is more than photosynthesis. These conditions usually occurred during warm, dry conditions (between DOY 150- 220 in 2004 and DOY 140-225 in 2005) when the ecosystem respiration exceeds GPP. In this humid boreal ecosystem, drier periods favored photosynthesis because of increased primary production due to increased stomatal conductance and N availability (Govind et al., 2008a). However, high temperature also increased ecosystem respiration (R_a and R_h) even more than the primary production, making the system a net C-source. However, on an annual basis, the amount of sources and sinks is nearly similar, making the system almost C-neutral on an annual basis.

We also need to consider some feedback mechanisms that are strengthened as a result of temporal variations in ecosystem respiration, photosynthesis, and ET to fully understand the C-balance of this humid boreal ecosystem. R_a is primarily determined by the temperature and the magnitude and physico-chemical nature of various biomass C-pools. However, R_h is determined by various controls such as soil temperature, moisture, and size of soil C-pools. Increased decomposition of soil C-pools under warm-dry conditions result in increased soil N mineralization resulting in increased leaf N. This increased N, in turn, affects primary production due to an increase in the maximum carboxylation rate. Thus, increased NEP immediately after dry periods could be partially attributed to increased N mineralization.

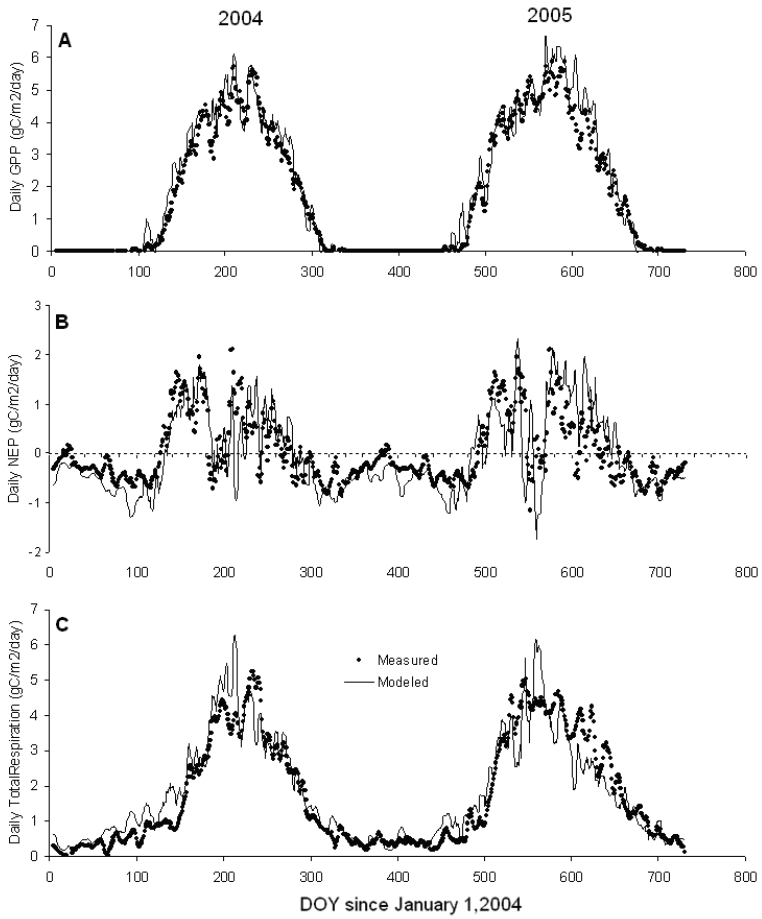

Figure 5-6. Comparison of measured and simulated (A) GPP (B) NEP (B) and (C) Ecosystem respiration (all 5 day moving averages shown for visual clarity) at the footprint region of the EOBS tower site, for two years 2004 and 2005.

Between the two years, seasonally, 2004 showed smaller shifts in the ecosystem status as a C-sink to C-source, resulting in a net sink of around 11 gC m^{-2} yr^{-1}. However, in 2005, although the annual GPP was high, annual NEP was reduced by increased respiration due to prolonged warm-dry periods. This resulted in changing the ecosystem's status as a weak C-source (-2 gC m^{-2} yr^{-1}).

The total ecosystem respiration is a highly fluctuating and influential portion of the C-balance that determines the NEP of an ecosystem. It is dynamic because of the presence of several

sub-component processes (growth R_g , maintenance R_m and heterotrophic R_h respirations) and the associated feedback mechanisms (e.g. N mineralization) that directly or indirectly modify the magnitude of the total respiration. Depending on the environmental controls (soil moisture and temperature), magnitudes, and physico-chemical nature (C:N ratios) of various ecosystem C-pools, the simulated total ecosystem respiration showed spatio-temporal variations that significantly affected the NEP. In Figure 5-5c, the simulated total respiration is compared to EC derived respiration for the years 2004 and 2005. During the winter season, when the air temperature is very low, primary production is almost negligible. However, the daily magnitude of total respiration is significant. During this time, near surface soil temperature (20 cm) remains almost uniform (near 0-1°C) due to the thermal insulation imparted by the snowpack facilitating active soil respiration, even if the air temperature dropped as low as -30 ^{o}C. The model is able to capture the annual trend of total ecosystem respiration with reasonable accuracy (R^2=0.84, RMSE= 0.54 gC m^{-2} day^{-1}, 2 years).

The annual ecosystem respiration at the EOBS footprint region was almost as large as the annual GPP, making the ecosystem almost C-neutral. The high respiration can be attributed to the age effects of the stand having increased R_a and R_h . From the measurement data collected from six coniferous boreal sites, Lavigne et al., (1997) reported for black spruce ecosystems, soil respiration accounts for as much as 48-71% of total ecosystem respiration. Black et al. (2005) also reported that the contribution from soil respiration can be as high as 80, 67, and 83% for boreal aspen, black spruce, and jack pine sites, respectively. These studies highlight the importance of soil respiration in determining the fate of C-cycling in boreal ecosystems. We realize that the presence of thick snowpack in the winter season in a boreal ecosystem has a great role in

determining the winter soil respiration that determines the annual NEP. Thus, modeling snow dynamics is critical to simulate soil temperature, heterotrophic respiration, and NEP.

5.8.3. Differences in the Simulated NEP under Hydrological Scenarios.

In order to investigate the role of topographically-driven baseflow in determining the local scale biogeochemical dynamics of C-sources or sinks, we analyzed the NEP simulated by various scenarios. Figure 5-7 shows the deviations in the simulated NEP under the *Implicit* and the *NoFlow* scenarios in comparison to the *Explicit* scenario. The plot is a pixel-to-pixel comparison of annual NEP simulated under these three scenarios (the *Explicit* vs. *Implicit* or *Noflow* scenarios) for the whole watershed (n= 35426). The plots clearly demonstrate that there are pronounced differences under these three hydrologically distinct scenarios (deviation from the 1:1 line). In general, both the *Non-Explicit* scenarios over-estimated annual NEP in comparison to the *Explicit* scenario.

The trend shown here is different from what Govind et al. (2008b) demonstrated for GPP where it is overestimated under the *Implicit* scenario and underestimated under the *NoFlow* scenario. Since NEP depends on many processes such as photosynthesis, respiration (autotrophic and heterotrophic), N mineralization, stomatal dynamics, and the associated feedback mechanisms, it is impossible to give a single reason for the observed differences in the simulated NEP under the *Non-Explicit* scenarios. It is probable that ecosystem respiration is greatly subdued under the *NoFlow* scenario, making the ecosystem a net C sink in spite of the lowered photosynthesis as a result of lowered stomatal conductance and N-mineralization. The deviation created by the *NoFlow* scenario resembles the type of bias inherently present in ecological models where only topographically driven SOLF is considered and impacts of soil-water partitioning on physiological and biogeochemical processes are ignored.

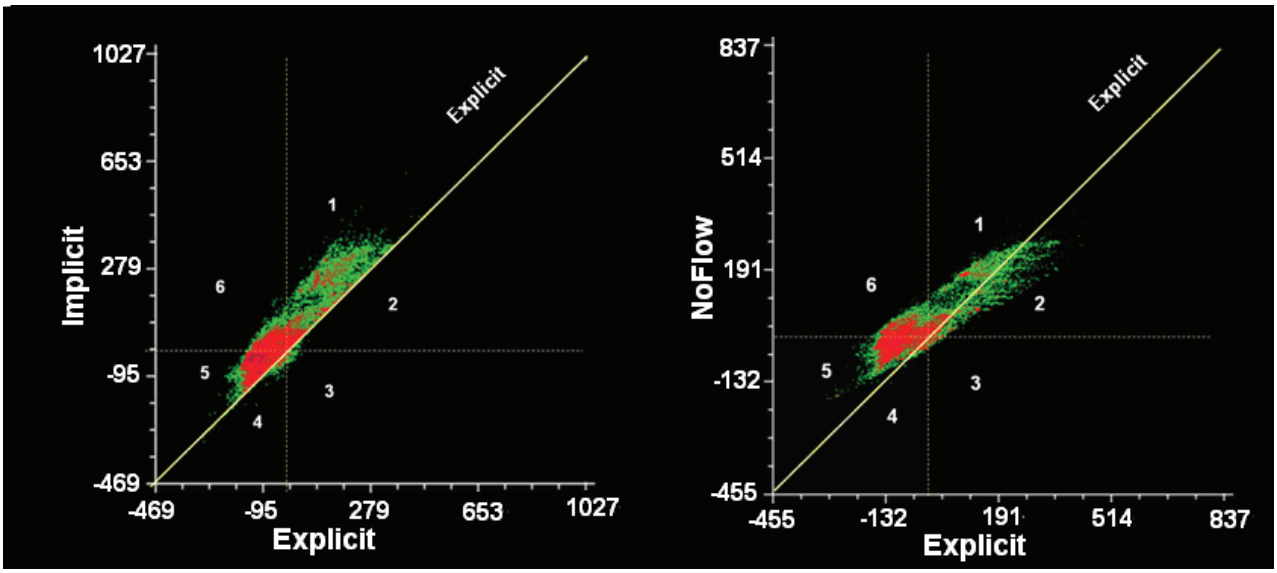

Figure 5-7. Plots between the NEP simulated under different baseflow scenarios. Left panel is the plot between the *Implicit* and the *Explicit* scenarios and right panel is between the *NoFlow* and the *Explicit* scenarios. In both, the line on slope=1 is the *Explicit* scenario, and departure from this line is considered as the bias.

The *Implicit* scenario also showed a general overestimation of the annual NEP in comparison to the *Explicit* scenario. This could be because of increased photosynthetic C-gains (from optimal stomatal conductance and increased N-availability) that dominated over increased respiratory C-losses (due to increased soil C-pool decomposition or increased autotrophic respiration). Implicit accounting of sub-surface baseflow assumes that within a soil profile if soil water has energy status above the field capacity, it is prone to gravitational flow. Baseflow in this type of calculation is not constrained by the topography. Thus, even on relatively flat areas where the slope is almost zero, soil moisture conditions remained conducive for both plant growth and soil C-pool decomposition because the volumetric water content in the soil profile always remained between the permanent wilting point(θ_{pwp}) and field capacity(θ_{fc}).

Figures 5-8a and 5-8c show the spatial distributions of the differences of the annual NEP as simulated by the *Non-Explicit* scenarios in comparison to the *Explicit* scenario. It is quite apparent that differences in the annual NEP were prominent in both the two *Non-Explicit* scenarios. These differences could be attributed to various landscape scale attributes such as topographic location, species composition, soil physical properties, etc. Topographic differences determine the WTD gradients that govern sub-surface baseflow. Baseflow fluxes are generally high on hill-slopes rather than on flat areas and the NEP differences among the scenarios are intense on hill slope locations than on flatter areas.

The spatial distribution of NEP differences between the *Implicit* and the *Explicit* scenarios (*Explicit-Implicit*) show that there is a marked overestimation by the *Implicit* scenario (dark blue tone, since low values represent overestimation). On flatter and soil-saturation-prone locations, NEP is substantially overestimated. Where the vegetation type is deciduous, photosynthesis and N-availability synergistically increases further enhancing NEP. On the other hand, on hill slope locations, the *Implicit* scenario create lesser baseflow fluxes than what *Explicit* scenario would simulate, leading to slight underestimations (red tone). Note that the maximum underestimation by the *Implicit* scenario on hill slopes is as low as 0.1 gC m^{-2} yr^{-1}, which indicates that the *Implicit* scenario only has weak tendency to underestimate NEP.

The spatial distribution of the annual NEP difference between the *NoFlow* and the *Explicit* scenarios also shows there was an overestimation (pixels with blue tones). This is because the respiratory losses in most of the locations are suppressed due to soil saturation. However, some locations show marked underestimation of NEP (locations with red tones). Land cover-specific ecophysiological parameters such as maximum stomatal conductance, clumping index, root depth, and architecture in combination with the effects of soil water determine the photosynthesis and, hence, the NEP.

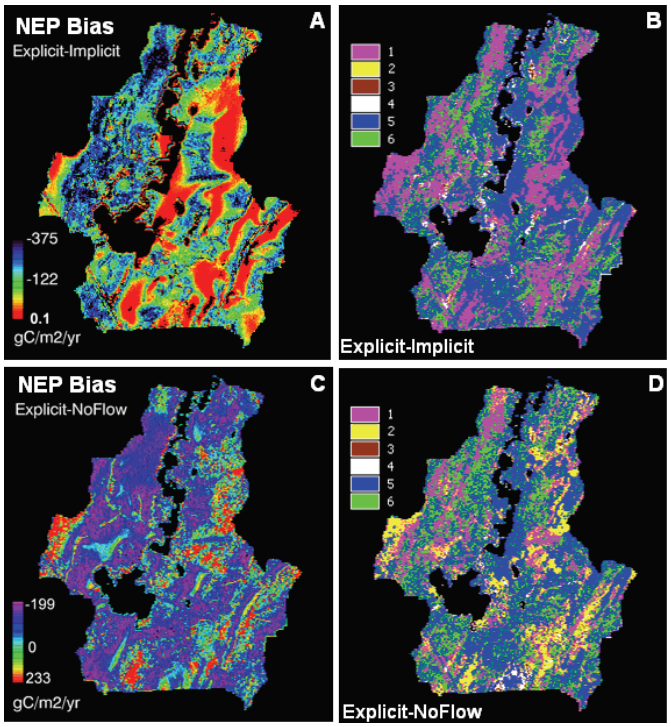

Figure 5-8. The spatial distribution of NEP bias under various hydrological scenarios. (A) by the *Implicit* scenario and (D) by the *NoFlow* scenario. Panels B and D show the spatial distribution of NEP difference-types for the *Implicit* and the *No Flow* scenarios, respectively.

It is insufficient to interpret the influence of sub-surface baseflow on NEP by relying only on the NEP difference maps. This is because various factors affect NEP simultaneously and differently. In the scatter plots shown in Figure 5-7, it is possible to delineate the NEP differences into six types of NEP. Each type has a different reason for its occurrence. The reasons can be summarized as:

***Type 1*:** This type of NEP-difference occurs when the NEP simulated by the *Non-Explicit* scenario is larger than the *Explicit* scenario. This is a case of intensification of an existing C-sink and arises either due to increase in photosynthesis (GPP) or reduction in ecosystem respiration.

***Type 2*:** This type of NEP-difference occurs when the NEP simulated by the *Non-Explicit* scenario is less than the *Explicit* NEP. This is a case of weakening C-sinks and arises either due to reduced GPP or increased ecosystem respiration.

***Type 3*:** This type of NEP-difference occurs when the NEP simulated by the *Non-Explicit* scenario results in a complete reversal of C-sinks (mostly weak sinks) to C-sources.

***Type 4*:** This type of NEP-difference occurs when the NEP simulated by the *Non-Explicit* scenario intensifies existing C-sources and mainly occurs due to increased heterotrophic respiration and reduced photosynthesis.

***Type 5*:** This type of NEP-difference occurs when the NEP simulated by the *Non-Explicit* scenario weaken the C sources but still remains as a C-source and mainly occurs due to a small decrease in heterotrophic respiration or small increase in photosynthesis. Type 5 differences are likely to be found on flat regions having mature (old growth) vegetation that are mostly weak C-sources.

***Type 6*:** This type of NEP-difference occurs when the NEP simulated by the *Non-Explicit* scenario results in a complete reversal of C-sources (mostly weak sources) to C-sinks and occurs mainly because of an increase in photosynthesis due to an increase in stomatal conductance or N-availability.

We mapped the NEP-difference types as shown in Figures 5-8b and 5-8d for the two *Non-Explicit* scenarios. It is obvious that Type 5 and Type 1 are the dominant forms under the *Implicit* scenario and Type 5, Type 1, and Type 2 in the *NoFlow* scenario. From these figures, it is clear that the differences in NEP on a landscape as a result of unrealistic hydrological representations can have various reasons for their existence. Figure 5-9 shows the relative contribution of different types of biases under the different *Non- Explicit* scenarios. It is clear that Type 5, Type 1, and Type 6 are the dominant types of errors. This suggests that ecological models that use *Non-*

Explicit forms of hydrological representation inherently could contain these types of errors in their NEP estimates.

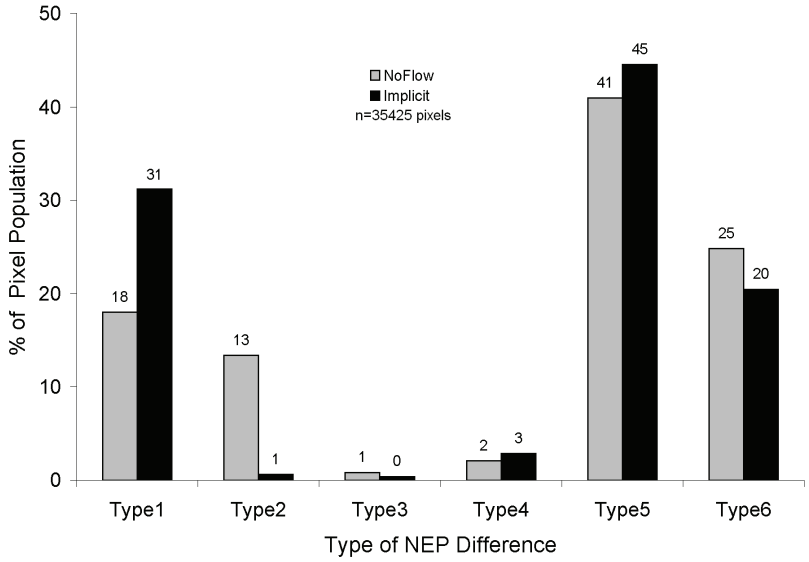

Figure 5-9. Relative occurrence of various NEP-difference types under different hydrological scenarios. Note that in both the *Non Explicit* scenarios, Type 5 is the dominant type.

5.8.4. Mechanisms of Hydrological Control on NEP

In the previous section, we demonstrated through the numerical experiment that local hydrological regimes can control the spatial distribution of terrestrial C-sources or sinks as affected by two important, hydrologically-controlled biogeochemical processes, i.e., photosynthesis and respiration. These processes are characterized by opposite directions of C-flux between the biosphere and the atmosphere. Factors such as the soil thermal regime and N-control on soil C-pool decomposition are some of the indirect effects of hydrological controls that govern NEP. Many processes have to be considered simultaneously while analyzing the NEP - differences as a result of variations in environmental, ecophysiological, biogeochemical, and hydrological processes in different scenarios. Table 5-2 summarizes the mechanisms of NEP-differences under various scenarios. In this table, ΔNEP, ΔGPP, ΔRa and ΔRh represent

percentage change in NEP, GPP, Ra, and Rh as a result of *Non-Explicit* hydrological representation from that of its *Explicit* (real) values. Due to non-linearities and feedback relationships, these changes are not additive in nature. From the Table 5-2, it can be seen that a Type 5 bias is mainly responsible for increased NEP in both *Implicit* and the *NoFlow* scenarios, and the reasons for its occurrence are different. For the *Implicit* scenario, a Type 5 bias accounts for 44.5% of the pixel population. This bias occurs due to a decrease in the magnitudes of C-sources. Under the *NoFlow* scenario, a Type 5 bias is still the dominant cause for differences from the *Explicit* scenario (41% of the pixel population).

Table 5-2. Differences in the magnitudes of various C-fluxes within various NEP-difference as a result of *Non-Explicit* hydrological representation.

Bias Type	**ΔNEP (as %)**	**ΔGPP (as %)**	**ΔRa (as %)**	**ΔRh (as %)**	**Dominant mechanism**	**Probability of occurrence ***
Implicit						
1	+60.1	+16.3	+8.3	+8.7	P dominated sink increase	31.2
2	-5.1	+31.3	+37.9	+37.3	R dominated sink decrease	0.6
3	-245.1	+119.5	+128.7	+131.9	R dominated sink to source	0.4
4	-17.4	+57.5	+52.7	+52.1	R dominated source increase	2.9
5	+52.4	+15.0	+7.3	+5.1	P dominated source decrease	44.5
6	+166.0	+25.9	+12.3	+9.6	P dominated source to sink	20.5
NoFlow						
1	+43.8	-21.7	-29.7	-31.7	P dominated sink increase	18.0
2	-24.2	-32.3	-33.2	-35.5	R dominated sink decrease	13.4
3	-172.5	-30.5	-24.5	-28.9	R dominated sink to source	0.8
4	-42.1	-18.9	-13.1	-18.0	R dominated source increase	2.1
5	+68.6	-35.9	-39.9	-40.7	R dominated source decrease	41.0
6	+138.0	-29.6	-38.2	-39.8	P dominated source to sink	24.8

P is Photosynthesis and R is Respiration * as percentage of n=35425 pixels

In the *Implicit* scenario, a Type 5 bias occurs due to a 15% increase in photosynthesis. However, under the *NoFlow* scenario, the increased C-sink is due to the large suppression of the total respiration (40%), even if the photosynthesis is reduced as much as 35%. The net effect in

both scenarios is a weakening of the existing C-sources (NEP becoming less negative). This reveals that ecological models having *Non-Explict* hydrological representation could have larger errors in determining the magnitudes of existing C-sources than the C-sinks.

5.8.5. Dynamics of Ecosystem C-Pools under Various Hydrological Scenarios

Although both photosynthesis and respiration determine the magnitudes of NEP, it is important to understand the nature of C-dynamics under various hydrological scenarios. Sizes of the soil C-pools affect the magnitude of NEP because of their roles in determining Rh or N-mineralization. Hence, we were interested to investigate the dynamics of various soil C-pools under hydrological scenarios. Moreover, uncertainties associated with the terrestrial C-cycle under climate change are mainly associated with the behavior of C-stocks in the soil (Cox et al., 2001). The temporal dynamics of various biomass and soil C-pools are shown in the Figure 5-10, averaged for the whole watershed. It is apparent that the differences among the scenarios are identifiable soon after the spring (~ DOY=150) when soil is saturated with snow-melt water and when the sub-surface baseflow begins.

Soil C-pools, $C_{cd}, C_{ssd}, C_{smd}, C_{fmd}, C_{fsd}, C_m, C_s$ and C_m accumulate under the *NoFlow* scenario and tend to deplete under the *Implicit* scenario. This is because the soil moisture regime in the former case is hypo-optimal for R_h or pool decomposition, whereas it is hyper-optimal for the latter case. Only the passive soil organic C-pool (Cp) showed a different trend and was the least in the *NoFlow* scenario. This is theoretically plausible because Cp is a conceptual pool that represents the most recalcitrant form of soil C comprising of humus which is the last product of organic matter decomposition. Since in the *Implicit* scenario the C-cycling is intense, Cp accumulates as opposed to the *NoFlow* scenario. Soil organic C decomposition under saturated

conditions (anaerobic) is considerably lower than under aerobic conditions. In the absence of oxygen, oxidation of soil C to CO_2 is incomplete, and much of the C remains as an intermediate products of decomposition.

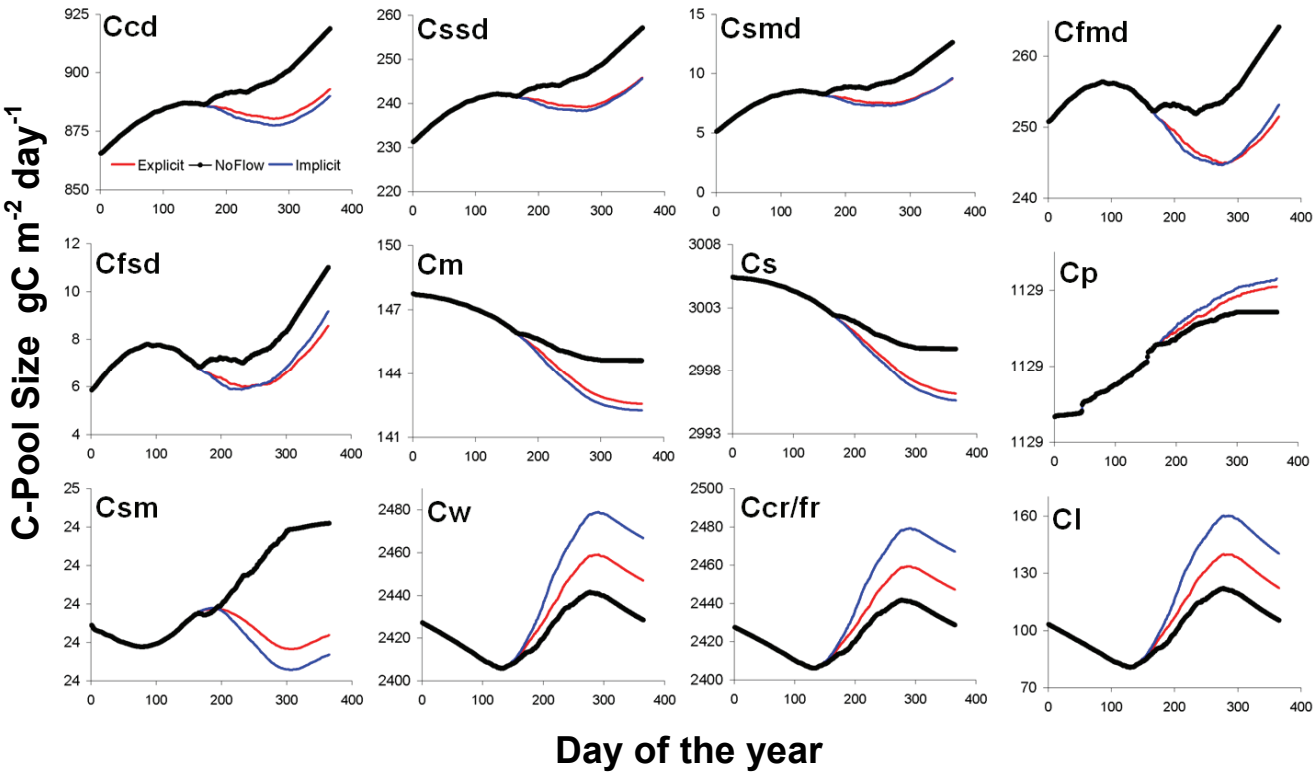

Figure 5-10. Temporal dynamics of various ecosystem C-pools under hydrological scenarios. The C-pools shown here are Woody biomass pool (C_w), Foliage biomass pool (C_l), Coarse root biomass pool (C_{cr}), Fine root biomass pool (C_{fr}), Coarse detritus pool (C_{cd}), Surface structural pool (C_{ssd}), Surface metabolic pool (C_{smd}), Surface microbial pool (C_{sm}), Soil structural litter pool (C_{fsd}),Soil metabolic pool (C_{fmd}), Soil microbial pool (C_m), Slow C pool(C_s), and Passive C pool(C_p)

Temporal dynamics of biomass C-pools (C_w, C_{cr}, C_{f_r} and C_l) among the different scenarios reveal that the *NoFlow* conditions result in lower biomass C-pools, and the *Implicit*

scenario results in higher biomass C-pools. The magnitude of the biomass C-pools and their variations under different scenarios looks similar because all of these C-pools are derived from NPP at a constant rate of biomass pool allocation. The seasonality of biomass allocation is not currently dynamic in BEPS-TerrainLab V2.0. The hydrological controls that directly affect the dynamics of biomass C-pools are: (1) change in stomatal conductance (2) variation in the autotrophic respiration, which is a function of the biomass C-pool itself and (3) N-mineralization.

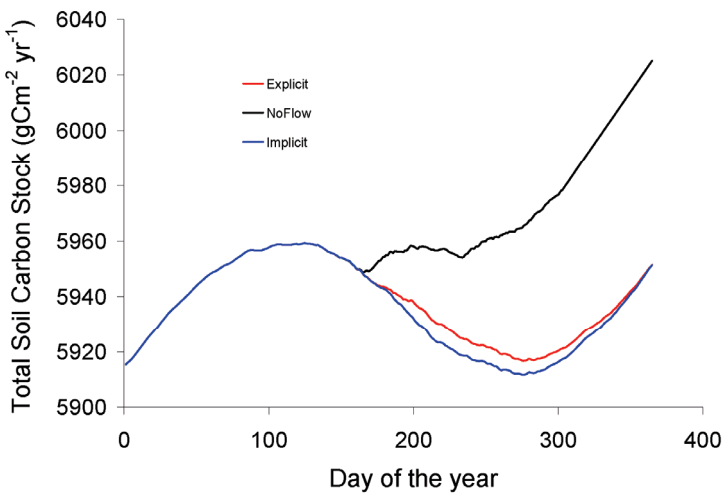

Figure 5-11. Temporal dynamics the total soil C-pools (sum of all the pools) under various hydrological scenarios.

Figure 5-11 demonstrates how the soil C-stocks (sum of all soil C-pools) build up in the *NoFlow* scenario. Under saturated conditions, these ecosystems behave similarly to temperate wetlands where the decomposition of soil organic matter is very limited. This behavior is consistent with the measurements made by Nakane et al. (1997), who reported the existence of twice as much soil C in places where the water table was shallow as opposed to places where the water table was deep (0.4m). However, under the *Implicit* scenario, the soil C-pools decompose

faster in the growing season, although sufficient replenishment of these C-pools occurs with increased photosynthesis and NPP.

5.8.6. Nutrient (N) Availability and Associated Feedback Mechanisms.

Nitrogen is required for plant growth because it is the primary constituent of important bio-molecules such as chlorophyll and enzymes. N-control on the C-cycle is represented in BEPS-Terrainlab V2.0 through leaf-N that affects the maximum carboxylation rate used in the photosynthesis model. Although a substantial amount of N is present in the soil organic matter, a majority of this is unavailable to plants. Since BEPS-Terrain Lab V2.0 simulates the seasonal patterns of individual soil C-pool in a comprehensive manner, it is also possible to simulate the dynamics of their C:N ratios (refer Appendix 2 for the equations).

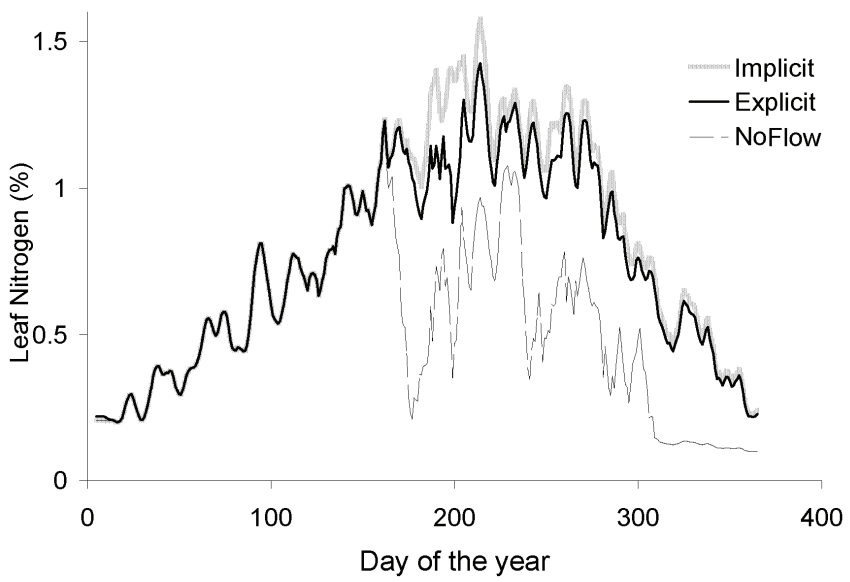

Figure 5-12. Temporal dynamics of leaf-N content under various hydrological scenarios. Note the pronounced N limitation under the *NoFlow* scenario which is primarily due to reduced soil C decomposition and N mineralization.

This facilitates the calculation of N-mineralization that occurs as a result of soil C-pool decomposition. Together with the N deposited from the atmosphere and biological N fixation, a part of the mineralized N is available to plants. This continuum of N cycling in the soil is strongly controlled by hydrological processes. Our results are consistent with the measurement studies conducted by Devito et al. (1999) who reported that annual rates of net N mineralization higher in forest soils of the deciduous and conifer-mixed stands than in peatland soils. The *Implicit* scenario mimics conditions that are seen in deciduous forests while the *NoFlow* scenario creates soil water regimes similar to a peatland.

Figure 5-12 shows the seasonal pattern of the leaf-N under various scenarios. Under all the scenarios, leaf-N remains minimal in the winter seasons, owing to weak decomposition of soil C-pools and N-availability. In the *NoFlow* scenario, the soil water balance is altered in such a way that the soil profile gets excessively saturated from the absence of topographically driven baseflow. Throughout the year, soil C-pools accumulate without decomposition, reducing N-mineralization. However, under the *Implicit* scenario, there is excessive of drainage even on flat locations and low lying areas of the landscape creating optimal conditions for N-mineralization and that directly affects the plant growth by increasing the maximum carboxylation rate, Vcmax, and thus overestimating the biomass. This increased biomass further increases soil organic matter and N mineralization, creating a positive feedback mechanism.

5.9. Summary and Conclusions

In order to understand better the strong coupling between water, C, and N cycles in terrestrial ecosystems in a spatially explicit manner, we developed a hydro-ecological model, BEPS-TerrainLab V2.0. We ran this model over a boreal landscape in North Central Quebec and compared the simulations with various measurements. Additionally, we conducted a modeling

experiment to understand better the hydrological influence on C and N cycling and the associated feedback mechanisms. From this study we draw the following conclusions.

1. The seasonal dynamics of modeled NEP and total ecosystem respiration at a daily time step agreed well with the eddy covariance measurements indicating that BEPS-TerrainLab V2.0 can capture these biogeochemical processes with reasonable accuracy and can be used further as a predictive tool.

2. The main factor governing the accuracy of the simulated NEP was the accuracy of the simulated GPP and respiration processes. While the former depends mainly on hydrologically-controlled stomatal dynamics and the leaf-N content, the latter was attributed to several factors that directly or indirectly depend on the soil water and temperature regimes in addition to the dynamics of various ecosystem C-pools.

3. The accuracy of heterotrophic respiration and N mineralization is thermally controlled. It is therefore essential to precisely model boreal edaphic thermal regimes in order to accurately map C-sources and sinks. This warrants the inclusion of snow dynamics and proper soil heat transfer schemes in models that simulate C-dynamics in boreal ecosystems.

4. In order to model comprehensively the soil C-dynamics in conjunction with other biogeochemical cycles, we believe that a proper initialization of current ecosystem C-pools is an essential requirement.

5. In general, hydrological simulations without the explicit consideration of sub-surface baseflow overestimate NEP. Generally, six types of NEP differences can be created due to simplified forms of hydrological representations. This occurs because of variations in ecophysiological and biogeochemical processes with the nature of the soil-water balance. The most common bias that could be created due to simplified hydrological representation is *an underestimation of the existing C-sources.*

6. Soil C-dynamics are significantly altered under simplified hydrological representations. Soil C-pools accumulate faster when the soil saturates due to decrease in respiration or deplete when soil moisture is maintained below field-capacity. This has significance in the N-availability, which indirectly affects primary production and C cycling.

In conclusion, we saw that hydrology plays a critical role in determining the spatio-temporal distribution of C-sources and sinks**.** Therefore, it is imperative to simulate realistic hydrological regimes within ecological models to accurately map spatio-temporal patterns of C-sources or sinks. Our results suggest that the lateral sub-surface flow does play a significant role in boreal C-distribution. Although the landscape we worked on is a humid boreal forest ecosystem where non-Hortinian run-off mechanisms predominate, we believe that even in drier ecosystems such differences can be observed if realistic hydrological representations are not implemented in ecosystem models.

5.10. Appendix 1

CN_x C:N ratio of pools x. e.g. CN_{cr} C:N ratio of coarse root biomass pool

Cx C content in pool x in gCm^{-2} . e.g. C_{cr} carbon content of coarse root biomass pool

F_m Partitioning fraction of leaf and fine-root litterfall into metabolic detritus C pool.

f Fraction of NPP allocated to a particular biomass pool

N_{dep} Net N déposition $gNm^{-2}day^{-1}$

N_{av} Available N $gNm^{-2}day^{-1}$

N_{fix} N fixation $gNm^{-2}day^{-1}$

$N_{\min}$ N mineralization $gNm^{-2}day^{-1}$

N_{up} N uptake by plants $gNm^{-2}day^{-1}$

N_{loss} N loss $gNm^{-2}day^{-1}$

N_l Actual leaf N content $gNm^{-2}day^{-1}$

Subscripts denoting various C pools.

a	C released to the atmosphere
cr	Coarse root biomass pool
fr	Fine root biomass pool
l	Leaf biomass pool
w	Wood biomass pool
cd	Coarse root and dead wood structural detritus pool
fd	Fine root structural detritus pool
md	Metabolic detritus pool
m	Microbial pool
p	Passive soil C pool
s	Slow soil C pool

5.10.1. Daily change in Ecosystem Carbon Pool

Using the soil C pool initialized using InTEC model for the year 2003, the daily dynamics of 2004 soil C pool is modeled using BEPS-TerrainLab V2.0 using an update mechanism as described earlier. The daily change in individual pool size is a function of decomposition rate manifested by hydrothermal controls and feedback relationships.

Daily change in woody biomass pool

$$\Delta C_{wi} = f_w.NPP_i - k_{w,cd}.C_{wi-1} \quad \text{(A1)}$$

Daily change in coarse root biomass pool

$$\Delta C_{cr\,i} = f_{cr}.NPP_i - k_{cr,cd}C_{cr\,i-1} \tag{A2}$$

Daily change in foliar biomass pool

$$\Delta C_{l\,i} = f_l.NPP_i - k_{l,sl}.C_{l\,i-1} \tag{A3}$$

Daily change in fine root biomass pool

$$\Delta C_{fr\,i} = f_{fr}.NPP_i - k_{fr,fl}.C_{fr\,i-1} \tag{A4}$$

Daily change in coarse detritus from woody and coarse root pool

$$\Delta C_{cd\,i} = \left[\frac{(k_{w,cd}.C_{w\,i-1} + k_{cr,cd}.C_{cr\,i-1})}{(1+(k_{cd,a}+k_{cd,m}+k_{cd,s}))} - \left[C_{cd\,i-1}.(k_{cd,a}+k_{cd,m}+k_{cd,s})\right]\right] \tag{A5}$$

Daily change in surface structural pool

$$\Delta C_{ssd\,i} = \left[\frac{(1-F_{m\,i}).k_{l,sl}.C_{l\,i-1}}{(1+(k_{ssd,a}+k_{ssd,sm}+k_{ssd,s}))} - \left(C_{ssd\,i-1}.(k_{ssd,a}+k_{ssd,sm}+k_{ssd,s})\right)\right] \tag{A6}$$

Daily change in surface metabolic pool

$$\Delta C_{smd\,i} = \left[\frac{F_{m\,i}.k_{l,sl}.C_{l\,i-1}}{1+(k_{smd,a}+k_{smd,sm})} - \left(C_{smd\,i-1}.(k_{smd,a}+k_{smd,sm})\right)\right] \tag{A7}$$

Daily change in soil structural Litter pool

$$\Delta C_{fsd\,i} = \left[\frac{(1-F_{m\,i}).k_{fr,fl}.C_{fr\,i-1}}{1+(k_{fsd,a}+k_{fsd,m}+k_{fsd,s})} - \left(C_{fsd\,i-1}.(k_{fsd,a}+k_{fsd,m}+k_{fsd,s})\right)\right] \tag{A8}$$

Daily change in soil metabolic pool

$$\Delta C_{fmd\,i} = \left[\frac{F_{m\,i}.k_{fr,fl}.C_{fr\,i-1}}{1+(k_{fmd,a}+k_{fmd,m})} - \left(C_{fmd\,i-1}.(k_{fmd,a}+k_{fmd,m})\right)\right] \tag{A9}$$

Daily change in surface microbial pool

$$\Delta C_{sm\,i} = \left(C_{ssd\,i}.k_{ssd,sm} + C_{smd\,i}.k_{smd,sm}\right) - \left(C_{sm\,i-1}.\left(k_{sm,a}+k_{sm,s}\right)\right) \tag{A10}$$

Daily change in soil microbial pool

$$\Delta C_{mi} = \left[(k_{fsd,m}.C_{fsd_i} + k_{fmd,m}.C_{fmd_i} + C_{cd\,i}.k_{cd,m}) + (C_{s\,i-1}.k_{s,m} + C_{p_{i-1}}.k_{p,m})\right] - \left[C_{m\,i-1}.(k_{m,a} + k_{m,s} + k_{m,p})\right] \quad \text{(A11)}$$

Daily change in slow C pool

$$\Delta C_{s\,i} = \left[\left(C_{m\,i}.k_{m,s} + C_{cd\,i}.k_{cd,s} + C_{fsdi}.k_{fsd,s}\right) + \left(C_{sm\,i}.k_{sm,s} + C_{ssd\,i}.k_{ssd,s}\right)\right] - \left[C_{s\,i-1}.\left(k_{s,a} + k_{s,p} + k_{s,m}\right)\right] \quad \text{(A12)}$$

Daily change in passive C pool

$$\Delta C_{p\,i} = (k_{m,p}.C_{m\,i} + k_{s,p}.C_{s\,i}) - (k_{p,m}.C_{p\,i-1} + k_{p,a}.C_{p\,i-1}) \quad \text{(A13)}$$

5.11. Appendix 2

5.11.1. Soil Nitrogen Dynamics

N mineralization is simulated based on the decomposition of soil C pools. In the process of soil C pool decomposition, amount of N mineralized depends on the C:N ratio of individual pools. Although we assume a constant C:N ratio for surface and soil microbial C pool at 12 because they are living beings, the dynamics of C:N ratio of C contained in non living materials is however, quite variable. They are calculated as follows:

Dynamics of Foliar biomass pool C N ratio

$$CN_{l\,i} = \frac{\left[(1-K_l).C_{l\,i-1} + f_l.NPP_{i-1}\right]}{\left[\left(\frac{(1-K_l).C_{l\,i-1}}{CN_{l\,i-1}}\right) + \left(\frac{f_l}{CN_{l\,i-1}}\right) \times \left(\frac{N_{up\,i}}{\left[\frac{f_l}{CN_{l\,i-1}}\right] + \left[\frac{f_{fr}}{CN_{fr\,i-1}}\right] + \left[\frac{f_w + f_{cr}}{CN_{w\,i-1}}\right]}\right)\right]} \quad \text{(A14)}$$

Dynamics of Fine root biomass pool C N ratio

$$CN_{fr\,i} = \frac{\left[\left(1-k_{fr}\right).C_{fr\,i-1} + f_{fr}.NPP_{i-1}\right]}{\left[\left(\frac{\left(1-k_{fr}\right).C_{fr\,i-1}}{CNfr_{i-1}}\right) + \left(\frac{f_{fr}}{CNfr_{i-1}}\right) \times \left(\frac{N_{up\,i}}{\left[\frac{f_l}{CN_{l\,i-1}}\right] + \left[\frac{f_{fr}}{CN_{fr\,i-1}}\right] + \left[\frac{f_w + f_{cr}}{CN_{w\,i-1}}\right]}\right)\right]} \tag{A15}$$

Dynamics of wood biomass pool C N ratio

$$CN_{w\,i} = \frac{\left[C_{w\,i-1} + C_{cr\,i-1} + \left(f_w + f_{cr}\right).NPP_{i-1}\right]}{\left[\left(\frac{C_{w\,i-1} + C_{cr\,i-1}}{CNw_{i-1}}\right) + \left(\frac{f_w + f_{cr}}{CNw_{i-1}}\right) \times \left(\frac{N_{up\,i}}{\left[\frac{f_l}{CN_{l\,i-1}}\right] + \left[\frac{f_{fr}}{CN_{fr\,i-1}}\right] + \left[\frac{f_w + f_{cr}}{CN_{w\,i-1}}\right]}\right)\right]} \tag{A16}$$

Dynamics of coarse detritus pool C N ratio

$$CN_{cd\,i} = \frac{C_{cd\,i}}{\left[\left(\frac{C_{cd\,i-1}}{CN_{cd\,i-1}}\right) + \left(\frac{k_{w,cd}.C_{w\,i} + k_{cr,cd}.C_{cr\,i}}{CN_{w\,i}}\right) - \left(\frac{C_{cd\,i-1}\left(k_{cd,m} + k_{cd,s} + k_{cd,a}\right)}{CN_{cd\,i-1}}\right)\right]} \tag{A17}$$

Dynamics of surface structural pool C N ratio

$$CN_{ssd\,i} = \frac{C_{ssd\,i}}{\left[\left(\frac{C_{ssd\,i-1}}{CN_{ssd\,i-1}}\right) + \left(\frac{k_l.C_{l\,i}\left(1-F_{m\,i}\right)}{CN_{l\,i}}\right) - \left(\frac{C_{ssd\,i-1}\left(k_{ssd,sm} + k_{ssd,s} + k_{ssd,a}\right)}{CN_{ssd\,i-1}}\right)\right]} \tag{A18}$$

Dynamics of surface metabolic pool C N ratio

$$CN_{smd\,i} = \frac{C_{smd\,i}}{\left[\left(\frac{C_{smd\,i-1}}{CN_{smd\,i-1}}\right) + \left(\frac{k_l.C_{l\,i}.F_{m\,i}}{CN_{l\,i}}\right) - \left(\frac{C_{smd\,i-1}\left(k_{smd,sm} + k_{smd,a}\right)}{CN_{smd\,i-1}}\right)\right]} \tag{A19}$$

Dynamics of soil structural litter pool C N ratio

$$CN_{fsd\,i} = \frac{C_{fsd\,i}}{\left[\left(\frac{C_{fsd\,i-1}}{CN_{fsd\,i-1}}\right) + \left(\frac{k_{fr}.C_{fr\,i}.(1-F_{m\,i})}{CN_{fr\,i}}\right) - \left(\frac{C_{fsd\,i-1}\left(k_{fsd,m} + k_{fsd,s} + k_{fsd,a}\right)}{CN_{fsd\,i-1}}\right)\right]} \tag{A20}$$

Dynamics of soil metabolic pool C N ratio

$$CN_{fmd\,i} = \frac{C_{fmd\,i}}{\left[\left(\frac{C_{fmd\,i-1}}{CN_{fmd\,i-1}}\right) + \left(\frac{k_{fr}.C_{fr\,i}.F_{m\,i}}{CN_{fr\,i}}\right) - \left(\frac{C_{fmd\,i-1}\left(k_{fmd,m} + k_{fmd,a}\right)}{CN_{fmd\,i-1}}\right)\right]} \tag{A21}$$

Dynamics of soil slow organic pool C N ratio

$$CN_{s\,i} = \frac{C_{s\,i}}{\left[\begin{array}{l}\left(\frac{C_{s\,i-1}}{CN_{s\,i-1}}\right) + \left(\frac{k_{ssd_s}.C_{ssd\,i-1}}{CN_{ssd\,i}}\right) + \left(\frac{k_{fsd_s}.C_{fsd\,i-1}}{CN_{fsd\,i}}\right) + \left(\frac{k_{cd,s}.C_{cd\,i-1}}{CN_{cd\,i}}\right) + \left(\frac{k_{m,s}.C_{m\,i-1}}{CN_{m\,i}}\right) \\ + \left(\frac{k_{sm,s}.C_{sm\,i-1}}{CN_{sm\,i}}\right) + \left(\frac{C_{s\,i-1}.\left(k_{s,m} + k_{s,p} + k_{s,a}\right)}{CN_{s\,i-1}}\right)\end{array}\right]} \tag{A22}$$

Dynamics of passive soil C pool C N ratio

$$CN_{p\,i} = \frac{C_{p\,i}}{\left[\left(\frac{C_{p\,i-1}}{CN_{p\,i-1}}\right) + \left(\frac{k_{s,p}.C_{s\,i-1}}{CN_{s\,i-1}}\right) + \left(\frac{k_{m,p}.C_{m\,i-1}}{12.0}\right) - \left(\frac{Cpi-1.\left(k_{p,m} + k_{p,a}\right)}{CN_{p\,i-1}}\right)\right]} \tag{A23}$$

$F_{m\,i}$ is the partitioning fraction of leaf and fine-root pools to metabolic C pool

$$F_{m\,i} = 0.85 - 0.6 \times 0.018 \times \left(CN_{l\,i} + CN_{fr\,i}\right) \tag{A24}$$

Consequent of the dynamics of the C:N ratios, the N mineralization is calculated as follows.

$$
\begin{aligned}
N_{\min i} = & \left[\frac{\left(k_{cd,a} + k_{cd,m} + k_{cd,s}\right).C_{cd_i}}{CN_{cd_i}}\right] + \left[\frac{\left(k_{ssd,sm} + k_{ssd,s} + k_{ssd,a}\right).C_{ssd\,i}}{CN_{ssd\,i}}\right] \\
& + \left[\frac{\left(k_{smd,sm} + k_{smd,a}\right).C_{smd\,i}}{CN_{smd\,i}}\right] + \left[\frac{\left(k_{fsd,m} + k_{fsd,s} + k_{fsd,a}\right).C_{fsd\,i}}{CN_{fsd\,i}}\right] \\
& + \left[\frac{\left(k_{fmd,m} + k_{fmd,a}\right).C_{fmd\,i}}{CN_{fmd\,i}}\right] + \left[\frac{\left(k_{sm,s} + K_{sm,a}\right).C_{sm\,i}}{CN_{sm\,i}}\right] \\
& + \left[\frac{\left(k_{m,s} + k_{m,p} + k_{m,a}\right).C_{m\,i}}{CN_{m\,i}}\right] + \left[\frac{\left(k_{s,m} + k_{s,p} + k_{s,a}\right).C_{s\,i}}{CN_{s\,i}}\right] \\
& + \left[\frac{\left(k_{p,m} + k_{p,s} + k_{p,a}\right).C_{p\,i}}{CN_{p\,i}}\right] \\
& - \left[\frac{\left(k_{sd,sm}.C_{ssd\,i}\right) + \left(k_{smd,sm}.C_{smd,sm\,i}\right)}{CN_{sm\,i}}\right] - \left[\frac{\left(k_{s,p}.C_{s\,i}\right) + \left(k_{m,p}.C_{m\,i}\right)}{CN_{p\,i}}\right] \\
& - \left[\frac{\left(k_{fsd,m}.C_{fsd\,i}\right) + \left(k_{fmd,s}.C_{fmd\,i}\right) + \left(k_{cd,m}.C_{cd\,i}\right) + \left(k_{s,m}.C_{s\,i}\right) + \left(k_{p,m}.C_{p\,i}\right)}{CN_{m\,i}}\right] \\
& - \left[\frac{\left(k_{fsd,s}.C_{fsd\,i}\right) + \left(k_{fmd,s}.C_{fmd\,i}\right) + \left(k_{cd,s}.C_{cd\,i}\right) + \left(k_{m,s}.C_{m\,i}\right) + \left(k_{p,s}.C_{p\,i}\right)}{CN_{s\,i}}\right]
\end{aligned}
\tag{A25}
$$

References

Bergeron, O., Margolis, H.A., Black, T.A., Coursolle, C., Dunn, A.L., Barr, A.G., and Wofsy, S.C.(2007). Comparison of Carbon Dioxide Fluxes Over Three Boreal Black Spruce Forests in Canada, *Global Change Biology* **13**, 89-107.

Black, T.A., Gaumont-Guay, D., Jassal, R.S., Amiro, B.D., Jarvis, P.G., Gower, S.T., Kelliher,F.M., Dunn, A., Wofsy, S.C. (2005). Measurement of CO2 exchange between boreal forest and the atmosphere. In: Griffiths, H., Jarvis, P.J. (Eds.), The Carbon Balance of Forest Biomes. Taylor and Francis Group, New York, NY, pp. 151-186.

Chen, J.M., Ju, W.M., Cihlar, J., Price, D., Liu, J., Chen, W.J., Pan, J.J., Black, A., and Barr, A.(2003). Spatial Distribution of Carbon Sources and Sinks in Canada's Forests, *Tellus Series B-Chemical and Physical Meteorology* **55**, 622-641.

Chen, J.M., Liu, J., Cihlar, J., and Goulden, M.L.(1999). Daily Canopy Photosynthesis Model Through Temporal and Spatial Scaling for Remote Sensing Applications, *Ecological Modelling* **124**, 99-119.

Chen, W.J., Chen, J., and Cihlar, J.(2000a). An Integrated Terrestrial Ecosystem Carbon-Budget Model Based on Changes in Disturbance, Climate, and Atmospheric Chemistry, *Ecological Modelling* **135**, 55-79.

Cox, P.M., Betts, R.A., Jones, C.D., Spall, S.A., and Totterdell, I.J.(2000). Acceleration of Global Warming Due to Carbon-Cycle Feedbacks in a Coupled Climate Model (Vol 408, Pg 184, 2000), *Nature* **408**, 750.

Devito, K.J., Westbrook, C.J., and Schiff, S.L.(1999). Nitrogen Mineralization and Nitrification in Upland and Peatland Forest Soils in Two Canadian Shield Catchments, *Canadian Journal of Forest Research-Revue Canadienne De Recherche Forestiere* **29**, 1793-1804.

Environment Canada . Canadian Climate Normals or Averages 1971-2000. 2006. 2007-05-15.

Giasson, M.A., Coursolle, C., and Margolis, H.A.(2006). Ecosystem-Level Co2 Fluxes From a Boreal Cutover in Eastern Canada Before and After Scarification, *Agricultural and Forest Meteorology* **140**, 23-40.

Govind, A., Chen, J.M., Margolis, H., Ju, W., Sonnentag, O., and Giasson, M.(2008a). A Spatially Explicit Hydro-Ecological Modeling Framework (BEPS-TerrainLab V2.0) Part 1: Model Description and Test in a Boreal Ecosystem in Eastern North America., *Journal of Hydrology*. Submitted

Govind, A., Chen, J.M., Ju, W., and Sonnentag, O.(2008b). A Spatially Explicit Hydro-ecological Modeling Framework (BEPS-TerrainLab V2.0) Part 2: Effect of Lateral Hydrological Processes on Photosynthesis and Evapotranspiration., *Journal of Hydrology*. Submitted

Govind, A., Chen, J.M., Bernier, P.Y., Guindon, L., Margolis, H., and Beaudoin, A. (2008c). Reconstructing the Carbon Balance of a Boreal Ecosystem under Climate Change, CO2

Fertilization, Nitrogen Deposition and Disturbance Effects. *Geoderma*. Submitted.

Grant, R.F.(2004). Modeling Topographic Effects on Net Ecosystem Productivity of Boreal Black Spruce Forests, *Tree Physiology* **24**, 1-18.

Ju, W.M. and Chen, J.M.(2005). Distribution of Soil Carbon Stocks in Canada's Forests and Wetlands Simulated Based on Drainage Class, Topography and Remotely Sensed Vegetation Parameters, *Hydrological Processes* **19**, 77-94.

Ju, W.M., Chen, J.M., Black, T.A., Barr, A.G., Liu, J., and Chen., B.Z.(2006). Modelling Multi-Year Coupled Carbon and Water Fluxes in a Boreal Apen Forest , *Agricultural and Forest Meteorology* **140**,136-151.

Ju, W.M., Chen, J.M., Harvey, D., and Wang, S. Future carbon balance of China's forests under climate change and increasing CO2: Carbon Sequestration In China's Forest Ecosystems. Journal of Environmental Management 85[3], 538-562. 2007.

Kljun, N., Calanca, P., Rotachhi, M.W., and Schmid, H.P.(2004). A Simple Parameterisation for Flux Footprint Predictions, *Boundary-Layer Meteorology* **112**, 503-523.

Lavigne, M.B., Ryan, M.G., Anderson, D.E., Baldocchi, D.D., Crill, P.M., Fitzjarrald, D.R., Goulden, M.L., Gower, S.T., Massheder, J.M., Mccaughey, J.H., Rayment, M., and Striegl, R.G.(1997). Comparing Nocturnal Eddy Covariance Measurements to Estimates of Ecosystem Respiration Made by Scaling Chamber Measurements at Six Coniferous Boreal Sites, *Journal of Geophysical Research-Atmospheres* **102**, 28977-28985.

Liu, J., Chen, J.M., Cihlar, J., and Chen, W.(1999). Net Primary Productivity Distribution in the Boreas Region From a Process Model Using Satellite and Surface Data, *Journal of Geophysical Research-Atmospheres* **104**, 27735-27754.

Nakane, K., Kohno, T., Horikoshi, T., and Nakatsubo, T.(1997). Soil Carbon Cycling at a Black Spruce (Picea Mariana) Forest Stand in Saskatchewan, Canada, *Journal of Geophysical Research-Atmospheres* **102**, 28785-28793.

Parton, W.J., Scurlock, J.M.O., Ojima, D.S., Gilmanov, T.G., Scholes, R.J., Schimel, D.S., Kirchner, T., Menaut, J.C., Seastedt, T., Moya, E.G., Kamnalrut, A., and Kinyamario, J.I.(1993). Observations and Modeling of Biomass and Soil Organic-Matter Dynamics for the Grassland Biome Worldwide, *Global Biogeochemical Cycles* **7**, 785-809.

Porporato, A., D'odorico, P., Laio, F., and Rodriguez-Iturbe, I.(2003). Hydrologic Controls on Soil Carbon and Nitrogen Cycles. I. Modeling Scheme, *Advances in Water Resources* **26**, 45-58.

Thompson, M.V., Randerson, J.T., Malmstrom, C.M., and Field, C.B.(1996). Change in Net Primary Production and Heterotrophic Respiration: How Much Is Necessary to Sustain the Terrestrial Carbon Sink?, *Global Biogeochemical Cycles* **10**, 711-726.

CHAPTER 6.

Summary and Conclusions

Currently there is much speculation surrounding the global carbon (C) balance, with considerable uncertainty associated with the terrestrial C cycling processes. Under the conditions of a rapidly changing climate, we need to understand better the magnitude of terrestrial C and its inter-annual variability. The dynamics of the terrestrial C-cycle depend on a number of environmental factors and have strong links to other biogeochemical or biogeophysical cycles, especially the hydrological cycle. Hence, a systems approach is required to understand precisely the C-cycle as it is affected by hydrological controls directly or indirectly, along with the associated feedback mechanisms.

For this research project, a modeling approach was used to investigate the links between C-cycling and hydrological processes. A process-based, spatially-distributed, hydro-ecological model, BEPS-TerrainLab V2.0 was further developed modifying a previously existing hydro-ecological model, BEPS-TerrainLab V1.0 (Chen et al., 2005, Chen et al., 2007). Several processes and modifications were added to the model which resulted in a stronger coupling of hydrological, biogeochemical, and eco-physiological processes. This model was tested with different high-frequency and high-precision measurements of carbon, water fluxes and various other parameters for two years. The comparisons revealed that the model can simulate various ecophysiological, hydrological and biogeochemical processes adequately. Further, BEPS-TerrainLab V2.0 was used as a tool to investigate the links between meso-scale hydrology, biogeochemistry, and eco-physiology.

6.1. Lessons Learned from this Research.

Boreal forests are unique in terms of hydrology, C-cycling and biogeochemical processes. In an attempt to model the coupled hydrological and C-cycling processes in a humid boreal ecosystem in eastern Canada, several facets were revealed and further challenges were identified. They are briefed below.

6.1.1. Understanding the Hydro-ecology of Humid Boreal Forests using BEPS-TerrainLab V2.0

Forest floors in boreal ecosystems are predominately covered by a moss-peat layer. Lateral water fluxes take preferential pathways through this highly permeable layer that comprise of both living and non-living parts. Realizing the importance of moss in boreal hydrological processes, a simple parameterization scheme was developed based on laboratory measurements of moss/peat hydraulic properties. This parameterization adequately simulated the baseflow fluxes which when tested against two other hydrological parameterizations appeared to provide better ecophysiological and biogeochemical estimates indicating that hydrological processes should be incorporated in C cycle models. More laboratory studies on moss/peat hydraulic properties are hence necessary for effective hydro-ecological modeling in boreal ecosystems.

Upscaling leaf-level ecophysiological processes to canopy scales by simultaneously considering fractions of LAI that correspond to different moisture and light regimes when used as weighting factors seemed to perform well and is a novel spatial upscaling approach. This quasi-physiological strategy could upscale the plant physiological process in a manner more effective than that of its predecessors. More detailed plant physiological upscaling strategies could be developed in similar lines by following a nested approach with fractions of LAI and their respective stomatal conductance as the basic idea.

This study showed that explicit modeling of aerodynamic resistance for each canopy layer (over-story, under-story, and moss/soil surface) can improve the simulation of ET at watershed scale. The magnitudes of the simulated ET play a great role in determining the local water balance and, therefore, C cycling in boreal ecosystems where the canopy is more open.

In humid boreal ecosystems such as eastern Canada, topographically-driven sub-surface baseflow is the main mechanism of ground water redistribution, which was almost 63-65% of the infiltrated soil water. Surface overland flow was rare because of the high infiltration capacity of boreal soil surfaces. Only under conditions of soil saturation or ground water ridging did surface overland flow occur. Hence it is concluded that proper accounting of sub-surface baseflow is critical to improve our understanding of how hydro-ecological connectivity is established at local scales. It was observed that the accuracy of DEM is the most critical factor for reliable baseflow simulations, which in turn determine the accuracy of the simulated hydrological processes.

6.1.2. Effect of Sub-surface Baseflow on Ecophysiological Processes

A numerical experiment was conducted to assess the importance of landscape scale lateral hydrological processes on local scale C-cycling using three modeling scenarios that primarily differed in the way lateral sub-surface baseflow was conceptualized. The results of the experiment showed that large differences were created in the simulated GPP under unrealistic hydrological representations. The spatial distributions of these biases depend on the type of scenario and the nature of the local water balance within each modeling unit. It was observed that if we neglect sub-surface baseflow (e.g., no lateral flow is allowed until the soil profile is saturated), GPP was underestimated on hill slopes as opposed to flat areas in comparison to realistic simulations. On the other hand, an implicit methodology having no topographic control overestimates GPP in flat regions and depressions in comparison to realistic simulations. The dynamics of ET are quite different from those of GPP under different hydrological

representations. In general, ET is both positively and negatively biased under unrealistic hydrological representations. This is because of the presence of sub-component processes that behave differently under various soil moisture conditions. The primary reasons for these biases (GPP and ET) were attributed to variations in stomatal conductance, N availability, and differences in the upscaling mechanism which is conceptualized as a function of the root zone water contents that affect the physiological status of leaves.

In order to ascertain the relative error contribution of various model parameters towards GPP and ET vis-à-vis the errors caused by hydrological misrepresentation, a sensitivity analysis was conducted using 14 parameters that are common to both ET and GPP calculation. This analysis revealed that the most sensitive parameters that affects the magnitudes of the simulated GPP and ET were LAI, clumping index, $g_{s\max}$, $g_{cuticle}$, ratio of overstory to understory $g_{s\max}$, soil porosity, saturated hydraulic conductivity, and K_s, in the order of precedence. Although this sensitivity analysis highlights the importance of accurate parameter values, since the magnitude of the errors in GPP or ET created due to parameter values was lower than what hydrological misrepresentation would produce, the importance of hydrology in C-cycle modeling is further reinforced.

6.1.3. Long-term Dynamics of C-cycling Processes

In order to test the ability of BEPS-Terrainlab V2.0 to simulate biogeochemical processes, explicit C or N cycles were incorporated within BEPS-TerrainLab V2.0. The biogeochemical module facilitated the simulation of the dynamics of various C and N-pools between the vegetation and the soil facilitating a comprehensive representation of processes such as heterotrophic respiration and N mineralization which paved the way for realistic calculations of NEP (C-source or sink) at a daily time step. Before simulating various biogeochemical processes,

much effort was put to comprehensively spin-up the current magnitudes of various ecosystem C-pool sizes and their CN ratios. This was achieved by reconstructing historical ecosystem C-balances using the InTEC model under a climate change, CO_2 change, N-deposition, and various disturbance events that occurred on this landscape in the recent past. These spun-up C-pools were validated with inventory plot measurements of above-ground biomass C-pools and soil C-pools, in addition to plant area index as an indicator of the amount of above ground biomass. The comparison showed that using InTEC model, about 80% in the variability of the current distribution of various C-pools could be achieved and that the C-pools estimated in this manner were adequate for further biogeochemical modeling at daily time steps by BEPS-TerrainLab V2.0.

6.1.4. Effect of Sub-surface Baseflow on Biogeochemical Processes

The seasonal dynamics of NEP and total respiration simulated by BEPS-TerrainLab V2.0 were comparable to the eddy covariance measurements, demonstrating that the model was capable of simulating these ecological processes with reasonable accuracy and can be further used as a predictive tool. The study showed that the main factors governing the accuracy of the simulated NEP were the accuracy of the simulated GPP and ecosystem respiration. While the former depended mainly on hydrologically-controlled stomatal dynamics and the leaf N-content that modify the ambient photosynthesis rate, the accuracy of the latter process was attributed to several factors that directly or indirectly depend on the soil hydrothermal conditions that determines the dynamics of various ecosystem C pools and its decomposition. The accuracy of heterotrophic respiration and N-mineralization is thermally controlled. Therefore, it is essential to accurately model boreal soil thermal regimes in order to simulate its biogeochemical processes. This necessitates explicit modeling of snow dynamics and the consequential soil heat flow in order to capture the boreal winter biogeochemical processes. Winter biogeochemical processes have a great influence on the annual magnitudes of ecosystem C fluxes.

Further investigation was conducted using the same numerical experiment mentioned above to explore the effect of sub-surface baseflow on C-sources and sinks (NEP). It was concluded that unrealistic hydrological representations overestimate NEP. However, the reasons for the overestimations were different under the various scenarios. Six types of biases were identified in the simulated NEP as a result of hydrological misrepresentation. These biases occur because of differences in the proportion of photosynthesis, respiration, and the associated feedback mechanisms. The most common type of NEP bias created due to unrealistic hydrological representation was *an underestimation of the existing C-sources*. This is a significant finding because it throws light on the fact that that our current bottom-up modeling endeavors that do not include explicit hydrological processes could underestimate the sizes of C sources on the Earth's surface. Soil C-dynamics is significantly altered under unrealistic hydrological scenarios. It was found out that generally, soil C-pools accumulate if we neglect sub-surface baseflow and deplete under implicit formulations of sub-surface baseflow. The dynamics of soil C-pools have great significance on the N-availability that indirectly affects primary production.

From these results it can be concluded that hydrology plays a critical role in determining the spatio-temporal distribution of C sources and sinks**.** Therefore, it is imperative to simulate realistic hydrological regimes within ecological models to realistically simulate spatio-temporal patterns of C sources or sinks. Results of this study suggest that topographically-driven, lateral water flow and its consequent alteration of soil water balance do play a significant role in the terrestrial C distribution. Therefore, it is appropriate to conclude that regional or global scale terrestrial C-estimates could have significant errors if proper hydrological constraints from the large topographic variation on the Earth's surface are not considered in the modeling of ecological processes.

6.2. Uncertainties in the Simulated Results

Although the current modeling exercise was carried out using a systems approach and simulations were validated using high-precision continuous measurements, there could still be room for uncertainties associated with this study. The source of uncertainties can be attributed to several factors. These are detailed below.

6.2.1. Parameters and Coefficients used in BEPS-TerrainLab V2.0 and InTEC.

In almost all existing simulation models, various coefficients are used to parameterize natural processes. Even if these coefficients are applied in a spatially distributed manner as a function of plant functional type or soil texture, it may not be a true representation of the reality. Parameter values were mostly obtained from the literature that are either based on laboratory or field measurements or based on other modeling studies. Considering the large size of the modeling unit (625 m^2), within which much heterogeneity can exist, it is still somewhat uncertain to use field-measured parameters for meso-scale calculations. It is plausible that these parameter values could vary for different situations and can create uncertainty in the simulations. This warrants the need for parameter estimation and rigorous sensitivity analysis using various techniques (Wang et al., 2001; Peddle et al., 2004). Such an exercise will help to identify the most sensitive parameter that needs to be accurately parameterized. There are various parameter estimation techniques, such as data assimilation using ensemble Kalman filters (Jones et al., 2004; Williams et al., 2005) to estimate the optimal parameter values. In an ideal modeling context, one should do such an analysis prior to running the model over an ecosystem.

6.2.2. Quality of Input Datasets Used in BEPS-TerrainLab V2.0 and InTEC.

There could be some errors associated with spatial inputs that are used for running BEPS-TerrainLab V2.0. These datasets originate from several sources and have different spatial resolutions. Therefore, they were resampled with a common spatial resolution before using them

as inputs. This resampling procedure is likely to cause some form of abstraction of the original information. In this study, much effort was devoted to minimizing such errors. For example, with land cover as a qualitative spatial data, resampling a land cover map is likely to create many errors. This was the motivation for choosing to resample all other datasets at the spatial resolution of the land cover map. Additionally, DEM is a critical spatial input that determines the accuracy of lateral hydrological processes. Although this study utilized a hydrologically consistent DEM, the spatial interpolation algorithms that are used to create DEMs using ground control points and could include some minor inconsistencies with reality. This error could have some effect on the simulated C-cycling process. Moreover, the ground control points used for the creation of DEM are usually collected using indirect methods, where some errors are also plausible.

6.2.3. Quality of Long-term Meteorological Records Used in InTEC.

This research work utilized long-term meteorological records to simulate the historical trends in the ecosystem C-balance. However, it is plausible that there could be minor errors associated with these meteorological datasets that might slightly affect the reconstructed C balance. Even for daily simulations, errors in meteorological data is plausible when it is temporally upscaled (half hourly to daily), due to issues such as missing values. A study by Matsushita et al. (2004) using a sophisticated sensitivity analysis technique called the Extension of Fourier Amplitude Sensitivity Test (EFAST) using the BEPS model demonstrated that the required accuracy for daily maximum temperature is ±2.9^{o}C, for daily minimum temperature is ±2.0^{o}C, for daily global solar radiation its is ±2.5 MJ m^{-2} day^{-1}, and for daily specific humidity it is ±3.4 g kg^{-1} in order to estimate NPP with an overall confidence coefficient of 95%.

6.2.4. Quasi-empiricism Existing in Process Models.

None of the currently existing process models are purely physical in nature. There are many instances where empirical approaches are employed to describe biophysical processes. This is because these processes are either not well studied by field or laboratory measurements or they are too highly complex in nature for us to comprehend them mathematically. Some of the empirical formulations currently existing in BEPS-Terrainlab V2.0 are similar to other process models. They are given below.

2. Pedo-transfer function that is used to calculate unsaturated hydraulic conductivity from saturated hydraulic conductivity.
3. Interception of precipitation by canopy using an interception coefficient
4. Calculation of Vcmax using temperature and nitrogen scalars.
5. Soil surface conductance as a function of soil water content
6. Moss surface conductance.

The empirical description of these processes leads to site-specific nature and warrants calibration of the model before actual use to reduce uncertainties in simulations.

6.3. Current Modeling Gaps or Topics for Future Research

There are several opportunities to further improve our understanding of how the terrestrial C-cycle, hydrology, and other biogeochemical cycles interact. These are the topics that can be incorporated in future bottom-up modeling endeavors or improving the present model. These topics are briefly described below.

6.3.1. Simulation of other Forms of Hydrologically Controlled C-Fluxes.

In the current model set up, the C-balance in forest ecosystems assumes that there is no C-flux associated with dissolved organic C (DOC) or methane emission. However, in reality, DOC is

transported along with lateral flow of water (Schiff et al., 1997; Shibata et al., 2003). From the current research, it was seen that 65% of the soil water is fractionated as sub-surface baseflow. It is plausible that the assumption of negligible DOC or other mechanisms of C-flux such as methane emission (Miyata et al., 2000; Zhuang et al., 2004) may not be valid. It is necessary to create new conceptualizations to represent these forms of C-fluxes in boreal ecosystems. With the spatially-explicit biogeochemical module that exists closely with the distributed hydrological processes within BEPS-Terrainlab V2.0, it is not difficult to simulate these types of C fluxes in the future.

6.3.2. Multilayer Soil Water Scheme Replacing the Two Layered Approach

Although BEPS-TerrainLab V2.0 has five conceptual soil layers for heat flow, only two conceptual soil layers currently exist with respect to soil water movement, i.e., saturated and unsaturated zones. Although this assumption is adequate for boreal shield applications where the water table is shallow, in order to use this model in places that have deep ground water (e.g. arid and semi-arid regions), we need to improve representations of the unsaturated zone hydrological processes by incorporating multi-layered unsaturated soil. This conceptualization of soil layers for soil moisture can be considered in conjunction with soil heat flow for explicitly calculating hydrothermal regimes. Hydrogeological approaches should be adopted to model ground water fluxes in places were complex sub-surface geology exists.

6.3.3. Root Water Uptake Schemes

In order to better represent plant water relations, it will be more realistic to have a multi-layered soil that conceptually has roots having mechanistic or quasi-mechanistic soil water uptake scheme constraining the dynamics of leaf water potential and stomatal conductance. Multi-layer soil having an explicit root water uptake scheme and a stomatal conductance model

that employs the Ball-Berry approach would be an ideal conceptualization of representing plant water relations to represent the soil-plant-atmosphere continuum of heat and mass.

6.3.4. Temporal upscaling of the Penman- Monteith equation

Theoretically, the Penman-Monteith equation is an instantaneous conceptualization of the vegetation-controlled surface energy balance. In this model, stomatal resistance or bulk surface resistance prevents water from escaping the boundary layer in spite of having other conducive conditions such as available energy or vapor pressure deficit. Hitherto scientists have been using this model for daily applications using daily mean values for the parameters that go into this equation. This is intuitively erroneous. We need to develop a temporal scaling algorithm that takes into consideration the diurnal variations in available radiation, vapor pressure deficit, stomatal resistance, and slope of the vapor pressure curve.

6.3.5. C-allocation Mechanism in InTEC and BEPS-TerrainLab V2.0.

The InTEC model is an efficient tool to reconstruct the sizes and nature (CN ratios) of various ecosystem C-pools in space and time. However, in this model, the C-allocations to various biomass pools are assumed to be constant even under varied plant physiological, meteorological, and CO_2 conditions. There are many studies that have shown that the allocation of biomass C change with age and environmental variables. Similarly, in BEPS-TerrainLab V2.0., the seasonal allocations of NPP to various biomass pools are kept constant. Studies have shown that the allocation of C to biomass pools also seasonally changes.

6.4. Contribution to Science

This research has made some new contributions to science by improving our understanding of how biogeochemical cycles interact with hydrological cycles at meso-scales or higher. Currently we rely on Atmospheric General Circulation models (AGCMs), which are

constructed based on sound physical or statistical principles to understand how climates change. Many of the existing AGCMs simulate the dynamics of terrestrial C or hydrological processes, which govern the climate using Land Surface Schemes, LSS (Sellers et al., 1997). Most of the existing LSS do not explicitly consider topographically-driven hydrological processes. Instead they use "bucket schemes" or have topographically driven saturation excess overland flow, overlooking the ecophysiological and biogeochemical consequences of unrealistic soil-water status. Although these simplified schemes are capable of simulating the trend and magnitudes of lateral hydrological responses, the fact that they abstract the fundamental mechanism (topographic control) and that they neglect the redistribution of water among hydrologically connected areas in the landscape could create substantial errors in the simulated global biogeochemical cycles (especially C). This is an issue that is mostly overlooked today and could further question the reliability of our climate predictions. Currently, we tend to believe that the effects of global warming may switch the status of the terrestrial biosphere from C-sinks to sources in the middle of this century (Cox et al., 2000; Cramer et al., 2001). However, if the lateral hydrological processes dominate due to increased melting of ice and snow in high latitude permafrost regions as a result of global warming (Zimov et al., 2006), it could lead to increased soil saturation, which could further suppress the currently anticipated rates of soil C-decomposition, leading to an increase in the existing C-sinks. Some recent GCM simulations demonstrate that historical variations in continental run-off altered stomatal conductance of global vegetation that had a positive feedback on the climate (Gedney et al., 2006) and vice versa (Betts et al., 2007). These studies hint that hydrologically-controlled ecological processes could affect biogeochemical cycles and hence the climate. Explicit hydrological representations, if realistically included within LSS, could give a better idea of the spatial distributions of terrestrial C-sources or sinks which could improve our climate predictions.

Climate change prediction needs to incorporate explicit consideration of Earth's topography because water and light are the major controls on plant growth that sequesters atmospheric CO_2. With the availability of cutting edge computing facilities such as the *Earth Simulator* (Normile, 2002), it is possible to incorporate topographic controls in our models. This research demonstrates to the scientific community that it is necessary that our land surface schemes within climate models are "rugged", in order to mimic Earth system processes more realistically.

References

Betts, R.A., Boucher, O., Collins, M., Cox, P.M., Falloon, P.D., Gedney, N., Hemming, D.L., Huntingford, C., Jones, C.D., Sexton, D.M.H., and Webb, M.J.(2007). Projected Increase in Continental Runoff Due to Plant Responses to Increasing Carbon Dioxide, *Nature* **448**, 1037-U5.

Chen, J.M., Chen, X.Y., Ju, W.M., and Geng, X.Y.(2005). Distributed Hydrological Model for Mapping Evapotranspiration Using Remote Sensing Inputs, *Journal of Hydrology* **305**, 15-39.

Cox, P.M., Betts, R.A., Jones, C.D., Spall, S.A., and Totterdell, I.J.(2000). Acceleration of Global Warming Due to Carbon-Cycle Feedbacks in a Coupled Climate Model (Vol 408, Pg 184, 2000), *Nature* **408**, 750.

Cramer, W., Bondeau, A., Woodward, F.I., Prentice, I.C., Betts, R.A., Brovkin, V., Cox, P.M., Fisher, V., Foley, J.A., Friend, A.D., Kucharik, C., Lomas, M.R., Ramankutty, N., Sitch, S., Smith, B., White, A., and Young-Molling, C.(2001). Global Response of Terrestrial Ecosystem Structure and Function to Co2 and Climate Change: Results From Six Dynamic Global Vegetation Models, *Global Change Biology* **7**, 357-373.

Gedney, N., Cox, P.M., Betts, R.A., Boucher, O., Huntingford, C., and Stott, P.A.(2006). Detection of a Direct Carbon Dioxide Effect in Continental River Runoff Records, *Nature* **439**, 835-838.

Jones, J.W., Graham, W.D., Wallach, D., Bostick, W.M., and Koo, J.(2004). Estimating Soil Carbon Levels Using an Ensemble Kalman Filter, *Transactions of the Asae* **47**, 331-339.

Laio, F., Porporato, A., Ridolfi, L., and Rodriguez-Iturbe, I.(2001). Plants in Water-Controlled Ecosystems: Active Role in Hydrologic Processes and Response to Water Stress - Ii. Probabilistic Soil Moisture Dynamics, *Advances in Water Resources* **24**, 707-723.

Matsushita, B., Xu, M., Chen, J., Kameyama, S., and Tamura, M.(2004). Estimation of Regional Net Primary Productivity (Npp) Using a Process-Based Ecosystem Model: How Important Is the Accuracy of Climate Data?, *Ecological Modelling* **178**, 371-388.

Miyata, A., Leuning, R., Denmead, O.T., Kim, J., and Harazono, Y.(2000). Carbon Dioxide and Methane Fluxes From an Intermittently Flooded Paddy Field, *Agricultural and Forest Meteorology* **102**, 287-303.

Normile, D.(2002). *Science* **295** , 1631-1633.

Paola, C., Foufoula-Georgiou, E., Dietrich, W.E., Hondzo, M., Mohrig, D., Parker, G., Power, M.E., Rodriguez-Iturbe, I., Voller, V., and Wilcock, P.(2006). Toward a Unified Science of the Earth's Surface: Opportunities for Synthesis Among Hydrology, Geomorphology, Geochemistry, and Ecology, *Water Resources Research* **42**.

Peddle, D.R., Johnson, R.L., Cihlar, J., and Latifovic, R.(2004). Large Area Forest Classification and Biophysical Parameter Estimation Using the 5-Scale Canopy Reflectance Model in Multiple-Forward-Mode, *Remote Sensing of Environment* **89**, 252-263.

Porporato, A., Laio, F., Ridolfi, L., and Rodriguez-Iturbe, I.(2001). Plants in Water-Controlled Ecosystems: Active Role in Hydrologic Processes and Response to Water Stress - Iii. Vegetation Water Stress, *Advances in Water Resources* **24**, 725-744.

Rodriguez-Iturbe, I., Porporato, A., Laio, F., and Ridolfi, L.(2001). Plants in Water-Controlled Ecosystems: Active Role in Hydrologic Processes and Response to Water Stress - I. Scope and General Outline, *Advances in Water Resources* **24**, 695-705.

Rodriguez-Iturbe, I., Porporato, A., Ridolfi, L., Isham, V., and Cox, D.R.(1999). Probabilistic Modelling of Water Balance at a Point: the Role of Climate, Soil and Vegetation, *Proceedings of the Royal Society of London Series a-Mathematical Physical and Engineering Sciences* **455**, 3789-3805.

Schiff, S.L., Aravena, R., Trumbore, S.E., Hinton, M.J., Elgood, R., and Dillon, P.J.(1997). Export of Doc From Forested Catchments on the Precambrian Shield of Central Ontario: Clues From C-13 and C-14, *Biogeochemistry* **36**, 43-65.

Sellers, P.J., Dickinson, R.E., Randall, D.A., Betts, A.K., Hall, F.G., Berry, J.A., Collatz, G.J., Denning, A.S., Mooney, H.A., Nobre, C.A., Sato, N., Field, C.B., and Hendersonsellers, A.(1997). Modeling the Exchanges of Energy, Water, and Carbon Between Continents and the Atmosphere, *Science* **275**, 502-509 .

Shibata, H., Petrone, K.C., Hinzman, L.D., and Boone, R.D.(2003). Effect of Fire on Dissolved Organic Carbon and Inorganic Solutes in Spruce Forest in the Permafrost Region of Interior Alaska, *Soil Science and Plant Nutrition* **49**, 25-29.

Wang, Y.P., Leuning, R., Cleugh, H.A., and Coppin, P.A.(2001). Parameter Estimation in Surface Exchange Models Using Nonlinear Inversion: How Many Parameters Can We Estimate and Which Measurements Are Most Useful?, *Global Change Biology* **7**, 495-510.

Williams, M., Schwarz, P.A., Law, B.E., Irvine, J., and Kurpius, M.R.(2005). An Improved Analysis of Forest Carbon Dynamics Using Data Assimilation, *Global Change Biology* **11**, 89-105.

Zhuang, Q., Melillo, J.M., Kicklighter, D.W., Prinn, R.G., Mcguire, A.D., Steudler, P.A., Felzer, B.S., and Hu, S.(2004). Methane Fluxes Between Terrestrial Ecosystems and the Atmosphere at Northern High Latitudes During the Past Century: a Retrospective Analysis With a Process-Based Biogeochemistry Model, *Global Biogeochemical Cycles* **18**.

Zimov, S.A., Schuur, E.A.G., and Chapin, F.S.(2006). Permafrost and the Global Carbon Budget, *Science* **312**, 1612-1613.